Maria Sklodowska-Curie
National Research Institute of Oncology

ANETA ŻEBROWSKA

MOLECULAR CHARACTERISTICS OF SMALL EXTRACELLULAR VESICLES ISOLATED FROM MELANOMA PATIENTS' PLASMA

Doctoral dissertation realized in the Center for Translational Research and Molecular Biology of Cancer

under the supervision of Monika Pietrowska, PhD, DSc

Gliwice, 2025

Supported in part by the National Science Centre grant no. 2016/22/M/NZ5/00667 (HARMONIA 8) and 2022/45/B/NZ5/03510 (OPUS 23)

I would like to express my sincere gratitude to the team at the collaborating laboratory for their invaluable support in preparing the samples for our analyses and to Professor Soldano Ferrone for his expertise and production of anti-CSPG4 mAbs, which have significantly contributed to the progress of this study.

I would like to thank

my Supervisor - Professor Monika Pietrowska for inspiration, scientific supervision, substantial assistance enabling me to carry out the research that became a part of this dissertation, and motivation for continuous development,

my Colleagues at the Center for Translational Research and Molecular Biology of Cancer, especially Dr. Marta Gawin and Dr. Mateusz Smolarz for their kindness and valuable guidance I received during the implementation of the presented research,

my Family and my Closest Friends for their unconditional support.

TABLE OF CONTENTS

LIST OF THE MOST FREQUENTLY USED ABBREVIATIONS

AML – acute myeloid leukemia

APCs – antigen-presenting cells

BAP1 – BRCA1-associated deubiquitinase 1 (gene)

BM – bone marrow

BMDCs – bone marrow-derived cells

BRAF – B-Raf proto-oncogene, serine/threonine kinase (gene)

CDK4 – cyclin dependent kinase 4 (gene)

CDKN2A – cyclin-dependent kinase inhibitor 2A (gene)

CAFs – cancer-associated fibroblasts

CAMs – cell adhesion molecules

CD3 – cluster of differentiation 3

CID – collision-induced dissociation

circRNA – circular ribonucleic acid

CSPG4 – chondroitin sulfate proteoglycan 4 (protein)

CTCs – circulating tumor cells

ctDNA – circulating tumor DNA

CYT-MAA – cytoplasmic melanoma-associated antigens

DCs – dendritic cells

DDA – data-dependent acquisition

DIA – data-independent acquisition

DTT – dithiothreitol

EI – electron impact ionization

EMT – epithelial-mesenchymal transition

ESCRT – endosomal sorting complex required for transport

ESI – electrospray ionization

EVs – extracellular vesicles

FAMMM – familial atypical multiple mole-melanoma

FA – formic acid

FASP – filter-aided sample preparation

FGF2 – fibroblast growth factor 2

gDNA – genomic deoxyribonucleic acid

GPC1 – glypican 1 (protein)

HD – healthy donor

HSP – heat shock protein

IAA – iodoacetamide

IFN-γ – interferon gamma

IHC – immunohistochemistry

IL-2R – interleukin-2 receptor

ISEV – International Society for Extracellular Vesicles

lEV – large extracellular vesicles

LB – lysis buffer

LC-MS/MS – liquid chromatography coupled to tandem mass spectrometry

LDH – lactate dehydrogenase

lncRNA – long non-coding ribonucleic acid

MAAs – melanoma-associated antigens

MAPK – mitogen-activated protein kinase signaling pathway

MAS - melanoma-astrocytoma syndrome

MC1R – melanocortin 1 receptor (gene)

miRNA – micro ribonucleic acid

MRM – multiple reaction monitoring

mRNA – messenger ribonucleic acid

MS2 – tandem mass spectrum

MSCs – myeloid-derived stem cells

MHC – major histocompatibility complex

MIA – melanoma inhibitory activity

MITF – melanocyte inducing transcription factor (gene)

MISEV – minimal information for studies of extracellular vesicles

MMP9 – matrix metalloproteinase 9

MS – mass spectrometry

mtDNA – mitochondrial deoxyribonucleic acid

MTEX – melanoma cell-derived small extracellular vesicles

MVBs – multivesicular bodies

MVs – microvesicles

MWCO – molecular weight cut-off

m/z – mass to charge ratio

NED – no evidence of disease

NF1 – neurofibromin 1 (gene)

NK – natural killer cells

NMTEX – non melanoma cell-derived small extracellular vesicles

NTA – nanoparticle tracking analysis

NTEX – non tumor-derived small extracellular vesicles

NRAS - neuroblastoma RAS viral oncogene homolog (gene)

OCA2 – oculocutaneous albinism 2 (gene)

PD – Proteome Discoverer (software)

PD-1 – programmed cell death protein 1

PDCD6IP – programmed cell death 6-interacting protein

PD-L1 – programmed cell death 1 ligand 1

PEG – poly(ethylene glycol)

POT1 – protection of telomeres 1 (gene)

PRM – parallel reaction monitoring

PTMs – post-translational modifications

RCF – relative centrifugal force

rpm – revolutions per minute

RTK – receptor tyrosine kinase

SDS-PAGE – sodium dodecyl sulfate-polyacrylamide gel electrophoresis

SEC – size exclusion chromatography

sEV – small extracellular vesicles

SLC45A2 – solute carrier family 45 member 2 (gene)

SRM – selected reaction monitoring

TCR – T cell receptor

TEM – transmission electron microscopy

TERF2IP – telomeric repeat binding factor 2, interacting protein (gene)

TERT – telomerase reverse transcriptase (gene)

TEX – tumor-derived small extracellular vesicles

TFA – trifluoroacetic acid

Th – T helper cell

TME – tumor microenvironment

TNF-α – tumor necrosis factor-alpha

TLR – Toll-like receptor

TOF – time-of-flight mass analyzer

Treg – regulatory T cell

TYR – tyrosinase (gene)

TYRP1 - tyrosinase-related protein 1 (gene)

UC – ultracentrifugation

UV – ultraviolet

VEGFa – vascular endothelial growth factor A

WB – western blotting

ABSTRACT

Melanoma is a highly invasive cancer the incidence of which is increasing worldwide. Currently, primary surgical treatment is supplemented by tailored adjuvant treatment with immune checkpoint inhibitors or BRAF or MEK kinase inhibitors. However, melanoma tends to escape immunological control and develops resistance to therapy, which remains a major therapeutic problem. A second clinical problem is the lack of predictive markers enabling to anticipate which melanoma patients will benefit most from the proposed treatment and which will not be sensitive to it.

Melanoma cells communicate with other cells present in the tumor microenvironment, including components of the immune system. Recent data indicate that this communication is mediated by small extracellular vesicles (sEV) derived from melanoma cells (MTEX). sEV are a subset of extracellular vesicles freely circulating in body fluids that are produced and released by all cells in the human body. Compared to normal cells, cancer cells produce more sEVs because they function under conditions of permanent stress (in a hypoxic, acidic and glucose-deprived environment), as well as being exposed to toxic physical (radiation therapy) or chemical (chemotherapy) agents during anticancer treatment. The molecular content of MTEX present in the plasma of patients resembles that of the melanoma cells from which they were released. Thus, the molecular composition of MTEX can serve as a surrogate for melanoma cells in plasma. This approach, called “liquid tumor biopsy,” allows diagnosis and non-invasive monitoring of melanoma progression or response to therapy.

The plasma of melanoma patients contains a heterogeneous mixture of sEV, which includes MTEX, sEV derived from body tissues, including circulating non-malignant cells like immune cells in the blood. As a result of this heterogeneity, sEV-mediated intercellular communication is difficult to understand. We hypothesize that selective assignment of the molecular content of sEVs in plasma to specific subsets of sEVs produced by malignant and non-malignant cells will expand knowledge of MTEX composition and function. Consequently, understanding of the mechanisms determining melanoma response to therapy will improve, and new markers may be identified that will potentially serve as predictors of such response.

The aim of the dissertation was to study the molecular composition of small extracellular vesicles derived from melanoma cells of the CSPG-4(+) phenotype and lymphocytes of the CD3(+) phenotype isolated from the plasma of patients diagnosed with melanoma and healthy subjects.

In the first stage of the PhD project, an immune capture strategy was used to separate tumor cell-derived sEV (TEX) from other subsets of sEV present in patients' plasma. This approach is only effective if specific tumor surface antigens are known and antibodies specific for such antigen are available. In my study, an anti-CSPG4 antibody [Pietrowska et al., 2021] specifically recognizing a melanoma cell antigen that is also present in the membranes of the sEVs they produce, was used to isolate MTEX from patient plasma. In the research presented in this dissertation I used the technique of high-resolution mass spectrometry coupled to nano-liquid chromatography (nano-LC-MS/MS) as a tool to assess the protein composition of sEV. The proteomes of sEVs divided into melanoma cell-derived (MTEX) and non-melanoma cell-derived (NMTEX) were compared, and statistical analysis identified an MTEX-related profile of 16 proteins that distinguished MTEX from NMTEX. Among the 75 proteins the levels of which were elevated in MTEX, the PDCD6IP (programmed cell death 6-interacting protein) had the greatest power to distinguish patients with progressive melanoma from those with no evidence of disease. Patients with progression had elevated levels of PDCD6IP in MTEX. This discovery motivated us to expand our research on the role of PDCD6IP protein detected in the cargo of MTEX present in plasma, in immune regulation and promotion of melanoma progression (OPUS project currently underway).

Continuing with the use of the immune capture strategy, we used antibodies specific for the CD3 antigen expressed only on TCR+ (T-cell receptor) cells. This strategy allowed us to isolate from plasma sEVs with CD3(+) phenotype, which are products of T lymphocytes, and with CD3(-) phenotype, which contain a mixture of sEVs produced by non-T cells, including MTEX produced by melanoma cells [Zebrowska et al., 2022]. In the plasma of melanoma patients, the CD3(-) fraction of sEVs contains MTEX and other sEVs (non-TEX) in different, individual-variant proportions. Using the above strategy for isolating sEVs from the plasma of melanoma patients, we have shown that

it is possible to selectively isolate and evaluate the protein profile of CD3(+) sEVs and then compare it with that of MTEX-enriched CD3(-) vesicles.

In conclusion, we have shown that the molecular composition of sEVs derived from melanoma cells and present in plasma distinguishes patients with progression from those with stable disease. The research technique used allows identification of proteins that can potentially serve as prognostic markers in melanoma. In addition, we found that the sEV capture method using antibodies is effective in studying the molecular composition of subpopulations of small extracellular vesicles present in body fluids.

Key words: melanoma, small extracellular vesicles, prognostic marker, proteomics, high-resolution mass spectrometry

STRESZCZENIE

Czerniak (melanoma) jest wysoce inwazyjnym nowotworem, którego częstość występowania wzrasta na całym świecie. Obecnie, uzupełnieniem pierwotnego leczenia chirurgicznego jest indywidualnie dobrane leczenie adjuwantowe inhibitorami immunologicznych punktów kontrolnych lub inhibitorami kinaz BRAF lub MEK. Czerniak ma jednak tendencję do wymykania się spod kontroli immunologicznej i rozwija oporność na terapię, co pozostaje głównym problemem terapeutycznym. Drugim problemem klinicznym jest brak markerów predykcyjnych umożliwiających przewidywanie, którzy chorzy na czerniaka odniosą najwyższy zysk z proponowanego leczenia, a którzy nie będą na nie wrażliwi.

Komórki czerniaka komunikują się z innymi komórkami obecnymi w mikrośrodowisku guza, w tym ze składnikami układu odpornościowego. Najnowsze dane wskazują, że w tej komunikacji pośredniczą małe pęcherzyki zewnątrzkomórkowe (sEV) pochodzące z komórek czerniaka (MTEX). sEV są podzbiorem pęcherzyków zewnątrzkomórkowych swobodnie krążących w płynach ustrojowych, które są wytwarzane i uwalniane przez wszystkie komórki ludzkiego ciała. W porównaniu z komórkami prawidłowymi, komórki nowotworowe wytwarzają więcej sEV ponieważ funkcjonują w warunkach permanentnego stresu (w środowisku niedotlenionym, kwaśnym i pozbawionym glukozy), a także podczas leczenia przeciwnowotworowego poddawane są działaniu toksycznych czynników fizycznych (radioterapia) lub chemicznych (chemioterapia). Zawartość molekularna MTEX obecnych w osoczu pacjentów przypomina zawartość komórek czerniaka, z których zostały uwolnione. Zatem skład molekularny MTEX może służyć jako surogat komórek czerniaka w osoczu. Takie podejście, zwane „płynną biopsją guza", pozwala na diagnozowanie i nieinwazyjne monitorowanie progresji czerniaka lub odpowiedzi na terapię.

Osocze chorych na czerniaka zawiera heterogeniczną mieszaninę sEV, w skład której wchodzą MTEX, sEV pochodzące z tkanek ciała, w tym krążących we krwi komórek niezłośliwych jak komórki odpornościowe. W wyniku tej heterogeniczności, międzykomórkowa komunikacja za pośrednictwem sEV jest trudna do zrozumienia. Zakładamy, że selektywne przypisanie zawartości molekularnej sEV w osoczu do określonych podzbiorów sEV wytwarzanych przez komórki złośliwe i niezłośliwe

poszerzy wiedzę o składzie i funkcjach MTEX. W konsekwencji, poprawi się zrozumienie mechanizmów determinujących odpowiedź czerniaka na terapię, a także mogą zostać zidentyfikowane nowe markery, które potencjalnie będą służyć jako predykcja takiej odpowiedzi.

Celem pracy doktorskiej było poznanie składu molekularnego małych pęcherzyków zewnątrzkomórkowych pochodzących z komórek czerniaka o fenotypie CSPG-4(+) oraz limfocytów o fenotypie CD3(+) izolowanych z osocza pacjentów z rozpoznaniem czerniaka oraz osób zdrowych.

W pierwszym etapie projektu doktorskiego zastosowano strategię wychwytu immunologicznego w celu oddzielenia sEV pochodzących z komórek nowotworowych (TEX) od innych podgrup sEV obecnych w osoczu pacjentów. Podejście to jest skuteczne tylko wtedy, gdy znane są specyficzne powierzchniowe antygeny nowotworowe oraz dostępne są przeciwciała specyficzne dla takiego antygenu. W moich badaniach do izolacji MTEX z osocza chorych zostało zastosowane przeciwciało anty-CSPG4 [Pietrowska i in., 2021] specyficznie rozpoznające antygen komórek czerniaka, który jest obecny także w błonach produkowanych przez nie sEV. W badaniach prezentowanych w niniejszej pracy doktorskiej wykorzystałam technikę wysokorozdzielczej spektrometrii mas sprzężonej z nano-chromatografią cieczową (nano-LC-MS/MS) jako narzędzie do oceny składu białkowego sEV. Porównano proteomy sEV podzielone na pochodzące z komórek czerniaka (MTEX) i pochodzące z komórek niezłośliwych (NMTEX), a analiza statystyczna zidentyfikowała związany z MTEX profil 16 białek, które odróżniały MTEX od NMETEX. Wśród 75 białek których poziom był podwyższony w MTEX największą moc odróżniania pacjentów z postępującym czerniakiem od pacjentów bez objawów choroby miało białko PDCD6IP (ang. programmed cell death 6-interacting protein). Pacjenci z progresją mieli podwyższony poziom PDCD6IP w MTEX. Odkrycie to zmotywowało nas do poszerzenia badań nad rolą białka PDCD6IP wykrytego w składzie MTEX obecnych w osoczu w regulacji immunologicznej i promowaniu progresji czerniaka (obecnie realizowany projekt OPUS).

Kontynuując wykorzystanie strategii wychwytu immunologicznego użyliśmy przeciwciał specyficznych dla antygenu CD3 wyrażanego tylko na komórkach TCR+ (T-cell

receptor). Strategia ta pozwoliła na wyizolowanie z osocza sEV o fenotypie CD3(+), które są produktami limfocytów T, oraz o fenotypie CD3(-), które zawierają mieszaninę sEV wytwarzanych przez komórki inne niż T, w tym MTEX produkowane przez komórki czerniaka [Żebrowska i in., 2022]. W osoczu pacjentów chorych na czerniaka frakcja CD3(-) sEV zawiera MTEX i pozostałe sEV (non-TEX) w różnych, osobniczo-zmiennych proporcjach. Stosując powyższą strategię izolacji sEV z osocza chorych na czerniaka, wykazaliśmy, że możliwe jest selektywne wyizolowanie i ocena profilu białkowego sEV CD3(+), a następnie porównanie go z profilem wzbogaconych w MTEX pęcherzyków CD3(-).

Podsumowując, wykazaliśmy, że skład molekularny sEV pochodzących z komórek czerniaka i obecnych w osoczu odróżnia pacjentów z progresją od pacjentów ze stabilną chorobą nowotworową. Zastosowana technika badawcza pozwala na identyfikację białek, które potencjalnie mogą służyć jako markery prognostyczne w czerniaku. Ponadto stwierdziliśmy, że metoda wychwytywania sEV z wykorzystaniem przeciwciał jest skuteczna w badaniu składu molekularnego subpopulacji małych pęcherzyków zewnątrzkomórkowych obecnych w płynach ustrojowych.

Słowa kluczowe: czerniak, małe pęcherzyki zewnątrzkomórkowe, marker prognostyczny, proteomika, wysokorozdzielcza spektrometria mas

1. INTRODUCTION

1.1. Melanoma - risk factors and pathogenesis.

Melanoma is a malignant cancer that develops from melanocytes. The majority of melanoma diagnoses are cutaneous (>90%), while mucosal and uveal melanomas are less common (<1-5% of diagnoses, depending on a nation) [Rashid et al. 2023, Elder et al. 2020]. The incidence of melanoma has increased in the developed, predominantly fair-skinned countries over the past decades. Cutaneous melanoma is one of the most aggressive forms of skin cancer and one of the leading causes of cancer-related mortality due to its high metastatic potential.

The pathogenesis of melanoma is multifactorial, involving environmental, and host (genetic) factors. Ultraviolet (UV) light exposure (both: UV-B and UV-A) is the main environmental risk factor for melanoma skin cancer development. UV light is a known DNA-damaging agent. It induces DNA lesions, such as pyrimidine dimers, which when not repaired by the DNA repair nucleotide excision repair (NER) system cause errors in DNA replication. This subsequently leads to mutations in genes encoding cell signaling molecules, and ultimately to carcinogenesis. UV-B light (wavelength: 280–320 nm) is considered 1000 times more genotoxic per photon than UV-A (320–400 nm). On the other hand, environmental exposure to UV-A is up to 20–40-times higher depending on time, season, latitude, and altitude [Saginala et al. 2021, Bowden et al. 2010]. Over 75% of cutaneous melanomas in White populations are estimated to be driven by the mutagenic effect of UV light [Long et al. 2023]. Multiple studies have linked sun exposure patterns and timing to an increased risk of melanoma. For example, severe and intermittent sun exposure (the typical history of sunburn) is associated with a higher risk than chronic continuous sun exposure, which is more often associated with non-melanoma skin malignancies [Gosman et al. 2023, Burns et al. 2019, Leonardi et al. 2018, Candido et al. 2014, Caini et al. 2009]. Moreover, a history of sunburn in childhood or adolescence is related to the highest risk of melanoma disease, severe sunburn experienced five times or more has a 2-fold greater risk of developing melanoma [Leonardi et al. 2018]. There is also a link between the risk of developing melanoma and exposure to UV from artificial sources (like sunbed use), particularly at a young age [Gordon et al. 2020, Colantionio et al. 2014, Vehner et al. 2014]. First

exposure at an early age (≤ 20 years) and frequent exposure (annual frequency ≥ 10 times) to indoor tanning showed increasing risk for melanoma (relative risk = 1.47, 1.16-1.85; relative risk = 1.52, 1.22-1.89; 95% confidence interval) [An et al. 2021].

Melanocytic nevi count or type are direct precursors and markers of an increased risk of melanoma. Approximately 30% of melanoma cases arise on a pre-existing nevus [Leonardi et al. 2018, Pampena et al. 2017]. In a meta-analysis on nevi as risk factors for melanoma, the highest risk (about 7-fold) of melanoma was observed in individuals with more than 100 nevi. What is more, the presence of several atypical nevi (at least 5 mm, with a flat component, variable pigmentation, irregular asymmetric outline, indistinct borders) was correlated with 6-fold higher risk of melanoma formation compared with the absence of atypical nevi [Gandini et al. 2005]. Total nevus count on the trunk and legs is more strongly associated with melanoma than on the head and arms [Caini et al. 2009]. Other important host risk factors of melanoma are individual phenotypic traits associated with heightened sensitivity to UV irradiation such as lighter skin tones, freckles, light eyes, red hair. Each of these phenotypic factors is positively associated with melanoma, on both usually and occasionally sun-exposed body sites [Long et al. 2023, Saginala et al. 2021, Caini et al. 2009]. Therefore, the incidence rate of cutaneous melanoma is greater in the White population compared to Hispanic, African-American, Indo-American, and Asian population [Gutiérrez-Castañeda et al. 2020].

A family history of melanoma is a strong risk factor for the disease. Familial (inherited) melanomas account for about 10% of all cases. Main high penetrance genes associated with the development of familial melanoma are as follows: tumor suppressor genes: CDKN2A (20-40% of hereditary melanomas) and BAP1 (<1%), CDK4 (cell cycle regulator), or genes coding proteins responsible for telomere maintenance: POT1, ACD, TERT, TERF2IP. Other significant contributors to the pathogenesis of hereditary melanoma are germline pathogenic mutations in pigmentation-related genes. Among these genes there are MITF, MITF-regulated MC1R, SLC45A, OCA2, melanosomal TYR and TYRP1 [Gosman et al. 2023, Timar et al. 2022, Zocchi et al. 2021, Saginala et al. 2021, Leonardi et al. 2018]. An increased risk of developing melanoma is also observed in families with genetic diseases such as familial atypical multiple mole-melanoma (FAMMM), melanoma-astrocytoma syndrome (MAS), familial

retinoblastoma, Li-Fraumeni cancer syndrome, and Lynch syndrome type II [Saginala et al. 2021, Leonardi et al. 2018, Soura et al. 2016, Markovic et al. 2007].

1.2. Therapeutic options for melanoma.

Within the last decades, the treatment of melanoma patients has evolved significantly, shifting from conventional surgical management toward a more integrated approach including systemic therapies. While radical surgery remains the cornerstone of melanoma treatment, particularly in early-stage disease, the risk of recurrence in high-risk patients (stages II–IV) remains substantial, ranging from 30% to 90%. To mitigate this, adjuvant systemic treatment options have been implemented. In general, two major therapeutic strategies have been approved for adjuvant use:

- Molecular targeted therapy (for BRAF-mutant melanoma) – a combination of BRAF and MEK inhibitors that targets the mitogen-activated protein kinase (MAPK) signaling pathway which is frequently activated in melanoma due to BRAF mutations. These inhibitors effectively reduce tumor growth and risk of recurrence in patients with BRAF-mutated melanoma.
- Immunotherapy (for all melanoma subtypes) – immune checkpoint inhibitors (anti-PD-1, anti-CTLA4, anti-LAG-3, interferon alfa-2b). These monoclonal antibodies restore the immune system's ability to recognize and eliminate melanoma cells by blocking respective checkpoint molecules. This approach has been shown to significantly reduce the risk of relapse in high-risk patients with resected melanoma. It is also recommended for preoperative treatment (neoadjuvant therapy) of melanoma patients with clinical lymph node metastases (grade IIIB-D), as it improves event-free survival [Garbe et al. 2024, Rutkowski et al. 2022].

1.3. Somatic mutations and key oncogenic signaling pathways involved in melanoma.

Alexandrov et al. studied mutational signatures of 7042 primary cancers of 30 different classes concluding that the prevalence of somatic mutations was highly variable between and within cancer classes, ranging from about 0.001/Mb to more than 400/Mb. Melanoma had the highest mutation frequency of all cancers analyzed [Alexandrov et al. 2013]. The most common somatic mutations in melanoma impact genes implicated in the phosphoinositol-3-kinase (PI3K)/AKT pathway and the

RAS/RAF/MEK/ERK signaling system, referred to as the MAPK pathway. BRAF, NRAS, NF1, PTEN, KIT, TP53, CDKN2A, and TERT are among the mutant genes [Tímár et al. 2022, Gutiérrez-Castañeda et al. 2020, Hayward et al. 2017, Hodis et al., 2012]. The landscape of somatic mutations varies substantially between melanoma subtypes, both in terms of driver oncogenes and a total number of mutations.

Melanomas from chronically sun-exposed skin tend to have the highest number of genomic alterations, with mutations in NF1, NRAS, and BRAF (V600K). Melanomas developed in intermittently sun-exposed skin are more likely to have BRAF (V600E) (40-50% of cases) or NRAS (15-20%) mutations. The total number of mutations is lower in mucosal, uveal, and acral melanomas with BRAF, NRAS, and KIT being the most frequently mutated in the acral subtype (up to 15% each), or with KIT mutations in 15% of cases and sporadic incidence of BRAF or NRAS mutations in the mucosal subtype. Uveal melanomas have different genetic background with GNAQ or GNA11 mutations in >90% of cases [Gutiérrez-Castañeda et al. 2020, Davis et al. 2018, Cancer Genome Atlas Network 2015].

Most of the melanoma mutations discussed above deregulate several cell signaling pathways that control cell proliferation, survival, invasion, and immune evasion, making them important targets for therapeutic intervention [Li et al. 2022, Guo et al. 2021, Paluncic et al. 2016].

The MAPK pathway is the most frequently altered signaling cascade in melanoma, primarily due to activating mutations in BRAF (V600E being the most common) and NRAS. This pathway is initiated by receptor tyrosine kinases (RTKs) or G-protein-coupled receptors, leading to RAS activation. RAS then stimulates RAF kinases (ARAF, BRAF, or CRAF), which phosphorylate and activate MEK1/2, ultimately leading to ERK1/2 activation. ERK drives cell proliferation and survival by modulating transcription factors and cell cycle regulators such as MYC and cyclin D1. Since BRAF-mutant melanoma is highly dependent on sustained MAPK signaling, several BRAF (e.g., vemurafenib, dabrafenib) and MEK (e.g., trametinib, cobimetinib) inhibitors have been implemented as effective drugs for melanoma treatment. However, alternative MAPK reactivation, RTK upregulation, or secondary mutations in NRAS or MEK result in the development of resistance to these inhibitors [Timar et al. 2022, Motwani et al. 2021, Dhillon et al. 2007].

The phosphoinositide 3-kinase (PI3K)/AKT pathway is another key oncogenic axis in melanoma, often activated via PTEN loss, NRAS mutations, or PI3K alterations. Activation of PI3K leads to phosphorylation of PIP2 to PIP3, subsequent recruitment of AKT to the membrane and its phosphorylation by PDK1 and mTORC2. Activated AKT promotes cell survival, proliferation, and metabolic adaptation by inhibiting pro-apoptotic factors (e.g., BAD, FOXO) and activating mTORC1, which enhances protein synthesis and tumor growth. PTEN, a tumor suppressor that dephosphorylates PIP3, is frequently lost in melanoma, leading to constitutive AKT activation. This effect can enhance resistance to MAPK inhibitors. Hence, dual targeting of MAPK and PI3K/AKT pathways is often required to prevent adaptive resistance mechanisms [Teixido et al. 2021, Paluncic et al. 2016].

Aberrant activation of the Wnt/β-catenin signaling pathway is associated with melanoma progression, therapy resistance, and immune evasion. In normal cells, Wnt ligands bind to Frizzled receptors and LRP5/6 co-receptors, inhibiting the β-catenin destruction complex (comprising APC, Axin, and GSK3β). This leads to β-catenin accumulation, nuclear translocation, and increased transcription of genes involved in cell proliferation and differentiation. High levels of β-catenin in melanoma are linked to reduced T cell infiltration and resistance to immune checkpoint inhibitors. β-catenin modulates immune evasion by downregulating chemokines such as CCL4, preventing dendritic cell recruitment and T cell priming. Thus, inhibition of Wnt signaling represents a potential strategy for improving immunotherapy response in melanoma [Motwani et al. 2021, Gajos-Michniewicz et al. 2020].

MITF is a lineage-specific master regulator that governs melanocyte development, differentiation, and survival. It is tightly regulated by MAPK, Wnt, and PI3K/AKT pathways, integrating oncogenic signals to promote melanoma cell proliferation or dormancy. High levels of MITF expression are linked to a differentiated phenotype, whereas low levels correlate with dedifferentiation, invasion, and therapy resistance. MITF downregulation leads to a switch toward a neural crest-like state, enabling metastatic spread and immune evasion [Li et al. 2022, Goding et al. 2019].

Other pathways contributing to melanoma progression are as follows: TGF-β signaling, which induces EMT process to promote invasion and metastasis [Marvine et al. 2023, Skarmoutsou et al. 2018]; Hippo signaling (e.g., YAP/TAZ activation), which

enhances melanoma stemness and drug resistance [Kazimierczak et al. 2024]; NF-κB signaling that promotes inflammation-driven immune suppression and tumor progression [Deng et al. 2020].

1.4. Biomarkers in melanoma.

Laboratory diagnostics in melanoma is essential for diagnostic purposes, evaluation of response to the treatment, and after therapy for patient monitoring . Identification of tumor markers in blood or tumor tissue may help determine the stage of disease, may have prognostic or predictive value, or help monitor the patient for potential recurrence after treatment. The current expert recommendations on diagnostic-therapeutic management of melanoma patients combine several well-established prognostic factors including clinical ABCDE system (preliminary identification of some of the melanomas), the Breslow thickness, mitotic rate, presence of ulceration, extent of metastasis, and serum lactate dehydrogenase (LDH) level [Garbe et al. 2024, Rutkowski et al. 2022]. Additionally, a panel of antibodies for immunohistochemistry testing of HMB45, Melan A, p16, SOX-10, Ki-67 is used to search for clinically undetected metastases in sentinel lymph nodes. Diagnostic molecular testing for the presence of mutations in BRAF gene (in formalin-fixed and paraffin embedded tumor material) is mandatory in patients with stage III, and IV, and recommended in stage IIC. In the absence of BRAF mutations, testing for NRAS and/or KIT mutations should be considered. In the case of spitzoid melanocytic lesions, mutational status of the TERT gene promoter and the HRAS gene is recommended to correctly classify a lesion, with particular emphasis on differentiation from melanoma [Rutkowski et al. 2022]. The markers mentioned above provide significant diagnostic insight and predictive value. However there is still unmet need to identify reliable prognostic biomarkers that would enable identification of patients at a high risk of relapse.

The search for potential novel melanoma biomarkers can be performed using a variety of biological materials. However, the richest and most readily accessible source is blood, which fits perfectly with the concept of minimally invasive but highly informative liquid biopsy. This approach enabled successful detection of several biomarkers such as circulating tumor cells (CTCs), circulating tumor DNA (ctDNA), proteins, metabolites, different classes of RNA, and tumor-derived extracellular

vesicles (TEX) [Ma et al. 2024]. At present, the most extensively studied protein biomarkers in melanoma are S100 calcium-binding protein B (S100B), melanoma inhibitory activity (MIA), and melanoma-associated antigens (MAAs).

S100B, a factor involved in cell-cycle regulation and differentiation, has been widely associated with melanoma progression. Elevated serum S100B levels correlate with poor prognosis, increased relapse risk, and reduced survival [Tarhini et al. 2009]. Some studies suggest that S100B may be a superior prognostic marker to LDH for predicting overall and long-term survival in metastatic melanoma patients [Krahn et al. 2001, Egberts et al. 2008]. The meta-analysis of six eligible studies, including 1,033 patients with cutaneous melanoma, revealed that serum S100B showed significantly greater discriminative ability in detecting disease relapse than serum LDH levels. The prognostic performance of serum S100B was independent but not superior to that of serum LDH [Mocellin et al. 2008].

MIA, a 12-kDa protein secreted by melanoma cells, has been shown by Sandru et al. as an independent prognostic biomarker [Sandru et al. 2014, Nwafor et al. 2023].

Melanoma-associated antigens (MAAs), such as Pmel-17/gp100 and MART-1/Melan-A, are proteins specifically expressed in melanoma cells. Due to their immunogenic properties, these proteins have been extensively examined as potential biomarkers for melanoma detection and prognosis. Studies have demonstrated a correlation between MAA expression and melanoma progression, with certain MAAs, such as MAGE-A3, being associated with poor survival outcomes. For instance, patients with elevated levels of cytoplasmic MAAs (CYT-MAA) exhibited 81% likelihood of disease recurrence compared to those with undetectable levels. A study involving 117 melanoma patients further reinforced the prognostic relevance of MAAs, particularly in the case of residual melanoma in patients with resected disease [Vergilis et al. 2005]. Melan-A was the focus of research over the past decade, yielding mixed findings. While some studies highlighted its high sensitivity (ca. 93%) and specificity (ca. 99%) in distinguishing primary melanoma from non-melanocytic cells, others reported lower sensitivity (ca. 86%) and raised concerns about its specificity. This is due to the fact that in the case of immunohistochemistry-based diagnostics anti-Melan-A staining can give positive results also in the case of other pigmented and non-

pigmented epithelial cells, such as retinal cells, Leydig cells, and adrenocortical tissue [Weinstein et al. 2014].

Several studies investigated CTCs in blood of melanoma patients and found association of CTC presence with poor prognosis and disease progression [Galanzha et al. 2019, Gray et al. 2015]. However, study-to-study differences in CTCs detection rates in melanoma patients (at the same stage) constitutes the main obstacle for applying CTC levels as a valuable marker in clinical settings (CTCs could be detected in 16%–80% of patient in stage I–III melanoma) [Khoja et al. 2015].

The search for diagnostic, prognostic and predictive biomarkers in melanoma is an active research area. In the last decade, the research field aimed at finding novel potential biomarkers has expanded to include analysis of circulating small extracellular vesicles (sEV) derived from melanoma (MTEX).

1.5. Classification and terminology of extracellular vesicles.

The term extracellular vesicles (EVs) covers a broad range of vesicles. The current definition of EVs describes them as nano-sized particles released from cells, bounded by a lipid bilayer membrane, and incapable of self-replication [Welsh et al. 2024]. EVs are a heterogeneous group of particles that differ in origin, size, release pathway, biochemical composition, and function. Due to this variability, the nomenclature of EVs used by researchers is inconsistent. Therefore, the International Society for Extracellular Vesicles (ISEV), the leading professional society for researchers and scientists involved in the study of EVs (https://www.isev.org/) is continuously working on guidelines on EVs terminology and minimal information for studies on EVs (MISEV). The latest guidelines announced in 2023 (MISEV 2023) recommend using operational terms based on the diameter of particles. The term small extracellular vesicles (sEV) is reserved for particles with a diameter below 200 nm, whereas large extracellular vesicles (lEV) refers to particles with a diameter above 200 nm [Welsh et al. 2024]. Furthermore, the classification of EVs based on their biogenesis distinguishes microvesicles (MVs), exosomes, and apoptotic bodies [Jin et al. 2022, Mathieu et al. 2019, Catalano et al. 2019]. Microvesicles (called also ectosomes, shedding vesicles, or microparticles) with a size varying between 100 nm and 1000 nm are formed by direct outward budding of the cell's plasma membranes. Exosomes, generally smaller than

200 nm, are formed by the inward budding of the endosomal membrane during the maturation of multivesicular bodies (MVBs) [Singh et al. 2024, Welsh et al. 2024, Mathieu et al. 2019]. The largest and most heterogeneous group of EVs are apoptotic bodies (50 - 5000 nm) derived from apoptotic cells [Miao et al. 2024, Santavanond et al. 2021]. Figure 1 presents a comparison of the size of the above-mentioned vesicles with viruses, lipoproteins and mitochondria. The subject of research of Prof. Monika Pietrowska's group, including my doctoral studies, are small EVs (sEV, sized below 200 nm), a group consisting mainly of exosomes, however it may also include other types of vesicles, for example, microvesicles. Thus, it should be borne in mind that the majority of isolation methods allow for enrichment of a given subgroup of EVs in a sample [Welsh et al. 2024, Skoczylas et al. 2024, Zebrowska et al. 2022, Pietrowska et al. 2021, Zebrowska et al 2020, Mathieu et al. 2019].

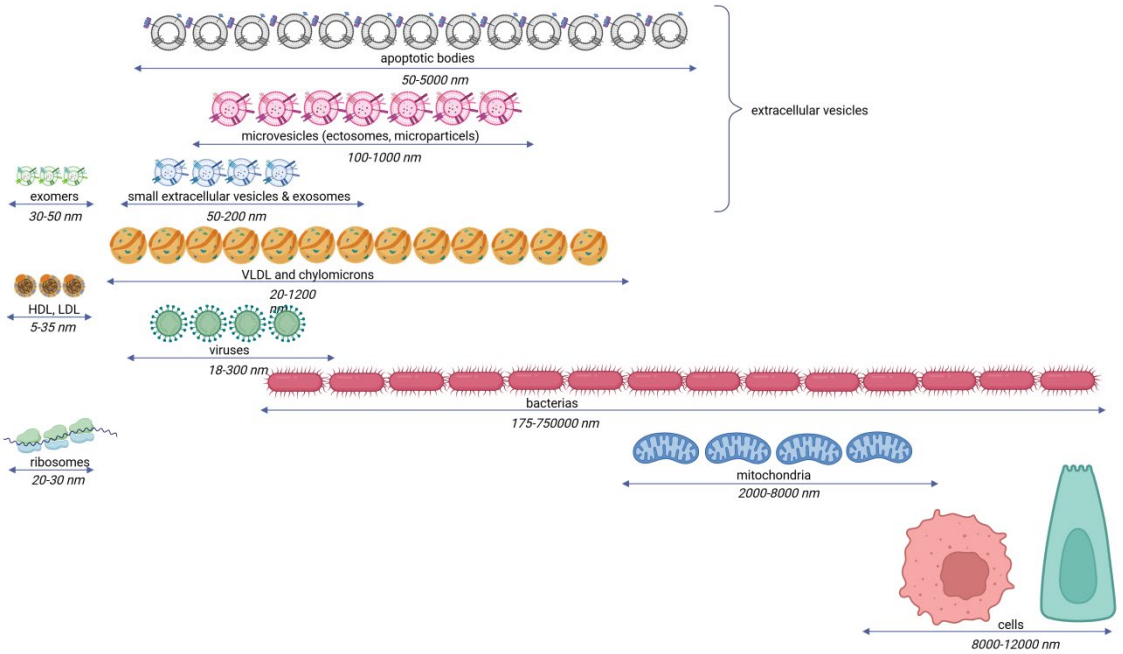

Figure 1. Division of extracellular vesicles: comparison of the size of sEV, MVs, apoptotic bodies with viruses, lipoproteins and mitochondria. *Created in https://BioRender.com.*

1.5.1. Small extracellular vesicles (sEV).

sEV are a diverse class of nano-sized (30-200 nm), cell-derived structures containing a lipid bilayer membrane, released by all cell types. They are present in all human body fluids, including plasma/serum, urine, semen, saliva, bronchial fluid, cerebral spinal fluid, milk, amniotic fluid, synovial fluid, peritoneal fluid, tears, lymph, bile [Nieuwland

et al. 2024, Singh et al. 2024, Tengler et al. 2024, Wang et al. 2024, Hadpech et al. 2024, Quiralte et al. 2024, Cross et al. 2023, Jonak et al. 2023, Hendrix et al. 2023, Kalluri & LeBleu, 2020]. sEV carry various bioactive molecules (proteins, lipids, nucleic acids), playing an important role in cell-to-cell communication under physiological and pathological conditions including the immune response, inflammation, and tumorigenesis. The molecular and genetic cargo of sEV reflects the content of their parent cells [Singh et al. 2024, Kalluri et al. 2020, Witwer et al. 2019]. Through their complex cargo, sEV can alter the phenotypes and functions of recipient cells [Singh et al. 2024, Hendrix et al. 2023, Pegtel et al. 2019]. All the above factors, combined with the presence of sEV in all body fluids, have directed researchers' attention to sEV as a promising component of "a liquid biopsy" with potential clinical importance as a biomarker.

1.5.2. sEV uptake and cargo delivery.

The uptake of sEV by recipient cells is a complex and multifaceted process influenced by factors such as vesicle surface composition (proteins, lipids, glycans), and the cellular environment (pH, extracellular matrix). This process involves several steps: targeting, internalization, and intracellular trafficking. The initial targeting of sEV to recipient cells can be either specific, dictated by receptor-ligand interactions, or nonspecific, relying on general endocytic pathways. The preferential uptake of sEV by a specific cell type is exemplified by several observations. Oligodendrocyte-derived sEV are preferentially internalized by microglia, whereas neuron-derived sEV selectively target other neurons [Chivet et al. 2014, Fitzner et al. 2011]. Melanoma-derived sEV were mainly taken up by the lungs and spleen [Takahashi et al. 2013]. Hoshino et al. observed organ specificity of sEV biodistribution: sEV from breast cancer cells were more efficiently uptaken in lung, whereas those released by pancreatic cancer cells were uptaken predominantly in the liver [Hoshino et al. 2015]. In contrast, some cells, such as HeLa cells, can indiscriminately uptake EVs from diverse sources, suggesting a more generalized internalization process [Costa Verdera et al. 2017].

The interactions of sEV with recipient cells can occur through various mechanisms, including ligand-to-receptor binding, macropinocytosis, and endocytosis. Several surface molecules, such as integrins, tetraspanins, T cell immunoglobulin, lectins, and

proteoglycans are implicated in receptor-mediated sEV uptake. However, it should be noted that no single receptor has been definitively identified as essential for this process [Sabatke et al. 2024, Mathieu et al. 2019, Yáñez-Mó et al. 2015].

Once bound to the recipient cell, sEV are internalized through multiple endocytic pathways, including clathrin-dependent and clathrin-independent mechanisms. Clathrin-mediated endocytosis enables the specific uptake of sEV via interactions with cell surface receptors. Caveolin-dependent endocytosis, a form of clathrin-independent uptake, seems to have a variable, experimental condition-dependent influence on sEV internalization [Horibe et al. 2018, Costa Verdera et al. 2017]. Macropinocytosis, a non-specific bulk uptake mechanism, is compatible with the internalization of small extracellular vesicles but not with larger EV aggregates.

The major route of sEV uptake is endosomal processing [Liu et al. 2023, Mathieu et al. 2019]. Once internalized, sEV enter the endosomal system where they can be sorted for degradation, recycling, or cargo release [O'Brien et al. 2022, Han et al. 2022, Kalluri et al. 2020, Hessvik et al. 2018]. A significant proportion of sEV are directed toward lysosomes for degradation, preventing excessive accumulation within the cell. Alternatively, sEV can be recycled and released back into the extracellular space [Sabatke et al. 2024, O'Brien et al. 2022, Zhang et al. 2019, Pegtel et al. 2019]. However, the primary function of EVs lies in their ability to transfer enclosed cargo to recipient cells. The cargo release typically occurs within endosomes, where membrane fusion facilitates the release of bioactive molecules into the cytosol. Acidic pH conditions in late endosomes may trigger EV-endosomal membrane fusion, akin to viral entry mechanisms. Lipid components such as cholesterol and phosphatidylserine may further modulate this process.

sEV serve as transporters of bioactive molecules. The composition and structure of sEV are inherently linked to the parental cell characteristics and its functional state. This causes structural and molecular diversity of sEV present in the body and determines their complex modulating effects on physiological and pathophysiological processes [Singh et al. 2024, Li et al. 2023, Witwer et al. 2019]. Structurally, sEV are enclosed by a lipid bilayer membrane essential for their stability and functional interactions with recipient cells. sEV lipidome is constituted to a large extent of membrane lipids, including glycerolipids, glycerophospholipids, sphingolipids, sterol

lipids, prenol lipids, and fatty acids [Lobasso et al. 2021, Kalluri & LeBleu, 2020, Zebrowska et al. 2019]. In comparison to their parent cells, sEV are enriched in sphingomyelins, cholesterol, glycosphingolipids, and phosphatidylserine, but contain lower levels of phosphatidylcholine and phosphatidylinositol. The lipid composition of sEV shows similarities with lipid rafts, making them more stable against detergents than microvesicles or lysosomes [Skotland et al. 2023, Donoso-Quezada et al. 2021, Skotland et al. 2019].

The protein content of sEV is diverse and includes molecules common to all sEV and proteins specific to parental cells. The common markers of sEV are membrane-associated tetraspanins (CD9, CD63, CD81, and CD82), which are involved in processes such as membrane fusion, cellular penetration, and cell signaling. Other groups of sEV markers are proteins involved in sEV formation, such as ESCRT complexes, Alix, TSG101, and Rab GTPases (e.g. Rab2, Rab7, Rab10, Rab27B, Rab33B), which play key roles in the sorting and trafficking of cargo within the vesicles. sEV also carry heat shock proteins (HSPs) such as chaperone proteins from the multigene families HSP70 and HSP90, which are involved in protein folding and cellular stress responses, as well as cytoskeletal proteins (actin, tubulin, myosin) that provide structural integrity to the vesicles. Furthermore, sEV carry major histocompatibility molecules MHC-I and II, cytokines (e.g. IL-6, IL-10, TNF-α, TGF-β), adhesion molecules (e.g. integrins, CAMs), and immune-modulatory proteins (e.g. FasL, TRAIL, PD-L1) which contribute to immune modulation, tumor progression, and cell-to-cell communication [Whiteside 2025, Welsh et al. 2024, Zebrowska et al. 2022, Whiteside et al 2021, Pietrowska et al. 2021, Kowal et al. 2016]. The above-mentioned set of proteins is supplemented with proteins specific to parental cells. An example is the presence of CD3 protein in sEV released by T lymphocytes [Theodoraki et al. 2018], glypican 1 (GPC1) in sEV produced by pancreatic cancer cells [Melo et al. 2015], or chondroitin sulfate proteoglycan 4 (CSPG4) in melanoma-derived sEV [Pietrowska et al. 2021, Sharma et al. 2020, Ferrone et al. 2020].

Apart from proteins and lipids, sEV carry nucleic acids such as mRNA, and non-coding RNAs (miRNAs, lncRNAs, circRNAs). The latter are involved in the regulation of gene expression in recipient cells, thus influencing cellular processes such as cell differentiation, metabolism, proliferation, or innate and adaptive immunity. Currently,

miRNAs have attracted growing attention in the research on sEV biology, since many publications reported differences in miRNA profile of sEV released by normal and malignant cells *in vitro* and *in vivo* [Li et al. 2023, Xie et al. 2022, Kalluri et al. 2020, Zebrowska et al. 2020]. Moreover, sEV cargo has been associated with different types of DNA, including mtDNA and gDNA, although this issue is still being investigated [Liu et al. 2022, Elzanowska et al. 2021]. sEV also contain metabolites (amino acids, sugars, alcohols, low-molecular-weight metabolites) that can modulate cellular metabolism in recipient cells [Bajaj et al. 2024, Ludwig et al. 2020, Zebrowska et al. 2019]. The structure of a small extracellular vesicle including the above-mentioned component groups is presented in Figure 2.

Overall, the molecular composition of sEV vary and depend on the molecular context of parental cells. Understanding the molecular diversity of sEV is crucial for research on the function of sEV in pathological processes. In this aspect it is worth noting that sEV released by tumor cells (tumor-derived sEV or TEX) exhibit distinct molecular profiles compared to those from non-malignant cells, reflecting their involvement in cancer progression and metastasis.

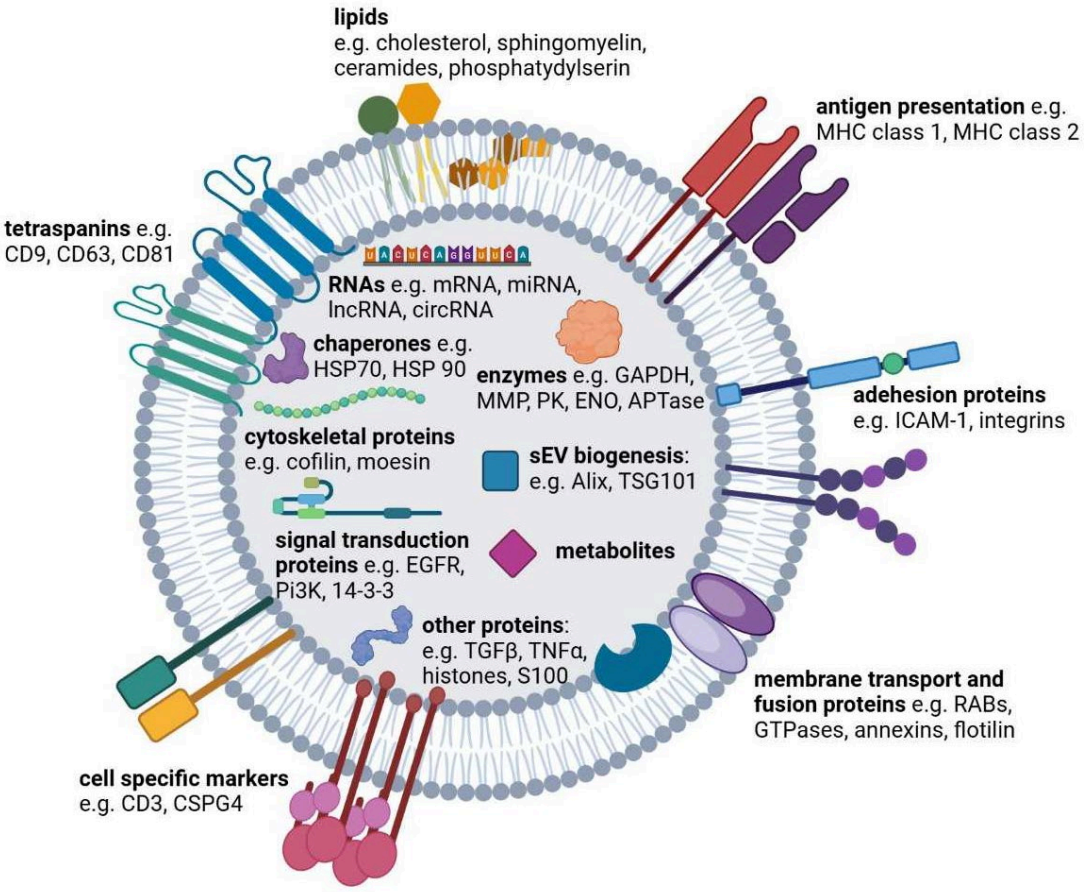

Figure 2. The structure of a small extracellular vesicle. *Created in https://BioRender.com.*

1.5.3. The role of sEV in pathogenic conditions.

According to the current state of knowledge sEV are implicated in a wide range of pathological conditions, including neurodegenerative diseases, liver disorders, cardiovascular diseases, and cancer. In this doctoral dissertation, I focus on the role of sEV in cancer. Tumor-derived extracellular vesicles (TEX) play a pivotal role in cancer biology by reshaping the tumor microenvironment (TME), driving cancer immune escape, promoting angiogenesis, inducing epithelial-mesenchymal transition (EMT), and driving metastasis. Their involvement in therapy resistance highlights their potential utility as therapeutic targets and biomarkers for cancer progression [Whiteside 2024, Zebrowska et al. 2020, Tung et al. 2019, Mashouri et al. 2019, Whiteside 2016].

TEX contribute to the TME remodeling by influencing the phenotype and functions of fibroblasts, endothelial cells, and infiltrating immune cells. The molecular cargo of TEX, which reflects the originating tumor cell, dictates the extent and nature of these

alterations. Under stress conditions such as hypoxia, nutrient deprivation, and acidosis, cancer cells enhance the release of TEX, leading to widespread TME reorganization. TEX stimulate extracellular receptor signaling and disrupt cell adhesion, facilitating tumor expansion and metastatic dissemination. The key molecules underlying these effects are integrins and their ligands within TEX, which are instrumental in the establishment of a pre-metastatic niche. For instance, exosomal integrins contribute to cancer cell colonization by promoting adhesion to specific distant organs, laying the groundwork for subsequent metastasis [Paolillo et al. 2017, Hoshino et al. 2015]. Colorectal cancer-derived TEX enriched with miR-25-3p modulate endothelial cell function by repressing key regulators such as KLF2 and KLF4, thereby enhancing vascular leakiness in pre-metastatic sites such as the liver and lungs [Zeng et al. 2018]. Moreover, TEX can reprogram fibroblasts into CAFs (cancer-associated fibroblasts), which in turn produce an array of pro-tumorigenic factors. For example, pancreatic CAFs exposed to gemcitabine upregulate Snail and miR-146a while increasing sEV release, which enhances epithelial proliferation. Additionally, CAF-derived sEV provide metabolic support to tumor cells by promoting glycolysis and diverting mitochondrial oxidative phosphorylation. This metabolic adaptation enables tumor cells to sustain growth even under hypoxic and nutrient-limited conditions [Zhang et al. 2018, Richards et al. 2017, Zhao et al. 2016].

Angiogenesis is a vital process for tumor progression, allowing for increased nutrient and oxygen supply. TEX from various cancer cells (glioblastoma, gastric, pancreatic and bladder, ovarian and breast cancer) are instrumental in promoting angiogenesis through delivering numerous pro-angiogenic factors, including proteins (VEGF, FGF, PDGF, TGF-β, glypican-1 and IL-8) and regulatory RNAs (miR-221, miR-1247-3p, miR-30b-5), to endothelial cells thus promoting proliferation and vessel formation [Liu et al. 2024, Chen et al. 2022, Liu et al. 2022, Qiu et al. 2022, Monteforte et al. 2017].

TEX facilitate epithelial-mesenchymal transition by delivering key signaling molecules such as TGF-β, HIF1α, β-catenin, and miRNAs. TEX promote downregulation of epithelial markers (e.g. E-cadherin) and upregulation of mesenchymal markers (e.g. N-cadherin, vimentin, and Snail) which are hallmarks of EMT. TEX carrying miR-301a-3p from pancreatic cancer cells induce macrophage polarization toward the M2

phenotype, further accelerating EMT [Mashouri et al. 2019, Whiteside 2017, Jeppesen et al. 2014].

TEX mediate a dialog between immune cells and cancer cells. The TEX-mediated modulation of the immune system mainly involves inhibition of antitumor immune response and promotion of immune evasion. TEX achieve this through direct interaction with immune cells, suppression of immune signaling pathways, and induction of apoptosis in key effector cells.

One of the primary mechanisms by which TEX interact with immune cells is through ligand-receptor recognition. TEX carry ligands that bind to specific receptors on lymphocytes, triggering inhibitory signaling pathways. Additionally, MHC molecules on TEX can bind to cellular MHC receptors, influencing antigen presentation and immune recognition. While professional antigen-presenting cells (APCs) such as macrophages and dendritic cells (DCs) readily internalize TEX, T cells primarily receive extracellular signals from these sEV, leading to sustained intracellular signaling changes. This interaction alters gene expression in recipient immune cells, skewing their function towards immunosuppression [Cao et al. 2023, Mu et al. 2017, Hiltbrunner et al. 2016].

Inhibition of T cell activation and proliferation is a key immunosuppressive function of TEX, which negatively regulate the T cell receptor (TCR) and interleukin-2 receptor (IL-2R) signaling pathways, impairing the activation of CD8+ cytotoxic T cells. TEX-mediated suppression of the JAK/STAT signaling pathway further prevents T cell proliferation and cytokine production. TEX also reprogram T cells by activating NF-κB and STAT3 signaling, which shifts T helper (Th) cells towards an immunosuppressive Th2 phenotype. This cytokine imbalance weakens the antitumor response, allowing cancer cells to evade immune surveillance [Bretz et al. 2013, Wieckowski et al. 2009, Calyton et al. 2007].

Beyond inhibition, TEX actively induce apoptosis in activated CD8+ effector T cells. Many circulating CD8+ T cells in cancer patients express death receptors such as Fas (CD95) and programmed cell death receptor 1 (PD-1), making them susceptible to apoptosis upon interaction with TEX carrying Fas ligand (FasL) or programmed cell death ligand 1 (PD-L1). Additionally, TEX-mediated downregulation of the PI3K/AKT survival pathway and upregulation of proapoptotic proteins such as Bax further drive

apoptosis in cytotoxic T cells [Whiteside 2023, Ludwig et al. 2022, Czystowska et al. 2011].

TEX also exert immunosuppressive effects on natural killer (NK) cells, which are essential for innate immune surveillance against tumors. TEX downregulate NK-activating receptors such as NKG2D, NKp30, and NKp46, reducing NK cell cytotoxicity. This suppression is mediated by TEX carrying TGF-β, which directly inhibits NK cell activation. In acute myeloid leukemia (AML) patients, TEX carrying MICA and MICB ligands further inhibit the function of NK cells [Hong et al. 2014, Mincheva-Nilsson et al. 2013, Szczepanski et al. 2011]. The role of TEX in establishing an immunosuppressive TME that promotes tumor progression is summarized in Figure 3.

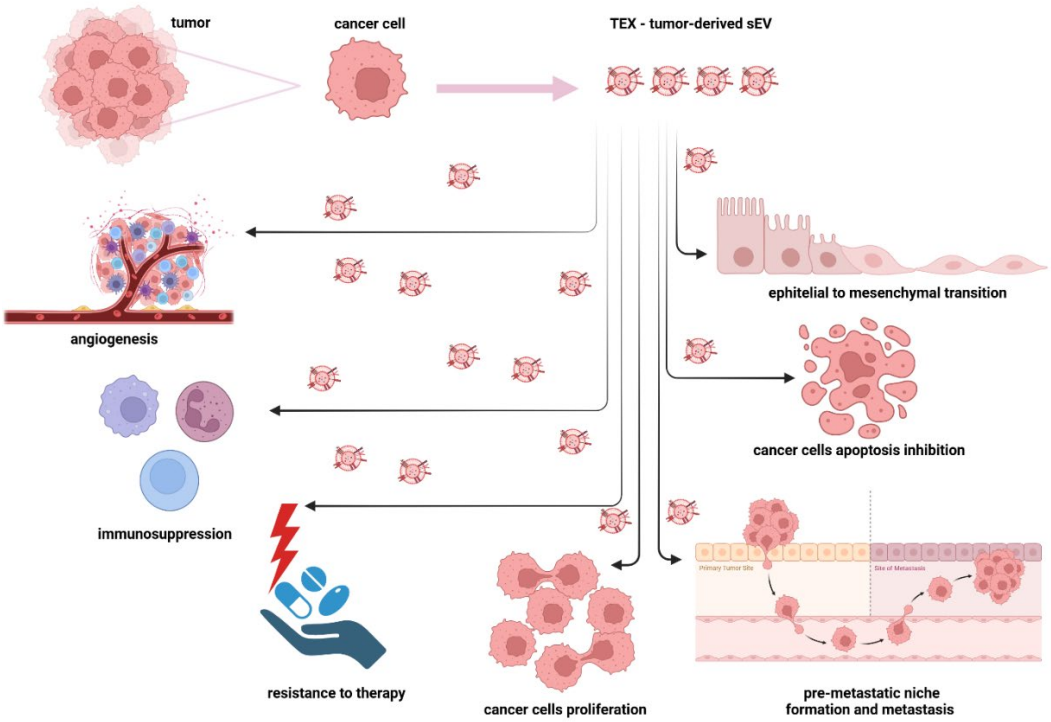

Figure 3. Immunesupresive impact of sEV in tumour microenviroment. *Created in https://BioRender.com.*

1.5.4. Heterogeneity of sEV in plasma and serum.

The blood contains a heterogeneous mixture of sEV produced by all cells and tissues (Fig. 4). In patients with cancer, blood contains also a subpopulation of sEV produced by tumor cells [Sharma et al. 2018, Kalluri et al. 2016] termed tumor-derived small extracellular vesicles (TEX).

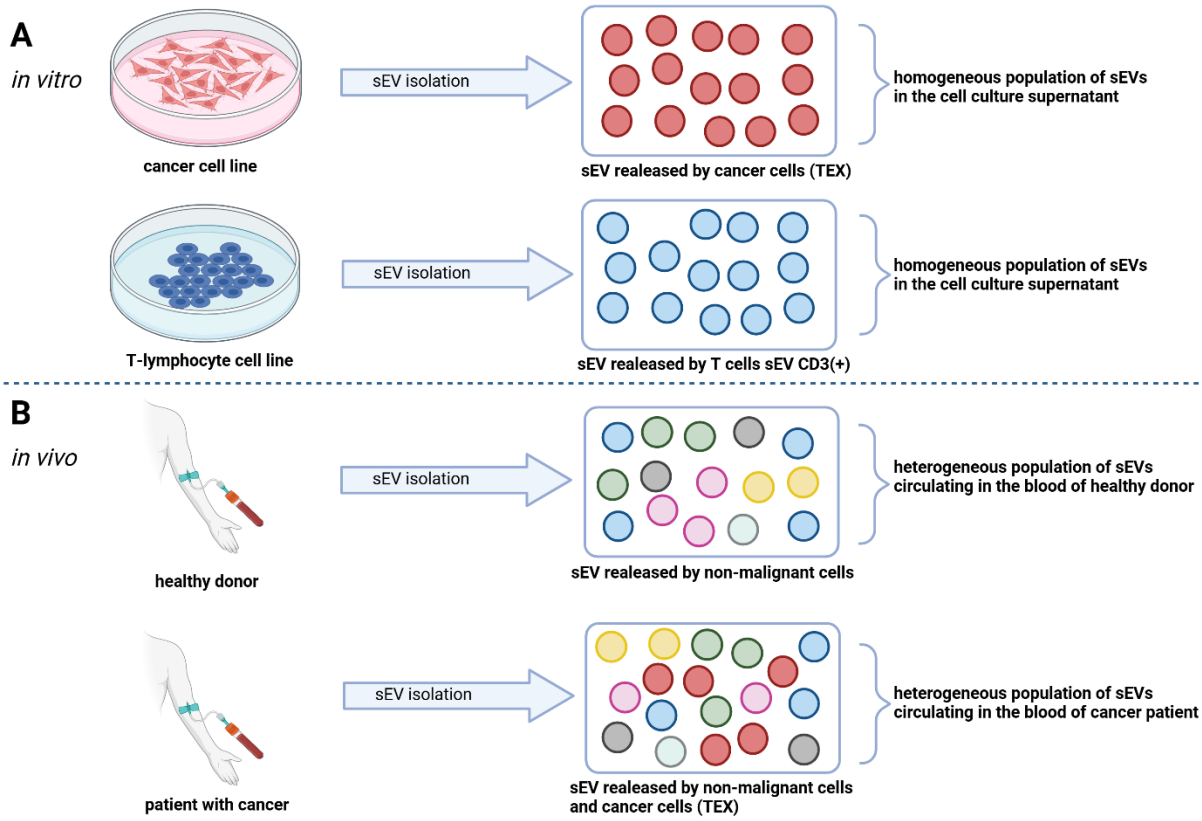

Figure 4. Populations of small extracellular vesicles present in material collected in *in vitro* and *in vivo* studies: A – homogeneous population of sEV present in cell culture supernatants, B – heterogeneous population of sEV present in human blood. *Created in https://BioRender.com.*

The largest group in the heterogeneous population of sEV circulating in the blood are sEV of lymphoid origin. They account for 38-54% of all sEV isolated from serum or plasma. Such a high representation of this subpopulation is due to the large number of lymphocytes in the blood, particularly T cells [Theodoraki et al. 2018]. Some sources report that sEV produced by platelets can account for up to 50% of all sEV circulating in the blood, suggesting that sEV of other origin are less represented [Tao et al. 2017]. Current studies show that these parameters may change in cancer patients. In the plasma of healthy individuals, the concentration of circulating sEV is estimated to be between 10^8 and 10^9 per milliliter. However, in cancer patients, TEX are present at significantly higher levels, with a total number of sEV ranging from 10^{10} to 10^{12} per milliliter of plasma. In cases of malignant melanoma, TEX constitute approximately 20% to 80% of the total plasma sEV population. Additionally, as melanoma advances, the proportion of TEX relative to non-tumor-derived sEV (NTEX) increases, indicating a

possible correlation between disease progression and TEX abundance [Sharma et al. 2020]. Higher number of sEV in blood of cancer patients was also confirmed for prostate cancer, breast cancer, pancreatic adenocarcinoma, hepatocellular carcinoma and ovarian cancer [Meng et al. 2018, Fang et al. 2017, Arbelaiz et al. 2017, Meng et al. 2016, Turay et al. 2016].

Thus, the plasma/serum of cancer patients contains a diverse mix of sEV from various cells and with different molecular cargo unlike sEV isolated from the medium from cells cultured *in vitro* in a monoculture, where all sEV have the same origin (Fig. 5A).

1.5.5. Methods of sEV isolation.

Current methods of sEV isolation are based on physicochemical properties of sEV and/or the presence of membrane receptors. Among the most commonly used methods are ultrafiltration, ultracentrifugation, size exclusion chromatography (SEC), methods based on extrusion, microfluidics and immunoprecipitation [Welsh et al. 2024, Singh et al 2024, Ludwig et al. 2019].

Techniques based on ultracentrifugation are among the most widely used for sEV isolation. They are density-, size- and shape-based sequential separations of particulate constituents and solutes, consisting of several centrifugation steps aiming to remove cells and debris, followed by collection of sEV. The technique has several disadvantages, especially for isolation of sEV from body fluids. Among the most important ones are: co-isolation of impurities (for example plasma proteins), low reproducibility, the potential damage of sEV and low sample throughput, that do not meet the requirements for a clinically useful protocol [Kurian et al. 2021, An et al 2018].

Ultrafiltration is based on size differences between sEV and other particulates. It uses porous membranes (or centrifugal filters) with different membrane types and pore sizes to trap particles of specific sizes. It is usually used in a combination with ultracentrifugation or size exclusion chromatography, to concentrate sEV on the porous membrane [Ansari et al. 2024, Mondal et al. 2021].

Size exclusion chromatography separates molecules according to their size by filtration through a column packed with a porous gel (e.g. Sepharose), which consists

of spherical beads containing pores with a specific size distribution. It allows for precise separation of large and small molecules removing a considerable (but not all) amount of impurities (plasma or cell culture medium components) without affecting sEV structure by shearing force [Zhang et al. 2019, Ludwig et al. 2019, Xu et al. 2016]. SEC is regarded as one of the most efficient methods to retain high concentrations of biologically active sEV from plasma specimens [Jablonska et al. 2019, Hong et al. 2016].

Another technique is precipitation using PEG 8000 polymers which bind water molecules causing precipitation of less soluble components in the sample, including sEV. The technique is simple and fast, but its disadvantage is co-isolation of other sample components and formation of sEV aggregates [Kurian et al. 2021].

Microfluidics technology allows for sEV separation due to the action of ultrasound, which separates sample components by their size and density using channels with dimensions of micrometers and capillary forces. The advantage of this method is the speed of isolation and the ability to reduce the sample volume, but it requires the use of complex equipment and is extremely expensive to implement [Lin et al. 2020].

The immunoprecipitation techniques are based on sEV fishing utilizing specific interactions between membrane-bound antigens (receptors) of sEV and immobilized antibodies (ligands). This technique enables selective isolation of a highly purified specific sEV subpopulation. The challenging requirement for this technique is a prior knowledge of specific membrane proteins for a given type of sEV. So far, this technique has been shown effective only for a few types of sEV fractionated according to their cellular origin [Skoczylas et al. 2024, Pietrowska et al. 2021, Mondal et al. 2021, Ferrone et al. 2020].

1.5.6. The role of sEV in melanoma.

It has become clear that melanoma-derived sEV (MTEX) facilitate cancer progression by promoting immune evasion, melanoma tumor growth and metastasis. MTEX participate in reprogramming immune cells, remodeling the tumor microenvironment (TME), and enhancing its metastatic potential [Wilczak et al. 2025, Gyukity-Sebestyén et al. 2019, Bland et al. 2018, Zhou et al. 2018, Wang et al. 2017]. A comprehensive understanding of their pleiotropic functions is essential for improving

melanoma diagnosis, treatment, and prognosis. The multi-level involvement of MTEX in melanoma growth is schematically depicted in Figure 5.

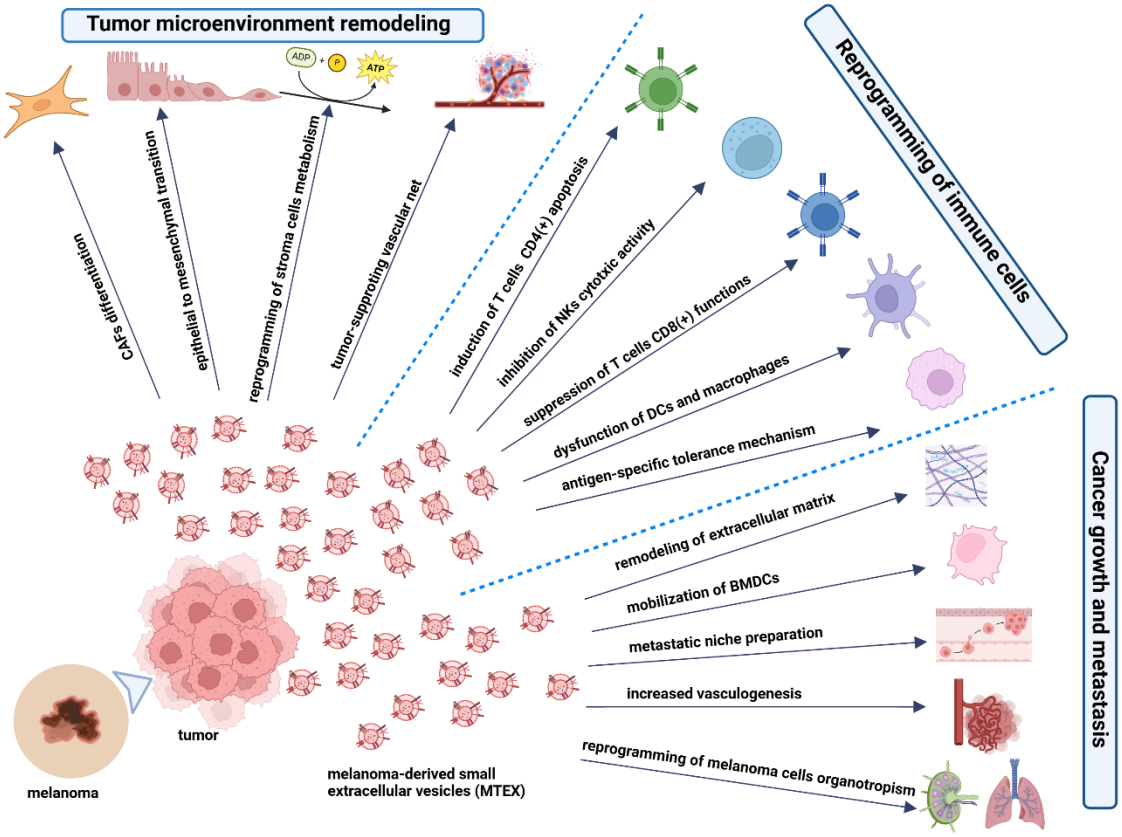

Figure 5. The multi-level contribution of MTEX to melanoma biology *Created in https://BioRender.com.*

Immune evasion is a fundamental requirement for melanoma progression, and MTEX have been identified as key mediators in this process. MTEX promote immunsuppression through antigen-specific mechanisms, including the transfer of MHC class I receptor proteins to antigen-presenting cells (APCs). Concurrently, co-stimulatory molecules such as CD86 and CD40 are downregulated, while the immunosuppressive cytokine IL-6 is upregulated [Düchler et al. 2019]. MTEX also deliver TGF-β, further contributing to immunosuppressive tolerance. MTEX-mediated immunosuppression extends to T cell function by increasing programmed cell death ligand 1 (PD-L1) expression, which interacts with PD-1 receptors on CD8+ T cells, leading to their functional inhibition. Furthermore, MTEX contain Fas ligand (FasL) and APO2 ligand (APO2L)/TRAIL, which induce apoptosis in T cells [Martínez-Lorenzo et al. 2004]. Another immunosuppressive mechanism involves upregulation of PTPN11, a protein that negatively regulates interferon and T cell receptor (TCR) signaling

pathways [Wu et al. 2017]. Additionally, MTEX influence cytokine signaling, reducing IL-12 receptor expression on CD8+ T cells and blocking T cell responses to IL-12 via WISP1-mediated inhibition [Wu et al. 2017, Kulkarni et al. 2012].

MTEX also alter T cell metabolic function by disrupting mitochondrial respiration and activating the Notch signaling pathway, further promoting immune evasion. They modulate TCR and IL-2 receptor signaling, inhibiting CD8+ T cell activation and inducing apoptosis. Moreover, MTEX promote the conversion of CD4+ T cells into regulatory T cells (Tregs), enhancing their suppressive function and dampening anti-tumor immunity [Raimondo et al. 2020, Wieckowski et al. 2009]. Their miRNA cargo, including miR-3187-3p, miR-498, and miR-122, suppresses TCR signaling and tumor necrosis factor-alpha (TNF-α) secretion, contributing to immune escape [Vignard et al. 2020].

The immunosuppressive effects of MTEX are further mediated by miR-21, which inhibits TNF-α and enhances IL-10 expression, leading to macrophage polarization towards an anti-inflammatory phenotype. Additionally, miR-21 acts as a ligand for Toll-like receptor (TLR) signaling, promoting pro-metastatic inflammatory responses. MTEX also interfere with dendritic cells (DC) function by engaging TLR2 receptors, leading to DC dysfunction and suppression of antigen presentation [Tang et al. 2015, Fabbri et al. 2012, Yang et al. 2011].

The tumor microenvironment (TME) plays a pivotal role in melanoma progression, and MTEX actively contribute to its remodeling. They facilitate epithelial-to-mesenchymal transition (EMT), a key process in metastasis, by activating the mitogen-activated protein kinase (MAPK) signaling pathway and modulating EMT-associated transcription factors such as ZEB2 and Snail 2 [Gyukity-Sebestyén et al. 2019, Caramel et al. 2013]. This results in decreased E-cadherin expression and increased vimentin levels, fostering a mesenchymal phenotype conducive to metastasis [Xiao et al. 2016]. MTEX interact with myeloid-derived stem cells (MSCs), inducing a tumor-promoting phenotype characterized by PD-1 and mTOR overexpression. Through gene expression modifications, MTEX influence multiple oncogenic pathways, including MET, Ras, RAF1, PI3K/Akt, and JAK/STAT3, further promoting tumor growth [Gyukity-Sebestyén et al. 2019].

A significant function of MTEX is their ability to transform fibroblasts into cancer-associated fibroblasts (CAFs), which support tumor progression by enhancing

angiogenesis [Hu et al. 2019, Zhao et al. 2015]. The MTEX cargo, particularly miR-155, drives this transformation by activating the JAK2/STAT3 pathway, leading to increased secretion of vascular endothelial growth factor A (VEGFa), fibroblast growth factor 2 (FGF2), and matrix metalloproteinase 9 (MMP9). Additionally, MTEX-mediated metabolic reprogramming of fibroblasts results in enhanced glycolysis and reduced oxidative phosphorylation, creating an acidic microenvironment that favors immune suppression and metastatic potential [Zhou et al. 2018, Shu et al. 2018, Zhao et al. 2015].

MTEX also contribute to tumor angiogenesis by transferring pro-angiogenic cytokines such as IL-1α, FGF, TNF-α, and VEGF. The transfer of miR-9 from melanoma cells to endothelial cells activates the JAK-STAT pathway, promoting endothelial cell migration and vascular network formation. Furthermore, WNT5A signaling in melanoma cells induces MTEX release enriched with VEGF and MMP2, further stimulating angiogenesis [Ekström et al. 2014, Zhuang et al. 2012].

MTEX directly influence melanoma cell proliferation and survival. Studies have demonstrated that MTEX enhance melanoma cell growth *in vitro* and *in vivo* by increasing cyclin D1 and phosphorylated Akt (p-Akt) levels while reducing apoptosis-related proteins such as Bax. Additionally, the oncoprotein MET which is enriched in MTEX, enhances tumorigenic potential and preconditions the bone marrow (BM) for metastasis by mobilizing bone marrow-derived cells (BMDCs) that support tumor invasion and vasculogenesis [Matsumoto et al. 2017, Peinado et al. 2016].

The metastatic potential of melanoma is significantly influenced by MTEX. They prepare the pre-metastatic niche by upregulating genes associated with extracellular matrix remodeling (Mapk14, uPA, laminin 5), vascular growth (VEGFB, HIF-1α, TNF-α), and immune evasion (S100A8, S100A9) [Peinado et al. 2016, Hood et al. 2011]. MTEX also promote osteotropism in melanoma cells through CXCR7 upregulation, facilitating bone metastasis [Hood et al. 2011].

1.6. Mass spectrometry-based proteomics.

Mass spectrometry (MS) is an analytical technique used to determine the molecular composition of a sample by measuring the mass-to-charge ratio (m/z) of ionized sample constituents. The analysis consists of three main steps: (i) transformation of

analytes into ions in the gas phase (e.g. by electrospray - ESI or electron impact ionization - EI); (ii) separation of ions according to m/z ratio in an analyzer (e.g. Orbitrap or time-of-flight, TOF); (iii) generation of an electrical signal proportional to the number of ions that can be recorded by a detector.

Because of the limited ability to ionize and measure the mass of molecules larger than peptides, in the case of mass spectrometry-based proteomic studies identification and analysis of proteins is usually accomplished via peptide analysis, which is referred to in the literature as the bottom-up strategy [Kraj et al. 2018, Ma 2010, Glish et al. 2003]. Analyzed peptides are obtained by proteolytic digestion of proteins present in a sample most often using specific enzymes thus enabling digestion of proteins in well-defined sites. A commonly used proteolytic enzyme is trypsin, which digest proteins into peptides with arginine (R) or lysine (K) at the C-terminus. Due to the presence of R and K amino acid residues at the C-terminus, thus obtained highly basic tryptic peptides are easily ionized. In addition, the resulting peptides consist of a few up to dozens of amino acids, resulting in a spectrum with a manageable range of m/z values. Application of a tandem mass spectrometer (i.e. containing at least two mass analyzers) enables to isolate a selected peptide ion with a specific m/z value (so called parent ion) in the first analyzer, and to perform its controllable fragmentation using a selected ion activation method, e.g. collision induced dissociation, CID. Thus obtained fragment (daughter) ions are subsequently analyzed in the second analyzer. The resulting MS/MS spectrum contains information on amino acid sequence of the fragmented peptide ion. For CID activation method, argon is usually used as an inert and low-energy gas, in the range of a few to 100 eV, resulting in dissociation of peptide bonds, thus enabling observation of b and y peptide ion series (containing the N-terminus and C-terminus of a peptide, respectively). Identification of the peptide sequence can be carried out by de novo sequencing or by matching the obtained MS/MS spectrum with theoretical MS/MS spectra contained in protein sequence databases using mass spectral analysis software (e.g. Mascot, Sequest, Peaks, Tandem), to find the greatest degree of similarity [Noor et al. 2021, Glish et al. 2003]. The bottom-up approach is still the most popular analytical solution used for large-scale protein analysis in a short time with satisfactory reproducibility. An alternative method to the bottom-up strategy is the top-down approach, in which mass

spectrometry is used to analyze intact proteins. Such direct analysis of structurally complete proteins offers the opportunity to answer questions that cannot be solved by the analysis of fragmented proteins. The greatest advantages of this technique is the ability to distinguish the individual proteoforms present in a sample to find information on post-translational modifications, and increase the sequence coverage of the proteins analyzed. Moreover, the use of the top-down approach eliminates the biggest limitation of bottom-up methods, that is, the correct assignment of the peptides that repeat in many proteins. The issue of highly homologous peptide occurrence in the structure of several different proteins is partially resolved in bottom-up analyses by assigning identified peptides not to an individual protein but to the entire protein group/family bearing similar amino acid sequences. Such an action reduces the risk of a wrong assignment of a peptide, and consequent errors in protein identification, but at the same time it does not provide information on the exact identity of the proteins present in the sample [Kraj et al. 2018, Ma 2010, El-Aneed et al. 2009].

1.6.1. Protein identification techniques in mass spectrometry.

Proteomics is a scientific discipline that emerged from genomics, building on the successful sequencing and mapping of various genomes, including the human genome. While genomics focuses on analyzing DNA, proteomics is dedicated to the study of the proteome e.g the complete set of proteins along with their post-translational modifications (PTMs) at a certain point of time. Unlike the genome, which remains relatively stable, the proteome is highly dynamic and changes depending on a cell type, developmental stage, environmental conditions, and signaling events. The complexity of proteomics far surpasses that of genomics, as an organism can have multiple proteomes due to influence of various biological and physiological states. Proteome research involves identifying proteins, determining their cellular localization, analyzing their interactions, and understanding their functions. Since proteins are the primary effectors of cellular processes and most diseases manifest themselves through changes in protein expression, structure, activity, or modifications, proteomics plays a key role in biomedical research. Proteomic studies provide critical insights into disease mechanisms by linking specific proteins and their modifications to pathological conditions. This knowledge accelerates the discovery of biomarkers for early diagnosis,

monitoring of treatment outcome, and prognosis, and the development of targeted therapeutics [Al-Amrani et al. 2021, Kraj et al. 2018]. Taking into account the enormous complexity of proteomes, the use of mass spectrometry for the analysis of non-volatile, high-molecular-weight organic compounds such as proteins and peptides has revolutionized proteomics.

Currently, proteomics distinguishes between several strategies for identifying proteins which can be divided e.g. by the type of an analyte: a mixture of peptides (bottom-up approach), an intact protein (top-down approach) addressed above, or by the goal of the study – whether it is carried out to analyze the entire proteome (non-targeted proteomics) or selected components of it (targeted proteomics) [Kraj et al. 2018, El-Aneed et al. 2021]. Moreover, the use of tandem mass spectrometers has made it possible to analyze more complex mixtures of peptides, but the method efficiency is highly dependent on the initial separation of a sample, which has been largely solved by combining high-performance liquid chromatographs with modern high-resolution mass spectrometers. Hyphenating the two methods and operating them in a continuous mode, however, besides the obvious advantages, generates significant limitations. After acquitition of an MS spectrum containing signals for multiple peptides present in an LC fraction reaching the spectrometer at a given time point, precursors are selected that further undergo fragmentation resulting in recording spectra of daughter ions characteristic for fragmented peptides. However, in the case of a continuous operation, the constant influx of analytes, the composition of which changes over time, makes it necessary to constantly monitor the spectra of precursor ions while simultaneously recording the fragmentation spectra of all selected precursors, which is challenging due to technical limitations. Due to the way of data collection and switching between modes of measurement of precursor and fragment spectra, bottom-up methods can be divided into those conducted in data dependent acquisition (DDA) and data independent acquisition (DIA) modes [Büyükköroğlu et al. 2018, Ma 2010].

Shotgun proteomics is a classic example of an approach characteristic of untargeted bottom-up proteomic methods and is currently the most widely used technique for identifying proteins in complex mixtures. The advantage of shotgun analysis is that it can identify thousands of proteins and their quantitative measurement in a series of

biological samples. It is commonly used to search for potential disease biomarker candidates, whose significantly elevated or reduced levels differentiate a given pathological condition. In the classic shotgun approach, an enzymatically digested protein sample is analyzed by liquid chromatography coupled to tandem mass spectrometry (LC-MS/MS) operated in DDA mode. Ion analysis in data-dependent acquisition mode consists of two steps. First, the spectrometer registers a full spectrum of parent ions (the so-called survey scan) in a pre-selected mass range and selects a few of the most intense precursor signals (e.g. top 10). In the second stage, these ions are isolated and directed to a collision chamber, where they are fragmented. This process produces series of fragment ions, which are recorded as MS/MS spectra (the so-called data-dependent scan) and which are then used along with the MS spectra to identify peptides. This method is very popular, but requires the use of very fast tandem mass spectrometers that allow continuous switching from the scan mode to the fragmentation mode. However, even the fastest instruments cannot record all parent ions in the scan mode and their fragment ions in MS/MS spectra, therefore some information on peptides with lower signal intensities may be lost in the DDA mode [Noor et al. 2021, El-Aneed et al. 2009].

DIA methods eliminate the problem of random selection of precursors thus increasing the repeatability and reproducibility of the obtained results. On the other hand, the lack of selection of ions for fragmentation means that a single MS/MS spectrum often contains fragment ions derived from several peptides. The limitation of the DIA method lies in high level of complexity of the obtained spectra, for the interpretation of which it is necessary to have a library of spectra built on the basis of prior DDA analyses of a specific sample. Obtaining of a spectral library is a time-consuming and labor-intensive process, moreover requiring an additional amount of sample [Pino et al. 2020].

The second analysis strategy, i.e. targeted proteomics, is used to detect and quantify a previously established set of proteins, testing specific hypotheses. It is characterized by high sensitivity, accuracy of quantitative measurements and reproducibility of analyses. It has been used as a reliable method for verification and validation of potential candidates for disease biomarkers determined in body fluids, tissues or cancer cells, selected during global, untargeted analysis. A commonly used

method in targeted proteomics is Multiple Reaction Monitoring (MRM), also known as Selected Reaction Monitoring (SRM), and Parallel Reaction Monitoring (PRM) [Doerr 2011].

1.6.2. Proteome of small extracellular vesicles in melanoma.

Recent research has increasingly focused on the proteomic characterization of small extracellular vesicles derived from cancer cells. However, studies specifically investigating the proteome of melanoma-derived tumor extracellular vesicles (MTEX) remain limited. The majority of available data have been obtained *in vitro* experiments utilizing MTEX isolated from the supernatants of various melanoma cell lines. Different proteomic methodologies have been employed in MTEX studies, with a majority relying on shotgun liquid chromatography-tandem mass spectrometry (LC-MS/MS) approaches, which involve protein digestion followed by high-resolution peptide analysis [Xiao et al. 2012, Lazar et al. 2015, Mushin-Sharafaldine et al. 2016]. Other studies have utilized LC-MS/MS to analyze proteins separated via one-dimensional (1D) or two-dimensional (2D) SDS-PAGE [Surman et al. 2019].

Mears et al. for the first time identified p120 catenin, syntaxin-binding proteins 1 and 2, septin 2 (Nedd5), ezrin, radixin, tryptophan/aspartic acid (WD) repeat-containing protein 1, and prostaglandin regulatory-like protein (PGRL) in MTEX [Mears et al. 2004]. Next, the proteome of MTEX released by A375 melanoma cells and melanocyte-derived EV was compared revealing different sets of proteins including annexin A1, HAPLN1, GRP78, endoplasmin precursor (gp 96), TUBA1B, PYGB), ferritin, heavy polypeptide 1 (MTEX-upregulated), annexin A2, syntenin-1, MFGE8, OXCT (MTEX-downregulated) [Xiao et al. 2012]. Analysis of MTEX proteins derived from nontumorigenic, tumorigenic, and metastatic human cell lines, showed distinct molecular profiles of proteins specific for MTEX isolated from metastatic cell lines: EGFR, PTK2/FAK1, EPHB2, SRC, LGALS1/LEG1, LGALS3/LEG3, NT5E/5NTD-CD73, NRAS, KIT, MCAM/MUC18, MET [Lazar et al. 2015]. On the other hand, the most abundant set of proteins in MTEX released by B16-F1 cells included: CD81, CD9, histones (H2A, H2B, H3.1, H4), heat shock proteins (HSPA5/GRP78, HSC71), syntetin-1 [Muhsin-Sharafaldin et al. 2016]. Another study reported changes in the proteome of MTEX released in acidic environment [Boussadia et al. 2018]. The proteins enriched in acidic

MTEX were the ones involved in melanoma metastasis (HRAS, GANAB, CFL2, HSP90B1, HSP90AB1, GSN, HSPA1L, NRAS, HSPA5, TIMP3, HYOU10).

Ex vivo studies involving small extracellular vesicles obtained from melanoma patient plasma or other biological fluids are relatively rare. Notably, sEV derived from melanoma cell lines represent a "pure" population of melanoma-derived small extracellular vesicles, whereas those isolated from biological fluids consist of a heterogeneous mixture originating from multiple cell types. The first comparative proteomic analysis of sEV isolated from plasma of melanoma patients was based on immunoaffinity techniques. Peinado et al. identified a specific “melanoma signature” comprising of TYRP2, VLA-4, HSP70, an HSP90 isoform, and MET in small extracellular vesicles from patients with advanced melanoma [Peinado et al. 2012]. Similarly, in another study, TYRP2 protein, along with MIA and S100B were increased in sEV from the plasma of stage IV melanoma patients in comparison to healthy individuals [Alegre et al. 2015]. There is also one proteomic study characterizing the proteome of plasma-derived and serum-derived sEV utilizing an LC-MS/MS approach [Lattmann et al. 2024]. It demonstrates different molecular profile between sEV from melanoma patients and healthy donors, but no clear distinctions between stage III and stage IV melanoma patients was found. Another proteomic analysis of sEV isolated from melanoma patients concentrated on tissue samples and lymphatic drainage fluid showing interesting results of a different experimental model in terms of understanding melanoma’s biology, however it was not related to the liquid biopsy concept. Despite all the advancements, our understanding of the melanoma-derived sEV proteome remains incomplete, and the heterogeneity of experimental models complicates direct comparisons across studies. A summary of data on *ex vivo* proteomic profiling of small extracellular vesicles are presented in Table 1.

Table 1. Review of proteomics profiling of sEV isolated form melanoma patients

Source of sEV	Method of sEV isolation and characterization	Proteomic approach	Major findings	Ref.
Serum and plasma of healthy controls, and melanoma patients stage III and stage IV	SEC/NTA, TEM	UHPLC-MS/MS	2896 sEV-associated proteins identified; plasma and serum sEV proteomes diverged healthy donors and melanoma patients, but no clear distinctions were revealed between stage III and stage IV melanoma patients; 348 proteins in plasma-derived sEV and 257 proteins in serum-derived sEV were upregulated in melanoma patients, with melanoma markers such as: MCAM, TNC, and TGFBI among them	Lattmann et al. 2024
Tumor tissues (in-transit metastases: lymph node metastases, bowel metastases, liver metastases) obtained from patients with stage III or IV metastatic malignant melanoma	UC/TEM, NTA, WB	nanoLC-MS/MS	Separation of subpopulations of sEV with different sizes and densities for 6 groups: large and small sEV, small low- and high-density sEV, large low- and high-density sEV; a total of 6870 proteins were identified and 742 proteins were differentially expressed among the sEV subpopulations; proteins identified in small low-density sEV were associated with "Endosome", "Plasma membrane" and "Extracellular exosome" GO terms, while proteomes of the large vesicles were more associated with "Mitochondria" and "Endoplasmic reticulum" terms; proteins enriched in individual EV subpopulations: ADAM10 and EHD4 in small LD EVs; the mitochondrial inner membrane protein mitofilin in large EVs and large LD EVs; GAPDH, fatty acid synthase and transitional endoplasmic reticulum ATPase in small EVs and small HD EVs	Crescitelli et al. 2020
Lymphatic exudate of patients with stage IIIA to 3C cutaneous melanoma obtained after lymphadenectomy	UC/TEM, NTA, WB	nanoLC-MS/MS	Proteome of lymph-derived EVs differentiated patients with no evidence of further nodal spread of cancer (LAN^{neg}) from patients with further nodal metastasis (LAN^{pos}); down-regulation of Rho GDP dissociation inhibitor signaling pathway (already known as a signature of highly metastatic breast cancer) and up-regulation of pathways associated with cell death, proliferation, and cancer-associated pathways were observed in EVs purified from LAN^{pos} patients; upregulated pathways associated with earlier stage of disease including actin signaling, cellular extravasation, integrin signaling, and VEGF pathways were observed for EVs from LAN^{neg} patients	Broggi et al. 2019
Lymphatic drainage and plasma of stage III melanoma patients obtained after lymphadenectomy	UC/TEM, NTA, WB	nanoLC-MS/MS	745 proteins significantly more abundant in lymphatic drainage (LD) than in plasma-derived EVs, including HSP90B, Annexin A1, S100 A4, NRAS, and Lactoferrin; significant enrichment in LD-derived EVs in pathways related to antigen presentation, endoplasmic reticulum-phagosome pathway, G2/M transition, and IL-12 family signaling; several RAS/RAF/MAPK-related pathways were enriched in LD-derived EVs from N3 melanoma patients compared with N1a patients	García-Silva et al. 2019
Tumor tissues from melanoma lymph node or skin metastases obtained from patients with stage III or IV metastatic malignant melanoma	UC/TEM, NTA, WB	nanoLC-MS/MS	Membrane proteome of EVs isolated from melanoma metastatic tissues from patients differs from surface proteome of EVs released by non-melanoma cell lines. Most importantly, melanoma tissue-derived EVs were highly enriched in mitochondrial membrane proteins (COX6c, SLC25A22, MT-CO2), HLA-DR (a plasma membrane protein) and Erlin2 (an endoplasmic reticulum membrane protein).	Jang et al. 2019

1.6.3. Melanoma-derived sEV as potential clinical biomarkers

Melanoma-derived small extracellular vesicles found in body fluids have emerged as promising candidates for prognostic biomarkers, offering a novel approach to liquid biopsy. Alegre et al. investigated established melanoma biomarkers, including MIA, S100B, and TYRP2, in small extracellular vesicles isolated from sera of stage IV melanoma patients, disease-free individuals (NED), and healthy donors (HD) [Alegre et al. 2016]. Their findings indicated significantly elevated levels of MIA and S100B in melanoma patients compared to NED and HD. Moreover, higher concentrations of MIA in sEV correlated with a shorter median survival (4 vs. 11 months, $p < 0.05$), suggesting a potential of the protein as a diagnostic and prognostic biomarker in serum sEV. Additionally, in another study MIA and GDF15 levels were significantly elevated in the secretome of uveal melanoma cells compared to non-malignant cells, reinforcing the findings of Alegre and co-workers [Angi et al. 2016]. MicroRNAs (miRNAs) in sEV have also been explored as potential classifiers of melanoma. Tenga et al. demonstrated that miR-532-5p and miR-106b in serum sEV could differentiate melanoma patients based on the metastatic status and disease stage [Tenga et al. 2018]. Furthermore, miR-17, miR-19a, miR-21, miR-126, and miR-149 were found at significantly higher levels in patients with metastatic sporadic melanoma than in familial melanoma cases or healthy controls [Pfeffer et al. 2015]. Conversely, miR-125b expression in sEV was notably lower in advanced melanoma patients compared to disease-free individuals and controls, though serum miR-125b levels did not show significant differences between groups [Alegre et al. 2014].

Moreover, there are emerging data suggesting an important role of small extracellular vesicles in understanding the mechanisms of therapy nonresponse and as biomarkers predicting therapy response and outcome. For example, elevated miR-497-5p level in circulating sEV during MAPKi-based therapy in metastatic melanoma patients with BRAFV600 mutations was significantly associated with improved progression-free survival (hazard ratio of 0.27) [Svedman et al. 2018]. Another study revealed that increased miR-497-5p levels correlated with prolonged post-recurrence survival in patients with resected metastatic disease [Segura et al. 2010]. Upregulation of miR-211-5p in melanoma patient-derived EV following vemurafenib and dabrafenib

treatment promoted melanoma cell survival, suggesting a role in resistance to BRAF inhibition. Transfection of miR-211 into low-expressing melanoma cells enhanced proliferation, while its inhibition reduced cell viability, highlighting its involvement in adaptive resistance mechanisms Lunavat et al. 2017].

Furthermore, positive correlation between sEV PD-L1 and IFN-γ levels, both *in vitro* and in metastatic melanoma patients was found [Chen et al. 2018]. Increased PD-L1 expression in response to IFN-γ resulted in functional suppression of CD8+ T cells, contributing to immune evasion and disease progression. Elevated sEV PD-L1 levels distinguished responders from non-responders to pembrolizumab, indicating its potential as an early biomarker of treatment response. A prospective clinical study by Cordonnier et al. further confirmed that sEV PD-L1 levels in melanoma patient plasma inversely correlated with therapeutic outcomes, supporting its role as a predictor of response to immune checkpoint inhibition [Cordonnier et al. 2020].

Literature data show a promising potential of small extracellular vesicles as melanoma biomarkers, although their clinical application is hindered by the challenge of isolating melanoma-specific vesicles from other sEV populations in circulation. Recent advances have introduced the use of anti-CSPG4 monoclonal antibodies for selective capture of melanoma-derived sEV, differentiating them from normal tissue-derived sEV [Ferrone et al. 2020, Mondal et al. 2021]. CSPG4+ MTEX isolated from melanoma patient plasma were found to be highly enriched in melanoma-associated antigens (MAAs) such as TYRP2, Melan-A, Gp100, and VLA4. Additionally, MTEX exhibited elevated levels of both immunostimulatory (CD40, CD40L, CD80, OX40, OX40L) and immunosuppressive (PD-L1, CD39, CD73, FasL, LAP-TGFβ, TRAIL, CTLA-4) molecules compared to sEV from healthy donors. Interestingly, NMTEX sEV also demonstrated immunomodulatory functions, with their ability to induce T cell apoptosis correlating with the disease stage [Sharma et al 2020, Sharma et al. 2018]. These findings provide a foundation for future development of MTEX-based biomarkers for melanoma detection, disease monitoring, and therapeutic response prediction.

2. THE OBJECTIVES OF THE DOCTORAL DISSERTATION

Despite meaningful advancements in melanoma therapy, including immunotherapy, tumor evasion from immune surveillance remains a critical challenge. Human malignancies establish an immunosuppressive microenvironment that impairs immune cell function while facilitating cancer progression. Among various mechanisms contributing to tumor-induced immune suppression, small extracellular vesicles (sEV) have emerged as key mediators. Tumor-derived small extracellular vesicles (TEX) present in body fluids of cancer patients may promote tumor growth and metastasis by transmitting immunosuppressive signals to immune cells, thereby disrupting anti-tumor immunity and potentially affecting therapeutic responses and clinical outcomes.

It is assumed that a better understanding of the role of melanoma-derived small extracellular vesicles (MTEX) in melanoma biology could be accomplished by defining their proteomic profile. This goal could be achieved by selectively separating MTEX from the broader pool of sEV present in the plasma of melanoma patients. Because the molecular content of MTEX mimics, at least in part, the content of their parent (tumor) cells, it could be assumed that it would provide a snapshot of the tumor microenvironment in real time, serving as an equivalent of a “liquid biopsy.” If so, MTEX can be considered a potential source of prognostic biomarkers in melanoma.

The first aim of this doctoral dissertation was to evaluate the potential prognostic significance of MTEX. In this respect, it is worth emphasizing that this study represents the first attempt to analyze the proteome of MTEX circulating in melanoma patients' plasma after their selective separation from all other sEV.

<u>The specific aims of this part of the work are as follows:</u>

1. Proteomic profiling of sEV isolated from plasma of melanoma patients after their fractionation, using immunocapture method and MTEX-specific antibodies (targeting the CSPG4 antigen), on (i) MTEX and ii) sEV released by non-malignant cells (NMTEX).
2. Searching for an MTEX proteomic signature associated with melanoma progression.

The immune competence of T cells in the tumor-bearing hosts is frequently compromised. It can be suspected that MTEX present in the body fluids of melanoma patients are responsible for delivering suppressive signals to immune cells and interfering with anti-tumor immunity. Moreover, it can be hypothesized that the composition of sEV released by MTEX-affected immune cells may differ from the

composition of sEV released by immune cells of healthy people. Since this hypothesis has not yet been tested in an *in vivo* model, it became the subject of the second part of the dissertation. We focused on sEV released from T cells (CD3(+) sEV) taking into account their contribution to crosstalk between immune cells and tissue-resident non-malignant and malignant cells. Knowing that the cargo of sEV reflects the features of their parent cells, the molecular profiling of CD3(+) sEV isolated from the plasma of melanoma patients may result in gaining knowledge of the functional status of T cells, thus serving as a "liquid T cell biopsy".

The specific aims of this part of the work are as follows:

1. Comparison of the proteome profile of T cells and sEV released by T cells (CD3(+) sEV) circulating in the blood of healthy donors.
2. Proteomic profiling of two subsets of sEV derived from melanoma patients' plasma and separated according to the presence of T cell-specific CD3 antigen using immunocapture method into:

a. sEV released by T cells (CD3(+))

b. sEV released by other cell types (CD3(-))

3. Identification of the potential differences in the proteomic profiles of sEV released by T cells (CD3(+) sEV) in healthy donors and melanoma patients.

3. MATERIALS AND METHODS

Study material

Blood samples were collected from melanoma patients receiving treatment at the UPMC Hillman Cancer Center Melanoma Program Outpatient Clinic, under the care of John M. Kirkwood, MD. The collection was conducted with approval from the University of Pittsburgh IRB (#970186), and all participants provided informed consent. The study analyzed samples from 15 melanoma patients (analysis of CSPG4(+)sEV and CSPG4(-)sEV), and from 10 melanoma patients (analysis of CD3(+)sEV and CD3(-)sEV), with detailed disease status and clinicopathological data provided in Table 2 and Table 3 respectivelly. Additionally, blood samples were obtained from ten healthy donors (HDs), who consented under IRB approval #04-001, for the purpose of proteomic analysis of total plasma small extracellular vesicles. Plasma was separated from blood samples, portioned into aliquots, and stored at −80°C until they were thawed for small extracellular vesicles isolation.

Table 2. Study population characteristic.

ID	Age at diagnosis /at blood draw	Gender	Clinical stage at diagnosis	Disease status at blood draw	Mutation status	Total sEV protein (TEP) level (µg/mL)	MTEX/total sEV protein ratio	MTEX/NMTEX protein ratio
1	56/58	M	IV	SD	BRAF codon 600 (p.K600V)	77	0,53	1,14
2	29/31	M	IIIC	PD	NRAS codon 61 (p.Q61K, c.181C>A)	74	0,47	0,90
3	68/71	M	IB	NED	BRAF codon 600 (p.V600E, c.1799T>A)	56	0,64	1,80
4	54/73	M	IB	PD	BRAF codon 600 (p.V600K, c.1798_1799GT>AA)	92	0,41	0,70
5	56/57	F	IVA	PD	BRAF/NRAS wildtype	62	0,35	0,55
6	36/41	M	IV	PD	unknown	77	0,75	3,05
7	57/63	M	NA	PD	unknown	83	0,39	0,63
8	32/33	F	NA	PD	unknown	74	0,35	0,54
9	56/57	M	III	PD	unknown	76	0,39	0,65
10	77/79	M	NA	PD	unknown	71	0,52	1,09
11	38/38	M	IIB	NED	unknown	66	0,39	0,65
12	65/65	M	IIIA	NED	unknown	54	0,56	1,25
13	71/71	M	IIIB	NED	unknown	68	0,32	0,48
14	63/63	M	IIB	NED	unknown	61	0,36	0,56
15	77/77	M	IIA	NED	unknown	59	0,54	1,19

NA: not available; SD: stable disease; NED: no evidence of disease; PD: progressive disease

Table 3. Study population characteristic.

Patient ID	Age at diagnosis/ at blood draw	Gender	Clinical stage at diagnosis	Disease status at blood draw	Mutation status	Total sEV protein (TEP) level (µg/mL)	Amount of protein in CD3(+) fraction (µg)	Amount of protein in CD3(-) fraction (µg)
1	56/58	M	IV	SD	BRAF codon 600 (p.K600V)	150	71	79
2	29/31	M	IIIC	PD	NRAS codon 61 (p.Q61K, c.181C>A)	148	86	62
3	68/71	M	IB	NED	BRAF codon 600 (p.V600E, c.1799T>A)	148	17	131
4	54/73	M	IB	PD	BRAF codon 600 (p.V600K, c.1798_1799GT>AA)	149	33	116
5	56/57	F	IVA	PD	BRAF/NRAS wildtype	171	64	107
6	36/41	M	IV	PD	unknown	77	34	43
7	57/63	M	NA	PD	unknown	150	72	78
8	32/33	F	NA	PD	unknown	97	34	63
9	56/57	M	III	PD	unknown	158	8	150
10	77/79	M	NA	PD	unknown	149	43	106

NA: not available; SD: stable disease; NED: no evidence of disease; PD: progressive disease

Samples of sEV (SEC isolation and immune capture) were isolated from plasma of melanoma patients and healthy donors in our colaborating laboratory of Theresa L. Whiteside in UPMC Hillman Cancer Center, Pittsburgh, USA and were send boiled to Poland for proteomic analysis. For immune capture and separation of total sEV for fractions the anti-CSPG4 mAb was used (separation for fractions with CSPG4(+) phenotype and CSPG4(-) phenotype) and anti-CD3 mAb (separation for fractions with CD3(+) phenotype) and CD3(-) phenotype). The anti-CSPG4 mAb used for the immune capture is the antibody produced by Soldano Ferrone, MD, PhD, Professor in Residence, at Massachusetts General Hospital at Harvard University.

Aliquots of subpopulations of small extracellular vesicles separated using the immunoaffinity capture approach were collected for analysis of protein cargo using quantitative untargeted bottom-up proteomic approach realized by nano-LC-MS/MS technique in data-dependent acquisition mode. The experimental work described in the presented dissertation is divided into three parts:

(i) preparation of sEV protein samples to nano-LC-MS/MS measurements,

(ii) acquisition of nano-LC-MS/MS data,

(iii) identification of proteins present in analyzed samples using bioinformatics tools.

Methods contained in this section and employed during realization of the doctoral project are an integral part of a broader experimental setup as shown in Figure 6. A list of consumables, chemicals and instruments used for realization of the doctoral project is collected in Tables 4-6, respectively.

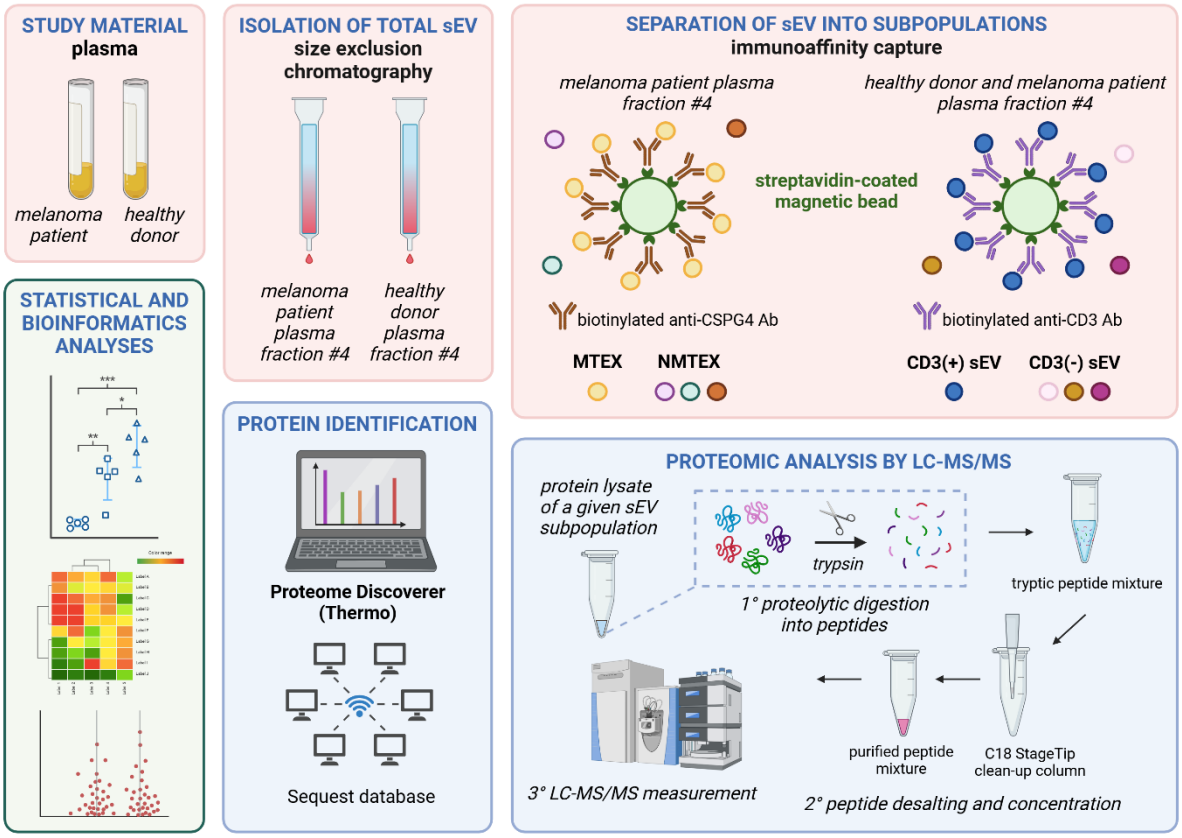

Figure 6. A general scheme of an experimental setup aiming at analysis of proteomic cargo of selected subpopulations of small extracellular vesicles, including the work performed during realization of the doctoral dissertation (contained within the blue region)

Table 4. List of consumables used during the experimental work conducted in the doctoral project

Category	Name	Product no.	Manufacturer
sample prep	Microcon® Centrifugal Filters NMWCO 30 kDa, Ultracel® regenerated cellulose membrane (low binding), sample volume 0.5 mL	MRCF0R030	Millipore
sample prep	Safe-Lock tubes, Eppendorf Quality, colorless, 0.5 mL	0030121023	Eppendorf
sample prep	Safe-Lock tubes, Eppendorf Quality, colorless, 2.0 mL	0030120094	Eppendorf
sample prep	epT.I.P.S.® Reloads, PCR clean, 0,1 – 10 µL,	0030073754	Eppendorf

	34 mm, colorless tips		
sample prep	epT.I.P.S.® Reloads, PCR clean, 2-200 µL, 53 mm, colorless tips	0030073819	Eppendorf
sample prep	epT.I.P.S.® Reloads, PCR clean, 50-1000 µL, 71 mm, colorless tips	0030073851	Eppendorf
sample prep	epT.I.P.S.® Standard Eppendorf Quality 0,1 – 5 mL, 120 mm, colorless tips	0030000978	Eppendorf
sample preparation	epT.I.P.S.® Standard Eppendorf Quality 0,5 – 10 mL, 165 mm, colorless tips	0030000765	Eppendorf
sample prep	Empore™ SPE Disks C18, diam. 47 mm	66883-U	Supelco
sample prep	16 gauge, Kel-F Hub Needle, 2 in, point style 3	90516	Hamilton
sample prep	Cell culture microplate, 384 well, PS, flat bottom, black, lid	781 086	Greiner
nano-LC	Acclaim PepMap™ 100, C18, 5 µm, 100 Å, 300 µm i.d. x 5 mm	160 454	Thermo Scientific
nano-LC	Acclaim PepMap™ 100, C18, 2 µm, 100 Å, 75 µm i.d. x 250 mm, Nano Viper	164 941	Thermo Scientific
nano-LC	0.3mL PP Snap ring micro-vials, 32x11.6mm, transparent	11 19 09 33	La-Pha-Pack
nano-LC	UltraClean closure: 11mm PE Snap ring cap, blue, centre hole, soft version, silicone white/PTFE red, 45° shore A, 1.3mm	11 15 18 54	La-Pha-Pack
mass spec	Stainless steel nano-bore emitters 40 mm OD, 1/32”	ES542	Thermo Scientific

Both in the case of sEV immunoselected using an anti-CSPG4 antibody and sEV immunoselected using an anti-CD3 antibody, protein samples were first subjected to Filter Aided Sample Preparation (FASP), according to Wiśniewski et al. [Wiśniewski et al. 2009]. This method utilizes the properties of an ultrafiltration membrane made of regenerated cellulose (integrated in a centrifugal unit) which acts as a molecular weight cut-off (MWCO 30kDa), enabling to retain proteins of interest on its surface and remove detergents (such as sodium dodecyl sulfate) and other components of an original sample which would otherwise interfere during proteolysis and/or mass spectrometric measurement. Protein lysates originating from a given subpopulation of sEV were prepared using a lysis buffer (LB) containing: 0.1M Tris-HCl pH 8.0, 0.1M DTT, 4% SDS. In the case of MTEX and NMTEX fractions or total plasma sEV from patients or healthy donors, sEV samples were mixed with LB in the volumetric ratio of 9:1, then boiled for 10 min. In the case of the CD3(+) and CD3(-) sEV fractions, proteins were precipitated with ice-cold methanol (final content of MeOH: 80%) and the obtained pellet was dissolved in 100 µL of LB, heated for 1 h at 99°C with shaking (800 rpm), then cooled down. The samples were subsequently centrifuged at 20,000 RCF for 10

min at room temperature and the supernatants were collected for nLC-MS/MS analysis.

Table 5. List of chemicals used during the experimental work conducted in the doctoral project

Name	Purity	Product no.	Manufacturer
Trizma® base ≥99.8% (T), crystalline	for molecular biology, BioUltra	93362	Sigma-Aldrich
Hydrochloric acid, fuming, ≥37%	puriss. p.a., ACS reagent	84422	Sigma-Aldrich
Dithiothreitol (DTT)	molecular biology grade	39759.03	SERVA
Sodium dodecyl sulfate (SDS) ≥98.5%	BioReagent, for molecular biology	L3771	Sigma-Aldrich
Urea	BioXtra	U0631	Sigma-Aldrich
Iodoacetamide (IAA)	BioUltra	I1149	Sigma-Aldrich
Ammonium bicarbonate ≥99.5%	BioUltra	09830	Sigma-Aldrich
Sequencing Grade Modified Trypsin, porcine, lyophilized	sequencing grade	V5111	Promega
L-Tryptophan	≥99%	0210315125	MP Biomedicals
methanol ≥99.9% (by GC), HiPerSolv CHROMANORM®, suitable for UPLC/UHPLC instruments	for LC-MS	83638.290	VWR Chemicals
acetonitrile ≥99.9%, HiPerSolv CHROMANORM®, suitable for UPLC/UHPLC instruments	for LC-MS	83640.290	VWR Chemicals
water, HiPerSolv CHROMANORM®, suitable for UPLC/UHPLC instruments	for LC-MS	83645.320P	VWR Chemicals
trifluoroacetic acid (TFA) ≥99.9%, HiPerSolv CHROMANORM® glass ampoule	for LC-MS	85049.001	VWR Chemicals
formic acid (FA) ≥99%, HiPerSolv CHROMANORM®	for LC-MS	84865.260	VWR Chemicals
Mass Spec-Compatible Human Protein Extract digest	mass spec grade	V6951	Promega
Pierce™ LTQ Velos ESI Positive Ion Calibration Solution	n/a	88323	Thermo Scientific

Table 6. List of instruments used during the experimental work conducted in the doctoral project

Name	Manufacturer
Q Exactive™ Plus Hybrid Quadrupole-Orbitrap™ Mass Spectrometer	Thermo Scientific
UltiMate™ 3000 RSLCnano liquid chromatograph	Thermo Scientific
Nanospray Flex ion source with USB cameras	Thermo Scientific
Savant DNA 120 SpeedVac concentrator	Thermo Scientific
Infinite M200 PRO multi-mode microplate reader	Tecan

Refrigerated Centrifuge 5804 R	Eppendorf
Thermomixer Comfort	Eppendorf
CLW 53 laboratory incubator	Pol-Eko-Aparatura
Vortex Genie-2 model G560	Scientific Industries

The FASP procedure was started with dissolving the protein lysates in urea buffer (8M urea in 0.1M Tris-HCl pH 8.5) in the volumetric ratio of 1:4 (50 µL of sample and 200 µL of urea buffer), followed with centrifugation in the Microcon unit at 14,000 RCF (room temperature) for 15 min. The proteins retained on the membrane of the unit were subsequently washed with 200 µL of urea buffer and alkylated with 50 mM iodoacetamide in urea buffer (50 µL of IAA solution was applied into the filter unit and alkylation reaction was conducted for 20 min at room temperature in darkness. After that time the alkylating solution was removed by centrifugation at 14,000 RCF, 15 min. The filter unit membrane was subsequently washed with three 100-µL portions of urea buffer: addition of each portion was followed with centrifugation at 14,000 RCF for 15 min, and then with three 100-µL portions of 50 mM NH_4HCO_3 (centrifugation as given above). Proteolytic digestion was carried out in 50 mM NH_4HCO_3 using Sequencing Grade Modified Trypsin with protein to enzyme ration of 1:100 (m/m) in the case of sEV immunoselected using an anti-CSPG4 antibody and 1:50 (m/m) in the case of sEV immunoselected using an anti-CD3 antibody. In both cases the digestion was carried out at 37°C for 18h.

Thus obtained tryptic peptides were released from the centrifugal unit by centrifugation (14,000 RCF, 15 min), and the membrane was additionally washed with two 80-µL portions of LC-MS grade water. Both washes were mixed with the peptide solution collected after first centrifugation, the whole was acidified with trifluoroacetic acid to reach the final TFA concentration of 0.2% (v/v) and subjected to peptide desalting and preconcentration using StageTip columns [Rappsilber et al. 2003] prepared by stacking 6 layers of Empore C18 disks in a 200-µL pipette tip. C18 bed pre-conditioning was performed by consecutive washes with 100 µL portion of: 100% methanol, eluent (i.e. 60% acetonitrile, 0.1% TFA) and 0.1% TFA; each wash followed by centrifugation (4,000 RCF, 5 min). Once the peptides were loaded onto the column (1,000 RCF, 10 min), the octadecyl bed was washed with three 100-µL portions of a wash solution (i.e. 5% MeOH, 0.1% TFA), followed by two additional washes with 0.1%

TFA (100 µL each); centrifugation conditions as in the pre-conditioning step. Finally, the tryptic peptides were released from the StageTip using two consecutive washes with the eluent: 50 µL, 1,000 RCF, 5 min each. The collected eluates were dried out in a vacuum concentrator (no heating, drying rate: low, 60 min). Then, the purified peptides were dissolved in 20 µL of LC-MS grade water and subjected to peptide assay according to the tryptophan fluorescence method by Wiśniewski and Gaugaz [Wiśniewski and Gaugaz 2015].

The tryptophan fluorescence method is a non-destructive method for peptide assay and once the signal is registered, each peptide sample can be collected form a well of a multi-well plate and subjected to nano-LC-MS/MS analysis. Six measurement series were acquired for each sample and tryptophan standard, the data were averaged and peptide concentration in each sample was calculated based on a linear regression equation obtained by the least square method. Before nano-LC-MS/MS analysis, the peptide samples were acidified to reach the final TFA concentration of 0.1% v/v.

Spectrometric measurements were realized using a nano-LC/MS system comprising of an UltiMate RSLCnano liquid chromatograph coupled to a Q Exactive Plus hybrid high-resolution mass spectrometer. Measurements were performed in a random order within a sample set, and control samples (i.e. Mass Spec-Compatible Human Protein Extract Digest, 1 µg/injection) were analyzed in the same conditions as real samples at the beginning of the measurement batch, after every 10^{th} sample and at the end of the batch. Instrumental settings of the measurements carried out for sEV immunoselected using an anti-CSPG4 antibody and anti-CD3 antibody are collected in Table 7A and Table 7B, respectively.

Table 7A. Instrumental settings of the nano-LC-MS/MS system used for measurements conducted for protein cargo of sEV immunoselected using anti-CSPG4 antibody

Chromatographic conditions	
Mobile phase	Water phase (phase A): 0.1% formic acid/H_2O Organic phase (phase B): 80% acetonitrile, 0.1% formic acid
Stationary phase	Octadecyl (C18)-modified silica, pore size: 100Å: - trap column: particle size 5µm, 300 µm i.d. x 5 mm - analytical (capillary) column: particle size 2µm,75 µm i.d. x 250 mm
Oven temperature	30°C
Acetonitrile gradient	4-60% B
Flowrate	300 nL/min

Total run time	180 min
Loading Buffer	0.1% formic acid/H_2O (flow rate: 8µL/min)
Injection routine	µL pickup
Tandem mass spectrometry conditions	
Ionization	ESI positive mode
Spray voltage	1.80 kV
Ion transfer capillary temp.	250°C
Sheath gas	0
Auxiliary gas	0
Sweep gas	0
S-lens RF	50.0
Acquisition type	Full-MS DDA (Top10)
Precursor scan	
Resolution	70,000 at m/z 200
AGC target	1e6
Max. injection time	50
Mass range	300-2000 m/z
Spectrum data type	Profile
Product ion scan	
Resolution	17,500 at m/z 200
Fragmentation mode	HCD
Normalized collision energy	25
Spectrum data type	Profile

Table 7B. Instrumental settings of the nano-LC-MS/MS system used for measurements conducted for protein cargo of sEV immunoselected using anti-CD3 antibody

Chromatographic conditions	
Mobile phase	Water phase (phase A): 0.1% formic acid/H_2O Organic phase (phase B): 80% acetonitrile, 0.1% formic acid
Stationary phase	Octadecyl (C18)-modified silica, pore size: 100Å: - trap column: particle size 5µm, 300 µm i.d. x 5 mm - analytical (capillary) column: particle size 2µm,75 µm i.d. x 250 mm
Oven temperature	30°C
Acetonitrile gradient	3-8% B for 7 min, 8-35% B for 130 min, 35-60% B for 20 min, 80% B for 20 min, 3% B for 20 min
Flowrate	300 nL/min
Total run time	200 min
Loading Buffer	0.1% formic acid/H_2O (flowrate: 8µL/min)
Injection routine	µL pickup
Tandem mass spectrometry conditions	
Ionization	ESI positive mode
Spray voltage	1.80 kV
Ion transfer capillary temp.	250°C
Sheath gas	0

Auxiliary gas	0
Sweep gas	0
S-lens RF	50.0
Acquisition type	Full-MS DDA (Top12)
Precursor scan	
Resolution	70,000 at m/z 200
AGC target	1e6
Max. injection time	50
Mass range	350–1500 m/z
Spectrum data type	Profile
Product ion scan	
Resolution	17,500 at m/z 200
Fragmentation mode	HCD
Normalized collision energy	25
Spectrum data type	Profile

Protein identification based on the acquired mass spec data was performed using a commercial software provided by the manufacturer of the nLC-MS system used, namely Proteome Discoverer (PD). Details regarding the the method setup are collected in Table 8. Abundance of identified proteins was estimated in PD using the Precursor Ions Area detector node, which calculates abundance of a given protein based on average intensity of three most intensive distinct peptides for this protein, with further normalization to the total ion current (TIC).

Table 8. Parameters set for protein identification and label-free quantitation based on the acquired nLC-MS/MS datasets using the Proteome Discoverer software

Parameter	**Description**
software	Proteome Discoverer version 1.4 (Thermo Scientific)
database	reviewed Swiss-Prot human database (release 2018_11_30 containing 11 378 269 sequence entries)
search engine	Sequest
mass tolerance	peptide masses: 10 ppm fragment ion masses: 0.02 Da
input data	Thermo raw files
terms for a protein considered as “identified”	If at least two peptides per protein found by the search engine; If peptide score reached the significance threshold FDR = 0.01 (assessed by the Percolator algorithm)
terms for a protein considered as “present”	If detected in at least one sample of a given type
method for estimation of abundance of identified proteins	Precursor Ions Area detector node

Statistical analysis of proteins identified in sEV with CSPG4(+) phenotype (MTEX) and CSPG4(-) phenotype (NMTEX).

Immunoglobulins were excluded from further examination. To identify proteins that differentiate MTEX from NMTEX, the identified protein set was divided into two categories based on the number of patients showing detectable levels. The first category consisted of proteins detected in at least 8 out of 15 patients in either the MTEX or NMTEX groups. These proteins were assessed using the non-parametric one-sided paired Wilcoxon test to evaluate whether their median abundance was higher in MTEX compared to NMTEX samples. Effect sizes were determined by calculating the rank-biserial correlation coefficient (RBCC) associated with the Wilcoxon test. The second category comprised the remaining proteins, which were analyzed based on their binary presence or absence in each sample. For this, the McNemar test, suitable for paired nominal data, was employed alongside Cohen's g statistic to measure the effect size. Proteins with p-values below 0.05 were considered significant, with functional analysis providing an additional layer of false discovery control.

To establish a set of proteins distinguishing melanoma patients with progressive disease (PD) from those with no evidence of disease or stable disease (NED/SD), the U Mann–Whitney test was used to compare the MTEX–NMTEX differential abundance, with effect sizes quantified using Wendt's rU. For rank-biserial coefficients (both RBCC and rU), a threshold of 0.5 indicated a large effect, while Cohen's g values of 0.25 or higher were also deemed indicative of a substantial effect size. All effect sizes were calculated using the absolute values of the corresponding statistics, with larger values representing stronger confidence in the observed differences. Finally, a decision tree classifier, validated through five-fold cross-validation, was employed to identify a protein signature capable of distinguishing PD patients from those with NED/SD. The classifier set was built through a stepwise selection process to prioritize proteins based on their predictive relevance.

A gene list corresponding to the differentially expressed proteins was utilized to identify enriched Gene Ontology (GO) terms and Reactome pathways using the Fisher's exact test. The analyses were performed with the Bioconductor packages ReactomePA and clusterProfiler. To reduce the risk of false positives, only those terms and pathways associated with a minimum of three and a maximum of 600 genes were

included in the analysis. For the enrichment of all proteins detected in MTEX, the entire human genome was used as the background reference set. In other enrichment analyses, the background consisted of genes corresponding to all identified proteins (totaling 573 proteins). The false discovery rate (FDR) for the GO terms and Reactome pathways was estimated using the Storey method, with a significance threshold set at a q-value of 0.05. Additionally, protein–protein interactions among selected proteins were predicted using the STRING database [Szklarczyk et al., 2019].

Statistical analysis of proteins identified in sEV with CD3(+) phenotype (T cell-derived sEV) and CD3(-) phenotype.

Given the presence of numerous zero values (indicating protein abundance below the detection threshold), the protein dataset was divided into two distinct subsets. The first subset included proteins that exhibited non-zero abundance in at least 12 out of 20 samples across both groups combined. Within this subset, differences in protein expression between melanoma patients (MP) and healthy donors (HD) were identified using the U Mann–Whitney test, with the rank-biserial correlation coefficient (RBCC) applied to estimate effect size based on abundance. To assign ranks, zero abundance values were replaced with half of the minimum non-zero abundance detected in the entire dataset. For the second subset, which consisted of the remaining proteins, differences between MP and HD were assessed based on the binary presence or absence of protein detection in each sample. Fisher's exact test was applied, with Cramér's V used to evaluate effect size. Statistical significance was set at $p = 0.05$, and the Benjamini-Hochberg procedure was employed to control the false discovery rate (FDR). Proteins were considered differentially expressed (DEPs) if they demonstrated at least a large effect size between the MP and HD groups.

Further functional analysis focused on Gene Ontology and Reactome pathways, with enrichment evaluated using the hypergeometric test. The hypothetical activation of selected pathways was assessed by calculating the Pathway Activation Score (PAS) for each sample. Pathway selection for PAS analysis followed a multi-step filtering process: (i) pathways with fewer proteins than the 1st decile were excluded; (ii) only pathways containing a number of detected proteins at or above the 3rd quartile were retained; (iii) pathways were further filtered to include those with measurement coverage of at

least the 3rd quartile across all samples. For each selected pathway, PAS was determined by calculating the median abundance of all proteins within that pathway in a given sample, substituting zero abundance values with half of the minimum non-zero abundance found in the dataset. To test the significance of pathway activation in MP samples (indicating elevated abundance of pathway components), the U Mann–Whitney test was applied along with RBCC for effect size measurement. A significance threshold of 0.05 was used, and FDR was again controlled using the Benjamini-Hochberg correction. Finally, the STRING database was utilized to evaluate the overrepresentation of associated pathways and to visualize potential interactions among selected proteins.

Statistical analysis was performed under the guidance of Prof Joanna Polańska and conducted by Justyna Mika (after protein identification in Proteome Discoverer analysis).

4. RESULTS

4.1. Characterization of sEV isolated from plasma of melanoma patients and healthy donors.

sEV were isolated from the plasma of melanoma patients and healthy donors by SEC (size exclusion chromatography) method. Total sEV-enriched fraction #4 was collected and subsequently characterized using three complementary techniques according to the MISEV 2018 recommendations [Thery et al. 2018]. At first, the presence of sEV protein markers (Alix, TSG101, CD9), and the absence of contamination by cytoplasmatic proteins (GRP94, Calnexin) were confirmed by Western blots (Fig. 7A). Secondly, the morphology and size of sEV were examined by TEM imaging (Fig. 7B). Lastly, the size range of vesicles was measured by nanoparticle tracking analysis (NTA) (Fig. 7C). All samples were enriched in sEV within the size range of 47,8 - 122,1 nm and were positive for Alix and TSG1010 markers, what confirmed the endocytic origin of sEV. Thus, the isolated vesicles met the MISEV criteria of both MISEV2018, which were in effect at the time of the experiments, and the latest MISEV2024 [Welsh et al. 2024, Thery et al. 2018].

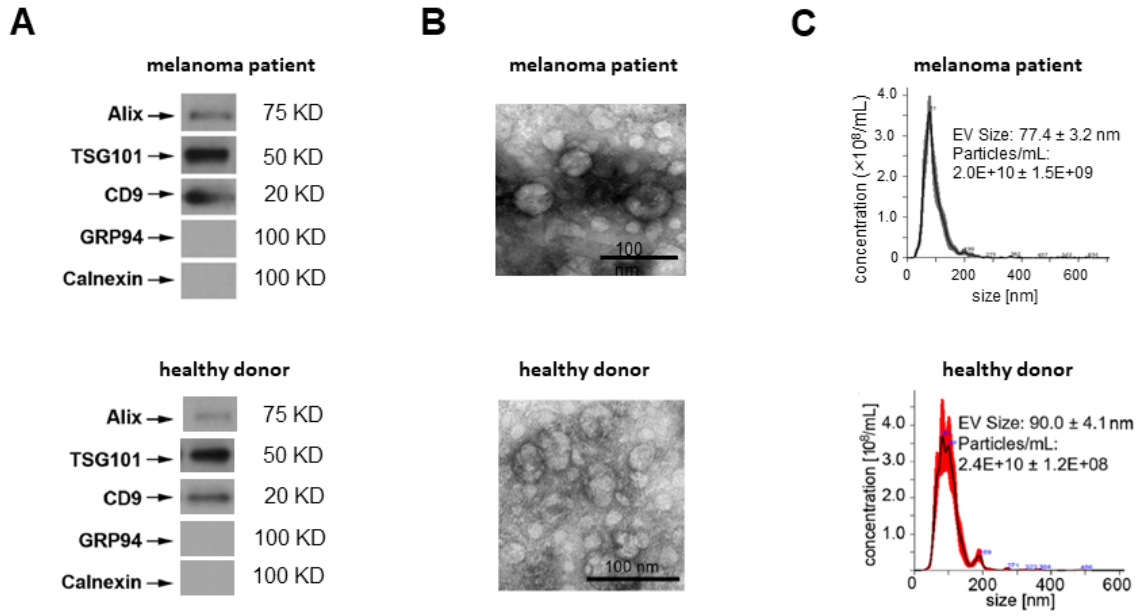

Figure 7. Representative characteristics of the plasma-derived small extracellular vesicles (sEV; total fraction#4). Western blot analysis of sEV markers and the absence of cytoplasmatic protein contamination (A), representative electronograms generated by transmission electron microscopy [TEM] showing vesicles morphology (B), histograms show results of nanoparticle tracking analysis (NTA), i.e. the size distribution and number of particles (C).

As the next step, the isolated sEV (fraction#4) were selectively separated by using the immunoaffinity capture method and two different strategies:

- the anti-CSPG4 monoclonal antibody (mAb) was used to separate melanoma cell-derived sEV (MTEX) from sEV produced by non-malignant cells (nonMTEX)
- the anti-CD3 mAb was used to separate T cell-derived sEV (CD3(+)) from non-T cell-derived sEV (CD3(-)).

CSPG4 (chondroitin sulphate proteoglycan 4) is a member of the CSPG family of cancer-associated proteins, which play multiple roles in supporting tumor growth and migration. CSPG4 is also referred to as molecular weight- melanoma-associated antigen (HMW-MAA) or melanoma-associated chondroitin sulfate proteoglycan (MCSP). The CSPG4 protein is highly expressed on melanoma cells (both differentiated and invading) in about 80% of primary and metastatic tumors with limited inter- and intra-lesional heterogeneity [Ferrone et al. 2020, Price et al. 2011]. The high specificity of anti-CSPG4 mAbs used in experiments was confirmed by Prof. Soldano [Ferrone et al. 2020] and repeatedly tested in our collaborative laboratory headed by Prof. Theresa L. Whiteside , PhD , in UPMC Hillman Cancer Center, Pittsburgh, USA, where the technique of sEV immune capture was developed [Mondal et al. 2021]. The published data show that 99% of MTEX (both in vitro and in vivo) are positive for CSPG4, whereas nonMTEX are negative [Sharma et al. 2020, Sharma et al. 2018]. Such a high detection rate and excellent specificity are critical for the effective immunoisolation of CSPG4-positive cells or sEV. In our experiments, for immunodetection and MTEX capture, we used the CSPG4-specific mAb clones 763.64 or 225.28 recognizing distinct and spatially distant CSPG4 epitopes, respectively. Both mAb clones selectively recognize epitopes abundantly expressed on melanoma cells, while showing no reactivity toward normal human tissues [Ferrone et al.2020, Sharma et al. 2020].

Immunocapture of MTEX, sEV with phenotype CSPG4(+), from total sEV sample (fraction#4) isolated from plasma of melanoma patients revealed that these vesicles carried different levels of CSPG4 on their surface (measured by quantitative on-bead flow cytometry) showing individual differences between patients (Fig. 8). As expected, on-bead flow cytometry confirmed that plasma of healthy donors does not contain sEV with the cancer antigen CSPG4 (Fig. 9).

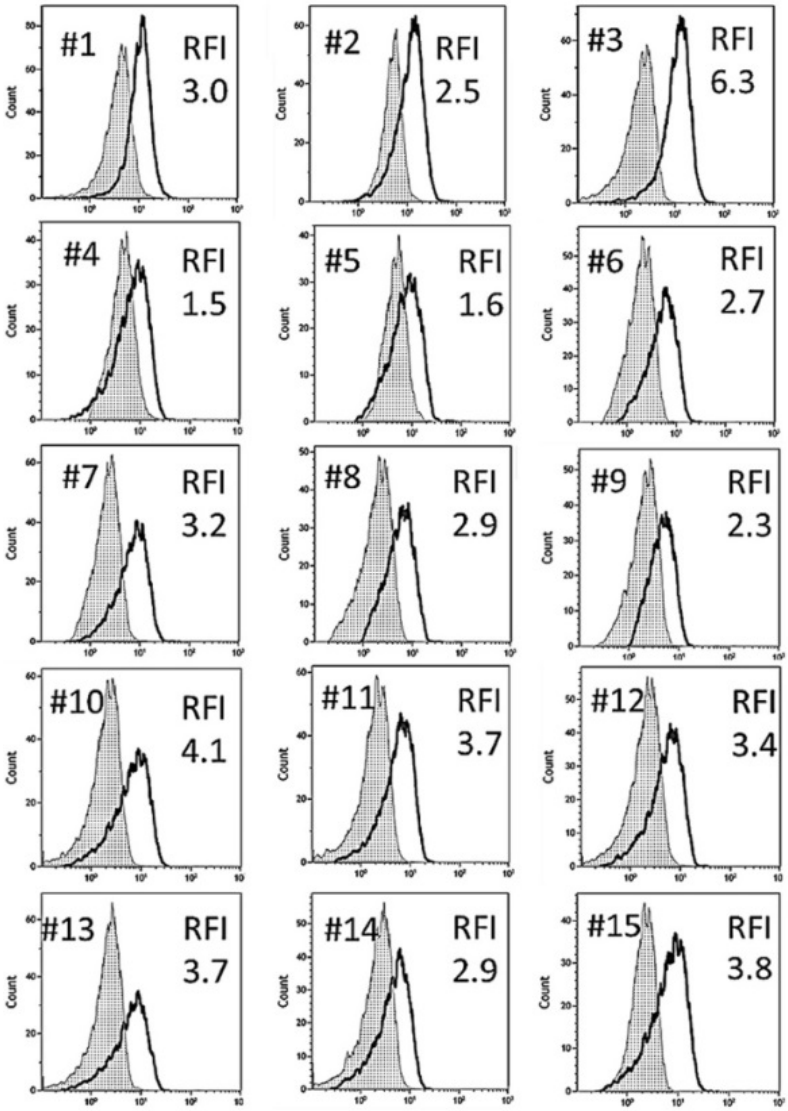

Figure 8. Results of on-bead flow cytometry analysis of sEV in fraction #4 isolated from plasma of melanoma patient (n = 15). sEV were immunocaptured on streptavidin beads using biotin-labeled anti-CD63 mAb. Detection was performed using PE-labeled anti-CSPG4 mAb. Relative fluorescence intensity (RFI) values differ among patients but CSPG4+ sEV are present in total plasma-derived sEV of all 15 patients. The histograms display relative fluorescence intensity on the x-axis and the number of events (cell count) on the y-axis.

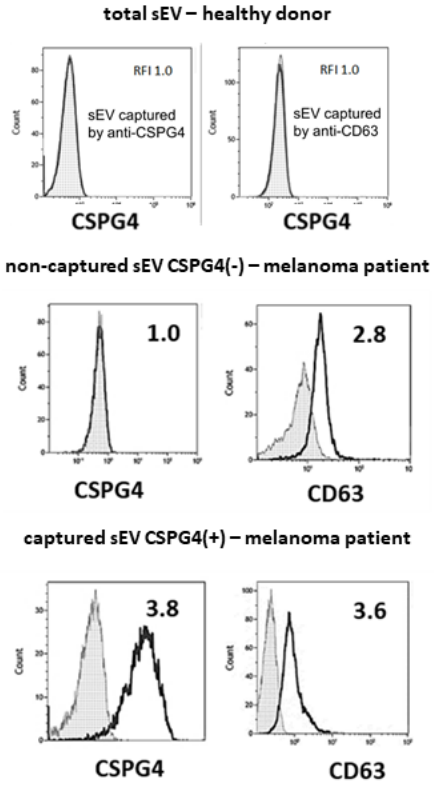

Figure 9. Detection of CSPG4, CD63 antigens in total sEV fraction (#4) isolated from plasma of a healthy donor, non-captured sEV CSPG4(-) or captured sEV CSPG4(+) from a melanoma patient. Relative fluorescence intensity (RFI) values confirm presence of CSPG4 antygen in captured sEV (CSPG4(+)) isolated from melanoma patients plasma and absence of CSPG4 antygen in sEV from plasma of healthy donors (sEV were captured by antiCSPG4 mAb and by antiCD63 mAb), as well as in non-captured sEV CSPG4(-) of melanoma patients. RFI values confirmed also dexpression of CD63 antygen in both – captured (CSPG4(+))and non-captured sEV (CSPG4(-)) of melaoma patients. The histograms display relative fluorescence intensity on the x-axis and the number of events (cell count) on the y-axis.

The CD3 protein is uniquely expressed by TCR+ cells, and anti-CD3 Abs was used to capture CD3(+)sEV, which are exclusively produced by T cells [Zebrowska et al. 2022, Theodoraki et al. 2018]. The immunocapture method with anti-CD3 antibody allowed for fractionation of total sEV (fraction#4) into 2 populations: (i) sEV released by T lymphocyte with CD3(+) phenotype; (II) sEV released by all other cells with CD3(-) phenotype (Fig. 10). Similarly as in the case of CSPG4 detection, the sEV in fraction#4 carried different levels of CD3 on their surface (measured by quantitative on-bead flow cytometry), revealing individual differences between melanoma patients (Fig. 11).

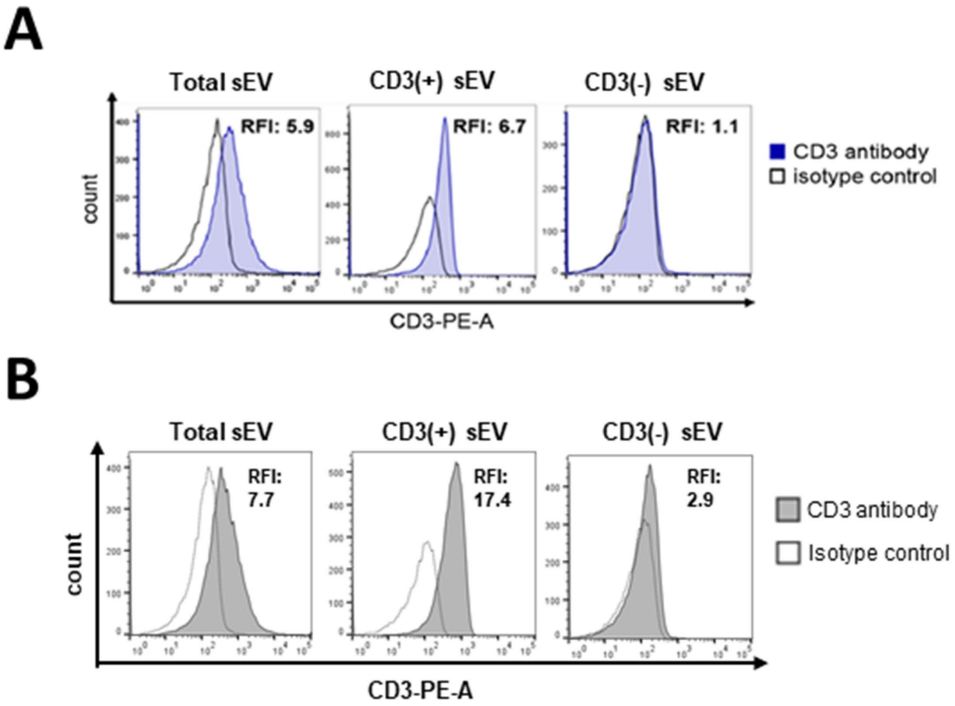

Figure 10. Representative results showing the detection of CD3 antigen in the total sEV fraction, and in the CD3(+) sEV and CD3(-) sEV fractions isolated from the plasma of healthy donor (panel A) and melanoma patients (B). The presence of CD3 was analyzed by on-bead flow cytometry. RFI, Relative fluorescence intensity, PE-A – antibody labelled with R-Phycoerythrin.

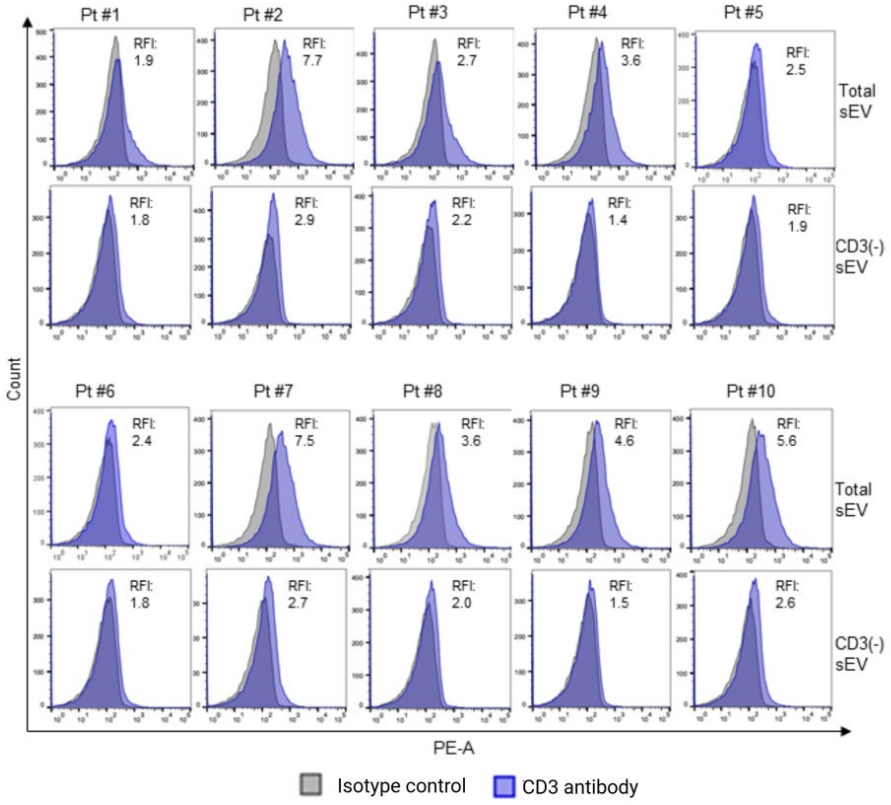

Figure 11. Expression of CD3 in total sEV and CD3(-) sEV isolated from plasma of all melanoma patients in this study (n=10). RFI - Relative fluorescence intensity, PE-A – antibody labelled with R-Phycoerythrin.

To summarize this part of results - sEVs were isolated from the plasma of melanoma patients and healthy donors via SEC. Fraction 4 (the so-called total sEV), which is a fraction enriched in small extracellular vesicles, was used for further studies. Total sEVs were characterized according to MISEV2018 / MISEV2024 guidelines, i.e. their size and morphology (NTA, TEM) and the presence of sEV markers (western blot) were confirmed. The total sEVs isolated in this way were separated into fractions by immunoblotting. First, anti-CSPG4 mAb was used to separate total sEV from melanoma patients into 2 fractions: CSPG4(+) (known as MTEX - melanoma-derived sEV) and CSPG4(-) (known as NMTEX - non-melanoma-derived sEV). The CSPG4 protein is a tumor-specific antigen for melanoma cells. The anti-CD3 mAb, on the other hand, was used in the second part of the study to separate total sEV from melanoma patients and healthy donors into 2 fractions: CD3(+) (T cell-derived sEV) and CD3(-) (non-T cell-derived sEV). The presence or absence (depending on the sEV fraction) of the corresponding antigens (CSPG4 and CD3) in the separated sEV fractions was verified by flow cytometry.

4.2. Molecular composition of sEV with CSPG4(+) phenotype (MTEX) isolated from plasma of melanoma patients.

4.2.1. Proteins identified in MTEX.

The MTEX (sEV with CSPG4(+) phenotype) and NMTEX (sEV with CSPG4(-) phenotype) isolated from plasma of 15 melanoma patients (please refer to Table 2 for details on the study population) were used for proteomic paired comparative analysis. Total sEV protein (TEP) levels (BCA assay based) varied between melanoma patients from 54 to 92 µg in 1 ml of plasma. Importantly, the average TEP level (63 µg/ml) for patients with non-evident or stable disease (NED/SD; n = 7) at the time of blood draw was significantly lower ($P < 0.02$) than that (78 µg/ml) for melanoma patients with progressive disease (PD; n = 8). The ratios of MTEX/TEP varied, ranging from 0.32 to 0.75, while those for MTEX/NMTEX varied from 0.48 to 3.05, and these ratios did not reflect disease activity (Table 2).

All MTEX and NMTEX samples were analyzed using a shotgun proteomics approach based on the high-resolution mass spectrometry (HRMS). This approach allowed the identification of 682 proteins in all analysed samples. Sample was normalized to TIC (Total Ion Current) value which have to be equal for all samples (Table 9).

Table 9. Calculated TIC value (the mean value of total abundances of proteins for each group).

MTEX only	**NMTEX only**
627,759,117,658	627,759,022,239

Identified proteins which were uncharacterized in human reviewed database (20 proteins) and 89 immunoglobulins were filtered out. Hence further analysis focused on 573 proteins encoded by the unique genes. An unsupervised principal component analysis (PCA) was used to analyze overall similarities between samples, which confirmed differences between MTEX and NMTEX (Fig. 12A). Even greater diversity was observed between samples obtained from 4 patients with PD (Fig. 12B). The abundance values of all proteins identified in analyzed samples are presented as a heat map in Figure 12C. The heat map reflects differences in protein abundance between MTEX and NMTEX samples. Interestingly, the heat map shows that the level of many proteins in patients with PD is higher than in patients with SD or NED. This difference is even more pronounced in 4 patients with PD (Fig. 12D). On the heat map showing proteins abundance in all samples, these 4 patients are represented as first 4 columns from the left sight of the heat map (Fig. 12C).

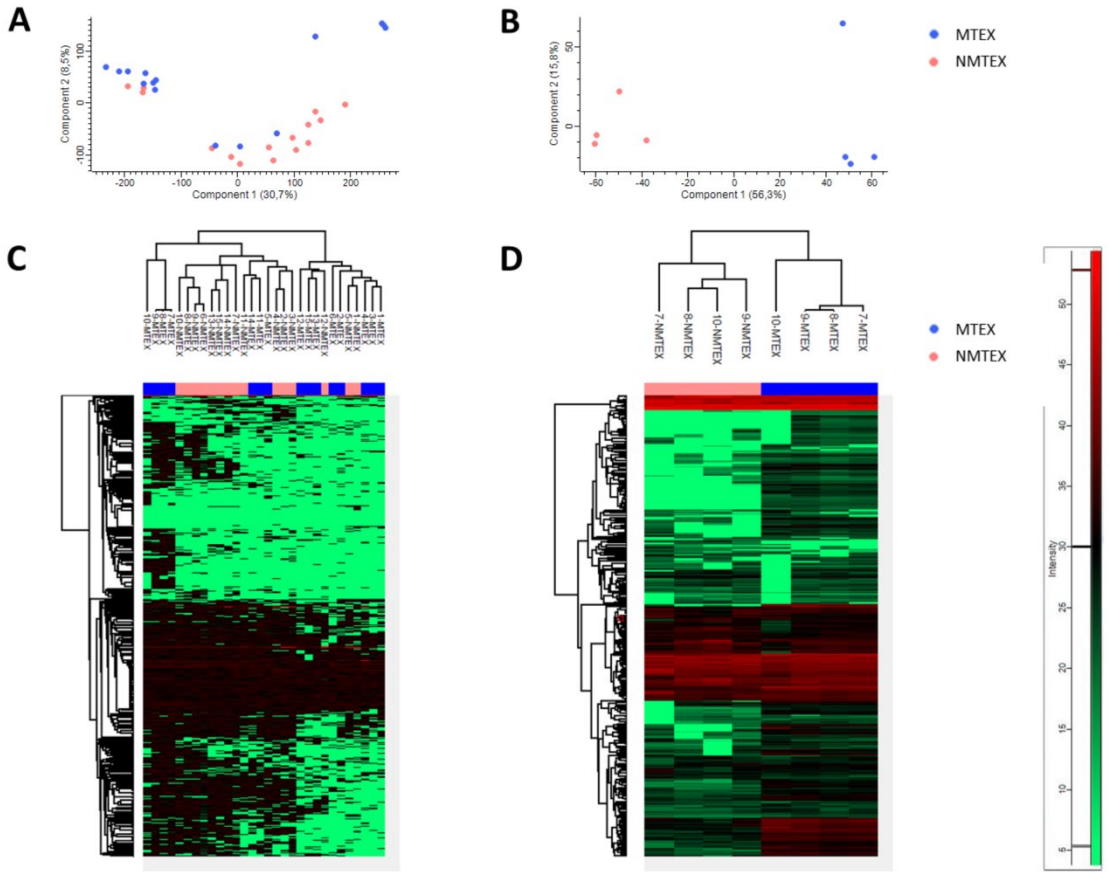

Figure 12. Principal component analysis (PCA) of overall similarities (all identified proteins) between MTEX and NMTEX for all 15 patients (panel A) and for 4 ptients with progressive disease (PD) and the highest level of proteins (panel B). The heat maps represent the abundance of all 573 proteins detected in MTEX and NMTEX samples of 15 melanoma patients (panel C) and 4 patients with PD and the highest level of proteins (panel D). The abundance of proteins is colour-coded according to the intensity of all normalized signals.

To identify which proteins discriminate MTEX and NMTEX, the ratio of individual protein levels in MTEX and NMTEX for each patient was determined. First, proteins for which the non-zero measurement was observed for at least 8 patients for MTEX, NMTEX, or both (8/15) were selected for the “continuous” mode of statistical testing. 384 proteins met this condition. A one-sided Wilcoxon test for paired data was used to compare MTEX and NMTEX with each other. It was applied to every protein separately. Effect size statistic was calculated using the rank-biserial coefficient correlation for Wilcoxon test (RBCC). Benjamini-Hochberg correction for multiple testing was applied (FDR). In MTEX 62 proteins were upregulated ($P > 0.05$ and RBCC ≥ 0.5) (Table 10).

Among them, 3 proteins (TUBA1A, GSN and FBLN1) had a false discovery rate at the level of 5% (Fig. 13). 54 proteins were classified as downregulated (RBCC ≤ -0.5). The complete list of proteins is shown in Table 11.

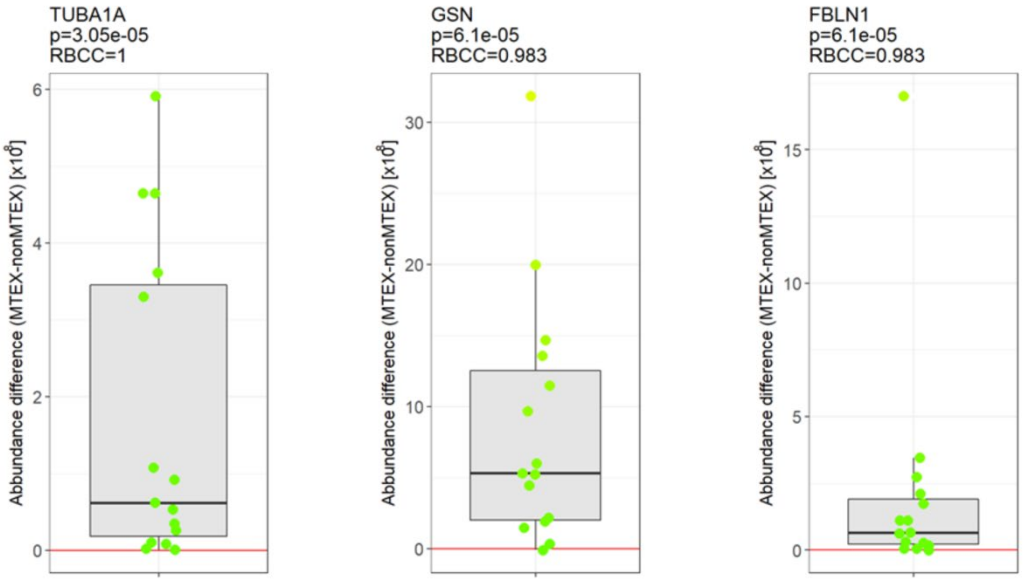

Figure 13. Box plots showing abundance difference (MTEX vs NMTEX) for 3 proteins upregulated in MTEX (FDR > 0.05).

The remaining 189 proteins which had more than 7 pairs of zero-observations were subjected to the binary/discrete mode of statistical testing. The comparison of proportions in groups samples (the present (detected by MS in group)/absent (non-detected) algorithm) was checked with McNemar test (due to related/paired observations) for each protein separately. Corresponding Cohen's g effect size for proportion was calculated. Analysis revealed an additional 11 proteins with increased levels in MTEX (p value > 0.05 and Cohen's g ≥ 0.5) and 23 proteins with decreased levels (Cohen's g ≤ 0.5). Although the power of statistical analysis for some of the downregulated proteins is low due to the small sample size, the p-value (and the multiple testing corrected p-value) is rather high, indicating no significant differences. Still, as the effect size for them is large (Cohen g ≤ -0.5), they are included in the classification as downregulated in MTEX. A list of all proteins up- and downregulated according to discrete analysis is placed in Table 12.

Table 10. List of proteins upregulated in MTEX (continuous analysis).

Accession	Protein Description	Gene Symbol	MTEX/NMTEX (median)	Type of analysis (continuous vs. binary)	Wilcoxon test p-value	Effect size (RBCC)	STATUS
P60709	Actin, cytoplasmic 1 OS=Homo sapiens OX=9606 GN=ACTB PE=1 SV=1	ACTB	1,69	C	0,0027	0,78	MTEX-UP
O00468	Agrin OS=Homo sapiens OX=9606 GN=AGRN PE=1 SV=6	AGRN	6,16	C	0,0128	0,65	MTEX-UP
P23526	Adenosylhomocysteinase OS=Homo sapiens OX=9606 GN=AHCY PE=1 SV=4	AHCY	20,11	C	0,0042	0,75	MTEX-UP
P04745	Alpha-amylase 1 OS=Homo sapiens OX=9606 GN=AMY1A PE=1 SV=2	AMY1A	15,46	C	0,0017	0,82	MTEX-UP
P04114	Apolipoprotein B-100 OS=Homo sapiens OX=9606 GN=APOB PE=1 SV=2	APOB	1,33	C	0,0277	0,57	MTEX-UP
P61204	ADP-ribosylation factor 3 OS=Homo sapiens OX=9606 GN=ARF3 PE=1 SV=2	ARF3	17,34	C	0,0017	0,82	MTEX-UP
P10643	Complement component C7 OS=Homo sapiens OX=9606 GN=C7 PE=1 SV=2	C7	7,31	C	0,0128	0,65	MTEX-UP
P16671	Platelet glycoprotein 4 OS=Homo sapiens OX=9606 GN=CD36 PE=1 SV=2	CD36	4,02	C	0,0319	0,55	MTEX-UP
P23528	Cofilin-1 OS=Homo sapiens OX=9606 GN=CFL1 PE=1 SV=3	CFL1	6,30	C	0,0277	0,57	MTEX-UP
Q9Y240	C-type lectin domain family 11 member A OS=Homo sapiens OX=9606 GN=CLEC11A PE=1 SV=1	CLEC11A	19,97	C	0,0075	0,70	MTEX-UP
Q12860	Contactin-1 OS=Homo sapiens OX=9606 GN=CNTN1 PE=1 SV=1	CNTN1	33,98	C	0,0062	0,72	MTEX-UP
P39059	Collagen alpha-1(XV) chain OS=Homo sapiens OX=9606 GN=COL15A1 PE=1 SV=2	COL15A1	24,27	C	0,0013	0,83	MTEX-UP
P02452	Collagen alpha-1(I) chain OS=Homo sapiens OX=9606 GN=COL1A1 PE=1 SV=5	COL1A1	2,19	C	0,0151	0,63	MTEX-UP
P02461	Collagen alpha-1(III) chain OS=Homo sapiens OX=9606 GN=COL3A1 PE=1 SV=4	COL3A1	3,49	C	0,0473	0,50	MTEX-UP
Q6UVK1	**Chondroitin sulfate proteoglycan 4 OS=Homo sapiens OX=9606 GN=CSPG4 PE=1 SV=2**	**CSPG4**	**18,68**	**C**	**0,0108**	**0,67**	**MTEX-UP**
P00742	Coagulation factor X OS=Homo sapiens OX=9606 GN=F10 PE=1 SV=2	F10	5,59	C	0,0090	0,68	MTEX-UP
P23142	Fibulin-1 OS=Homo sapiens OX=9606 GN=FBLN1 PE=1 SV=4	FBLN1	7,76	C	0,0001	0,98	MTEX-UP
Q14254	Flotillin-2 OS=Homo sapiens OX=9606 GN=FLOT2 PE=1 SV=2	FLOT2	4,67	C	0,0365	0,53	MTEX-UP
P04406	Glyceraldehyde-3-phosphate dehydrogenase OS=Homo sapiens OX=9606 GN=GAPDH PE=1	GAPDH	6,60	C	0,0062	0,72	MTEX-UP
P06396	Gelsolin OS=Homo sapiens OX=9606 GN=GSN PE=1 SV=1	GSN	12,58	C	0,0001	0,98	MTEX-UP
Q96S86	Hyaluronan and proteoglycan link protein 3 OS=Homo sapiens OX=9606 GN=HAPLN3 PE=2 SV=1	HAPLN3	>100	C	0,0128	0,65	MTEX-UP

Q5QNW6	Histone H2B type 2-F OS=Homo sapiens OX=9606 GN=HIST2H2BF PE=1 SV=3	HIST2H2BF	2,04	C	0,0177	0,62	MTEX-UP
P07900	Heat shock protein HSP 90-alpha OS=Homo sapiens OX=9606 GN=HSP90AA1 PE=1 SV=5	HSP90AA1	13,72	C	0,0128	0,65	MTEX-UP
P08238	Heat shock protein HSP 90-beta OS=Homo sapiens OX=9606 GN=HSP90AB1 PE=1 SV=4	HSP90AB1	16,64	C	0,0319	0,55	MTEX-UP
P11142	Heat shock cognate 71 kDa protein OS=Homo sapiens OX=9606 GN=HSPA8 PE=1 SV=1	HSPA8	2,42	C	0,0319	0,55	MTEX-UP
P98160	Basement membrane-specific heparan sulfate proteoglycan core protein OS=Homo sapiens	HSPG2	5,32	C	0,0206	0,60	MTEX-UP
O75874	Isocitrate dehydrogenase [NADP] cytoplasmic OS=Homo sapiens OX=9606 GN=IDH1 PE=1 SV=2	IDH1	>100	C	0,0042	0,75	MTEX-UP
Q06033	Inter-alpha-trypsin inhibitor heavy chain H3 OS=Homo sapiens OX=9606 GN=ITIH3 PE=1 SV=2	ITIH3	3,35	C	0,0365	0,53	MTEX-UP
P11047	Laminin subunit gamma-1 OS=Homo sapiens OX=9606 GN=LAMC1 PE=1 SV=3	LAMC1	5,53	C	0,0319	0,55	MTEX-UP
P00338	L-lactate dehydrogenase A chain OS=Homo sapiens OX=9606 GN=LDHA PE=1 SV=2	LDHA	>100	C	0,0003	0,92	MTEX-UP
P08519	Apolipoprotein(a) OS=Homo sapiens OX=9606 GN=LPA PE=1 SV=1	LPA	3,44	C	0,0151	0,63	MTEX-UP
Q07954	Prolow-density lipoprotein receptor-related protein 1 OS=Homo sapiens OX=9606 GN=LRP1	LRP1	2,30	C	0,0008	0,87	MTEX-UP
P43121	Cell surface glycoprotein MUC18 OS=Homo sapiens OX=9606 GN=MCAM PE=1 SV=2	MCAM	>100	C	0,0206	0,60	MTEX-UP
Q13201	Multimerin-1 OS=Homo sapiens OX=9606 GN=MMRN1 PE=1 SV=3	MMRN1	4,08	C	0,0416	0,52	MTEX-UP
P26038	Moesin OS=Homo sapiens OX=9606 GN=MSN PE=1 SV=3	MSN	3,03	C	0,0034	0,77	MTEX-UP
P35579	Myosin-9 OS=Homo sapiens OX=9606 GN=MYH9 PE=1 SV=4	MYH9	6,99	C	0,0003	0,92	MTEX-UP
Q04721	Neurogenic locus notch homolog protein 2 OS=Homo sapiens OX=9606 GN=NOTCH2 PE=1 SV=3	NOTCH2	>100	C	0,0042	0,75	MTEX-UP
Q8WUM4	Programmed cell death 6-interacting protein OS=Homo sapiens OX=9606 GN=PDCD6IP PE=1	PDCD6IP	14,19	C	0,0002	0,95	MTEX-UP
P00558	Phosphoglycerate kinase 1 OS=Homo sapiens OX=9606 GN=PGK1 PE=1 SV=3	PGK1	>100	C	0,0021	0,80	MTEX-UP
O43175	D-3-phosphoglycerate dehydrogenase OS=Homo sapiens OX=9606 GN=PHGDH PE=1 SV=4	PHGDH	>100	C	0,0365	0,53	MTEX-UP
Q9P2B2	Prostaglandin F2 receptor negative regulator OS=Homo sapiens OX=9606 GN=PTGFRN PE=1	PTGFRN	>100	C	0,0027	0,78	MTEX-UP
Q9H0U4	Ras-related protein Rab-1B OS=Homo sapiens OX=9606 GN=RAB1B PE=1 SV=1	RAB1B	2,31	C	0,0240	0,58	MTEX-UP
P61224	Ras-related protein Rap-1b OS=Homo sapiens OX=9606 GN=RAP1B PE=1 SV=1	RAP1B	4,28	C	0,0017	0,82	MTEX-UP
O00560	Syntenin-1 OS=Homo sapiens OX=9606 GN=SDCBP PE=1 SV=1	SDCBP	19,79	C	0,0108	0,67	MTEX-UP
P01008	Antithrombin-III OS=Homo sapiens OX=9606 GN=SERPINC1 PE=1 SV=1	SERPINC1	2,08	C	0,0021	0,80	MTEX-UP
P36955	Pigment epithelium-derived factor OS=Homo sapiens OX=9606 GN=SERPINF1 PE=1 SV=4	SERPINF1	8,10	C	0,0240	0,58	MTEX-UP

P08697	Alpha-2-antiplasmin OS=Homo sapiens OX=9606 GN=SERPINF2 PE=1 SV=3	SERPINF2	5,21	C	0,0277	0,57	MTEX-UP
P43007	Neutral amino acid transporter A OS=Homo sapiens OX=9606 GN=SLC1A4 PE=1 SV=1	SLC1A4	>100	C	0,0416	0,52	MTEX-UP
P11166	Solute carrier family 2, facilitated glucose transporter member 1 OS=Homo sapiens OX=9606	SLC2A1	2,21	C	0,0473	0,50	MTEX-UP
P07996	Thrombospondin-1 OS=Homo sapiens OX=9606 GN=THBS1 PE=1 SV=2	THBS1	4,21	C	0,0008	0,87	MTEX-UP
Q9Y490	Talin-1 OS=Homo sapiens OX=9606 GN=TLN1 PE=1 SV=3	TLN1	2,52	C	0,0004	0,90	MTEX-UP
Q99816	Tumor susceptibility gene 101 protein OS=Homo sapiens OX=9606 GN=TSG101 PE=1 SV=2	TSG101	>100	C	0,0151	0,63	MTEX-UP
Q71U36	Tubulin alpha-1A chain OS=Homo sapiens OX=9606 GN=TUBA1A PE=1 SV=1	TUBA1A	5,63	C	0,0000	1,00	MTEX-UP
P68366	Tubulin alpha-4A chain OS=Homo sapiens OX=9606 GN=TUBA4A PE=1 SV=1	TUBA4A	19,78	C	0,0206	0,60	MTEX-UP
P07437	Tubulin beta chain OS=Homo sapiens OX=9606 GN=TUBB PE=1 SV=2	TUBB	3,45	C	0,0319	0,55	MTEX-UP
P62987	Ubiquitin-60S ribosomal protein L40 OS=Homo sapiens OX=9606 GN=UBA52 PE=1 SV=2	UBA52	12,46	C	0,0013	0,83	MTEX-UP
O15240	Neurosecretory protein VGF OS=Homo sapiens OX=9606 GN=VGF PE=1 SV=2	VGF	8,69	C	0,0416	0,52	MTEX-UP
P04004	Vitronectin OS=Homo sapiens OX=9606 GN=VTN PE=1 SV=1	VTN	1,94	C	0,0240	0,58	MTEX-UP
P04275	von Willebrand factor OS=Homo sapiens OX=9606 GN=VWF PE=1 SV=4	VWF	1,87	C	0,0365	0,53	MTEX-UP
O75083	WD repeat-containing protein 1 OS=Homo sapiens OX=9606 GN=WDR1 PE=1 SV=4	WDR1	>100	C	0,0206	0,60	MTEX-UP
P62258	14-3-3 protein epsilon OS=Homo sapiens OX=9606 GN=YWHAE PE=1 SV=1	YWHAE	2,22	C	0,0240	0,58	MTEX-UP
P63104	14-3-3 protein zeta/delta OS=Homo sapiens OX=9606 GN=YWHAZ PE=1 SV=1	YWHAZ	2,53	C	0,0240	0,58	MTEX-UP

Table 11. List of proteins downregulated in MTEX (continuous analysis).

Accession	Protein Description	Gene Symbol	MTEX/NMTEX (median)	Type of analysis (continuous vs. binary)	Wilcoxon test p-value	Effect size (RBCC)	STATUS
P01023	Alpha-2-macroglobulin OS=Homo sapiens OX=9606 GN=A2M PE=1 SV=3	A2M	0,51	C	0,9794	-0,58	MTEX-down
P02760	Protein AMBP OS=Homo sapiens OX=9606 GN=AMBP PE=1 SV=1	AMBP	0,34	C	0,9949	-0,72	MTEX-down
P15144	Aminopeptidase N OS=Homo sapiens OX=9606 GN=ANPEP PE=1 SV=4	ANPEP	0,29	C	0,9966	-0,75	MTEX-down
P55056	Apolipoprotein C-IV OS=Homo sapiens OX=9606 GN=APOC4 PE=1 SV=1	APOC4	0,47	C	0,9584	-0,50	MTEX-down
P02749	Beta-2-glycoprotein 1 OS=Homo sapiens OX=9606 GN=APOH PE=1 SV=3	APOH	<0,01	C	0,9949	-0,72	MTEX-down
P25311	Zinc-alpha-2-glycoprotein OS=Homo sapiens OX=9606 GN=AZGP1 PE=1 SV=2	AZGP1	<0,01	C	0,9996	-0,88	MTEX-down
Q8TDL5	BPI fold-containing family B member 1 OS=Homo sapiens OX=9606 GN=BPIFB1 PE=1 SV=1	BPIFB1	<0,01	C	0,9849	-0,62	MTEX-down
P02746	Complement C1q subcomponent subunit B OS=Homo sapiens OX=9606 GN=C1QB PE=1	C1QB	0,35	C	0,9999	-0,97	MTEX-down
P02747	Complement C1q subcomponent subunit C OS=Homo sapiens OX=9606 GN=C1QC PE=1	C1QC	0,50	C	0,9996	-0,88	MTEX-down
P00736	Complement C1r subcomponent OS=Homo sapiens OX=9606 GN=C1R PE=1 SV=2	C1R	0,64	C	0,9584	-0,50	MTEX-down
P0C0L5	Complement C4-B OS=Homo sapiens OX=9606 GN=C4B PE=1 SV=2	C4B	0,27	C	0,9635	-0,52	MTEX-down
P04003	C4b-binding protein alpha chain OS=Homo sapiens OX=9606 GN=C4BPA PE=1 SV=2	C4BPA	0,85	C	0,9681	-0,53	MTEX-down
P20851	C4b-binding protein beta chain OS=Homo sapiens OX=9606 GN=C4BPB PE=1 SV=1	C4BPB	0,33	C	0,9983	-0,80	MTEX-down
P0DP25	Calmodulin-3 OS=Homo sapiens OX=9606 GN=CALM3 PE=1 SV=1	CALM3	<0,01	C	0,9823	-0,60	MTEX-down
Q6ZRK6	Coiled-coil domain-containing protein 73 OS=Homo sapiens OX=9606 GN=CCDC73 PE=2	CCDC73	<0,01	C	0,9925	-0,68	MTEX-down
P08571	Monocyte differentiation antigen CD14 OS=Homo sapiens OX=9606 GN=CD14 PE=1 SV=2	CD14	0,01	C	0,9584	-0,50	MTEX-down
Q08722	Leukocyte surface antigen CD47 OS=Homo sapiens OX=9606 GN=CD47 PE=1 SV=1	CD47	0,03	C	0,9892	-0,65	MTEX-down
O43866	CD5 antigen-like OS=Homo sapiens OX=9606 GN=CD5L PE=1 SV=1	CD5L	0,50	C	0,9584	-0,50	MTEX-down
Q96KN2	Beta-Ala-His dipeptidase OS=Homo sapiens OX=9606 GN=CNDP1 PE=1 SV=4	CNDP1	<0,01	C	0,9994	-0,87	MTEX-down
Q96IY4	Carboxypeptidase B2 OS=Homo sapiens OX=9606 GN=CPB2 PE=1 SV=2	CPB2	<0,01	C	1,0000	-1,00	MTEX-down

P27487	Dipeptidyl peptidase 4 OS=Homo sapiens OX=9606 GN=DPP4 PE=1 SV=2	DPP4	<0,01	C	0,9584	-0,50	MTEX-down
Q02413	Desmoglein-1 OS=Homo sapiens OX=9606 GN=DSG1 PE=1 SV=2	DSG1	<0,01	C	0,9760	-0,57	MTEX-down
Q15485	Ficolin-2 OS=Homo sapiens OX=9606 GN=FCN2 PE=1 SV=2	FCN2	0,62	C	0,9723	-0,55	MTEX-down
O75636	Ficolin-3 OS=Homo sapiens OX=9606 GN=FCN3 PE=1 SV=2	FCN3	0,36	C	0,9794	-0,58	MTEX-down
P02774	Vitamin D-binding protein OS=Homo sapiens OX=9606 GN=GC PE=1 SV=2	GC	0,34	C	0,9584	-0,50	MTEX-down
P80108	Phosphatidylinositol-glycan-specific phospholipase D OS=Homo sapiens OX=9606 GN=GPLD1	GPLD1	<0,01	C	0,9973	-0,77	MTEX-down
Q9ULI3	Protein HEG homolog 1 OS=Homo sapiens OX=9606 GN=HEG1 PE=1 SV=3	HEG1	0,01	C	0,9635	-0,52	MTEX-down
P62805	Histone H4 OS=Homo sapiens OX=9606 GN=HIST1H4A PE=1 SV=2	HIST1H4A	0,31	C	0,9958	-0,73	MTEX-down
P00738	Haptoglobin OS=Homo sapiens OX=9606 GN=HP PE=1 SV=1	HP	0,64	C	0,9635	-0,52	MTEX-down
P17936	Insulin-like growth factor-binding protein 3 OS=Homo sapiens OX=9606 GN=IGFBP3 PE=1	IGFBP3	0,33	C	0,9823	-0,60	MTEX-down
P03952	Plasma kallikrein OS=Homo sapiens OX=9606 GN=KLKB1 PE=1 SV=1	KLKB1	0,13	C	0,9997	-0,90	MTEX-down
P08779	Keratin, type I cytoskeletal 16 OS=Homo sapiens OX=9606 GN=KRT16 PE=1 SV=4	KRT16	<0,01	C	0,9958	-0,73	MTEX-down
Q04695	Keratin, type I cytoskeletal 17 OS=Homo sapiens OX=9606 GN=KRT17 PE=1 SV=2	KRT17	<0,01	C	0,9760	-0,57	MTEX-down
P13647	Keratin, type II cytoskeletal 5 OS=Homo sapiens OX=9606 GN=KRT5 PE=1 SV=3	KRT5	0,21	C	0,9990	-0,83	MTEX-down
P02538	Keratin, type II cytoskeletal 6A OS=Homo sapiens OX=9606 GN=KRT6A PE=1 SV=3	KRT6A	0,15	C	0,9794	-0,58	MTEX-down
P04259	Keratin, type II cytoskeletal 6B OS=Homo sapiens OX=9606 GN=KRT6B PE=1 SV=5	KRT6B	<0,01	C	0,9910	-0,67	MTEX-down
Q14CN4	Keratin, type II cytoskeletal 72 OS=Homo sapiens OX=9606 GN=KRT72 PE=1 SV=2	KRT72	0,41	C	0,9872	-0,63	MTEX-down
P02750	Leucine-rich alpha-2-glycoprotein OS=Homo sapiens OX=9606 GN=LRG1 PE=1 SV=2	LRG1	0,01	C	0,9823	-0,60	MTEX-down
Q14766	Latent-transforming growth factor beta-binding protein 1 OS=Homo sapiens OX=9606	LTBP1	<0,01	C	0,9990	-0,83	MTEX-down
Q9HC84	Mucin-5B OS=Homo sapiens OX=9606 GN=MUC5B PE=1 SV=3	MUC5B	0,05	C	0,9997	-0,90	MTEX-down
P02763	Alpha-1-acid glycoprotein 1 OS=Homo sapiens OX=9606 GN=ORM1 PE=1 SV=1	ORM1	0,18	C	0,9723	-0,55	MTEX-down
P07237	Protein disulfide-isomerase OS=Homo sapiens OX=9606 GN=P4HB PE=1 SV=3	P4HB	0,45	C	0,9681	-0,53	MTEX-down
Q9UHG3	Prenylcysteine oxidase 1 OS=Homo sapiens OX=9606 GN=PCYOX1 PE=1 SV=3	PCYOX1	0,30	C	0,9973	-0,77	MTEX-down
P01833	Polymeric immunoglobulin receptor OS=Homo sapiens OX=9606 GN=PIGR PE=1 SV=4	PIGR	0,50	C	0,9723	-0,55	MTEX-down
O00444	Serine/threonine-protein kinase PLK4 OS=Homo sapiens OX=9606 GN=PLK4 PE=1 SV=3	PLK4	<0,01	C	0,9794	-0,58	MTEX-down

O00592	Podocalyxin OS=Homo sapiens OX=9606 GN=PODXL PE=1 SV=2	PODXL	<0,01	C	0,9635	-0,52	MTEX-down
P07225	Vitamin K-dependent protein S OS=Homo sapiens OX=9606 GN=PROS1 PE=1 SV=1	PROS1	0,67	C	0,9760	-0,57	MTEX-down
O00391	Sulfhydryl oxidase 1 OS=Homo sapiens OX=9606 GN=QSOX1 PE=1 SV=3	QSOX1	<0,01	C	0,9872	-0,63	MTEX-down
P05109	Protein S100-A8 OS=Homo sapiens OX=9606 GN=S100A8 PE=1 SV=1	S100A8	<0,01	C	0,9635	-0,52	MTEX-down
P29622	Kallistatin OS=Homo sapiens OX=9606 GN=SERPINA4 PE=1 SV=3	SERPINA4	0,17	C	0,9849	-0,62	MTEX-down
Q9H299	SH3 domain-binding glutamic acid-rich-like protein 3 OS=Homo sapiens OX=9606	SH3BGRL3	<0,01	C	1,0000	-1,00	MTEX-down
Q8IWA5	Choline transporter-like protein 2 OS=Homo sapiens OX=9606 GN=SLC44A2 PE=1 SV=3	SLC44A2	0,37	C	0,9910	-0,67	MTEX-down
P11277	Spectrin beta chain, erythrocytic OS=Homo sapiens OX=9606 GN=SPTB PE=1 SV=5	SPTB	<0,01	C	0,9892	-0,65	MTEX-down
P02787	Serotransferrin OS=Homo sapiens OX=9606 GN=TF PE=1 SV=3	TF	0,49	C	0,9723	-0,55	MTEX-down

Table 12. List of proteins up- and downregulated in MTEX (binary/descrete analysis).

Accession	Protein Description	Gene Symbol	Type of analysis (continuous vs. binary)	MTEX/NMTEX (median)	McNemar test p-value	Effect Size (Coehn g)	STATUS
Q76LX8	A disintegrin and metalloproteinase with thrombospondin motifs 13 OS=Homo sapiens OX=9606 GN=ADAMTS13 PE=1 SV=1	ADAMTS13	B	>100	0,037	0,500	MTEX-UP
P52895	Aldo-keto reductase family 1 member C2 OS=Homo sapiens OX=9606 GN=AKR1C2 PE=1 SV=3	AKR1C2	B	>100	0,037	0,500	MTEX-UP
Q7RTV2	Glutathione S-transferase A5 OS=Homo sapiens OX=9606 GN=GSTA5 PE=1 SV=1	GSTA5	B	>100	0,037	0,500	MTEX-UP
P55268	Laminin subunit beta-2 OS=Homo sapiens OX=9606 GN=LAMB2 PE=1 SV=2	LAMB2	B	>100	0,037	0,500	MTEX-UP
Q02809	Procollagen-lysine,2-oxoglutarate 5-dioxygenase 1 OS=Homo sapiens OX=9606 GN=PLOD1 PE=1	PLOD1	B	>100	0,037	0,500	MTEX-UP
O15305	Phosphomannomutase 2 OS=Homo sapiens OX=9606 GN=PMM2 PE=1 SV=1	PMM2	B	>100	0,012	0,500	MTEX-UP
O43490	Prominin-1 OS=Homo sapiens OX=9606 GN=PROM1 PE=1 SV=1	PROM1	B	>100	0,037	0,500	MTEX-UP
P51812	Ribosomal protein S6 kinase alpha-3 OS=Homo sapiens OX=9606 GN=RPS6KA3 PE=1 SV=1	RPS6KA3	B	>100	0,037	0,500	MTEX-UP
P31947	14-3-3 protein sigma OS=Homo sapiens OX=9606 GN=SFN PE=1 SV=1	SFN	B	>100	0,037	0,500	MTEX-UP
O43556	Epsilon-sarcoglycan OS=Homo sapiens OX=9606 GN=SGCE PE=1 SV=6	SGCE	B	46,2	0,037	0,500	MTEX-UP
A0AVT1	Ubiquitin-like modifier-activating enzyme 6 OS=Homo sapiens OX=9606 GN=UBA6 PE=1 SV=1	UBA6	B	>100	0,037	0,500	MTEX-UP
Q8TD06	Anterior gradient protein 3 OS=Homo sapiens OX=9606 GN=AGR3 PE=1 SV=1	AGR3	B	2,21	0,5000	-0,50	MTEX-down
P16157	Ankyrin-1 OS=Homo sapiens OX=9606 GN=ANK1 PE=1 SV=3	ANK1	B	<0,01	0,8759	-0,50	MTEX-down
Q9BQE5	Apolipoprotein L2 OS=Homo sapiens OX=9606 GN=APOL2 PE=1 SV=1	APOL2	B	0,01	0,9883	-0,50	MTEX-down
Q68EM7	Rho GTPase-activating protein 17 OS=Homo sapiens OX=9606 GN=ARHGAP17 PE=1 SV=1	ARHGAP17	B	<0,01	0,9332	-0,50	MTEX-down
P80723	Brain acid soluble protein 1 OS=Homo sapiens OX=9606 GN=BASP1 PE=1 SV=2	BASP1	B	0,40	0,5000	-0,50	MTEX-down
Q03591	Complement factor H-related protein 1 OS=Homo sapiens OX=9606 GN=CFHR1 PE=1 SV=2	CFHR1	B	<0,01	0,9632	-0,50	MTEX-down
P09172	Dopamine beta-hydroxylase OS=Homo sapiens OX=9606 GN=DBH PE=1 SV=3	DBH	B	0,01	0,8759	-0,50	MTEX-down

Q9Y6C2	EMILIN-1 OS=Homo sapiens OX=9606 GN=EMILIN1 PE=1 SV=3	EMILIN1	B	<0,01	0,9632	-0,50	MTEX-down
O00602	Ficolin-1 OS=Homo sapiens OX=9606 GN=FCN1 PE=1 SV=2	FCN1	B	<0,01	0,9332	-0,50	MTEX-down
P20930	Filaggrin OS=Homo sapiens OX=9606 GN=FLG PE=1 SV=3	FLG	B	<0,01	0,5000	-0,50	MTEX-down
Q5VW36	Focadhesin OS=Homo sapiens OX=9606 GN=FOCAD PE=1 SV=1	FOCAD	B	0,05	0,7602	-0,50	MTEX-down
P69891	Hemoglobin subunit gamma-1 OS=Homo sapiens OX=9606 GN=HBG1 PE=1 SV=2	HBG1	B	<0,01	0,9632	-0,50	MTEX-down
Q01629	Interferon-induced transmembrane protein 2 OS=Homo sapiens OX=9606 GN=IFITM2 PE=1	IFITM2	B	<0,01	0,9332	-0,50	MTEX-down
Q14525	Keratin, type I cuticular Ha3-II OS=Homo sapiens OX=9606 GN=KRT33B PE=1 SV=3	KRT33B	B	<0,01	0,5000	-0,50	MTEX-down
O95678	Keratin, type II cytoskeletal 75 OS=Homo sapiens OX=9606 GN=KRT75 PE=1 SV=2	KRT75	B	<0,01	0,7602	-0,50	MTEX-down
P78386	Keratin, type II cuticular Hb5 OS=Homo sapiens OX=9606 GN=KRT85 PE=1 SV=1	KRT85	B	<0,01	0,5000	-0,50	MTEX-down
Q96S97	Myeloid-associated differentiation marker OS=Homo sapiens OX=9606 GN=MYADM PE=1 SV=2	MYADM	B	0,23	0,8759	-0,50	MTEX-down
P24844	Myosin regulatory light polypeptide 9 OS=Homo sapiens OX=9606 GN=MYL9 PE=1 SV=4	MYL9	B	5,09	0,5000	-0,50	MTEX-down
Q15149	Plectin OS=Homo sapiens OX=9606 GN=PLEC PE=1 SV=3	PLEC	B	<0,01	0,5000	-0,50	MTEX-down
P02549	Spectrin alpha chain, erythrocytic 1 OS=Homo sapiens OX=9606 GN=SPTA1 PE=1 SV=5	SPTA1	B	<0,01	0,8759	-0,50	MTEX-down
Q658P3	Metalloreductase STEAP3 OS=Homo sapiens OX=9606 GN=STEAP3 PE=1 SV=2	STEAP3	B	<0,01	0,9632	-0,50	MTEX-down
Q8WUA8	Tsukushin OS=Homo sapiens OX=9606 GN=TSKU PE=2 SV=3	TSKU	B	<0,01	0,5000	-0,50	MTEX-down
Q8WZ42	Titin OS=Homo sapiens OX=9606 GN=TTN PE=1 SV=4	TTN	B	<0,01	0,5000	-0,50	MTEX-down

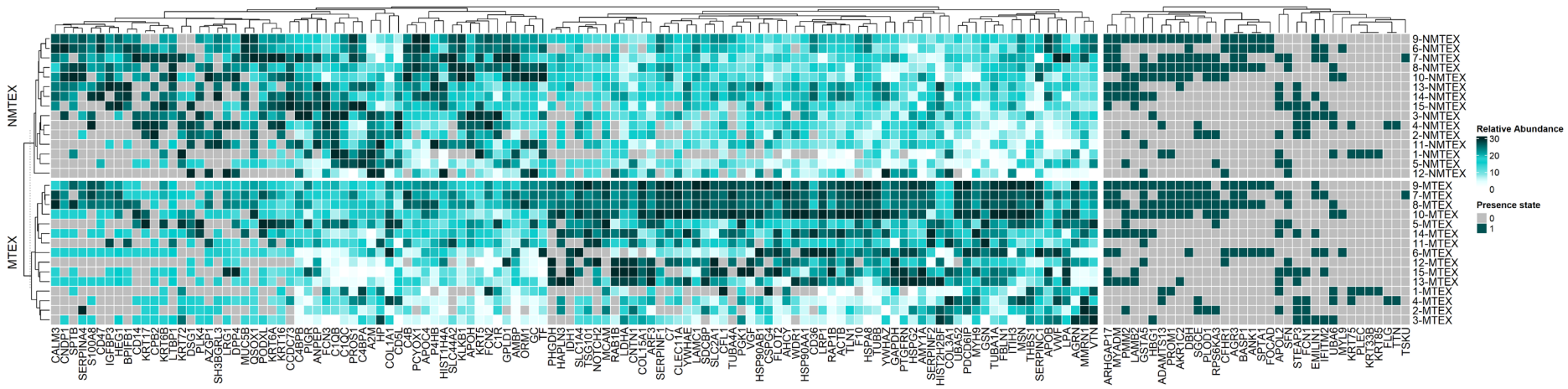

Figure 14. The heat map represents the abundance difference of differentially expressed proteins (DEPs) discriminating MTEX from NMTEX in melanoma patients. Left side shows DEPs from continuous analysis (RBCC > 0.5; abundances are color-coded according to ranks of all normalized signals). Right part shows DEPs from discrete analysis (Crammer's V effect size > 0.5). The abundance is color-coded according to present/absent status as yes/no (1 or 0, respectively).

Out of 73 proteins overexpressed in MTEX (continuous and binary analysis), 16 proteins were selected as a proposal to form a panel distinguishing MTEX from NMTEX, which can be potentially used in differential analysis of sEV in plasma of melanoma patients. The criteria for selection were: (i) detection in more than half of MTEX samples; (ii) existing evidence for their involvement in cancer growth and progression. The potential discriminating panel includes: adenosylhomocysteinase (AHCY), L-lactate dehydrogenase (LDHA), gelsolin (GSN), neurogenic locus notch homolog protein (NOTCH2), thrombospondin (THBS1), ubiquitin-60S ribosomal protein (UBA52), talin (TLN1), phosphoglycerate kinase 1 (PGK1), pigment epithelium-derived factor (SERPINF2), WD repeat-containing protein 1 (WDR1), chondroitin sulfate proteoglycan 4 (CSPG4), moesin (MSN), neutral amino acid transporter A (SLC1A4), 14-3-3 protein epsilon (YWHAE), tumor susceptibility gene 101 protein (TSG101), ras-related protein Rap-1b (RAP1B) (Fig. 15). It is worth noting that tumor antigen CSPG4 used for immunocapture of MTEX from the rest of sEV circulating in plasma, was detected by LC-MS/MS in all MTEX samples. In MTEX, CSPG4 was significantly overexpressed with 19-fold median upregulation compared to NMTEX.

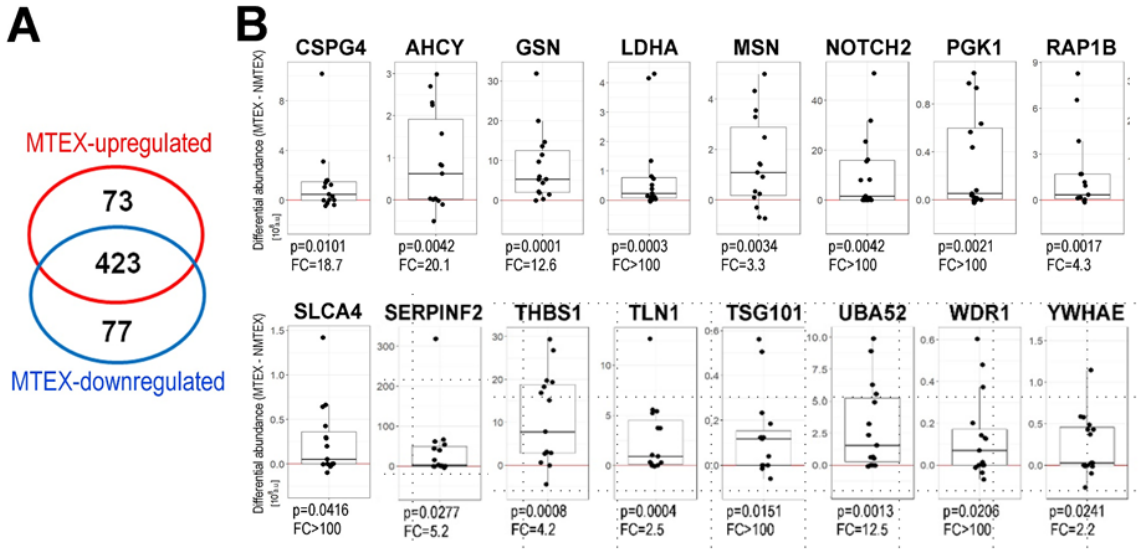

Figure 15. Differentially expressed proteins in MTEX relative to NMTEX. Panel A – the Venn diagram shows the numbers of proteins upregulated or downregulated in MTEX. Panel B – differences in the levels of specific proteins between paired MTEX and NMTEX samples; boxplots show median, upper and lower quartile, maximum and minimum (dots represent individual patients; the red line represents no difference between MTEX and NMTEX, FC – average fold-change) [modified Pietrowska et al. 2021].

What's more, the protein upregulated in MTEX were verified if present in melanoma cells. For this reason dataset of upregulated proteins in melanoma-derived sEV was compared with , immunohistochemical data from the Human Protein Atlas (https://www.proteinatlas.org/) and with transcriptomic data in the TCGA melanoma dataset (https://www.cancer.gov/ccg/research/genome-sequencing/tcga). It's appeared that the majority of proteins upregulated in MTEX were found in both of the aforementioned databases of proteins specific for melanoma tissue (Table 13). Notably, 10 of the MTEX-associated proteins were identified within the melanosome compartment (GO:0042470). These results confirm the origin of MTEX, as sEV released by melanoma cells and possibility they could serve as "liquid cancer biopsy".

Table 13. Expression of MTEX-upregulated proteins in melanoma tissue.

Gene Symbol	Protein Description	Transcript level (TCGA data) [FPKM value]	Protein expression (Protein Atlas data)	Melanosome (GO:0042470)
ACTB	Actin, cytoplasmic 1 OS=Homo sapiens OX=9606 GN=ACTB PE=1 SV=1	1415,16	Medium*	
ADAMTS13	A disintegrin and metalloproteinase with thrombospondin motifs 13 OS=Homo sapiens OX=9606 GN=ADAMTS13 PE=1 SV=1	0,83	Medium*	
AGRN	Agrin OS=Homo sapiens OX=9606 GN=AGRN PE=1 SV=6	32,4	Low	
AHCY	Adenosylhomocysteinase OS=Homo sapiens OX=9606 GN=AHCY PE=1 SV=4	62,17	Medium*	YES
AKR1C2	Aldo-keto reductase family 1 member C2 OS=Homo sapiens OX=9606 GN=AKR1C2 PE=1 SV=3	0,19	Not detected	
AMY1A	Alpha-amylase 1 OS=Homo sapiens OX=9606 GN=AMY1A PE=1 SV=2	N/A	Not detected	
APOB	Apolipoprotein B-100 OS=Homo sapiens OX=9606 GN=APOB PE=1 SV=2	0,0	Not detected	
ARF3	ADP-ribosylation factor 3 OS=Homo sapiens OX=9606 GN=ARF3 PE=1 SV=2	54,65	N/A	
C7	Complement component C7 OS=Homo sapiens OX=9606 GN=C7 PE=1 SV=2	0,05	Low	
CD36	Platelet glycoprotein 4 OS=Homo sapiens OX=9606 GN=CD36 PE=1 SV=2	0,84	Not detected	
CFL1	Cofilin-1 OS=Homo sapiens OX=9606 GN=CFL1 PE=1 SV=3	190,73	Medium*	
CLEC11A	C-type lectin domain family 11 member A OS=Homo sapiens OX=9606 GN=CLEC11A PE=1 SV=1	27,21	Low	
CNTN1	Contactin-1 OS=Homo sapiens OX=9606 GN=CNTN1 PE=1 SV=1	0,58	Not detected	
COL15A1	Collagen alpha-1(XV) chain OS=Homo sapiens OX=9606 GN=COL15A1 PE=1 SV=2	12,02	Low*	
COL1A1	Collagen alpha-1(I) chain OS=Homo sapiens OX=9606 GN=COL1A1 PE=1 SV=5	141,57	Not detected	
COL3A1	Collagen alpha-1(III) chain OS=Homo sapiens OX=9606 GN=COL3A1 PE=1 SV=4	86,56	Not detected*	
CSPG4	Chondroitin sulfate proteoglycan 4 OS=Homo sapiens OX=9606 GN=CSPG4 PE=1 SV=2	59,79	High*	

F10	Coagulation factor X OS=Homo sapiens OX=9606 GN=F10 PE=1 SV=2	0,48	N/A	
FBLN1	Fibulin-1 OS=Homo sapiens OX=9606 GN=FBLN1 PE=1 SV=4	8,09	Not detected	
FLOT2	Flotillin-2 OS=Homo sapiens OX=9606 GN=FLOT2 PE=1 SV=2	40,59	High*	
GAPDH	Glyceraldehyde-3-phosphate dehydrogenase OS=Homo sapiens OX=9606 GN=GAPDH PE=1 SV=3	1550,8	Medium*	
GSN	Gelsolin OS=Homo sapiens OX=9606 GN=GSN PE=1 SV=1	63,45	Medium*	
GSTA5	Glutathione S-transferase A5 OS=Homo sapiens OX=9606 GN=GSTA5 PE=1 SV=1	N/A	Low*	
HAPLN3	Hyaluronan and proteoglycan link protein 3 OS=Homo sapiens OX=9606 GN=HAPLN3 PE=2 SV=1	6,25	Low	
HIST2H2BF	Histone H2B type 2-F OS=Homo sapiens OX=9606 GN=HIST2H2BF PE=1 SV=3	0,11	High*	
HSP90AA1	Heat shock protein HSP 90-alpha OS=Homo sapiens OX=9606 GN=HSP90AA1 PE=1 SV=5	203,76	Not detected	YES
HSP90AB1	Heat shock protein HSP 90-beta OS=Homo sapiens OX=9606 GN=HSP90AB1 PE=1 SV=4	681,64	High*	YES
HSPA8	Heat shock cognate 71 kDa protein OS=Homo sapiens OX=9606 GN=HSPA8 PE=1 SV=1	266,06	Low*	YES
HSPG2	Basement membrane-specific heparan sulfate proteoglycan core protein OS=Homo sapiens OX=9606	16,03	Medium*	
IDH1	Isocitrate dehydrogenase [NADP] cytoplasmic OS=Homo sapiens OX=9606 GN=IDH1 PE=1 SV=2	11,84	Not detected	
ITIH3	Inter-alpha-trypsin inhibitor heavy chain H3 OS=Homo sapiens OX=9606 GN=ITIH3 PE=1 SV=2	0,09	Medium	
LAMB2	Laminin subunit beta-2 OS=Homo sapiens OX=9606 GN=LAMB2 PE=1 SV=2	58,33	High*	
LAMC1	Laminin subunit gamma-1 OS=Homo sapiens OX=9606 GN=LAMC1 PE=1 SV=3	34,97	Medium*	
LDHA	L-lactate dehydrogenase A chain OS=Homo sapiens OX=9606 GN=LDHA PE=1 SV=2	142,71	High*	
LPA	Apolipoprotein(a) OS=Homo sapiens OX=9606 GN=LPA PE=1 SV=1	N/A	Low	
LRP1	Prolow-density lipoprotein receptor-related protein 1 OS=Homo sapiens OX=9606 GN=LRP1 PE=1 SV=2	11,9	Not detected	

MCAM	Cell surface glycoprotein MUC18 OS=Homo sapiens OX=9606 GN=MCAM PE=1 SV=2	53,65	High	
MMRN1	Multimerin-1 OS=Homo sapiens OX=9606 GN=MMRN1 PE=1 SV=3	0,12	Not detected	
MSN	Moesin OS=Homo sapiens OX=9606 GN=MSN PE=1 SV=3	130,08	Medium*	
MYH9	Myosin-9 OS=Homo sapiens OX=9606 GN=MYH9 PE=1 SV=4	114,36	Medium*	
NOTCH2	Neurogenic locus notch homolog protein 2 OS=Homo sapiens OX=9606 GN=NOTCH2 PE=1 SV=3	10,19	Medium	
PDCD6IP	Programmed cell death 6-interacting protein OS=Homo sapiens OX=9606 GN=PDCD6IP PE=1 SV=1	15,45	Not detected	YES
PGK1	Phosphoglycerate kinase 1 OS=Homo sapiens OX=9606 GN=PGK1 PE=1 SV=3	98,94	High*	
PHGDH	D-3-phosphoglycerate dehydrogenase OS=Homo sapiens OX=9606 GN=PHGDH PE=1 SV=4	15,52	High	
PLOD1	Procollagen-lysine,2-oxoglutarate 5-dioxygenase 1 OS=Homo sapiens OX=9606 GN=PLOD1 PE=1 SV=2	64,57	Medium*	
PMM2	Phosphomannomutase 2 OS=Homo sapiens OX=9606 GN=PMM2 PE=1 SV=1	2,11	Low	
PROM1	Prominin-1 OS=Homo sapiens OX=9606 GN=PROM1 PE=1 SV=1	0,2	Low*	
PTGFRN	Prostaglandin F2 receptor negative regulator OS=Homo sapiens OX=9606 GN=PTGFRN PE=1 SV=2	14,94	Low	
RAB1B	Ras-related protein Rab-1B OS=Homo sapiens OX=9606 GN=RAB1B PE=1 SV=1	108,72	Medium	
RAP1B	Ras-related protein Rap-1b OS=Homo sapiens OX=9606 GN=RAP1B PE=1 SV=1	2,06	N/A	
RPS6KA3	Ribosomal protein S6 kinase alpha-3 OS=Homo sapiens OX=9606 GN=RPS6KA3 PE=1 SV=1	7,72	Medium*	
SDCBP	Syntenin-1 OS=Homo sapiens OX=9606 GN=SDCBP PE=1 SV=1	203,54	High	YES
SERPINC1	Antithrombin-III OS=Homo sapiens OX=9606 GN=SERPINC1 PE=1 SV=1	0,04	Low*	
SERPINF1	Pigment epithelium-derived factor OS=Homo sapiens OX=9606 GN=SERPINF1 PE=1 SV=4	84,98	Medium	YES
SERPINF2	Alpha-2-antiplasmin OS=Homo sapiens OX=9606 GN=SERPINF2 PE=1 SV=3	0,92	Medium*	

SFN	14-3-3 protein sigma OS=Homo sapiens OX=9606 GN=SFN PE=1 SV=1	26,99	Low*	
SGCE	Epsilon-sarcoglycan OS=Homo sapiens OX=9606 GN=SGCE PE=1 SV=6	15,12	N/A	
SLC1A4	Neutral amino acid transporter A OS=Homo sapiens OX=9606 GN=SLC1A4 PE=1 SV=1	17,78	High	YES
SLC2A1	Solute carrier family 2, facilitated glucose transporter member 1 OS=Homo sapiens OX=9606 GN=SLC2A1	17,29	Low*	
THBS1	Thrombospondin-1 OS=Homo sapiens OX=9606 GN=THBS1 PE=1 SV=2	6,63	Medium	
TLN1	Talin-1 OS=Homo sapiens OX=9606 GN=TLN1 PE=1 SV=3	43,02	Medium	
TSG101	Tumor susceptibility gene 101 protein OS=Homo sapiens OX=9606 GN=TSG101 PE=1 SV=2	18,31	Medium*	
TUBA1A	Tubulin alpha-1A chain OS=Homo sapiens OX=9606 GN=TUBA1A PE=1 SV=1	70,52	High*	
TUBA4A	Tubulin alpha-4A chain OS=Homo sapiens OX=9606 GN=TUBA4A PE=1 SV=1	3,99	High*	
TUBB	Tubulin beta chain OS=Homo sapiens OX=9606 GN=TUBB PE=1 SV=2	364,11	Medium*	
UBA52	Ubiquitin-60S ribosomal protein L40 OS=Homo sapiens OX=9606 GN=UBA52 PE=1 SV=2	127,79	Medium*	
UBA6	Ubiquitin-like modifier-activating enzyme 6 OS=Homo sapiens OX=9606 GN=UBA6 PE=1 SV=1	3,08	Not detected	
VGF	Neurosecretory protein VGF OS=Homo sapiens OX=9606 GN=VGF PE=1 SV=2	23,26	Not detected	
VTN	Vitronectin OS=Homo sapiens OX=9606 GN=VTN PE=1 SV=1	0,29	Not detected	
VWF	von Willebrand factor OS=Homo sapiens OX=9606 GN=VWF PE=1 SV=4	5,15	Not detected	
WDR1	WD repeat-containing protein 1 OS=Homo sapiens OX=9606 GN=WDR1 PE=1 SV=4	56,08	High*	
YWHAE	14-3-3 protein epsilon OS=Homo sapiens OX=9606 GN=YWHAE PE=1 SV=1	130,78	Medium*	YES
YWHAZ	14-3-3 protein zeta/delta OS=Homo sapiens OX=9606 GN=YWHAZ PE=1 SV=1	88,9	High	YES

Additionally, in the preliminary proteomic analysis, the NMTEX proteome was compared with the proteome of total sEV fraction#4 isolated from the plasma of healthy donors (n=10). Since the plasma of healthy donors does not contain MTEX, there was no possibility of comparing MTEX/NTMEX from melanoma patients vs healthy donors. Analysis showed that 431 proteins were shared between the total sEV fraction of healthy donors and NMTEX (Fig. 16A). 75 proteins were upregulated in NMTEX. These data suggest that the proteomic profiles of NMTEX and sEV isolated from the plasma of healthy donors are partly distinct (Fig. 16B), and that the biological significance of these differences deserves to be independently evaluated in future studies.

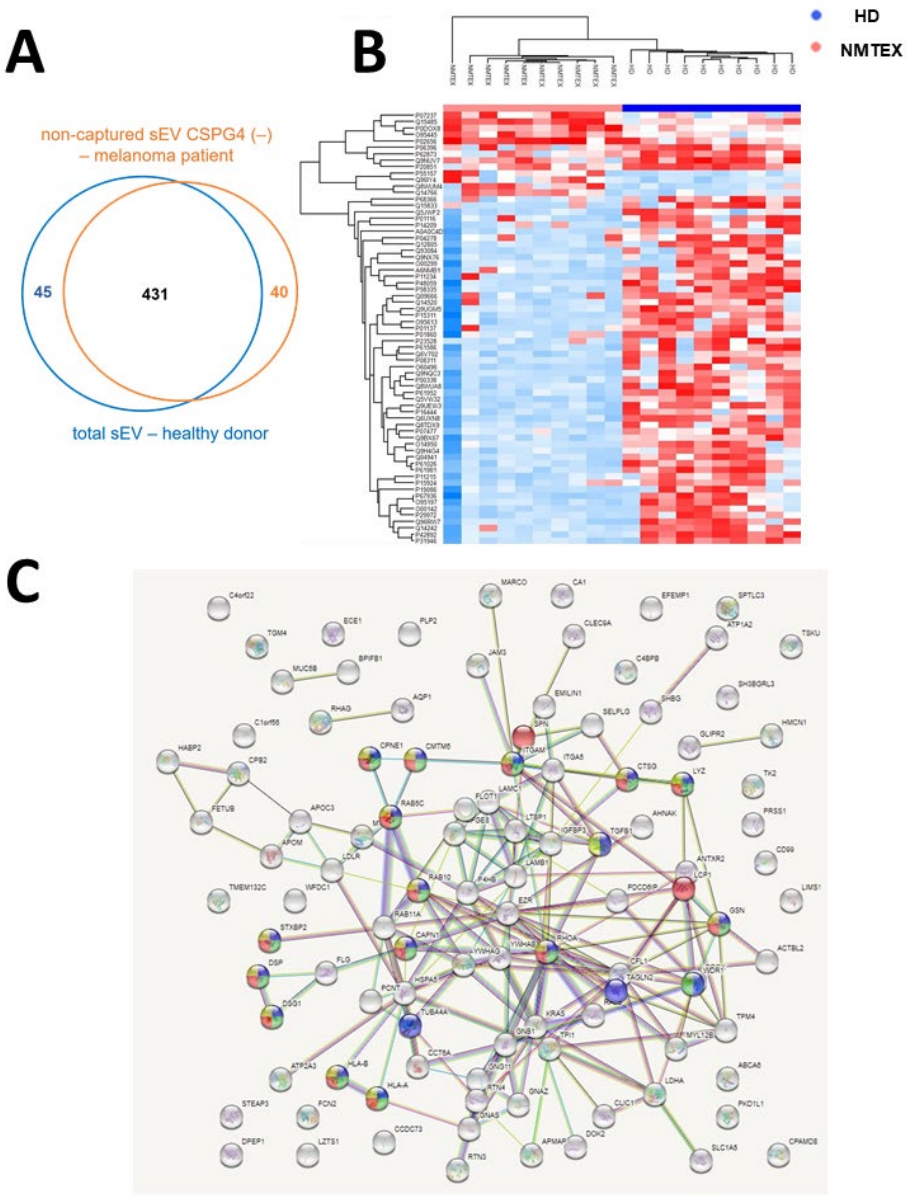

Figure 16. Comparison of the proteomic profile of non-captured sEV from melanoma patients (NMTEX) with total sEV from healthy donors. Panel A: Venn diagram showing the number of proteins present in NMTEX and total sEV from healthy donors. Panel B: A heat map presenting differential protein levels between total sEV of individual healthy donors (n=10) and NMTEX of melanoma patients (n=10). Panel C: The network of potential interactions between proteins differentiating sEV of healthy donors from NMTEX of melanoma patients – String db - database; color coding blue: GO: 0045055 Regulated exocytosis (FDR=3.16x10^{-6}); green – GO: 0002446 Neutrophil-mediated immunity (FDR=5.33x10^{-6}); red – GO: 0002366 Leukocyte activation involved in immune response (FDR=1.04x10^{-5}); yellow – GO: 0002271 Myeloid leukocyte activation (FDR: 1.64x10^{-5}); the strength of interactions is below 0,7 for all proteins in these GO terms.

4.2.2. Biological pathways associated with MTEX proteins.

To further describe the potential functional significance of proteins identified in MTEX, the gene ontology (GO) enrichment analysis was performed. For analysis, 496 proteins expressed in MTEX and their annotated genes were selected (proteins downregulated in MTEX and immunoglobulins were filtered out). Of the 2665 statistically overrepresented GO terms, 2012 had FDR below 0.05. Among them were terms: extracellular structure organization (81 proteins), extracellular matrix organization (57 proteins), wound healing (87 proteins), acute inflammatory response (44 proteins), neutrophil activation involved in immune response (76 proteins), neutrophil mediated immunity (79 proteins), myeloid leukocyte mediated immunity (79 proteins), regulation of vesicle-mediated transport (54 proteins).

Analyses were then narrowed to identify biological pathways associated with 73 proteins upregulated in MTEX, with all 573 identified proteins used as reference. Only terms with at least 3 and at most 600 genes assigned were tested using a classic hypergeometric test. The results show that 393 terms were statistically significant: 320 for biological processes, 44 for the cellular compartment, and 29 for molecular function. One term „establishment of cell polarity" had an FDR equal to 0.048. Proteins assigned to this term and overexpressed in MTEX are: CFL1, FLOT2, GSN, HSP90AA1, HSP90AB1, MSN, MYH9, RAP1B. The KEGG enrichment analysis showed three significantly enriched pathways: PI3K-Akt signaling pathway, pathogenic Escherichia coli infection, ECM-receptor interaction (p-value <0.05). No pathway had FDR<0.05. On the other hand, Reactom pathway enrichment analysis showed that 36 pathways were overrepresented in a gene set (at the level of 5% (p value)). However, twelve pathways linked with signal transduction, cell cycle, vesicle-mediated transport, cell adhesion, and protein glycosylation stayed with statistical significance after the FDR correction ($q < 0.05$) (Fig. 17).

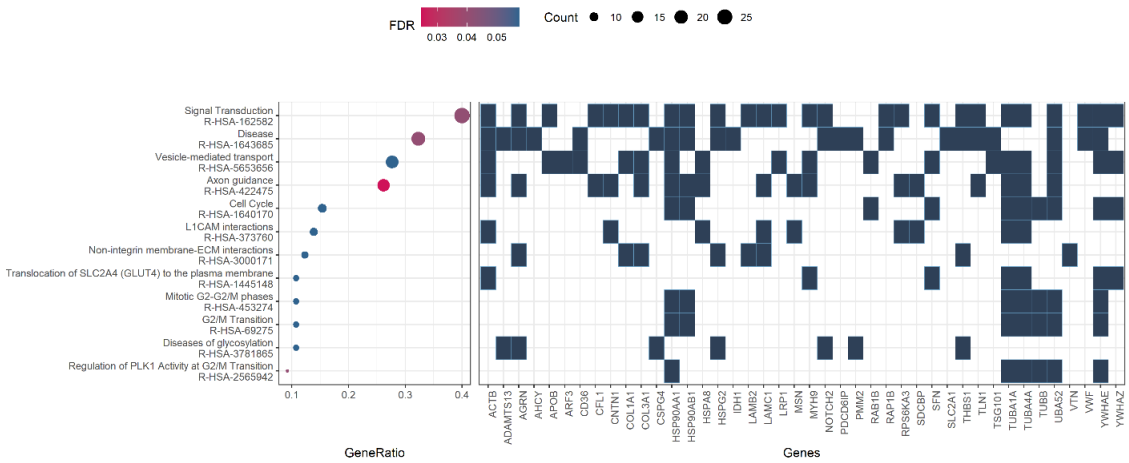

Figure 17. Results of Reactom pathway enrichment analysis: the left side of the panel shows a dot-plot with significantly enriched Reactome pathways (q < 0.05) coloured by FDR, right side of the panel shows proteins/genes ratio for each pathway.

The String-db database was used to illustrate possible interactions among all 73 proteins upregulated in MTEX (Szklarczyk et al. 2019). Potential functional enrichments in the protein network were related to the regulation of biological and cellular processes, response to stimulus, and anatomical structure development (Fig. 18).

Enriched molecular functions (GO) of the overexpressed protein set were connected with cell adhesion, extracellular matrix and cytoskeleton, and signaling receptor binding (Fig. 19). To sum up, our result allows us to speculate that proteins detected in MTEX are specifically linked to processes connected with cell cycle, signal transduction, extracellular matrix / cytoskeleton remodeling and functions of the immune system.

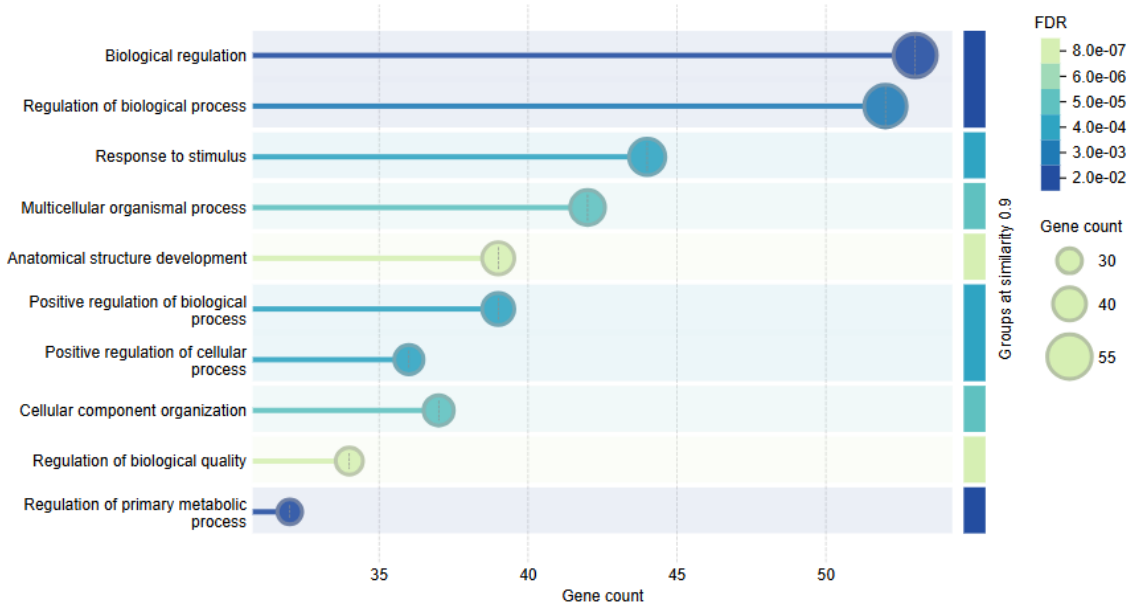

Figure 18. Biological process (GO) enrichment for the network of 73 proteins upregulated in MTEX, the whole genome was used as a reference (String-db database).

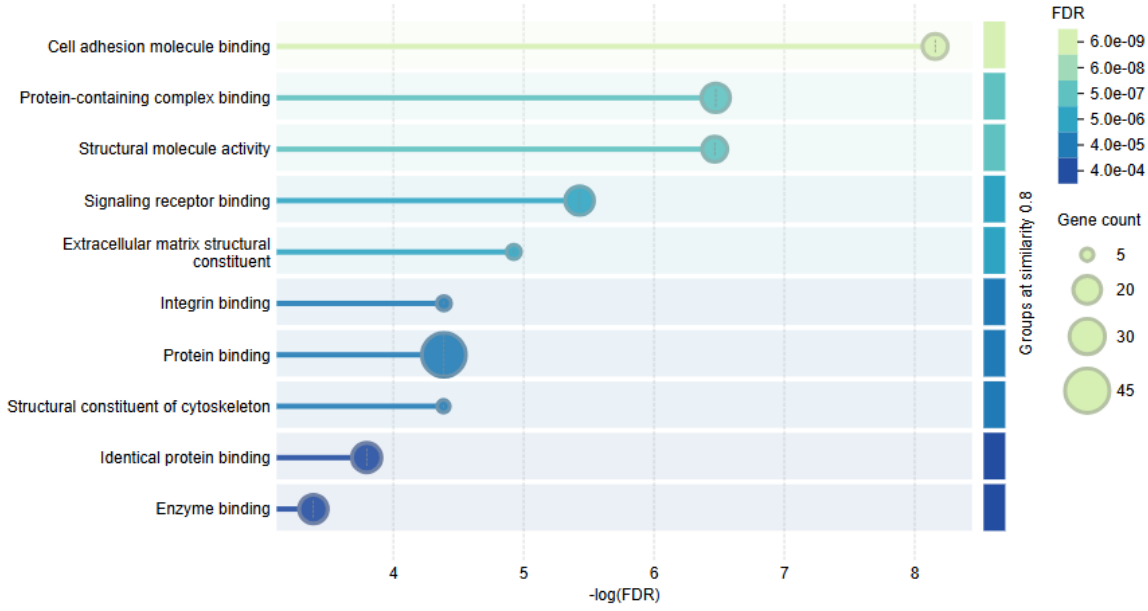

Figure 19. Molecular function (GO) enrichment for the network of 73 proteins upregulated in MTEX, where whole genome was used as reference (String-db database).

4.2.3. Proteomic signature of melanoma progression.

At the last stage of the MTEX molecular composition analysis, we addressed whether the proteomic signature of MTEX reflects the patient's health state. The group of melanoma patients (n=15) under study included individuals with no evidence of or stable disease (NED/SD, n=8), or with disease progression (PD, n=7) at the time of the

blood draw (Table 7). All patients received previous treatment for metastatic melanoma. To tackle this question the protein content of MTEX was compared between both groups of patients using the U-Mann-Whitney test with corresponding Wendt effect size. Among 83 proteins differentially expressed in NED/SD versus PD group ($p < 0.05$) (Table 14), 75 proteins had higher expression levels in the PD group with 12 proteins significantly upregulated in MTEX relative to NMTEX. These proteins are: PDCD6IP, HSP90AB1, ITIH3, MSN, THBS1, TUBB, UBA52, F10, PLOD1, RPS6KA3, SGCE, ADAMTS13 (the data for eight of these proteins are shown in Figure 20A). On the other hand, eight proteins exhibited significantly lower levels in MTEX of patients with PD than in those with NED/SD. The data for three of these proteins, including CNTM1 (contactin1, the only protein consistently upregulated in MTEX of NED/SD patients), are shown in Figure 20B.

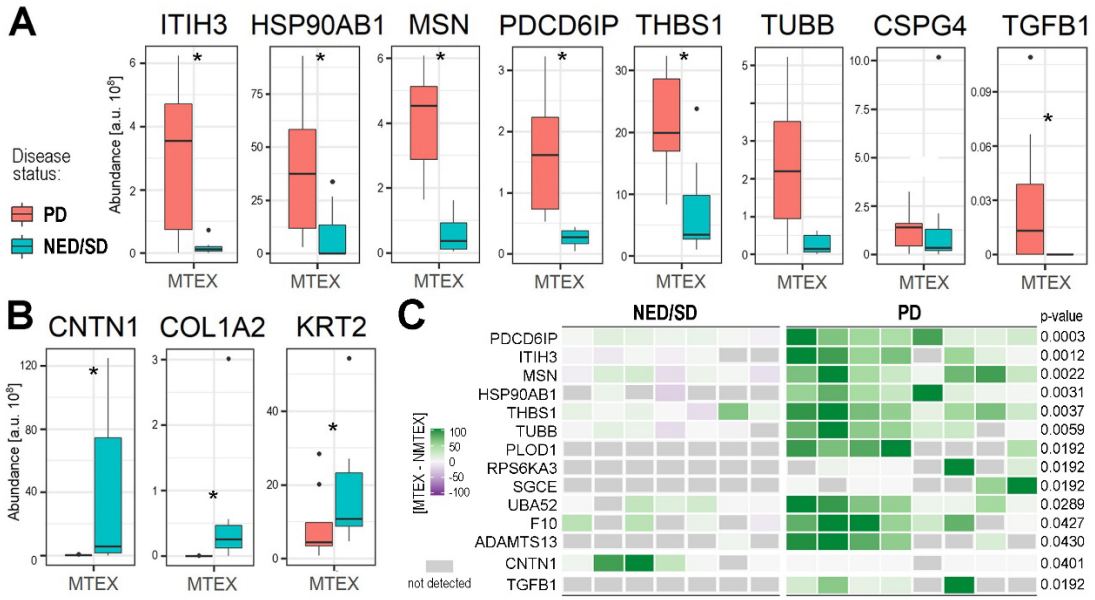

Figure 20. Differentially expressed proteins in MTEX of melanoma patients with PD relative to MTEX of melanoma patients with NED/SD. Panel A – MTEX proteins with significantly higher levels in patients with PD. Panel B – MTEX proteins with significantly higher levels in patients with NED/SD. Boxplots show median, upper and lower quartile, maximum, and minimum; dots represent outliers. The statistical significance of differences between patient subgroups ($P < 0.05$) is marked with asterisks. Panel C – A heat map presenting the differential (MTEX-NMTEX) protein levels in individual melanoma patients with NED/SD (n = 7) or PD (n = 8). Twelve proteins found to be upregulated in MTEX of melanoma patients with PD are listed. Moreover, the levels of CNTN1 and TGFβ1 are presented in the corresponding samples. The relative levels of the listed proteins is colour-coded where gray boxes represent not detected proteins; P-values represent the significance of the difference between patients' subgroups of the differential (MTEX-NMTEX) value [Pietrowska et al. 2021].

Table 14. List of proteins differentiating patients with different disease status.

Accession	Protein Description	Gene Symbol	differential (MTEX-NMTEX) abundances in patients with a different disease status [p-value]	differential (MTEX-NMTEX) abundances in patients with a different disease status [Wendt effect size rU]	progressing disease vs. stable disease
P01023	Alpha-2-macroglobulin OS=Homo sapiens OX=9606 GN=A2M PE=1 SV=3	A2M	0,0037	-0,857	HIGHER
P16112	Aggrecan core protein OS=Homo sapiens OX=9606 GN=ACAN PE=1 SV=3	ACAN	0,0270	-0,679	HIGHER
P12821	Angiotensin-converting enzyme OS=Homo sapiens OX=9606 GN=ACE PE=1 SV=1	ACE	0,0223	-0,643	HIGHER
P21399	Cytoplasmic aconitate hydratase OS=Homo sapiens OX=9606 GN=ACO1 PE=1 SV=3	ACO1	0,0327	-0,571	HIGHER
P68133	Actin, alpha skeletal muscle OS=Homo sapiens OX=9606 GN=ACTA1 PE=1 SV=1	ACTA1	0,0371	-0,661	HIGHER
Q76LX8	A disintegrin and metalloproteinase with thrombospondin motifs 13	ADAMTS13	0,0430	-0,571	HIGHER
Q9Y653	Adhesion G-protein coupled receptor G1 OS=Homo sapiens OX=9606 GN=ADGRG1 PE=1 SV=2	ADGRG1	0,0450	-0,500	HIGHER
P02771	Alpha-fetoprotein OS=Homo sapiens OX=9606 GN=AFP PE=1 SV=1	AFP	0,0192	-0,625	HIGHER
P14550	Alcohol dehydrogenase [NADP(+)] OS=Homo sapiens OX=9606 GN=AKR1A1 PE=1 SV=3	AKR1A1	0,0195	-0,732	HIGHER
P05023	Sodium/potassium-transporting ATPase subunit alpha-1 OS=Homo sapiens	ATP1A1	0,0278	-0,696	HIGHER
O43505	Beta-1,4-glucuronyltransferase 1 OS=Homo sapiens OX=9606 GN=B4GAT1 PE=1 SV=1	B4GAT1	0,0328	-0,643	HIGHER
P80723	Brain acid soluble protein 1 OS=Homo sapiens OX=9606 GN=BASP1 PE=1 SV=2	BASP1	0,0450	0,500	LOWER
P21810	Biglycan OS=Homo sapiens OX=9606 GN=BGN PE=1 SV=2	BGN	0,0450	-0,500	HIGHER
Q5VW32	BRO1 domain-containing protein BROX OS=Homo sapiens OX=9606 GN=BROX PE=1 SV=1	BROX	0,0223	-0,643	HIGHER
P09871	Complement C1s subcomponent OS=Homo sapiens OX=9606 GN=C1S PE=1 SV=1	C1S	0,0401	0,643	LOWER
P23435	Cerebellin-1 OS=Homo sapiens OX=9606 GN=CBLN1 PE=1 SV=1	CBLN1	0,0121	-0,732	HIGHER
P50991	T-complex protein 1 subunit delta OS=Homo sapiens OX=9606 GN=CCT4 PE=1 SV=4	CCT4	0,0328	-0,643	HIGHER
Q9BZP6	Acidic mammalian chitinase OS=Homo sapiens OX=9606 GN=CHIA PE=1 SV=1	CHIA	0,0450	-0,500	HIGHER
O94985	Calsyntenin-1 OS=Homo sapiens OX=9606 GN=CLSTN1 PE=1 SV=1	CLSTN1	0,0192	-0,625	HIGHER
Q12860	Contactin-1 OS=Homo sapiens OX=9606 GN=CNTN1 PE=1 SV=1	CNTN1	0,0401	0,643	LOWER
P08123	Collagen alpha-2(I) chain OS=Homo sapiens OX=9606 GN=COL1A2 PE=1 SV=7	COL1A2	0,0113	0,786	LOWER
P12109	Collagen alpha-1(VI) chain OS=Homo sapiens OX=9606 GN=COL6A1 PE=1 SV=3	COL6A1	0,0289	-0,679	HIGHER
P15169	Carboxypeptidase N catalytic chain OS=Homo sapiens OX=9606 GN=CPN1 PE=1 SV=1	CPN1	0,0065	-0,857	HIGHER
Q99829	Copine-1 OS=Homo sapiens OX=9606 GN=CPNE1 PE=1 SV=1	CPNE1	0,0328	-0,643	HIGHER
Q9H3Z4	DnaJ homolog subfamily C member 5 OS=Homo sapiens OX=9606 GN=DNAJC5 PE=1 SV=1	DNAJC5	0,0450	-0,500	HIGHER
P13639	Elongation factor 2 OS=Homo sapiens OX=9606 GN=EEF2 PE=1 SV=4	EEF2	0,0328	-0,643	HIGHER
P00742	Coagulation factor X OS=Homo sapiens OX=9606 GN=F10 PE=1 SV=2	F10	0,0427	-0,643	HIGHER

B1AL88	Transmembrane protein FAM155A OS=Homo sapiens OX=9606 GN=FAM155A PE=2 SV=1	FAM155A	0,0329	-0,625	HIGHER
P49327	Fatty acid synthase OS=Homo sapiens OX=9606 GN=FASN PE=1 SV=3	FASN	0,0450	-0,500	HIGHER
O75955	Flotillin-1 OS=Homo sapiens OX=9606 GN=FLOT1 PE=1 SV=3	FLOT1	0,0289	-0,679	HIGHER
P02794	Ferritin heavy chain OS=Homo sapiens OX=9606 GN=FTH1 PE=1 SV=2	FTH1	0,0446	-0,589	HIGHER
P50395	Rab GDP dissociation inhibitor beta OS=Homo sapiens OX=9606 GN=GDI2 PE=1 SV=2	GDI2	0,0205	-0,732	HIGHER
Q92820	Gamma-glutamyl hydrolase OS=Homo sapiens OX=9606 GN=GGH PE=1 SV=2	GGH	0,0144	-0,714	HIGHER
Q5JWF2	Guanine nucleotide-binding protein G(s) subunit alpha isoforms XLas OS=Homo sapiens	GNAS	0,0450	-0,500	HIGHER
P80108	Phosphatidylinositol-glycan-specific phospholipase D OS=Homo sapiens OX=9606 GN=GPLD1	GPLD1	0,0093	0,786	LOWER
P22352	Glutathione peroxidase 3 OS=Homo sapiens OX=9606 GN=GPX3 PE=1 SV=2	GPX3	0,0450	-0,500	HIGHER
P28161	Glutathione S-transferase Mu 2 OS=Homo sapiens OX=9606 GN=GSTM2 PE=1 SV=2	GSTM2	0,0223	-0,643	HIGHER
P84243	Histone H3.3 OS=Homo sapiens OX=9606 GN=H3F3A PE=1 SV=2	H3F3A	0,0401	-0,643	HIGHER
Q14520	Hyaluronan-binding protein 2 OS=Homo sapiens OX=9606 GN=HABP2 PE=1 SV=1	HABP2	0,0157	-0,679	HIGHER
P08238	Heat shock protein HSP 90-beta OS=Homo sapiens OX=9606 GN=HSP90AB1 PE=1 SV=4	HSP90AB1	0,0031	-0,929	HIGHER
Q92743	Serine protease HTRA1 OS=Homo sapiens OX=9606 GN=HTRA1 PE=1 SV=1	HTRA1	0,0450	-0,500	HIGHER
P46940	Ras GTPase-activating-like protein IQGAP1 OS=Homo sapiens OX=9606 GN=IQGAP1 PE=1 SV=1	IQGAP1	0,0387	-0,554	HIGHER
Q06033	Inter-alpha-trypsin inhibitor heavy chain H3 OS=Homo sapiens OX=9606 GN=ITIH3 PE=1 SV=2	ITIH3	0,0012	-0,929	HIGHER
P04264	Keratin, type II cytoskeletal 1 OS=Homo sapiens OX=9606 GN=KRT1 PE=1 SV=6	KRT1	0,0401	0,643	LOWER
P35908	Keratin, type II cytoskeletal 2 epidermal OS=Homo sapiens OX=9606 GN=KRT2 PE=1 SV=2	KRT2	0,0093	0,786	LOWER
P25391	Laminin subunit alpha-1 OS=Homo sapiens OX=9606 GN=LAMA1 PE=1 SV=2	LAMA1	0,0401	-0,643	HIGHER
P24043	Laminin subunit alpha-2 OS=Homo sapiens OX=9606 GN=LAMA2 PE=1 SV=4	LAMA2	0,0223	-0,643	HIGHER
Q00266	S-adenosylmethionine synthase isoform type-1 OS=Homo sapiens OX=9606 GN=MAT1A PE=1	MAT1A	0,0450	-0,500	HIGHER
P26038	Moesin OS=Homo sapiens OX=9606 GN=MSN PE=1 SV=3	MSN	0,0022	-0,893	HIGHER
P14543	Nidogen-1 OS=Homo sapiens OX=9606 GN=NID1 PE=1 SV=3	NID1	0,0038	-0,911	HIGHER
P20774	Mimecan OS=Homo sapiens OX=9606 GN=OGN PE=1 SV=1	OGN	0,0061	-0,857	HIGHER
Q9NRN5	Olfactomedin-like protein 3 OS=Homo sapiens OX=9606 GN=OLFML3 PE=2 SV=1	OLFML3	0,0223	-0,643	HIGHER
O75340	Programmed cell death protein 6 OS=Homo sapiens OX=9606 GN=PDCD6 PE=1 SV=1	PDCD6	0,0223	-0,643	HIGHER
Q8WUM4	Programmed cell death 6-interacting protein OS=Homo sapiens OX=9606 GN=PDCD6IP PE=1	PDCD6IP	0,0003	-1,000	HIGHER
P07737	Profilin-1 OS=Homo sapiens OX=9606 GN=PFN1 PE=1 SV=2	PFN1	0,0093	-0,786	HIGHER
Q8N0Y7	Probable phosphoglycerate mutase 4 OS=Homo sapiens OX=9606 GN=PGAM4 PE=3 SV=1	PGAM4	0,0450	-0,500	HIGHER
P36871	Phosphoglucomutase-1 OS=Homo sapiens OX=9606 GN=PGM1 PE=1 SV=3	PGM1	0,0387	-0,554	HIGHER
Q02809	Procollagen-lysine,2-oxoglutarate 5-dioxygenase 1 OS=Homo sapiens OX=9606 GN=PLOD1 PE=1	PLOD1	0,0192	-0,625	HIGHER
Q9NZ53	Podocalyxin-like protein 2 OS=Homo sapiens OX=9606 GN=PODXL2 PE=1 SV=1	PODXL2	0,0450	-0,500	HIGHER
P27169	Serum paraoxonase/arylesterase 1 OS=Homo sapiens OX=9606 GN=PON1 PE=1 SV=3	PON1	0,0401	0,643	LOWER

P62937	Peptidyl-prolyl cis-trans isomerase A OS=Homo sapiens OX=9606 GN=PPIA PE=1 SV=2	PPIA	0,0427	-0,643	HIGHER
P32119	Peroxiredoxin-2 OS=Homo sapiens OX=9606 GN=PRDX2 PE=1 SV=5	PRDX2	0,0327	-0,571	HIGHER
P30041	Peroxiredoxin-6 OS=Homo sapiens OX=9606 GN=PRDX6 PE=1 SV=3	PRDX6	0,0450	-0,500	HIGHER
P51149	Ras-related protein Rab-7a OS=Homo sapiens OX=9606 GN=RAB7A PE=1 SV=1	RAB7A	0,0021	-0,964	HIGHER
Q15493	Regucalcin OS=Homo sapiens OX=9606 GN=RGN PE=1 SV=1	RGN	0,0192	-0,625	HIGHER
P51812	Ribosomal protein S6 kinase alpha-3 OS=Homo sapiens OX=9606 GN=RPS6KA3 PE=1 SV=1	RPS6KA3	0,0192	-0,625	HIGHER
P07093	Glia-derived nexin OS=Homo sapiens OX=9606 GN=SERPINE2 PE=1 SV=1	SERPINE2	0,0307	-0,679	HIGHER
P50454	Serpin H1 OS=Homo sapiens OX=9606 GN=SERPINH1 PE=1 SV=2	SERPINH1	0,0450	-0,500	HIGHER
O43556	Epsilon-sarcoglycan OS=Homo sapiens OX=9606 GN=SGCE PE=1 SV=6	SGCE	0,0192	-0,625	HIGHER
P08195	4F2 cell-surface antigen heavy chain OS=Homo sapiens OX=9606 GN=SLC3A2 PE=1 SV=3	SLC3A2	0,0070	-0,786	HIGHER
Q01650	Large neutral amino acids transporter small subunit 1 OS=Homo sapiens OX=9606 GN=SLC7A5	SLC7A5	0,0223	-0,643	HIGHER
Q9H3E2	Sorting nexin-25 OS=Homo sapiens OX=9606 GN=SNX25 PE=1 SV=2	SNX25	0,0450	-0,500	HIGHER
Q15833	Syntaxin-binding protein 2 OS=Homo sapiens OX=9606 GN=STXBP2 PE=1 SV=2	STXBP2	0,0327	-0,571	HIGHER
P37802	Transgelin-2 OS=Homo sapiens OX=9606 GN=TAGLN2 PE=1 SV=3	TAGLN2	0,0486	-0,607	HIGHER
P01137	Transforming growth factor beta-1 proprotein OS=Homo sapiens OX=9606 GN=TGFB1 PE=1	TGFB1	0,0192	-0,625	HIGHER
P07996	Thrombospondin-1 OS=Homo sapiens OX=9606 GN=THBS1 PE=1 SV=2	THBS1	0,0037	-0,857	HIGHER
P24821	Tenascin OS=Homo sapiens OX=9606 GN=TNC PE=1 SV=3	TNC	0,0093	-0,786	HIGHER
P07437	Tubulin beta chain OS=Homo sapiens OX=9606 GN=TUBB PE=1 SV=2	TUBB	0,0059	-0,821	HIGHER
Q9H4B7	Tubulin beta-1 chain OS=Homo sapiens OX=9606 GN=TUBB1 PE=1 SV=1	TUBB1	0,0060	-0,839	HIGHER
P62987	Ubiquitin-60S ribosomal protein L40 OS=Homo sapiens OX=9606 GN=UBA52 PE=1 SV=2	UBA52	0,0289	-0,679	HIGHER
Q16851	UTP--glucose-1-phosphate uridylyltransferase OS=Homo sapiens OX=9606 GN=UGP2 PE=1 SV=5	UGP2	0,0441	-0,607	HIGHER
P50552	Vasodilator-stimulated phosphoprotein OS=Homo sapiens OX=9606 GN=VASP PE=1 SV=3	VASP	0,0328	-0,643	HIGHER
P13611	Versican core protein OS=Homo sapiens OX=9606 GN=VCAN PE=1 SV=3	VCAN	0,0205	-0,714	HIGHER

4.3. Molecular composition of sEV with CD3(+) phenotype (T cell-derived sEV) isolated from plasma of melanoma patients and healthy donors.

4.3.1. T cell proteins identified in CD3(+) sEV isolated from plasma of melanoma patients and healthy donors.

After the separation of sEV isolated from plasma of healthy donors (HD) and melanoma patients (MP) into CD3(+) and CD3(-) fractions, samples were assessed by mass spectrometry. The characteristic of the study population is placed in Table 3. Total sEV protein (TEP) levels (BCA assay based) varied between melanoma patients from 90 to 316.8 µg/ml plasma. The amount of protein used for immunocapture protocol varied from 148 to 171 µg for 8 patients and from 77 to 97 µg for 2 patients. After immunocapture, 40-90% of total sEV protein was retained in the CD3(-) sEV subfraction (the average = 65%). Hence, CD3(+) fraction of sEV represented a third of total plasma sEV, on average, with differences among patients from 5 to 58%. The protein profile of CD3(+) sEV was assessed in each healthy donor (n=10) and melanoma patient (n=10). Every sample was normalized as was given previously (page 53). Using a shotgun proteomics approach, 496 proteins were identified, including 94 immunoglobulin variants, which were excluded from further analysis. There were 92 common proteins for all samples. The distribution of identified proteins within sample groups is presented in Figure 21.

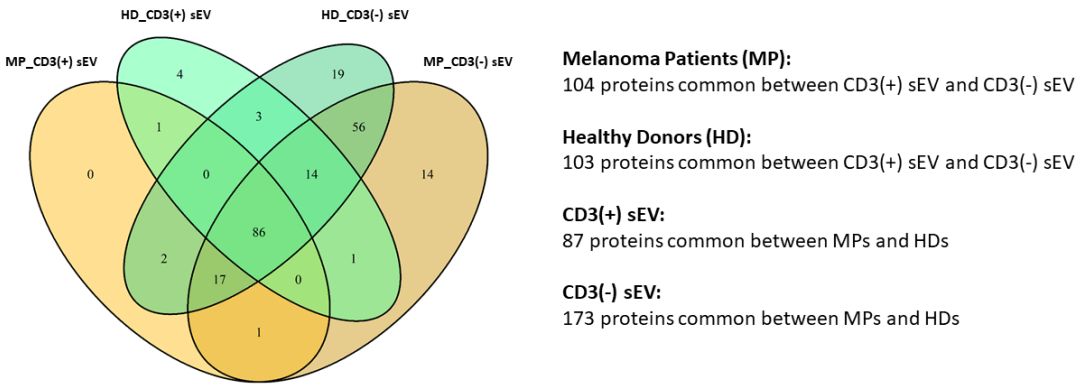

Figure 21. Quadruple Venn diagram showing contribution of identified proteins in each group.

The set of 402 proteins (after the exclusion of 94 immunoglobulins) included 108 proteins typically identified in serum/plasma specimens, which usually co-purify with

sEV isolated from the serum or plasma [Skoczylas et al. 2024, Smolarz et al. 2019]. To compare the components of T cells and T cell-derived proteome, putative plasma proteins were excluded from the analysis, and the remaining 271 proteins for the MP group, and 263 proteins for the HD group were considered sEV-specific. As a reference of T cells proteome were used combined data of:

- set of 6572 proteins provided by Joshi and coworkers, who performed an in-depth analysis of CD3+/CD4+/CD8− T cells from healthy donors [Joshi et al. 2019]
- set of 3281 proteins identified in T cell lysates of 10 melanoma patients (T cells were purified from the plasma of 10 MPs whose total plasma was subsequently used for immune capture of CD3(+) sEV), the lysates were prepared by our colleagues in the laboratory of Prof. Theresa Whiteside in UPMC, Pittsburgh, USA, and were send to Poland for analysis.

Both datasets generated a list of 6901 proteins present in the T cell proteome, which served as a reference for the annotation of proteins detected in the CD3(+) sEV fraction isolated from the plasma of melanoma patients. On the other hand, to compare the protein composition of CD3(+) sEV from healthy individuals and their parental cells, data set of 6572 proteins detected in T cells of healthy donors was used. Out of 263 proteins identified in the CD3(+)sEV fraction of healthy donors and considered sEV-specific, 65% of them (171 proteins) were co-annotated in the T cell proteome (Fig. 22). Whereas, among 271 proteins identified in the CD3(+)sEV fraction of melanoma patients and considered sEV-specific, 168 proteins (62%) were co-annotated in the T cell proteome (Fig. 22).

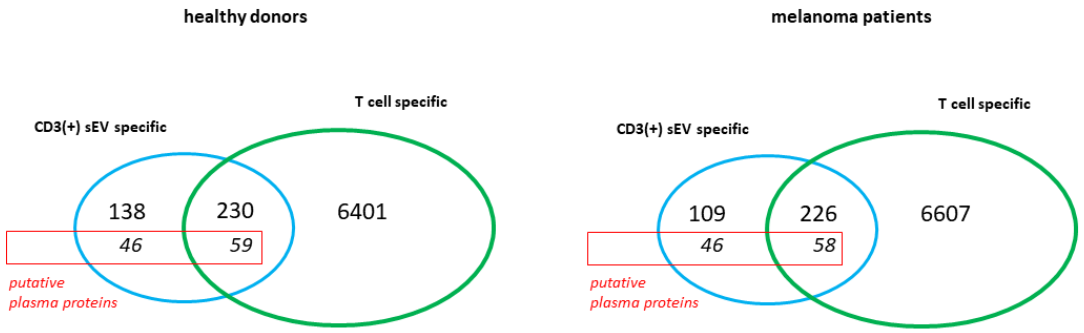

Figure 22. Venn diagrams showing the overlap between T cell-specific proteins and CD3(+) sEV-specific proteins isolated from plasma of healthy donors and melanoma patients.

The Gene Ontology pathway enrichment analysis revealed that putative T cell-derived sEV proteins were primarily associated with the terms: regulation of cellular processes and response to stimulus (Fig. 23A), the immune system, and signal transduction (Fig. 23B).

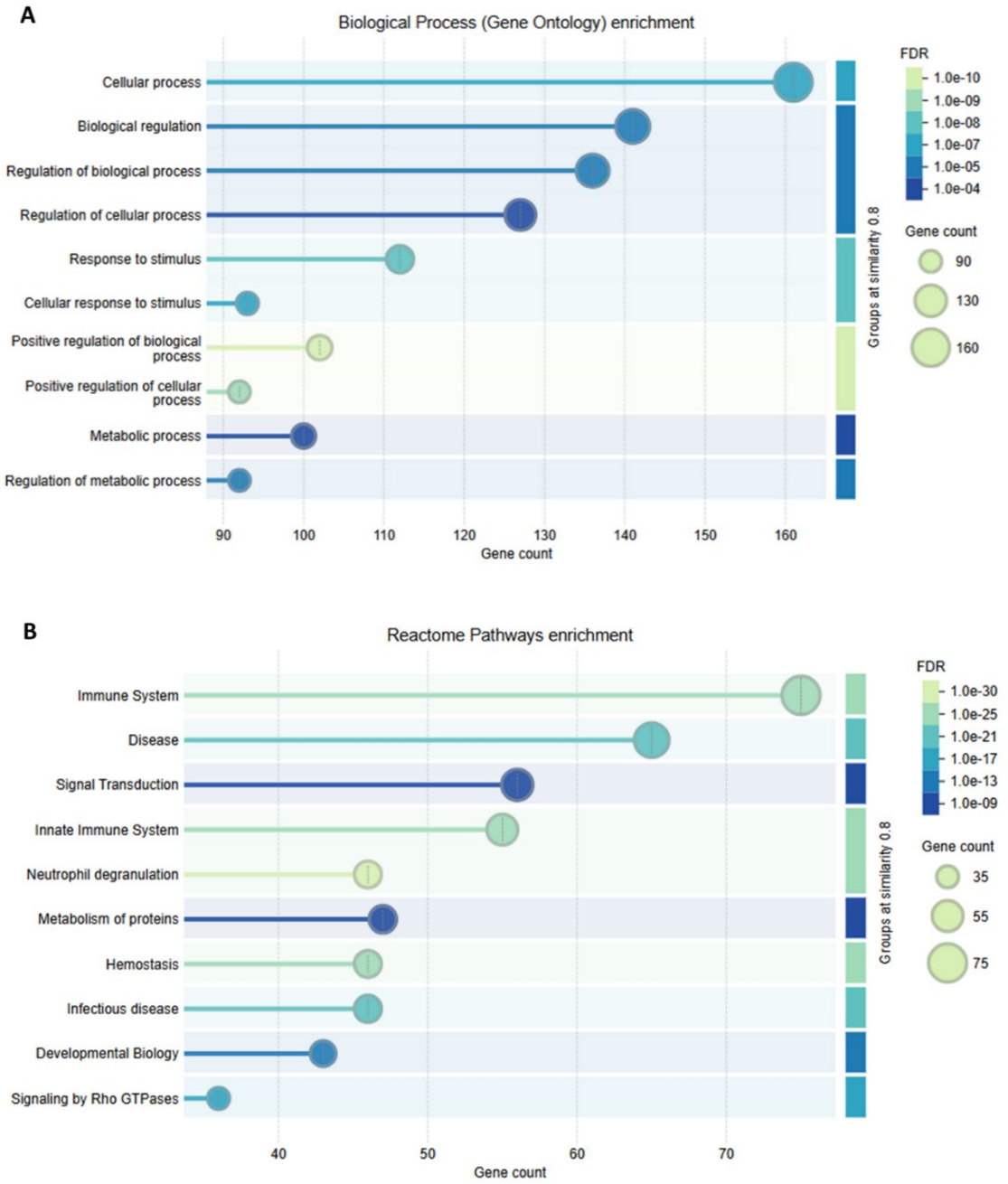

Figure 23. Functional enrichment in networks of proteins detected in the CD3(+) sEV fraction that were annotated in T cell proteome. Panel A: Biological processes (Gene Ontology), Panel B: Reactom Pathways. Processes are sorted by gene count (number of proteins annotated to the process) and FDR (color-coded). For the enrichment analysis, whole genome as a statistical background was assumed (String-db database).

On the other hand, proteins detected in CD3(+) sEV fraction, but not annotated in the T cells proteome were associated with cell adhesion and processes involved in tissues / organs development (Fig. 24A), localized to the extracellular region (Fig. 24B). Looking at the functions of the core set of proteins identified in CD3(+) sEV purified from plasma it can be concluded, that they represent the specific content of sEV released by T cells and could be considered as a ”T cell biopsy”.

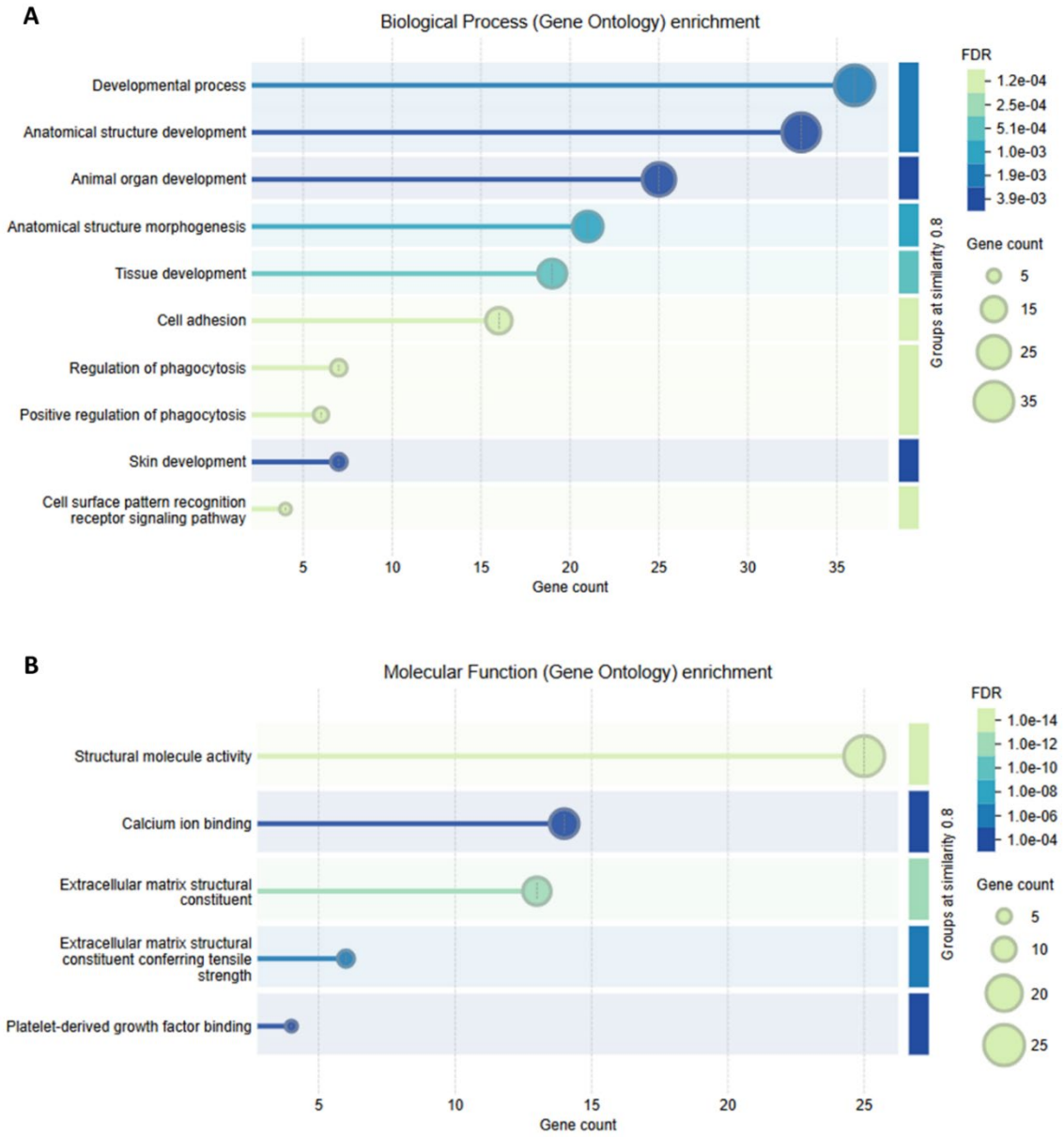

Figure 24. Functional enrichment in networks of proteins detected in the CD3(+) sEV fraction that were not annotated in T cell proteome. Panel A: Biological processes (Gene Ontology), Panel B: Molecular functions (Gene Ontology). Processes sorted by gene count (number of proteins annotated to the process) and FDR (color-coded). For the enrichment analysis, whole genome as a statistical background was assumed (String-db database).

4.3.2. Proteom profile of T cell-derived sEV in melanoma patients and healthy donors.

To identify which CD3(+) sV-specific proteins can discriminate between melanoma patients (MPs) and healthy donors (HDs), the ratio of individual protein levels in CD3(+) sEV samples for each patient was determined. At least 12 observations (protein measurements) were required to perform a test in both groups (12/20). 81 proteins met this criterion and were subjected to continuous quantitative analysis performed separately for each protein. Non-parametric U Mann-Whitney test was used. Effect size statistic was calculated using the rank-biserial coefficient correlation for Wilcoxon test (RBCC). Benjamini-Hochberg correction for multiple testing was applied (FDR). The levels of 37 proteins were significantly different between the MP and HD groups, with 28 proteins upregulated (Table 15) and 7 proteins downregulated (Table 16) in the MP group (p value > 0.05 and RBCC ≥ 0.5). Taking into account the strictest criteria of statistical significance (p value > 0.05, FDR > 0.05 and RBCC ≥ 0.5), the panel of 23 differentially expressed proteins in CD3(+) sEV MPs relative to CD3(+) sEV HDs was identified (21 with increased levels and 2 with decreased levels (Figure 25).

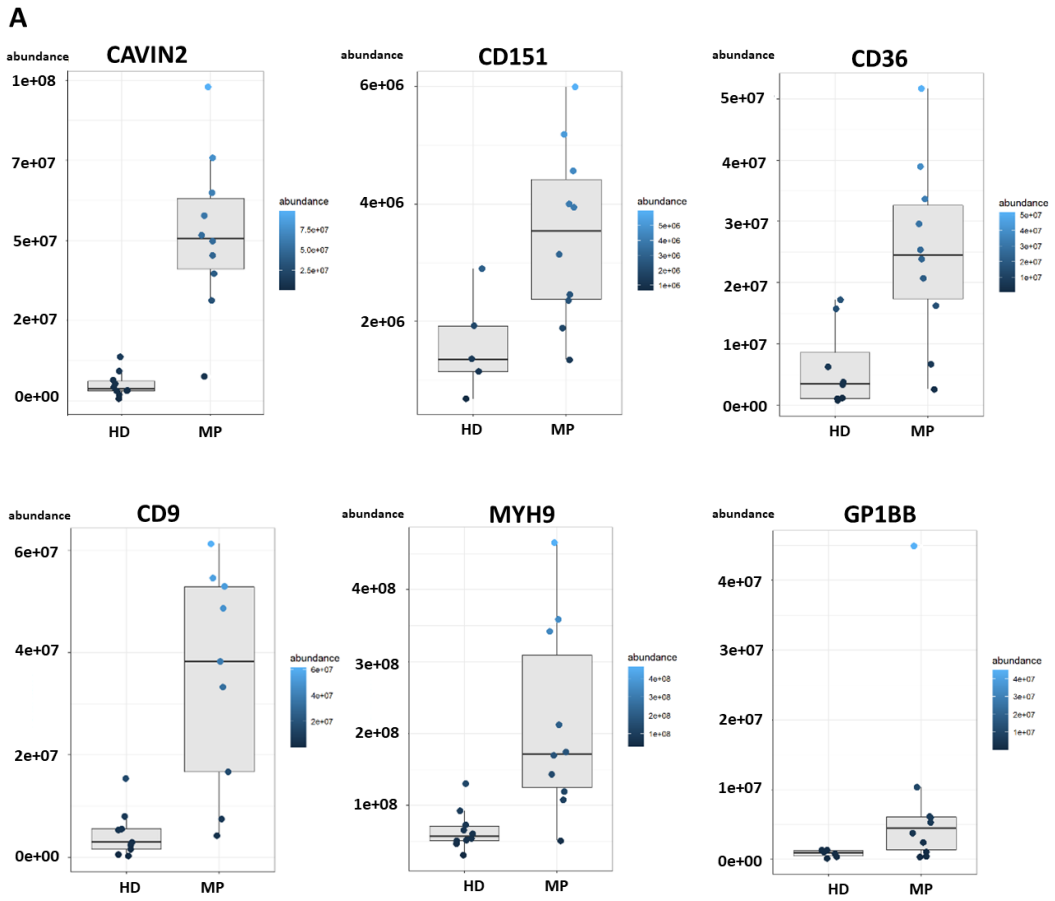

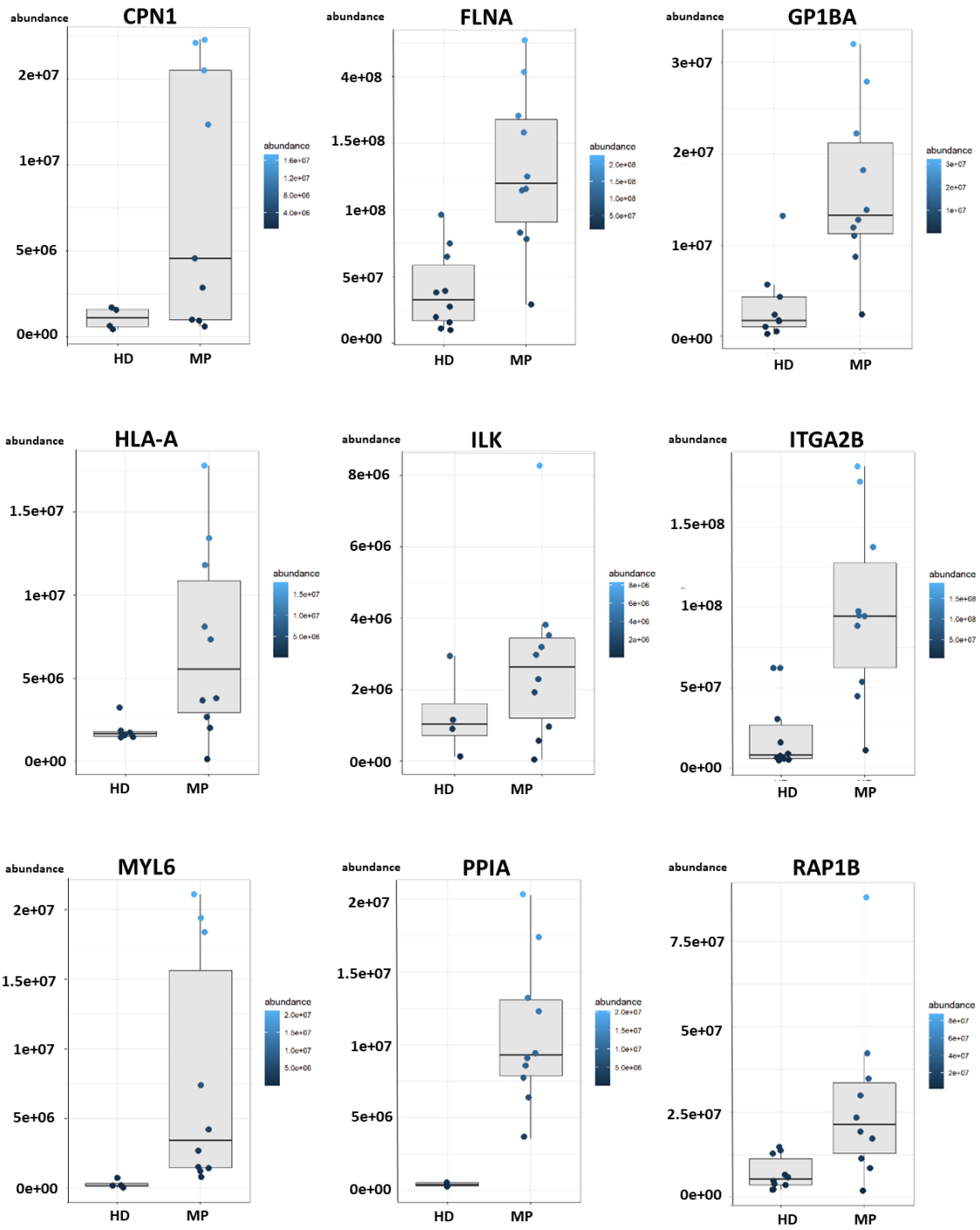
CPN1
abundance
2e+07
1e+07
5e+06
0e+00
HD
MP
FLNA
4e+08
1.5e+08
1e+08
5e+07
GP1BA
3e+07
HLA-A
1.5e+07
ILK
8e+06
6e+06
4e+06
2e+06
ITGA2B
MYL6
PPIA
RAP1B
7.5e+07
5e+07
2.5e+07

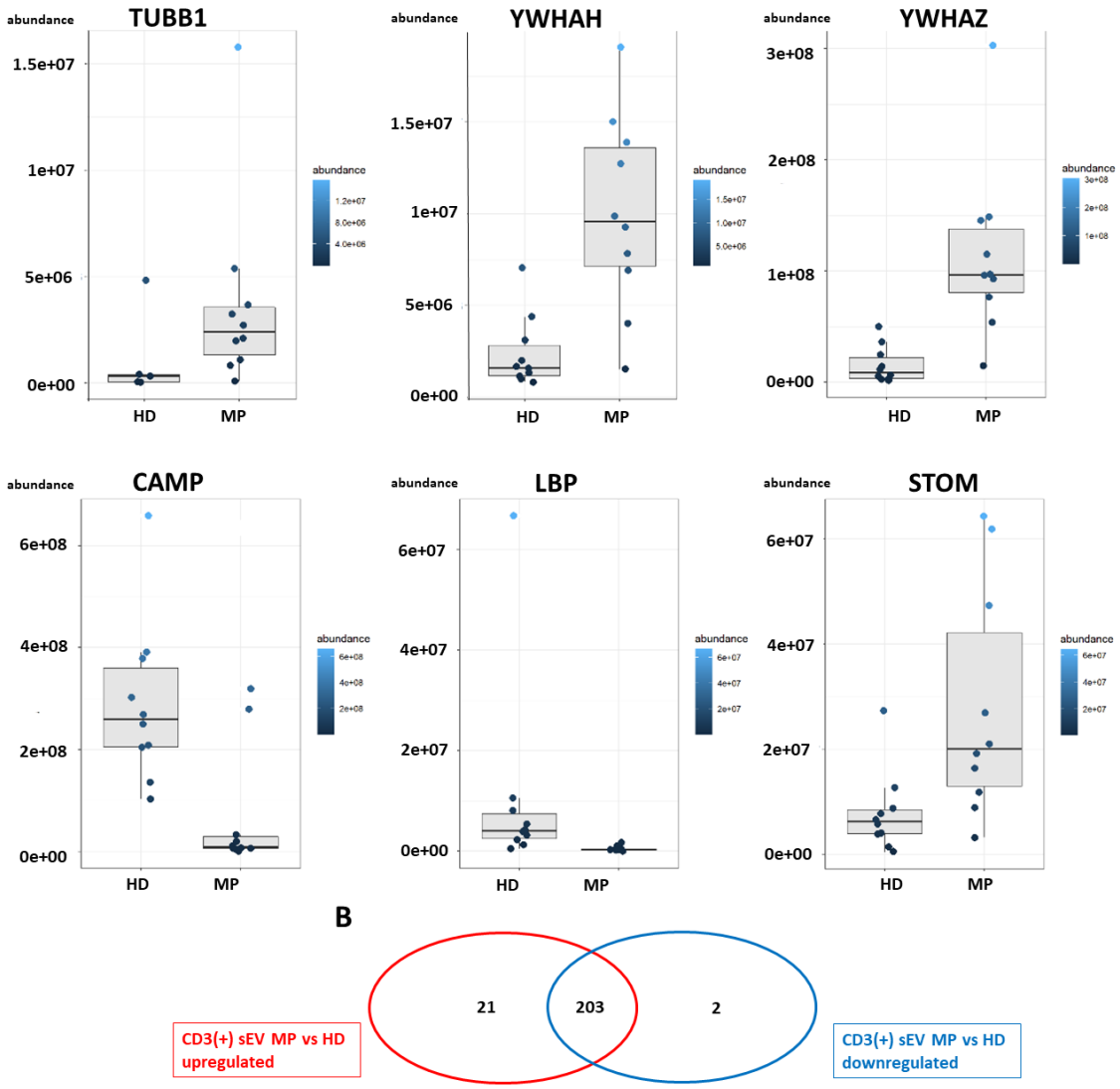

Figure 25. A panel of 23 differentially expressed proteins in CD3(+) sEV MPs relative to CD3(+) sEV HDs (p value > 0.05, FDR > 0.05 and RBCC ≥ 0.5). Panel A – abundance level of DEP in CD3(+) sEV MPs and CD3(+) sEV; boxplots show median, upper and lower quartile, maximum and minimum (dots represent individual patients – protein abundance color-coded). Panel B – the Venn diagram shows the numbers of proteins upregulated or downregulated in CD3(+) sEV MPs relative to CD3(+) sEV HDs.

In the subset of 145 sEV proteins subjected to discrete binary analysis (Fischer test, effect size – Crammer V test), the levels of 10 proteins exhibited significant differences between the MP and HD groups (p value > 0.05 and V ≥ 0.5). Taking into account only size effect, 28 differentially expressed proteins (large and very large effect size; V > 0.5) were found, including 11 proteins upregulated and 17 proteins downregulated in the MP group (Table 17).

Joint results of continuous and binary analyses show 66 differentially expressed proteins (DEPs) with 41 upregulated and 25 downregulated proteins in the MP group, thus discriminating CD3(+) sEV isolated from the plasma of MPs versus HD (Fig. 26).

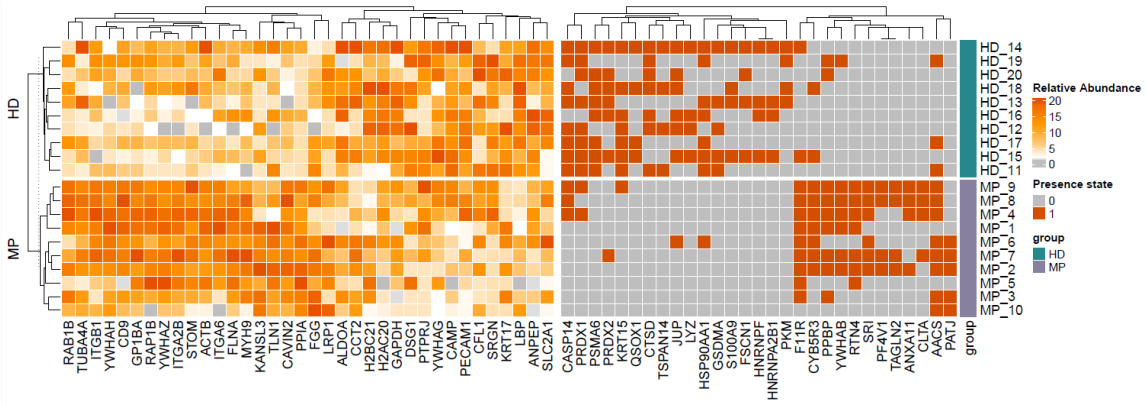

Figure 26. The heat map representing the abundance of DEPs differentaiting T-cell-derived CD3(+) sEV MPs from CD3(+) sEV HDs. Left side: shows DEPs from continuous analysis (RBCC > 0.5; abundances are color-coded according to ranks of all normalized signals), right part shows DEPs from discrete analysis (Crammer's V effect size > 0.5). The abundance is color-coded according to present/absent status as yes/no (1 or 0, respectively).

Table 15. List of proteins upregulated in CD3(+) sEV in melanoma patients (continuous analysis).

ProteinName	Protein Description	p-value (U-test)	FDR (U-test)	Effect size (RBCC)	Type of analysis (continuous vs. binary)	Size of effect	change in MP vs. HD
ACTB	Actin, cytoplasmic 1	0,0185	0,0600	-0,620	C	large	UP
ANXA7	Annexin A7	0,0464	0,1309	-0,530	C	large	UP
CANX	Calnexin	0,0139	0,0539	-0,640	C	large	UP
CAVIN2	Caveolae-associated protein 2	0,00004	0,0024	-0,960	C	very large	UP
CD151	CD151 antigen	0,0012	0,0121	-0,860	C	very large	UP
CD36	Platelet glycoprotein 4	0,0017	0,0156	-0,840	C	very large	UP
CD9	CD9 antigen	0,0081	0,0409	-0,710	C	very large	UP
CDC42	Cell division control protein 42 homolog	0,0172	0,0592	-0,640	C	large	UP
CPN1	Carboxypeptidase N catalytic chain	0,0061	0,0336	-0,720	C	very large	UP
FLNA	Filamin-A	0,0007	0,0080	-0,840	C	very large	UP
GP1BA	Platelet glycoprotein Ib alpha chain	0,0005	0,0067	-0,860	C	very large	UP
GP1BB	Platelet glycoprotein Ib beta chain	0,0035	0,0226	-0,780	C	very large	UP
HLA-A	HLA class I histocompatibility antigen, A alpha chain	0,0027	0,0198	-0,800	C	very large	UP
ILK	Integrin-linked protein kinase	0,0041	0,0249	-0,760	C	very large	UP
ITGA2B	Integrin alpha-IIb	0,0007	0,0080	-0,840	C	very large	UP
ITGA6	Integrin alpha-6	0,0433	0,1286	-0,540	C	large	UP
ITGB1	Integrin beta-1	0,0147	0,0539	-0,640	C	large	UP
KANSL3	KAT8 regulatory NSL complex subunit 3	0,0185	0,0600	-0,620	C	large	UP
MYH9	Myosin-9	0,0021	0,0177	-0,780	C	very large	UP
MYL12B	Myosin regulatory light chain 12B	0,0171	0,0592	-0,640	C	large	UP
MYL6	Myosin light polypeptide 6	0,0001	0,0027	-1,000	C	very large	UP

PPIA	Peptidyl-prolyl cis-trans isomerase A	0,0001	0,0027	-1,000	C	very large	UP
RAB1B	Ras-related protein Rab-1B	0,0317	0,0970	-0,560	C	large	UP
RAP1B	Ras-related protein Rap-1b	0,0089	0,0409	-0,680	C	large	UP
STOM	Stomatin	0,0089	0,0409	-0,680	C	large	UP
TUBB1	Tubulin beta-1 chain	0,0026	0,0198	-0,800	C	very large	UP
YWHAH	14-3-3 protein eta	0,0003	0,0051	-0,880	C	very large	UP
YWHAZ	14-3-3 protein zeta/delta	0,0001	0,0027	-0,920	C	very large	UP

Table 16. List of proteins downregulated in CD3(+) sEV in melanoma patients (continuous analysis).

ProteinName	Protein Description	p-value (U-test)	FDR (U-test)	Effect size (RBCC)	Type of analysis (continuous vs. binary)	Size of effect	change in MP vs. HD
ANPEP	Aminopeptidase N	0,0140	0,0539	0,660	C	large	DOWN
CAMP	Cathelicidin antimicrobial peptide	0,0029	0,0198	0,760	C	very large	DOWN
DSG1	Desmoglein-1	0,0489	0,1345	0,520	C	large	DOWN
GAPDH	Glyceraldehyde-3-phosphate dehydrogenase	0,0451	0,1305	0,540	C	large	DOWN
H2AC20	Histone H2A type 2-C	0,0147	0,0539	0,640	C	large	DOWN
LBP	Lipopolysaccharide-binding protein	0,0001	0,0027	0,940	C	very large	DOWN
PECAM1	Platelet endothelial cell adhesion molecule	0,0207	0,0649	0,620	C	large	DOWN

Table 17. List of proteins up- and downregulated in CD3(+) sEV in melanoma patients (binary/descrete analysis).

ProteinName	Protein Description	p-value (Fisher test)	FDR (Fisher test)	Effect size (Crammer V)	Type of analysis (continuous vs. binary)	Size of effect	change in MP vs. HD
AACS	Acetoacetyl-CoA synthetase	0,0698	0,6823	0,503	B	large	UP
ANXA11	Annexin A11	0,0867	0,6823	0,500	B	large	UP
CASP14	Caspase-14	0,0698	0,6823	0,503	B	large	DOWN
CLTA	Clathrin light chain A	0,0867	0,6823	0,500	B	large	UP
CTSD	Cathepsin D	0,0031	0,2632	0,734	B	very large	DOWN
CYB5R3	NADH-cytochrome b5 reductase 3	0,0698	0,6823	0,503	B	large	UP
F11R	Junctional adhesion molecule A	0,0055	0,3880	0,704	B	very large	UP
FSCN1	Fascin	0,0867	0,6823	0,500	B	large	DOWN
GSDMA	Gasdermin-A	0,0325	0,5757	0,577	B	large	DOWN
HNRNPA2B1	Heterogeneous nuclear ribonucleoproteins A2/B1	0,0867	0,6823	0,500	B	large	DOWN
HNRNPF	Heterogeneous nuclear ribonucleoprotein F	0,0867	0,6823	0,500	B	large	DOWN
HSP90AA1	Heat shock protein HSP 90-alpha	0,0198	0,5757	0,612	B	large	DOWN
JUP	Junction plakoglobin	0,0573	0,6823	0,524	B	large	DOWN
KRT15	Keratin, type I cytoskeletal 15	0,0198	0,5757	0,612	B	large	DOWN
LYZ	Lysozyme C	0,0867	0,6823	0,500	B	large	DOWN
PATJ	InaD-like protein	0,0325	0,5757	0,577	B	large	UP
PF4V1	Platelet factor 4 variant	0,0867	0,6823	0,500	B	large	UP
PKM	Pyruvate kinase PKM	0,0867	0,6823	0,500	B	large	DOWN
PRDX1	Peroxiredoxin-1	0,0230	0,5757	0,600	B	large	DOWN
PRDX2	Peroxiredoxin-2	0,0573	0,6823	0,524	B	large	DOWN
PSMA6	Proteasome subunit alpha type-6	0,0007	0,1518	0,817	B	very large	DOWN
QSOX1	Sulfhydryl oxidase 1	0,0867	0,6823	0,500	B	large	DOWN

RTN4	Reticulon-4	0,0031	0,2632	0,734	B	very large	UP
S100A9	Protein S100-A9	0,0867	0,6823	0,500	B	large	DOWN
SRI	Sorcin	0,0108	0,4605	0,655	B	large	UP
TAGLN2	Transgelin-2	0,0867	0,6823	0,500	B	large	UP
TSPAN14	Tetraspanin-14	0,0867	0,6823	0,500	B	large	DOWN
YWHAB	14-3-3 protein beta/alpha	0,0573	0,6823	0,524	B	large	UP
GC	Vitamin D-binding protein	0,0198	0,5757	0,612	B	large	UP
PPBP	Platelet basic protein	0,0698	0,6823	0,503	B	large	UP

4.3.3. Proteins pathway activities in T cell-derived sEV in melanoma patients and healthy donors.

The complete set of differentially expressed proteins (DEPs) was subjected to a pathway enrichment analysis (Table 18). Large subsets of DEPs were linked with pathways related to cancer-associated processes, including developmental biology, regulation of stimulus response or signal transduction, immune function, cell migration, and gene regulation. DEPs upregulated in MPs were associated with prominent categories involving immune system pathways (18 proteins) and signal transduction mechanisms (18 proteins). Specifically, this group contained 12 proteins linked to Rho GTPase signaling, 9 proteins associated with cytokine-mediated pathways, and 6 proteins participating in MAPK cascade signaling. Notably, 5 proteins within this subset (ACTB, ITGA2B, RAP1B, TLN1, YWHAB) were connected to pathways activated by mutant BRAF variants. In contrast, among the DEPs downregulated in MPs-derived sEVs, the largest category (17 proteins) was related to immune system functions, with 6 proteins involved in interleukin signaling, another 6 in Rho GTPase pathways, and 4 proteins associated with apoptosis.

Table 18. REACTOME pathways associated with Differentially Expressed Proteins (p value > 0.05)

REACTOME ID	REACTOME pathway	arbitrary category	# all proteins	# DEPs	p.value
R-HSA-74160	Gene expression (Transcription)	cancer-related	1547	24	0,0016
R-HSA-5625740	RHO GTPases activate PKNs	cancer-related	94	11	0,0028
R-HSA-1500931	Cell-Cell communication	immune-related	153	12	0,0065
R-HSA-446353	Cell-extracellular matrix interactions	cancer-related	18	4	0,0068
R-HSA-430116	GP1b-IX-V activation signalling	cancer-related	12	4	0,0068
R-HSA-195258	RHO GTPase Effectors	cancer-related	326	27	0,0072
R-HSA-168256	Immune System	immune-related	2068	90	0,0073
R-HSA-76009	Platelet Aggregation (Plug Formation)	cancer-related	39	6	0,0088
R-HSA-5627123	RHO GTPases activate PAKs	cancer-related	24	6	0,0088
R-HSA-449147	Signaling by Interleukins	immune-related	473	25	0,0095
R-HSA-162582	Signal Transduction	cancer-related	2599	66	0,0109
R-HSA-1280218	Adaptive Immune System	immune-related	770	29	0,0162
R-HSA-5628897	TP53 Regulates Metabolic Genes	cancer-related	87	9	0,0199
R-HSA-9006934	Signaling by Receptor Tyrosine Kinases	cancer-related	532	19	0,0219
R-HSA-5674135	MAP2K and MAPK activation	cancer-related	40	7	0,0237
R-HSA-6802948	Signaling by high-kinase activity BRAF mutants	cancer-related	36	7	0,0237
R-HSA-6785807	Interleukin-4 and Interleukin-13 signaling	immune-related	108	7	0,0237

R-HSA-421270	Cell-cell junction organization	cancer-related	88	3	0,0241
R-HSA-9614085	FOXO-mediated transcription	cancer-related	65	3	0,0241
R-HSA-9614399	Regulation of localization of FOXO transcription factors	cancer-related	11	3	0,0241
R-HSA-392517	Rap1 signalling	immune-related	16	3	0,0241
R-HSA-1280215	Cytokine Signaling in Immune system	immune-related	792	36	0,0255
R-HSA-109606	Intrinsic Pathway for Apoptosis	cancer-related	55	5	0,0264
R-HSA-111447	Activation of BAD and translocation to mitochondria	cancer-related	15	5	0,0264
R-HSA-114452	Activation of BH3-only proteins	cancer-related	30	5	0,0264
R-HSA-75035	Chk1/Chk2(Cds1) mediated inactivation of Cyclin B:Cdk1 complex	cancer-related	13	5	0,0264
R-HSA-194315	Signaling by Rho GTPases	cancer-related	706	42	0,0266
R-HSA-9716542	Signaling by Rho GTPases, Miro GTPases and RHOBTB3	cancer-related	722	42	0,0266
R-HSA-1640170	Cell Cycle	cancer-related	691	17	0,0287
R-HSA-1474244	Extracellular matrix organization	cancer-related	300	12	0,0297
R-HSA-1445148	Translocation of SLC2A4 (GLUT4) to the plasma membrane	cancer-related	72	12	0,0297
R-HSA-109582	Hemostasis	cancer-related	623	52	0,0342
R-HSA-2682334	EPH-Ephrin signaling	cancer-related	92	10	0,0382
R-HSA-6802952	Signaling by BRAF and RAF1 fusions	cancer-related	67	8	0,0488
R-HSA-9656223	Signaling by RAF1 mutants	cancer-related	43	8	0,0488
R-HSA-5683057	MAPK family signaling cascades	cancer-related	325	13	0,0493

In addition to the classical overrepresentation analysis based on the pre-selected subset of DEPs, the hypothetical activation status of individual pathways was assessed by calculating Pathway Activation Scores (PAS) derived from the abundance of all annotated proteins. To ensure a representative yet focused analysis, 50 Reactome pathways were selected using stringent filtering criteria, and their PAS values were compared between CD3(+) sEVs isolated from MPs and HDs. This comparison found 22 pathways with statistically significant differences, all demonstrating large or very large effect sizes (Figure 26). Among pathways showing moderate upregulation in MPs (21 out of 22), the most prominent were those related to cancer-associated signaling cascades, notably MAPK signaling (9 pathways) and Rho GTPase signaling (4 pathways). In turn, the only pathway showing downregulation in MPs was the pathway linked to the immune responses, specifically the uptake and activity of bacterial toxins.

Notably, 10 proteins identified in CD3(+) sEVs (ACTB, CALM3, FGG, ITGA2B, ITGB3, PHB, RAP1B, TLN1, VCL, YWHAB) are components of the oncogenic MAPK signaling associated with mutant BRAF activity. In line with the PAS findings, this pathway was enriched in sEVs from the MP group. Given that BRAF mutation status was available for

five MP donors (2 with wild-type BRAF and 3 harboring BRAF V600 mutations), a potential relationship between the abundance of these proteins and BRAF mutational status in MP-derived sEVs was investigated. Preliminary analysis revealed that ITGB3 and YWHAB levels were lower in CD3(+) sEV from melanoma patients with wild-type BRAF than with BRAF-mutant tumors (Figure 27). These very preliminary observations suggest that protein signatures within CD3(+) sEVs, particularly those linked to BRAF-related pathways, may offer potential utility as diagnostic biomarkers in melanoma.

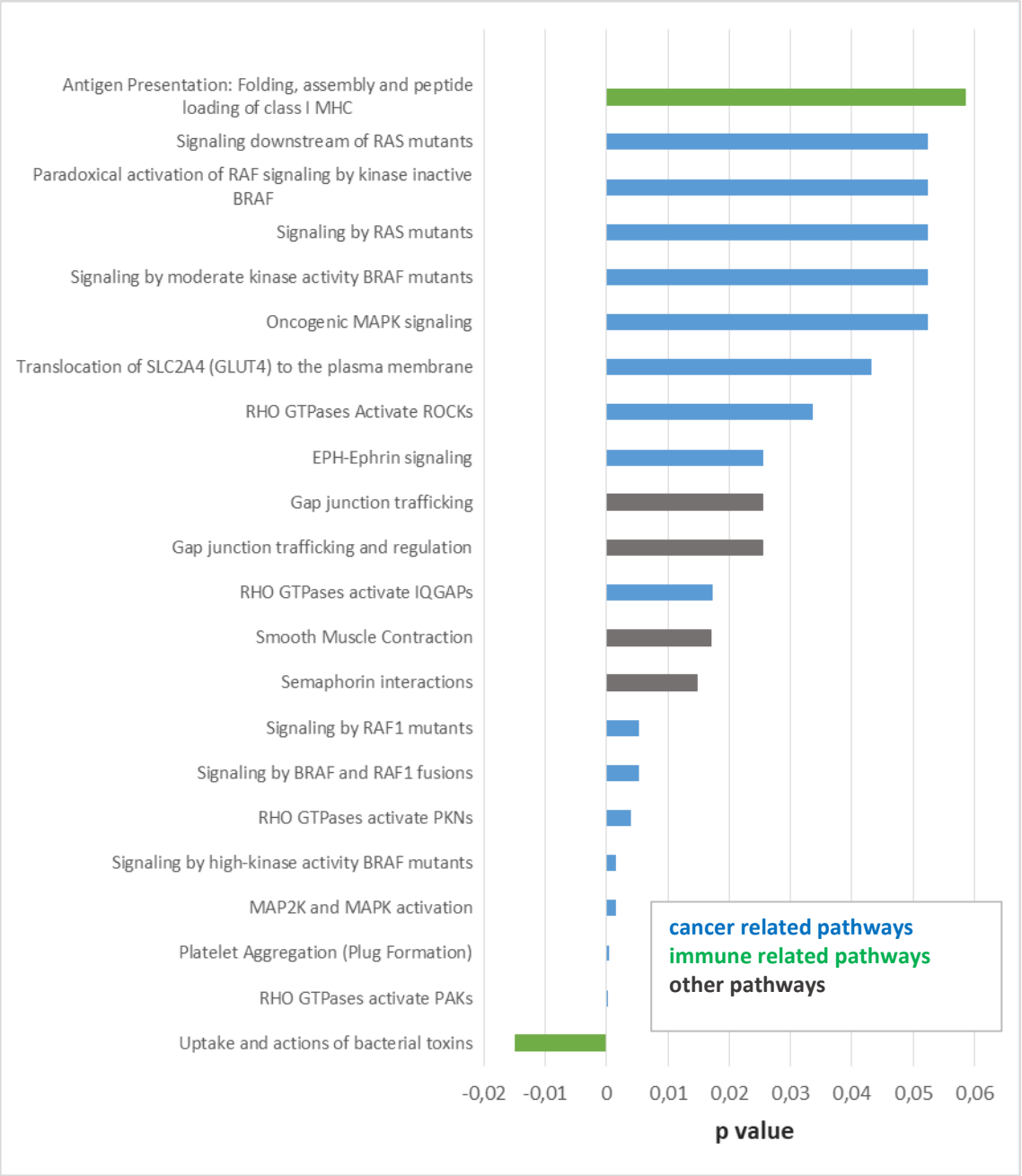

Figure 26. REACTOME pathways for which the Pathway Activation Score (PAS) values were different between the MP and HD groups (RBCC > 0.05).

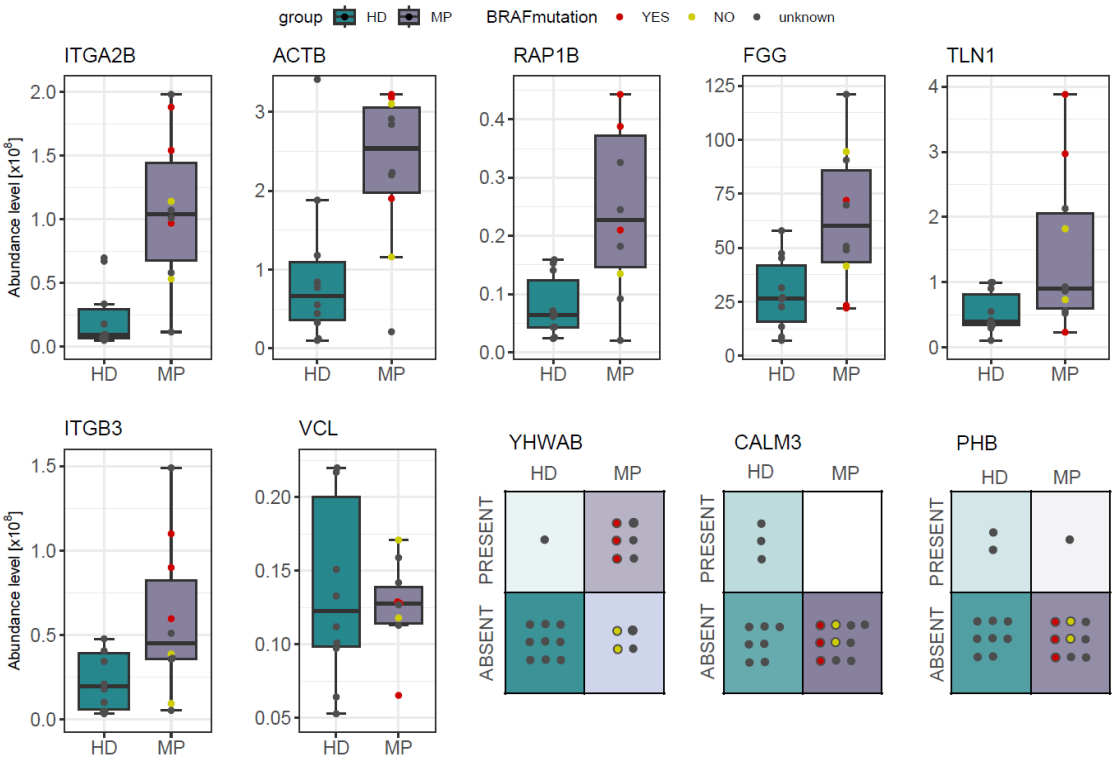

Figure 27. Abundance of selected proteins associated with BRAF-related pathways in CD3(+) sEV from MPs with the different BRAF gene status.

4.3.4. Proteome profile of CD3(-) sEV in melanoma patients and healthy donors.

To check which proteins detected in CD3(-) sEV discriminate melanoma patients (MPs) and healthy donors (HDs), the ratio of individual protein levels in CD3(-) sEV samples for each patient was determined. Minimum 12 protein measurements were required to perform a test in both groups (12/20). 160 proteins met this conditions and were subjected to continuous quantitative analysis applied to each protein separately. The levels of 49 proteins were significantly different between the MP and HD groups, with 41 proteins upregulated (Table 19) and 8 proteins downregulated (Table 20) in the MP group (p value > 0.05 and RBCC ≥ 0.5). Taking into account the stringent criteria of statistical significance (p value > 0.05, FDR > 0.05 and RBCC ≥ 0.5), the panel of 19 differentially expressed proteins in CD3(+) sEV in MPs relative to CD3(+) sEV in HDs was identified (with 15 proteins upregulated and 4 downregulated) (Figure 28).

A

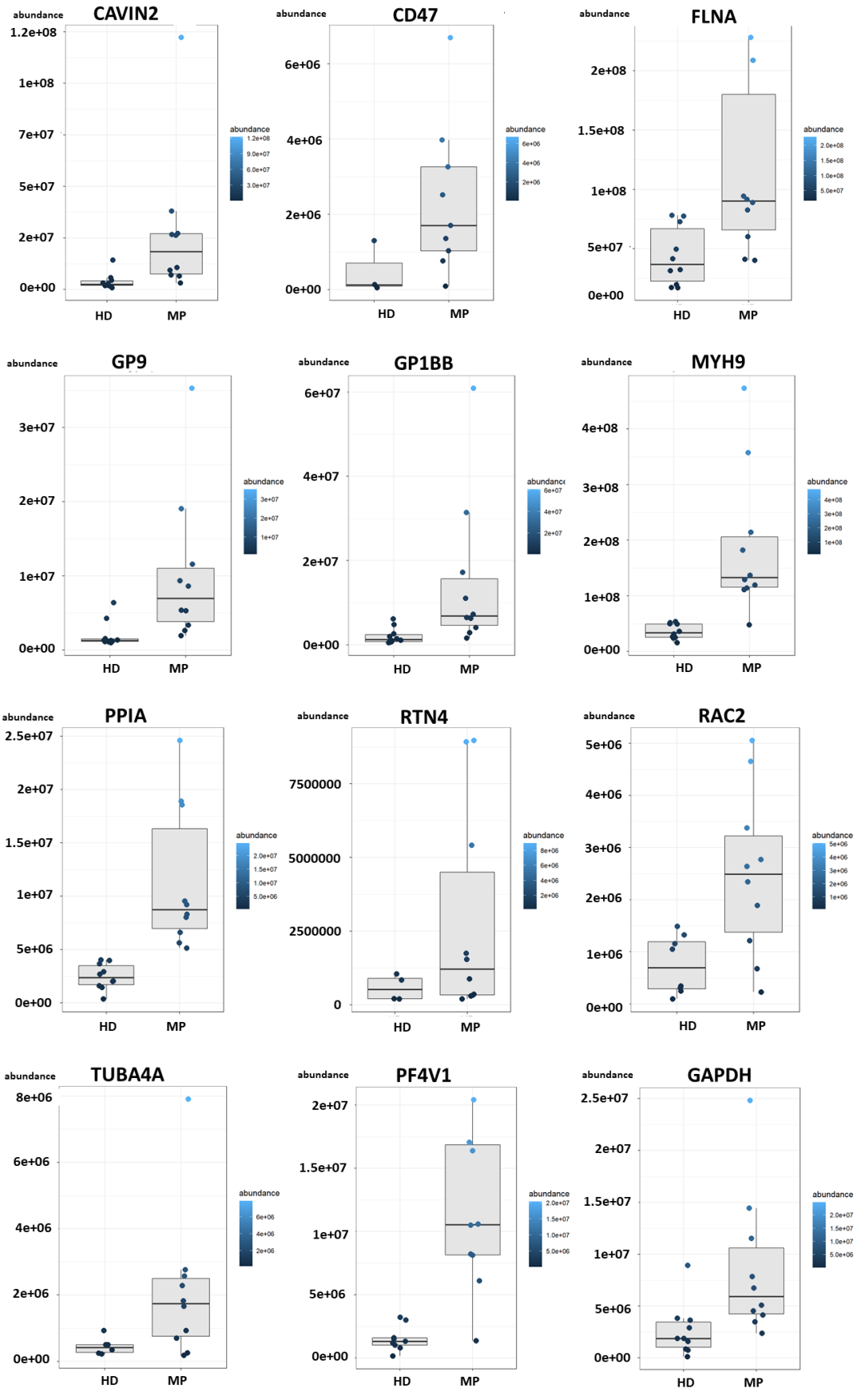
CAVIN2
CD47
FLNA
GP9
GP1BB
MYH9
PPIA
RTN4
RAC2
TUBA4A
PF4V1
GAPDH
abundance
HD
MP

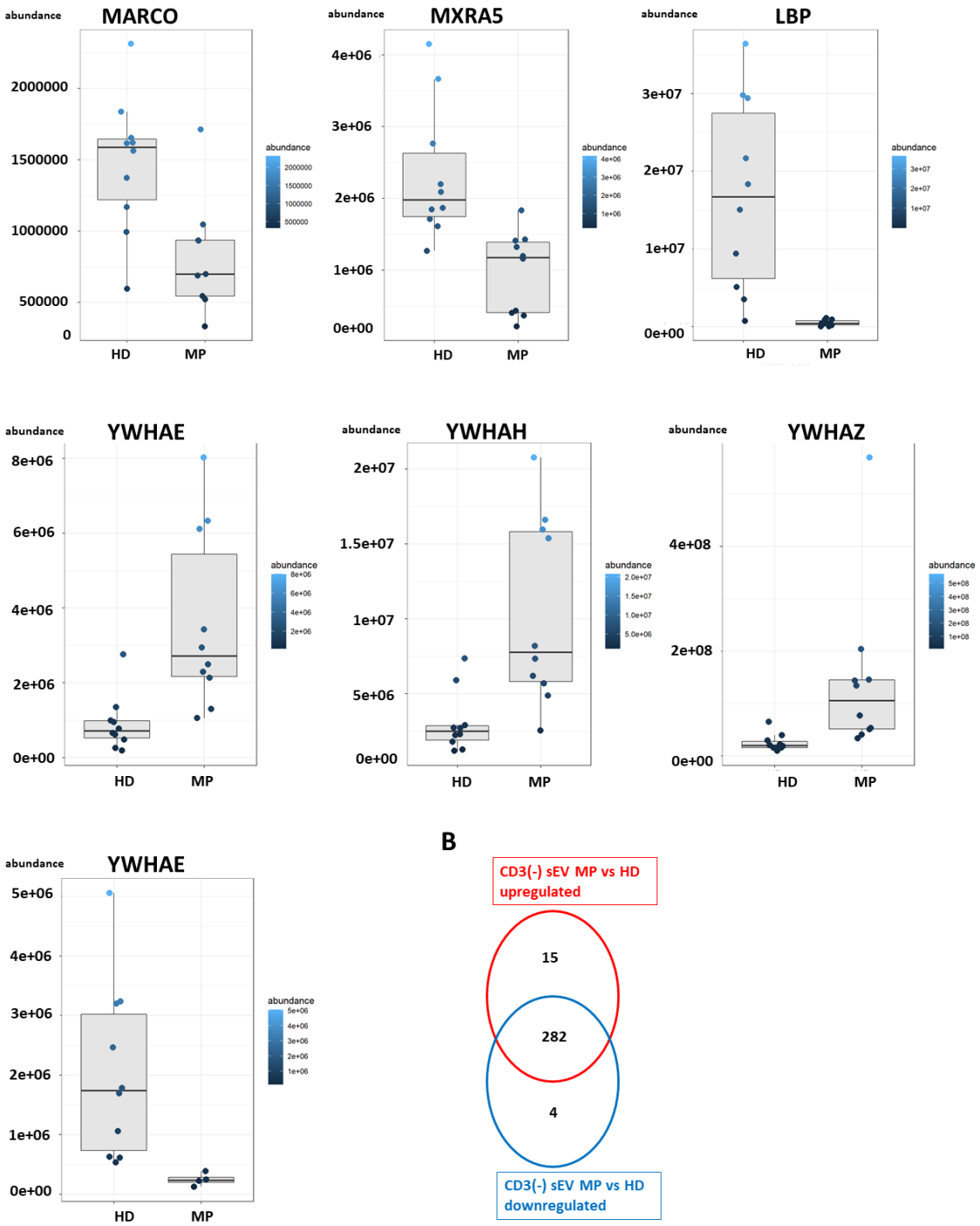

Figure 28. A panel of 19 differentially expressed proteins (DEPs) in CD3(-) sEV in MPs relative to CD3(-) sEV in HDs (p-value> 0.05, FDR > 0.05, and RBCC ≥ 0.5). Panel A – abundance level of DEPs in CD3(-) sEV and CD3(-) sEV in MPs and HDs; boxplots show median, upper and lower quartile, maximum, and minimum (dots represent individual patients). Panel B – the Venn diagram shows the numbers of proteins upregulated or downregulated in CD3(-) sEV in MPs relative to CD3(-) sEV in HDs.

In the subset of 46 sEV proteins subjected to discrete analysis (Fischer test, effect size – Crammer V test), the levels of 8 proteins were significantly different between the MP and HD groups (V ≥ 0.5) (Table 21).

Collectively, 64 differentially expressed proteins (DEPs) with large and very large size effects were identified in continuous and binary analyses, with 51 upregulated and 13 downregulated in the MP group, thus discriminating CD3(+) sEV isolated from plasma of 10 MPs and 10 HD (Fig. 29).

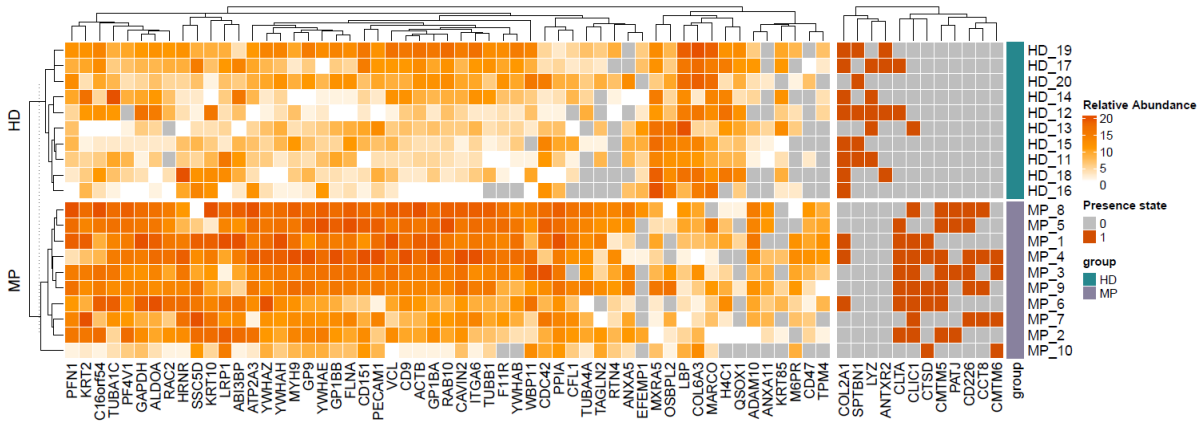

Figure 29. The heat map representing the abundance of DEPs differentiating T-cell-derived CD3(-) sEV in MPs from CD3(-) sEV in HDs. The left side shows DEPs from continuous analysis (RBCC > 0.5; abundances are color-coded according to ranks of all normalized signals). The right part shows DEPs from discrete analysis (Crammer's V effect size > 0.5). The abundance is color-coded according to present/absent status as yes/no (1 or 0, respectively).

Table 19. List of upregulated proteins in CD3(-) sEV in melanoma patients (continuous analysis).

Protein Name	Protein Description	p.val_U-test	FDR_U-test	Effect size - RBCC	Type of analysis (continuous vs. binary)	Size of effect	Side of change (regarding MP)
PPIA	Peptidyl-prolyl cis-trans isomerase A	0,0000	0,0017	-1,000	C	very large	UP
MYH9	Myosin-9	0,0001	0,0040	-0,940	C	very large	UP
PF4V1	Platelet factor 4 variant	0,0001	0,0047	-0,920	C	very large	UP
YWHAZ	14-3-3 protein zeta/delta	0,0002	0,0047	-0,900	C	very large	UP
YWHAE	14-3-3 protein epsilon	0,0002	0,0047	-0,900	C	very large	UP
GP9	Platelet glycoprotein IX	0,0005	0,0097	-0,860	C	very large	UP
CAVIN2	Caveolae-associated protein 2	0,0007	0,0129	-0,840	C	very large	UP
YWHAH	14-3-3 protein eta	0,0015	0,0201	-0,800	C	very large	UP
GP1BB	Platelet glycoprotein Ib beta chain	0,0015	0,0201	-0,800	C	very large	UP
RTN4	Reticulon-4	0,0019	0,0236	-0,820	C	very large	UP
GAPDH	Glyceraldehyde-3-phosphate dehydrogenase	0,0029	0,0320	-0,760	C	very large	UP
CD47	Leukocyte surface antigen CD47	0,0030	0,0320	-0,770	C	very large	UP
FLNA	Filamin-A	0,0039	0,0366	-0,740	C	very large	UP
TUBA4A	Tubulin alpha-4A chain	0,0044	0,0385	-0,760	C	very large	UP
RAC2	Ras-related C3 botulinum toxin substrate 2	0,0046	0,0385	-0,760	C	very large	UP
ALDOA	Fructose-bisphosphate aldolase A	0,0068	0,0513	-0,700	C	very large	UP
TUBB1	Tubulin beta-1 chain	0,0068	0,0513	-0,700	C	very large	UP
ANXA11	Annexin A11	0,0071	0,0513	-0,700	C	very large	UP
CD151	CD151 antigen	0,0089	0,0600	-0,680	C	large	UP
CFL1	Cofilin-1	0,0090	0,0600	-0,700	C	very large	UP
GP1BA	Platelet glycoprotein Ib alpha chain	0,0115	0,0707	-0,660	C	Large	UP

ATP2A3	Sarcoplasmic/endoplasmic reticulum calcium ATPase 3	0,0147	0,0870	-0,640	C	Large	UP
PFN1	Profilin-1	0,0185	0,0933	-0,620	C	Large	UP
CD9	CD9 antigen	0,0185	0,0933	-0,620	C	Large	UP
CDC42	Cell division control protein 42 homolog	0,0185	0,0933	-0,620	C	Large	UP
ADAM10	Disintegrin and metalloproteinase domain-containing protein 10	0,0187	0,0933	-0,630	C	Large	UP
LRP1	Prolow-density lipoprotein receptor-related protein 1	0,0232	0,1062	-0,600	C	Large	UP
PECAM1	Platelet endothelial cell adhesion molecule	0,0232	0,1062	-0,600	C	Large	UP
KRT2	Keratin, type II cytoskeletal 2 epidermal	0,0288	0,1280	-0,580	C	Large	UP
F11R	Junctional adhesion molecule A	0,0342	0,1379	-0,570	C	Large	UP
ACTB	Actin, cytoplasmic 1	0,0355	0,1379	-0,560	C	Large	UP
HRNR	Hornerin	0,0355	0,1379	-0,560	C	Large	UP
TUBA1C	Tubulin alpha-1C chain	0,0355	0,1379	-0,560	C	Large	UP
ITGA6	Integrin alpha-6	0,0355	0,1379	-0,560	C	Large	UP
TAGLN2	Transgelin-2	0,0362	0,1379	-0,560	C	Large	UP
TPM4	Tropomyosin alpha-4 chain	0,0385	0,1432	-0,540	C	Large	UP
M6PR	Cation-dependent mannose-6-phosphate receptor	0,0407	0,1464	-0,540	C	Large	UP
KRT10	Keratin, type I cytoskeletal 10	0,0433	0,1464	-0,540	C	Large	UP
RAB10	Ras-related protein Rab-10	0,0433	0,1464	-0,540	C	Large	UP
WBP11	WW domain-binding protein 11	0,0433	0,1464	-0,540	C	Large	UP
ANXA5	Annexin A5	0,0443	0,1464	-0,540	C	Large	UP
SSC5D	Soluble scavenger receptor cysteine-rich domain-containing protein SSC5D	0,0524	0,1553	-0,520	C	Large	UP
VCL	Vinculin	0,0524	0,1553	-0,520	C	Large	UP
ABI3BP	Target of Nesh-SH3	0,0524	0,1553	-0,520	C	Large	UP
C16orf54	Transmembrane protein C16orf54	0,0524	0,1553	-0,520	C	Large	UP
YWHAB	14-3-3 protein beta/alpha	0,0587	0,1707	-0,510	C	Large	UP

Table 20. List of downregulated proteins in CD3(-) sEV in melanoma patients (continuous analysis).

ProteinName	Protein Description	p.val_U-test	FDR_U-test	Effect size - RBCC	Type of analysis (continuous vs. binary)	Size of effect	Side of change (regarding MP)
LBP	Lipopolysaccharide-binding protein	0,0001	0,0040	0,940	C	very large	DOWN
QSOX1	Sulfhydryl oxidase 1	0,0002	0,0047	0,980	C	very large	DOWN
MXRA5	Matrix-remodeling-associated protein 5	0,0015	0,0201	0,800	C	very large	DOWN
MARCO	Macrophage receptor MARCO	0,0039	0,0366	0,740	C	very large	DOWN
COL6A3	Collagen alpha-3(VI) chain	0,0115	0,0707	0,660	C	Large	DOWN
KRT85	Keratin, type II cuticular Hb5	0,0185	0,0933	0,620	C	Large	DOWN
OSBPL2	Oxysterol-binding protein-related protein 2	0,0209	0,1015	0,620	C	Large	DOWN
H4C1	Histone H4	0,0448	0,1464	0,540	C	Large	DOWN

Table 21. List of up- and downregulated proteins in CD3(-) sEV in melanoma patients (binary analysis).

ProteinName	Protein Description	p.val_Fisher	FDR_Fisher	Effect size - CrammerV	Type of analysis (continuous vs. binary)	Size of effect	Side of change (regarding MP)
CMTM5	CKLF-like MARVEL transmembrane domain-containing protein 5	0,0031	0,6111	0,734	B	very large	UP
CLIC1	Chloride intracellular channel protein 1	0,0055	0,6111	0,704	B	very large	UP
CD226	CD226 antigen	0,0108	0,6111	0,655	B	Large	UP
CTSD	Cathepsin D	0,0325	0,9167	0,577	B	Large	UP
CLTA	Clathrin light chain A	0,0698	1,0000	0,503	B	Large	UP
CCT8	T-complex protein 1 subunit theta	0,0867	1,0000	0,500	B	Large	UP
CMTM6	CKLF-like MARVEL transmembrane domain-containing protein 6	0,0867	1,0000	0,500	B	Large	UP
PATJ	InaD-like protein	0,0867	1,0000	0,500	B	Large	UP

4.3.5. Pathway enriched in CD3(-) sEV in melanoma patients and healthy donors.

Differentially expressed proteins (DEPs) detected in CD3(-) sEV discriminating melanoma patients from healthy donors were mainly involved in biological processes connected with platelets and blood coagulation, wound healing, and cell adhesion (Figure 30A). Looking at potential Reactome pathways enrichment, DEPs were associated with pathways related to platelet activation, signaling and aggregation, GP1b-IX-V activation signaling, Rho GTPase signaling, immune system, and vesicle-mediated transport (Figure 30B). This suggests that sEV released by platelets and immune cells other than T lymphocytes constitute a large part of CD3(-) sEV fraction.

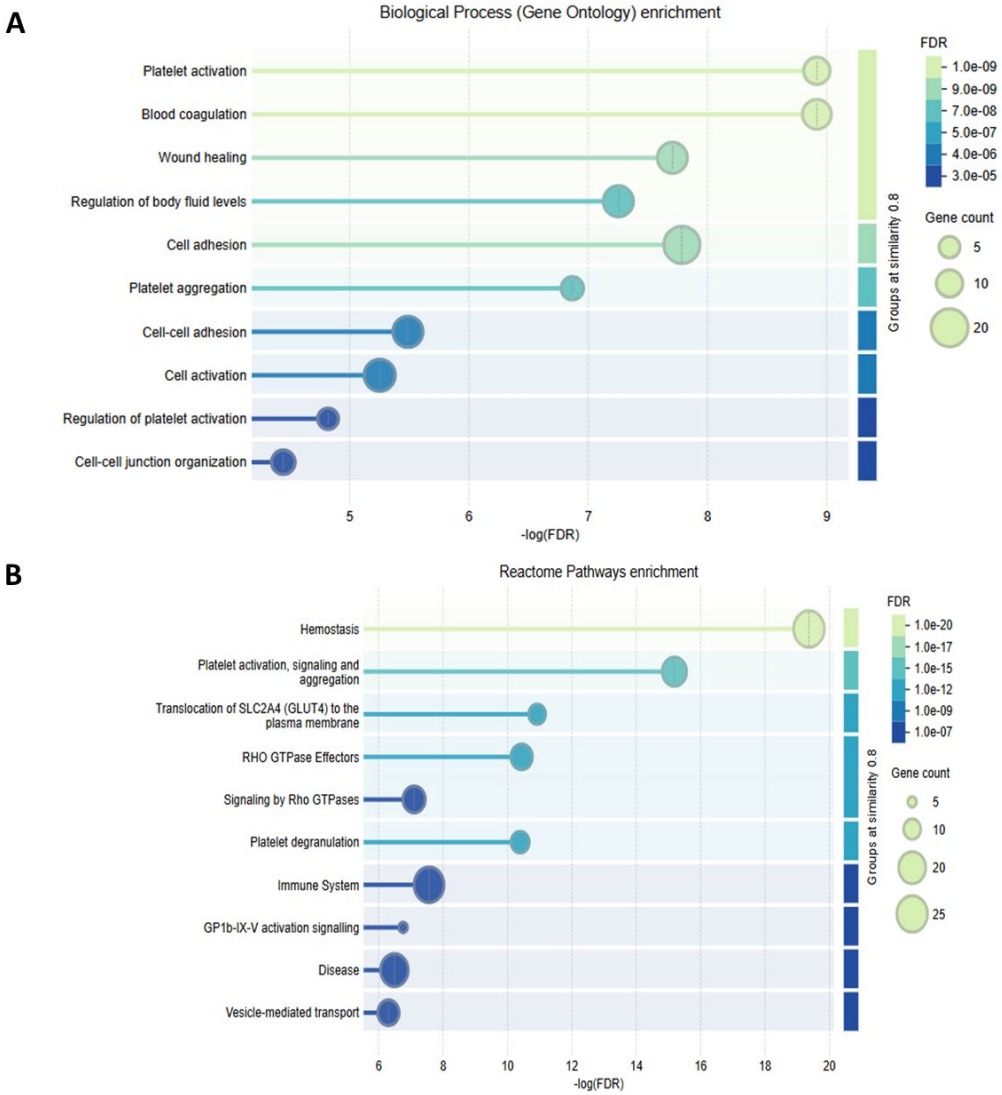

Figure 30. Functional enrichment in networks of proteins detected in the CD3(-) sEV fraction that were not annotated in T cell proteome. Panel A: Biological processes (Gene Ontology), Panel B: Molecular functions (Gene Ontology). Processes sorted by gene count (number of proteins annotated to the process) and FDR (color-coded). For the enrichment analysis, whole genome as a statistical background was assumed (String-db database).

5. DISCUSSION

5.1. Immunocapture Strategies for Small Extracellular Vesicle Isolation in Mass Spectrometry-Based Proteomics.

Small extracellular vesicles (sEV), have emerged as critical mediators of intercellular communication, carrying a diverse cargo of proteins, lipids, and nucleic acids that reflect the physiological and pathological states of their cells of origin [Singh et al. 2024, Whiteside 2024, Tung et al. 2019, Mashouri et al. 2019]. Consequently, proteomic profiling of sEV offers a promising avenue for biomarker discovery and insights into disease mechanisms, particularly in cancer and inflammatory diseases. Mass spectrometry based proteomics has become a cornerstone technique for such analyses, owing to its sensitivity and depth of coverage. However, a significant bottleneck in this workflow remains the efficient and selective isolation of sEV from complex biological matrices like plasma or serum. Among the various isolation approaches, immunoaffinity capture has gained attention for its potential to enrich vesicle subpopulations with higher specificity. Nevertheless, this strategy presents both opportunities and limitations that merit careful consideration [Skoczylas et al. 2024].

Proteomic analysis of sEV is inherently challenging due to several factors. First, the heterogeneity of vesicles complicates isolation and downstream analysis. sEV populations are not only diverse in size but also in their molecular composition, influenced by the cellular source and physiological context. Standard isolation techniques such as ultracentrifugation, size-exclusion chromatography, and polymer-based precipitation often yield heterogeneous vesicle preparations contaminated with protein aggregates, lipoproteins, and other extracellular components. These contaminants can obscure the detection of low-abundance vesicle-specific proteins, thereby limiting the sensitivity and specificity of MS-based proteomic profiling.

Additionally, the typically low protein content of sEV - estimated at the microgram level from milliliter volumes of biofluids - poses a significant analytical challenge. To achieve sufficient material for in-depth proteomic analysis, large sample volumes and efficient enrichment strategies are often required. Even when adequate quantities are

obtained, the dynamic range of vesicular proteins - spanning from highly abundant structural proteins to scarce signaling molecules - complicates comprehensive proteome coverage.

Finally, technical variability introduced during sample preparation, including vesicle lysis, protein digestion, and peptide clean-up, can significantly affect data reproducibility. Given these complexities, the development of robust and reproducible isolation methods is pivotal for advancing sEV proteomics [Fochtman et al. 2024, Kassem et al. 2021, Chandramoul et al. 2009].

Immunocapture-based isolation leverages the specific binding of antibodies to vesicle-associated surface proteins, such as tetraspanins (CD9, CD63, CD81) or cell-type-specific markers (for example CSPG4, CD3, CD34) enabling the targeted enrichment of sEV from complex samples [Ferrone et al. 2020, Sharma et al. 2020, Theodoraki et al. 2018]. This selectivity offers several distinct advantages.

Foremost, immunocapture reduces sample complexity by selectively isolating vesicles of interest while excluding contaminants and non-vesicular particles. Such enrichment enhances the signal-to-noise ratio in MS analyses, improving the detection of low-abundance vesicular proteins that might otherwise be masked by abundant extracellular proteins. This specificity is particularly valuable in biofluids like plasma or serum, where proteinaceous contaminants are prevalent. Furthermore, immunocapture facilitates the isolation of vesicles from specific cellular origins or disease contexts, allowing for more targeted biomarker discovery. For example, tumor-derived sEV can be enriched using antibodies against cancer-specific surface markers, potentially increasing the clinical relevance of identified protein signatures. The compatibility of immunocapture with small sample volumes also makes it an attractive approach for clinical studies, where sample availability can be limited. Coupled with recent advances in microfluidic platforms and automated workflows, immunocapture has the potential to enhance throughput and reproducibility, addressing some of the technical limitations of conventional methods. [Skoczylas et al. 2024, Zarovni et al. 2015, Hong et al. 2014].

Despite its advantages, immunocapture is not without challenges. A primary concern is the potential bias introduced by selective targeting. By focusing on a subset of vesicles expressing specific markers, immunocapture may overlook vesicle

populations that lack or have low expression of the targeted proteins. This selective capture could skew the proteomic profile, limiting the comprehensiveness of the analysis. Moreover, the efficiency of immunocapture is highly dependent on antibody quality, including specificity, affinity, and epitope accessibility. Non-specific binding or cross-reactivity can compromise the purity of the isolated vesicles, reintroducing contaminants that the method seeks to avoid. The orientation and density of target proteins on vesicle surfaces also influence capture efficiency, which can vary across biological conditions and vesicle subtypes [Fochtman et al. 2024].

Another technical limitation relates to the elution of captured vesicles or proteins for downstream MS analysis. Harsh elution conditions may be required to release bound vesicles or proteins from the antibody-coated surfaces, potentially leading to sample loss or protein denaturation, thereby impacting proteomic data quality. Finally, immunocapture approaches are often more costly than traditional isolation methods, due to the expense of high-quality antibodies and specialized reagents or equipment. This can pose a barrier to scalability, particularly for large cohort studies.

5.2. Proteomic signature of MTEX (small extracellular vesicles released by melanoma cells) isolated from plasma of melanoma patients.

Efforts to identify reliable biomarkers for melanoma progression and therapeutic response, including those based on advanced genomic and multi-omics methodologies, have yielded a range of promising protein candidates [Gowda et al. 2020]. However, to date, none of these putative biomarkers have been clinically validated. Soluble lactate dehydrogenase (sLDH) remains the only protein consistently correlated with tumour burden in certain patients with metastatic melanoma [Garbe et al. 2024, Rutkowski et al. 2022]. Despite intensive research, attempts to establish meaningful associations between sLDH levels and specific molecular, immunological, or metabolic characteristics have been unsuccessful [Gowda et al. 2020]. Consequently, the need for predictive biomarkers to guide therapy in melanoma remains a significant and unresolved clinical challenge.

Recently, small extracellular vesicles (sEV) have emerged as a promising platform for melanoma diagnostics and prognostics. Multiple studies, have demonstrated the

presence of factors implicated in angiogenesis, immune suppression, stromal remodeling, lymphatic dissemination, and tumour progression within sEV isolated from the plasma of melanoma patients [Sharma et al. 2020, Boussadia et al. 2018, Alegre et al. 2016]. Prior evidence suggests that tumour-derived sEV (TEX), in particular, may offer superior biomarker potential compared to analyses of tumour tissue or plasma-soluble factors alone [Rodriguez-Cerdeira et al. 2018, Byström et al. 2017].

Historically, studies on melanoma-derived TEX primarily utilized vesicles derived from established melanoma cell lines. Comprehensive proteomic analysis of TEX from a panel of melanoma cell lines (1205Lu, 501MEL, A375M, Daju, G1, MNT-1, SK-MEL-28) identified a total of 917 proteins, with individual cell lines contributing between 486 and 632 proteins each [Lazar et al. 2015]. Approximately 25% of these proteins were conserved across cell lines, encompassing ESCRT components, tetraspanins (CD9, CD63, CD81), small GTPases, annexins, cytoskeletal, and motor proteins. Notably, distinct subsets of proteins were identified: 22 unique to non-tumorigenic cell line TEX, 29 exclusive to tumorigenic TEX, and 112 specific to TEX from metastatic lines. The latter group included proteins with established roles in melanoma biology, such as EGFR, EPHB2, KIT, LGALS1, LGALS3, MCAM, MET, NRAS, NT5E (CD73), PTK2 (FAK1), and SRC [Lazar et al. 2015].

Proteomic analyses of small extracellular vesicles (sEV) isolated from the plasma or serum of melanoma patients could provide valuable insights, although the field remains fragmented. The initial comparative proteomic study, but using immunoaffinity-based isolation methods identified a distinct melanoma-associated sEV signature, including TYRP2, VLA-4, HSP70, an isoform of HSP90, and MET, specifically in patients with advanced melanoma [Peinado et al., 2012]. Supporting these findings, another investigation reported elevated levels of TYRP2, MIA, and S100B in plasma-derived sEV from stage IV melanoma patients compared to healthy controls [Alegre et al. 2015]. More recently, a comprehensive proteomic analysis employing LC-MS/MS characterized both plasma- and serum-derived sEV, revealing distinct molecular profiles between melanoma patients and healthy individuals, though no significant differences were observed between stage III and stage IV disease [Lattmann et al. 2024]. Additional studies focusing on sEV from tissue samples and lymphatic fluid have

provided useful biological insights but are less applicable to the liquid biopsy approach [Crescitelli et al. 2020, García-Silva et al. 2019, Broggi et al. 2019]. Moreover, the ex vivo analyses mentioned above involved a heterogeneous population of sEVs isolated from the plasma/serum of patients, representing a mixture of sEVs from different cells (non-malignant and malignant), rather than a homogeneous fraction of MTEX. Circulating sEV expressing PD-L1 have been investigated as dynamic biomarkers in melanoma patients receiving immune checkpoint inhibitors (ICIs) [Cordonnier et al. 2020]. Consistent with findings in other solid tumours, fluctuations in PD-L1 levels in sEV were found to correlate with disease activity and response to immunotherapy [Ricklefs et al. 2018; Theodoraki et al. 2018]. Despite these promising associations, the precise tumoural origin of PD-L1 in sEV remains uncertain, as these vesicles have not been conclusively validated as TEX and may partially derive from non-malignant PD-L1-positive cells. Overall, despite progress, the proteomic landscape of melanoma-derived sEV remains incompletely defined, and methodological variability continues to hinder direct comparison across studies.

One of the aims of this doctoral dissertation was to evaluate whether melanoma-derived sEV (MTEX), isolated from patient plasma, could function as a non-invasive liquid biopsy to predict disease progression or therapeutic outcomes. The rationale for comparing proteomic profiles of MTEX with non-malignant sEV (NMTEX) was based on the hypothesis that MTEX provide a tumour-specific vesicular signature, potentially superior to analyses of total plasma sEVs. Utilizing a previously established immunocapture method employing anti-CSPG4 monoclonal antibodies [Ferrone et al. 2020, Sharma et al. 2020], MTEX from NMTEX populations were successfully separated. High-resolution LC-MS/MS analysis of paired MTEX and NMTEX samples was then performed to elucidate differential protein cargo profiles. Building on earlier flow cytometric characterization of these vesicles [Sharma et al. 2020], it could have been anticipated that the identification of a distinct proteomic signature unique to MTEX that could serve as an indicator of melanoma progression or therapeutic responsiveness.

It is important to mention, that immune capture of MTEX was possible thanks to cooperation with Prof. Theresa Whiteside and Prof. Soldano Ferrone, who produced and investigated the anti-CSPG4 mAbs. CSPG4 is a tumor antigen, highly expressed on

melanoma cells (80% of primary and metastatic tumors) and on malignant melanoma initiating cells.

The anti-CSPG4 antibodies produced by S. Ferrone are very specific, selectively recognizing epitopes abundantly expressed on melanoma cells, while showing no reactivity toward normal human tissues. This happens because antigens in tumors have their own specific, unique pattern of epitope glycosylation [Ren et al. 2024]. The data regarding CSPG4 expression in normal human tissues remain inconsistent. Based on the investigations of Ferrone and his collaborators, immunohistochemical analyses employing monoclonal antibodies directed against distinct CSPG4 epitopes have not revealed any expression of this antigen in normal tissues, with the notable exception of activated pericytes within the tumor microenvironment [Ferrone et al. 2020]. Comparable findings have been reported independently by Beard et al, who utilized alternative methodological approaches [Beard et al. 2014]. Contrasting with these findings, the Protein Atlas database, which relies on commercially available anti-CSPG4 antibodies, reports a widespread distribution of CSPG4 across normal tissues. This discrepancy likely stems from the limited specificity of certain commercial antibodies employed in generating the Protein Atlas data. For example, a rabbit antiserum supplied by Sigma appears non-specific, as it detects a protein with a molecular weight distinct from CSPG4 in Western blot assays. Moreover, this antibody continues to bind cells with CSPG4 knock-out by CRISPR, what further indicating its lack of specificity. This divergence between Ferrone et al validated results and the findings presented in the Protein Atlas has contributed to confusion among researchers utilizing commercial anti-CSPG4 mAbs for immune capture applications. In contrast, several commercially available anti-CSPG4 antibodies do not achieve comparable tumor cell specificity, rendering them unreliable for immune capture of melanoma-derived sEV [Ferrone et al. 2020].

Notably, the proteome analysis of small extracellular vesicles released by melanoma cells and isolated from patients plasma presented in this doctoral dissertation remains unique immunoaffinity-based proteomic profiling of melanoma-derived sEV. No comparable immunoaffinity-based studies have since been reported for MTEX. There are studies in other cancers where immunocapture is also used to separate sEVs. For example glypican 1 (GPC1) was used to isolate TEX from plasma of patients with

pancreatic cancer [Melo et al. 2015], prostate-specific membrane antigen (PSMA) was used to isolate TEX from plasma of prostate cancer patients [Mizutani et al. 2014, and CD34 antigen, was used to immune capture TEX from the plasma of patients with acute myeloid leukemia [Hong et al. 2014].

Presented analyses revealed a panel of 73 proteins either uniquely present or significantly overexpressed in MTEX relative to NMTEX. Guided by clinical relevance and proteomic criteria - such as known involvement in oncogenic processes, frequent detection across patient samples, membrane association, and inclusion in the ExoCarta database [Chen et al. 2024], a subset of 16 proteins as an "MTEX differentiating panel" was defined. Functional enrichment analysis (GO) of the 73 MTEX-associated proteins revealed predominant roles in signalling cascades and immunoregulatory functions, aligning with prior findings (Sharma et al., 2020) and further substantiating the functional distinction between MTEX and NMTEX.

Importantly, this study also identified a subset of MTEX proteins - namely ADAMTS13, CNTN1, F10, HSP90AB1, ITIH3, MSN, PDCD6IP, PLOD1, RPS6KA3, SGCE, THBS1, TUBB, and UBA52 - whose expression levels discriminated between patients exhibiting progressive disease (PD) and those with no evidence of disease (NED) or stable disease (SD) post-therapy. This protein subset forms the basis of a putative MTEX-derived prognostic signature. Notably, despite the modest sample size, differential expression patterns within MTEX encompassed proteins associated with extracellular matrix organization, metabolic processes, stress responses, and immune modulation, what further supporting the clinical relevance of this vesicle population. Concordantly, another group reported a similar enrichment of progression-associated proteins in EVs derived from exudative seroma following lymphadenectomy in melanoma patients [García-Silva et al. 2019].

Among the prognostic candidates, PDCD6IP (also known as ALIX) emerged as a particularly potent discriminator between PD and NED/SD cohorts. ALIX, a multifunctional component of the ESCRT machinery, is pivotal for endocytosis, multivesicular body formation, membrane repair, cytokinesis, and apoptosis [Pust et al. 2023, Qiu et al. 2022, Larios et al. 2020]. Beyond its structural roles, ALIX has been implicated in regulating tumour cell survival, immunosuppression, and PD-L1

expression [García-Silva et al. 2019]. Intriguingly, four proteins - HSP90AB1, TUBB, TUBB1, and PFN1 - exhibited strong expression correlations with ALIX, suggesting the existence of an interconnected functional network. Collectively, the identified molecular signature - comprising ALIX, its correlated proteins (HSP90AB1, TUBB, TUBB1, PFN1), along with CNTN1 (expressed in MTEX but absent in PD patients) - holds significant prognostic potential in melanoma.

Taken together, these findings demonstrate that the proteomic cargo of MTEX reflects the molecular landscape of melanoma cells and supports the potential application of MTEX as a non-invasive liquid biopsy for monitoring disease progression and therapeutic response. Further validation in larger cohorts is warranted to establish MTEX profiling as a surrogate marker for melanoma progression. In fact, the potential role of PDCD6IP protein carried on plasma-derived MTEX in immune regulation and promotion of melanoma progression become the subject of new, ongoing research.

5.3. Proteomic signature of T cell-derived small extracellular vesicles (CD3(+) phenotype) isolated from plasma of melanoma patients.

The dual role of immune cells in either restraining or facilitating tumor progression is well established, and patients with advanced malignancies frequently exhibit compromised immune competence. Consequently, the evaluation of immune cells - whether within the tumor microenvironment (TME) or in systemic circulation - has become pivotal for assessing immune status and therapeutic responsiveness, particularly in the context of immunotherapies. However, conventional approaches that rely on tissue biopsies or serial blood sampling are inherently invasive and labor - intensive [Singh et al. 2023, Zugazagoitia et al. 2020]. Beyond their utility as proxies for tumor-derived materials in liquid biopsy applications, sEV also mirror the characteristics of immune cells, encapsulating both phenotypic and functional signatures of their parental cells.

Previous investigations have demonstrated that plasma-derived sEV can effectively substitute for direct analysis of tumor or immune cells, serving as biomarkers for tumor progression and immune cell functionality, especially T cell competence [Theodoraki et al. 2018]. Nonetheless, the heterogeneity of plasma sEV populations,

each with distinct biogenetic origins and molecular profiles, complicates the identification of functionally relevant subsets. To address this challenge, a hypothesis has been put forward that targeting specific sEV subpopulations through surface marker-based enrichment could enhance the informativeness of the resulting analysis.

In this part of the doctoral dissertation, immunoaffinity capture using antibodies targeting the CD3 antigen - a definitive marker of T lymphocytes was employed to isolate CD3-positive (CD3(+)) sEVs from plasma. This approach enabled the successful separation of T cell-derived vesicles from CD3-negative (CD3(-)) sEVs, which predominantly originate from non-T-cell sources. Prior to this work, the feasibility of this method and its ability to yield critical data regarding the functional state of T cells in patients was demonstrated with head and neck cancer patients [Theodoraki et al. 2018].

It is well understood that tumors exploit various mechanisms to subvert immune surveillance, often via TEX-mediated suppression of anti-tumor immune responses. Through complex crosstalk, TEX influence the functional fate of T cells and other immune populations, leading to diminished anti-tumor activity or, paradoxically, the acquisition of tumor-supporting roles [Whiteside et al. 2023]. As TEX remodel the TME and propagate immunosuppressive signals, sEVs secreted by functionally altered T cells contribute further to immune dysregulation, with implications for disease progression and treatment response [Theodoraki et al. 2018]. Results of this study support the concept that both TEX and T cell-derived sEV circulating in patient plasma act as non-invasive surrogates for monitoring tumor and immune dynamics. Specifically, T cell-derived vesicles offer a window into systemic and tumor-localized T cell status, effectively functioning as a "liquid T cell biopsy."

By applying immunocapture techniques to isolate CD3(+) sEV from melanoma patient plasma, we were able to delineate the proteomic landscape of T cell-derived vesicles and compare it to that of healthy donors. The analysis revealed distinct proteomic signatures between patient and control groups. Notably, proteins enriched in CD3(+) sEVs from MPs were predominantly associated with immune regulation and included key molecules involved in cancer-related processes such as developmental regulation, cellular motility, transcriptional control, and signal transduction pathways. Intriguingly, there was an upregulation of proteins linked to Rho GTPase signaling and

the MAPK cascade - particularly those involving BRAF kinase. While correlative, these observations suggest that T cells in melanoma patients may undergo malignant reprogramming, leading them to secrete sEV bearing protein signatures typically associated with melanoma cells themselves. This needs further investigation to find the molecular mechanisms underlying this phenomenon. Elucidating these molecular alterations, including the activation of Rho GTPase and MAPK/BRAF pathways in CD3(+) sEV, may provide critical insights into the extent of T cell reprogramming in the tumor context. Such understanding could enhance the utility of CD3(+) sEV as biomarkers for monitoring disease progression and therapeutic efficacy.

The immunocapture-based separation of T cell-derived sEV (CD3-positive) and TEX-enriched CD3-negative sEV represents a promising dual-biomarker strategy, enabling simultaneous "liquid biopsies" of both the immune and tumor compartments from a single plasma sample.

6. SUMMARY

1. Small extracellular vesicles released by melanoma cells can be effectively separated from other types of sEVs present in human plasma by immunocapture using antibodies specific for the CSPG4 antigen and small extracellular vesicles released by T cells can be efficiently separated from other types of sEVs present in human plasma by immunocapture using antibodies specific for the CD3 antigen.
2. The isolated, immunoselected sEVs are suitable material for mass spectrometry-based high-throughput proteome profiling. The analyses performed allowed the identification of proteins differentiating MTEX from NMTEX in melanoma patients and differentiating the CD3(+) and CD3(-) fractions of sEVs in the plasma of healthy donors and melanoma patients.
3. Paired MTEX vs. NMTEX analysis allowed the identification of 150 proteins differentiating MTEX from NMTEX isolated from melanoma patients (73 proteins with statistically significantly higher levels and 77 proteins showing statistically significant lower levels). Among them, the top 16 MTEX-upregulated proteins are proposed panel discriminating MTEX from NMTEX. All 16 proteins are functionally associated with cancer progression, signaling or immune regulation.
4. The MTEX protein profile reflects melanoma progression and differentiates between NED patients and PD patients after cancer therapy. Among the 12 proteins significantly upregulated in patients with PD, PDCD6IP (ALIX) had the highest discriminating value at $p<0.0003$.
5. There were identified 418 proteins in the CD3(+) sEV proteome of healthy donors and 406 proteins in the CD3(+) sEV proteome of patients diagnosed with melanoma. Among the identified proteins, 65 of them were proteins differentiating the CD3(+) sEV proteome of melanoma patients from healthy donors (26 proteins showing statistically significantly higher levels and 38 proteins showing statistically significant lower levels). In case of CD3(-) sEV , there were 51 proteins showing statistically significantly higher levels and 13 proteins showing statistically significant lower levels, thus dicrciminating CD3(-) sEV of MPs vs HDs.

6. The proteins identified in CD3(+) extracellular vesicles reflected known molecular features of T cells, suggesting that sEVs isolated from human plasma using immune capture with anti-CD3 antibodies could serve as a “liquid T-cell biopsy.”

7. REFERENCES:

1. Alexandrov LB, Nik-Zainal S, Wedge DC, Aparicio SA, Behjati S, Biankin AV, Bignell GR, Bolli N, Borg A, Børresen-Dale AL, Boyault S, Burkhardt B, Butler AP, Caldas C, Davies HR, Desmedt C, Eils R, Eyfjörd JE, Foekens JA, Greaves M, Hosoda F, Hutter B, Ilicic T, Imbeaud S, Imielinski M, Jäger N, Jones DT, Jones D, Knappskog S, Kool M, Lakhani SR, López-Otín C, Martin S, Munshi NC, Nakamura H, Northcott PA, Pajic M, Papaemmanuil E, Paradiso A, Pearson JV, Puente XS, Raine K, Ramakrishna M, Richardson AL, Richter J, Rosenstiel P, Schlesner M, Schumacher TN, Span PN, Teague JW, Totoki Y, Tutt AN, Valdés-Mas R, van Buuren MM, van 't Veer L, Vincent-Salomon A, Waddell N, Yates LR; Australian Pancreatic Cancer Genome Initiative; ICGC Breast Cancer Consortium; ICGC MMML-Seq Consortium; ICGC PedBrain; Zucman-Rossi J, Futreal PA, McDermott U, Lichter P, Meyerson M, Grimmond SM, Siebert R, Campo E, Shibata T, Pfister SM, Campbell PJ, Stratton MR. Signatures of mutational processes in human cancer. Nature. 2013;500(7463):415-21.Erratum in: Nature. 2013 Oct 10;502(7470):258. Imielinsk, Marcin [corrected to Imielinski, Marcin].
2. An M, Wu J, Zhu J, Lubman DM. Comparison of an Optimized Ultracentrifugation Method versus Size-Exclusion Chromatography for Isolation of Exosomes from Human Serum. J Proteome Res. 2018;17(10):3599-3605.
3. An S, Kim K, Moon S, Ko KP, Kim I, Lee JE, Park SK. Indoor Tanning and the Risk of Overall and Early-Onset Melanoma and Non-Melanoma Skin Cancer: Systematic Review and Meta-Analysis. Cancers (Basel). 2021;13(23):5940.
4. Ansari FJ, Tafti HA, Amanzadeh A, Rabbani S, Shokrgozar MA, Heidari R, Behroozi J, Eyni H, Uversky VN, Ghanbari H. Comparison of the efficiency of ultrafiltration, precipitation, and ultracentrifugation methods for exosome isolation. Biochem Biophys Rep. 2024;38:101668.
5. Arbelaiz A, Azkargorta M, Krawczyk M, Santos-Laso A, Lapitz A, Perugorria MJ, Erice O, Gonzalez E, Jimenez-Agüero R, Lacasta A, Ibarra C, Sanchez-Campos A, Jimeno JP, Lammert F, Milkiewicz P, Marzioni M, Macias RIR, Marin JJG, Patel T, Gores GJ, Martinez I, Elortza F, Falcon-Perez JM, Bujanda L, Banales JM. Serum extracellular vesicles contain protein biomarkers for primary sclerosing cholangitis and cholangiocarcinoma. Hepatology. 2017;66(4):1125-1143.
6. Arbelaiz A, Azkargorta M, Krawczyk M, Santos-Laso A, Lapitz A, Perugorria MJ, Erice O, Gonzalez E, Jimenez-Agüero R, Lacasta A, Ibarra C, Sanchez-Campos A, Jimeno JP, Lammert F, Milkiewicz P, Marzioni M, Macias RIR, Marin JJG, Patel T, Gores GJ, Martinez I, Elortza F, Falcon-Perez JM, Bujanda L, Banales JM. Serum extracellular vesicles contain protein biomarkers for primary sclerosing cholangitis and cholangiocarcinoma. Hepatology. 2017;66(4):1125-1143.
7. Arnold M, Singh D, Laversanne M, Vignat J, Vaccarella S, Meheus F, Cust AE, de Vries E, Whiteman DC, Bray F. Global Burden of Cutaneous Melanoma in 2020 and Projections to 2040. JAMA Dermatol. 2022;158(5):495-503.
8. Bajaj N, Sharma D. Uncovering metabolic signatures in cancer-derived exosomes: LC-MS/MS and NMR profiling. Nanoscale. 2024;17(1):287-303.

9. Beard RE, Zheng Z, Lagisetty KH, Burns WR, Tran E, Hewitt SM, Abate-Daga D, Rosati SF, Fine HA, Ferrone S, Rosenberg SA, Morgan RA. Multiple chimeric antigen receptors successfully target chondroitin sulfate proteoglycan 4 in several different cancer histologies and cancer stem cells. J Immunother Cancer. 2014;2:25.
10. Bland CL, Byrne-Hoffman CN, Fernandez A, Rellick SL, Deng W, Klinke DJ 2nd. Exosomes derived from B16F0 melanoma cells alter the transcriptome of cytotoxic T cells that impacts mitochondrial respiration. FEBS J. 2018;285(6):1033-1050
11. Bonsergent E, Grisard E, Buchrieser J, Schwartz O, Théry C, Lavieu G. Quantitative characterization of extracellular vesicle uptake and content delivery within mammalian cells. Nat Commun. 2021;12(1):1864.
12. Bowden NA, Ashton KA, Avery-Kiejda KA, Zhang XD, Hersey P, Scott RJ. Nucleotide excision repair gene expression after Cisplatin treatment in melanoma. Cancer Res. 2010;70(20):7918-26.
13. Bretz NP, Ridinger J, Rupp AK, Rimbach K, Keller S, Rupp C, Marmé F, Umansky L, Umansky V, Eigenbrod T, Sammar M, Altevogt P. Body fluid exosomes promote secretion of inflammatory cytokines in monocytic cells via Toll-like receptor signaling. J Biol Chem. 2013;288(51):36691-702.
14. Broggi MAS, Maillat L, Clement CC, Bordry N, Corthésy P, Auger A, Matter M, Hamelin R, Potin L, Demurtas D, Romano E, Harari A, Speiser DE, Santambrogio L, Swartz MA. Tumor-associated factors are enriched in lymphatic exudate compared to plasma in metastatic melanoma patients. J Exp Med. 2019;216(5):1091-1107.
15. Burns D, George J, Aucoin D, Bower J, Burrell S, Gilbert R, Bower N. The Pathogenesis and Clinical Management of Cutaneous Melanoma: An Evidence-Based Review. J. Med. Imaging Radiat. Sci. 2019;50:460–469.e1.
16. Byström S, Fredolini C, Edqvist PH, Nyaiesh EN, Drobin K, Uhlén M, Bergqvist M, Pontén F, Schwenk JM. Affinity Proteomics Exploration of Melanoma Identifies Proteins in Serum with Associations to T-Stage and Recurrence. Transl Oncol. 2017;10(3):385-395.
17. Caini S, Gandini S, Sera F, Raimondi S, Fargnoli MC, Boniol M, Armstrong BK. Meta-analysis of risk factors for cutaneous melanoma according to anatomical site and clinico-pathological variant. Eur J Cancer. 2009;45(17):3054-63.
18. Cancer Genome Atlas Network. Genomic Classification of Cutaneous Melanoma. Cell. 2015;161(7):1681-96.
19. Candido S, Rapisarda V, Marconi A, Malaponte G, Bevelacqua V, Gangemi P, Scalisi A, McCubrey JA, Maestro R, Spandidos DA, et al. Analysis of the B-RafV600E mutation in cutaneous melanoma patients with occupational sun exposure. Oncol Rep. 2014;31:1079–1082.
20. Cao Y, Xu P, Shen Y, Wu W, Chen M, Wang F, Zhu Y, Yan F, Gu W, Lin Y. Exosomes and cancer immunotherapy: A review of recent cancer research. Front Oncol. 2023;12:1118101.
21. Caramel J, Papadogeorgakis E, Hill L, Browne GJ, Richard G, Wierinckx A, Saldanha G, Osborne J, Hutchinson P, Tse G, Lachuer J, Puisieux A, Pringle JH, Ansieau S, Tulchinsky E. A switch in the expression of embryonic EMT-inducers drives the development of malignant melanoma. Cancer Cell. 2013;24(4):466-80.

22. Chandramouli K, Qian PY. Proteomics: challenges, techniques and possibilities to overcome biological sample complexity. Hum Genomics Proteomics. 2009;2009:239204.
23. Chapuy-Regaud S, Dubois M, Plisson-Chastang C, Bonnefois T, Lhomme S, Bertrand-Michel J, You B, Simoneau S, Gleizes PE, Flan B, Abravanel F, Izopet J. Characterization of the lipid envelope of exosome encapsulated HEV particles protected from the immune response. Biochimie. 2017;141:70-79.
24. Chen J, Lin JJ, Wang W, Huang H, Pan Z, Ye G, Dong S, Lin Y, Lin C, Huang Q. EV-COMM: A database of interspecies and intercellular interactions mediated by extracellular vesicles. J Extracell Vesicles. 2024;13(4):e12442
25. Chen K, Wang Q, Liu X, Wang F, Yang Y, Tian X. Hypoxic pancreatic cancer derived exosomal miR-30b-5p promotes tumor angiogenesis by inhibiting GJA1 expression. Int J Biol Sci. 2022;18(3):1220-1237.
26. Chivet M, Javalet C, Laulagnier K, Blot B, Hemming FJ, Sadoul R. Exosomes secreted by cortical neurons upon glutamatergic synapse activation specifically interact with neurons. J Extracell Vesicles. 2014;3:24722.
27. Clayton A, Mitchell JP, Court J, Mason MD, Tabi Z. Human tumor-derived exosomes selectively impair lymphocyte responses to interleukin-2. Cancer Res. 2007;67(15):7458-66
28. Colantonio S, Bracken MB, Beecker J. The association of indoor tanning and melanoma in adults: systematic review and meta-analysis. J Am Acad Dermatol. 2014;70(5):847-57.e1-18.
29. Cordonnier M, Nardin C, Chanteloup G, Derangere V, Algros MP, Arnould L, Garrido C, Aubin F, Gobbo J. Tracking the evolution of circulating exosomal-PD-L1 to monitor melanoma patients. J Extracell Vesicles. 2020;9(1):1710899.
30. Costa Verdera H, Gitz-Francois JJ, Schiffelers RM, Vader P. Cellular uptake of extracellular vesicles is mediated by clathrin-independent endocytosis and macropinocytosis. J Control Release. 2017;266:100-108.
31. Crescitelli R, Lässer C, Jang SC, Cvjetkovic A, Malmhäll C, Karimi N, Höög JL, Johansson I, Fuchs J, Thorsell A, Gho YS, Olofsson Bagge R, Lötvall J. Subpopulations of extracellular vesicles from human metastatic melanoma tissue identified by quantitative proteomics after optimized isolation. J Extracell Vesicles. 2020;9(1):1722433.
32. Cross T, Øvstebø R, Brusletto BS, Trøseid A-MS, Olstad OK, Aspelin T, Jackson CJ, Chen X, Utheim TP, Haug KBF. RNA Profiles of Tear Fluid Extracellular Vesicles in Patients with Dry Eye-Related Symptoms. Int. J. Mol. Sci. 2023;24:15390.
33. Czystowska M, Szczepanski MJ, Szajnik M, Quadrini K, Brandwein H, Hadden JW, Whiteside TL. Mechanisms of T-cell protection from death by IRX-2: a new immunotherapeutic. Cancer Immunol Immunother. 2011;60(4):495-506.
34. Davis EJ, Johnson DB, Sosman JA, Chandra S. Melanoma: What do all the mutations mean? Cancer. 2018;124(17):3490-3499.
35. Deng G, Zeng F, Su J, Zhao S, Hu R, Zhu W, Hu S, Chen X, Yin M. BET inhibitor suppresses melanoma progression via the noncanonical NF-κB/SPP1 pathway. Theranostics. 2020;10(25):11428-11443.

36. Dhillon AS, Hagan S, Rath O, Kolch W. MAP kinase signalling pathways in cancer. Oncogene. 2007;26(22):3279-90. doi: 10.1038/sj.onc.1210421. PMID: 17496922.
37. Donoso-Quezada J, Ayala-Mar S, González-Valdez J. The role of lipids in exosome biology and intercellular communication: Function, analytics and applications. Traffic. 2021;22(7):204-220.
38. Düchler M, Czernek L, Peczek L, Cypryk W, Sztiller-Sikorska M, Czyz M. Melanoma-Derived Extracellular Vesicles Bear the Potential for the Induction of Antigen-Specific Tolerance. Cells. 2019;8(7):665.
39. Ekström EJ, Bergenfelz C, von Bülow V, Serifler F, Carlemalm E, Jönsson G, Andersson T, Leandersson K. WNT5A induces release of exosomes containing pro-angiogenic and immunosuppressive factors from malignant melanoma cells. Mol Cancer. 2014;13:88.
40. Elder DE, Barnhil R, Bastian BC, Cook MG, de la Fouchardière A, Gerami P, et al.. "Melanocytic Tumour Classification and the Pathway Concept". In: Elder DE, Massi D, Scolyer RA, Willemze R, editors. Who Classification of Skin Tumours, 4th Edition. Lyon, F: IARC; (2018). p. 66–71.
41. Elder DE, Bastian BC, Cree IA, Massi D, Scolyer RA. The 2018 World Health Organization Classification of Cutaneous, Mucosal, and Uveal Melanoma: Detailed Analysis of 9 Distinct Subtypes Defined by Their Evolutionary Pathway. Arch Pathol Lab Med. 2020;144(4):500-522.
42. Elzanowska J, Semira C, Costa-Silva B. DNA in extracellular vesicles: biological and clinical aspects. Mol Oncol. 2021;15(6):1701-1714.
43. Fabbri M, Paone A, Calore F, Galli R, Gaudio E, Santhanam R, Lovat F, Fadda P, Mao C, Nuovo GJ, Zanesi N, Crawford M, Ozer GH, Wernicke D, Alder H, Caligiuri MA, Nana-Sinkam P, Perrotti D, Croce CM. MicroRNAs bind to Toll-like receptors to induce prometastatic inflammatory response. Proc Natl Acad Sci U S A. 2012;109(31):E2110-6.
44. Fang S, Tian H, Li X, Jin D, Li X, Kong J, Yang C, Yang X, Lu Y, Luo Y, Lin B, Niu W, Liu T. Clinical application of a microfluidic chip for immunocapture and quantification of circulating exosomes to assist breast cancer diagnosis and molecular classification. PLoS One. 2017;12(4):e0175050.
45. Ferrone S, Whiteside TL. Targeting CSPG4 for isolation of melanoma cell-derived exosomes from body fluids. HNO. 2020;68(2):100-105.
46. Fitzner D, Schnaars M, van Rossum D, Krishnamoorthy G, Dibaj P, Bakhti M, Regen T, Hanisch UK, Simons M. Selective transfer of exosomes from oligodendrocytes to microglia by macropinocytosis. J Cell Sci. 2011;124(Pt 3):447-58.
47. Gajos-Michniewicz A, Czyz M. WNT Signaling in Melanoma. Int J Mol Sci. 2020;21(14):4852.
48. Gandini S., Sera F., Cattaruzza M.S., Pasquini P., Abeni D., Boyle P., Melchi C.F. Meta-analysis of risk factors for cutaneous melanoma: I. Common and atypical naevi. Eur. J. Cancer. 2005;41:28–44.
49. Garbe C, Amaral T, Peris K, Hauschild A, Arenberger P, Basset-Seguin N, Bastholt L, Bataille V, Brochez L, Del Marmol V, Dréno B, Eggermont AMM, Fargnoli MC, Forsea AM, Höller C, Kaufmann R, Kelleners-Smeets N, Lallas A, Lebbé C, Leiter U,

Longo C, Malvehy J, Moreno-Ramirez D, Nathan P, Pellacani G, Saiag P, Stockfleth E, Stratigos AJ, Van Akkooi ACJ, Vieira R, Zalaudek I, Lorigan P, Mandala M; European Association of Dermato-Oncology (EADO), the European Dermatology Forum (EDF), and the European Organization for Research and Treatment of Cancer (EORTC). European consensus-based interdisciplinary guideline for melanoma. Part 2: Treatment - Update 2024. Eur J Cancer. 2025;215:115153.

50. Garbe C, Amaral T, Peris K, Hauschild A, Arenberger P, Basset-Seguin N, Bastholt L, Bataille V, Del Marmol V, Dréno B, Fargnoli MC, Forsea AM, Grob JJ, Höller C, Kaufmann R, Kelleners-Smeets N, Lallas A, Lebbé C, Lytvynenko B, Malvehy J, Moreno-Ramirez D, Nathan P, Pellacani G, Saiag P, Stratigos AJ, Van Akkooi ACJ, Vieira R, Zalaudek I, Lorigan P; European Dermatology Forum (EDF), the European Association of Dermato-Oncology (EADO), and the European Organization for Research and Treatment of Cancer (EORTC). European consensus-based interdisciplinary guideline for melanoma. Part 1: Diagnostics: Update 2022. Eur J Cancer. 2022;170:236-255.
51. García-Silva S, Benito-Martín A, Sánchez-Redondo S, Hernández-Barranco A, Ximénez-Embún P, Nogués L, Mazariegos MS, Brinkmann K, Amor López A, Meyer L, Rodríguez C, García-Martín C, Boskovic J, Letón R, Montero C, Robledo M, Santambrogio L, Sue Brady M, Szumera-Ciećkiewicz A, Kalinowska I, Skog J, Noerholm M, Muñoz J, Ortiz-Romero PL, Ruano Y, Rodríguez-Peralto JL, Rutkowski P, Peinado H. Use of extracellular vesicles from lymphatic drainage as surrogate markers of melanoma progression and BRAFV600E mutation. J Exp Med. 2019;216(5):1061-1070.
52. Goding CR, Arnheiter H. MITF-the first 25 years. Genes Dev. 2019;33(15-16):983-1007.
53. Gordon LG, Rodriguez-Acevedo AJ, Køster B, Guy GP, Jr Sinclair C, Van Deventer E, Green AC. Association of Indoor Tanning Regulations With Health and Economic Outcomes in North America and Europe. JAMA Dermatol. 2020;156:401–410.
54. Gosman LM, Țăpoi DA, Costache M. Cutaneous Melanoma: A Review of Multifactorial Pathogenesis, Immunohistochemistry, and Emerging Biomarkers for Early Detection and Management. Int J Mol Sci. 2023;24(21):15881.
55. Gowda R, Robertson BM, Iyer S, Barry J, Dinavahi SS, Robertson GP. The role of exosomes in metastasis and progression of melanoma. Cancer Treat Rev. 2020;85:101975.
56. Guo W, Wang H, Li C. Signal pathways of melanoma and targeted therapy. Signal Transduct Target Ther. 2021;6(1):424.
57. Gutiérrez-Castañeda LD, Nova JA, Tovar-Parra JD. Frequency of mutations in BRAF, NRAS, and KIT in different populations and histological subtypes of melanoma: a systemic review. Melanoma Research 2020;30(1): 62-70.
58. Gyukity-Sebestyén E, Harmati M, Dobra G, Németh IB, Mihály J, Zvara Á, Hunyadi-Gulyás É, Katona R, Nagy I, Horváth P, Bálind Á, Szkalisity Á, Kovács M, Pankotai T, Borsos B, Erdélyi M, Szegletes Z, Veréb ZJ, Buzás EI, Kemény L, Bíró T, Buzás K. Melanoma-Derived Exosomes Induce PD-1 Overexpression and Tumor Progression

via Mesenchymal Stem Cell Oncogenic Reprogramming. Front Immunol. 2019;10:2459.
59. Hadpech S, Chaiyarit S, Phuangkham S, Sukphan S, Thongboonkerd V. The Modulatory Effects of Large and Small Extracellular Vesicles from Normal Human Urine on Calcium Oxalate Crystallization, Growth, Aggregation, Adhesion on Renal Cells, and Invasion through Extracellular Matrix: An in Vitro Study. Biomed. Pharmacother. 2024;173:116393.
60. Hánělová K, Raudenská M, Masařík M, Balvan J. Protein cargo in extracellular vesicles as the key mediator in the progression of cancer. Cell Commun Signal. 2024;22(1):25.
61. Hayward NK, Wilmott JS, Waddell N, Johansson PA, Field MA, Nones K, Patch AM, Kakavand H, Alexandrov LB, Burke H, Jakrot V, Kazakoff S, Holmes O, Leonard C, Sabarinathan R, Mularoni L, Wood S, Xu Q, Waddell N, Tembe V, Pupo GM, De Paoli-Iseppi R, Vilain RE, Shang P, Lau LMS, Dagg RA, Schramm SJ, Pritchard A, Dutton-Regester K, Newell F, Fitzgerald A, Shang CA, Grimmond SM, Pickett HA, Yang JY, Stretch JR, Behren A, Kefford RF, Hersey P, Long GV, Cebon J, Shackleton M, Spillane AJ, Saw RPM, López-Bigas N, Pearson JV, Thompson JF, Scolyer RA, Mann GJ. Whole-genome landscapes of major melanoma subtypes. Nature. 2017;545(7653):175-180.
62. Hendrix A, Lippens L, Pinheiro C, Thery C, Martin-Jaular L, Lotwall J, Lasser C, Hill AF, Witwer KW. Extracellular vesicle analysis. Nat Rev Methods Primers 2023; 3, 56.
63. Hiltbrunner S, Larssen P, Eldh M, Martinez-Bravo MJ, Wagner AK, Karlsson MC, Gabrielsson S. Exosomal cancer immunotherapy is independent of MHC molecules on exosomes. Oncotarget. 2016;7(25):38707-38717.
64. Hodis E, Watson IR, Kryukov GV, Arold ST, Imielinski M, Theurillat JP, Nickerson E, Auclair D, Li L, Place C, Dicara D, Ramos AH, Lawrence MS, Cibulskis K, Sivachenko A, Voet D, Saksena G, Stransky N, Onofrio RC, Winckler W, Ardlie K, Wagle N, Wargo J, Chong K, Morton DL, Stemke-Hale K, Chen G, Noble M, Meyerson M, Ladbury JE, Davies MA, Gershenwald JE, Wagner SN, Hoon DS, Schadendorf D, Lander ES, Gabriel SB, Getz G, Garraway LA, Chin L. A landscape of driver mutations in melanoma. Cell. 2012;150(2):251-63.
65. Hong C.S., Muller L., Boyiadzis M., Whiteside T.L. Isolation and characterization of CD34+ blast-derived exosomes in acute myeloid leukemia. PLoS ONE. 2014;9:e103310.
66. Hong CS, Funk S, Muller L, Boyiadzis M, Whiteside TL. Isolation of biologically active and morphologically intact exosomes from plasma of patients with cancer. J Extracell Vesicles. 2016;5:29289.
67. Hong CS, Muller L, Whiteside TL, Boyiadzis M. Plasma exosomes as markers of therapeutic response in patients with acute myeloid leukemia. Front Immunol. 2014;5:160.
68. Hood JL, San RS, Wickline SA. Exosomes released by melanoma cells prepare sentinel lymph nodes for tumor metastasis. Cancer Res. 2011;71(11):3792-801.

69. Horibe S, Tanahashi T, Kawauchi S, Murakami Y, Rikitake Y. Mechanism of recipient cell-dependent differences in exosome uptake. BMC Cancer. 2018 ;18(1):47.
70. Hoshino A, Costa-Silva B, Shen TL, Rodrigues G, Hashimoto A, Tesic Mark M, Molina H, Kohsaka S, Di Giannatale A, Ceder S, Singh S, Williams C, Soplop N, Uryu K, Pharmer L, King T, Bojmar L, Davies AE, Ararso Y, Zhang T, Zhang H, Hernandez J, Weiss JM, Dumont-Cole VD, Kramer K, Wexler LH, Narendran A, Schwartz GK, Healey JH, Sandstrom P, Labori KJ, Kure EH, Grandgenett PM, Hollingsworth MA, de Sousa M, Kaur S, Jain M, Mallya K, Batra SK, Jarnagin WR, Brady MS, Fodstad O, Muller V, Pantel K, Minn AJ, Bissell MJ, Garcia BA, Kang Y, Rajasekhar VK, Ghajar CM, Matei I, Peinado H, Bromberg J, Lyden D. Tumour exosome integrins determine organotropic metastasis. Nature. 2015;527(7578):329-35.
71. Hu T, Hu J. Melanoma-derived exosomes induce reprogramming fibroblasts into cancer-associated fibroblasts via Gm26809 delivery. Cell Cycle. 2019;18(22):3085-3094.
72. Jablonska J, Pietrowska M, Ludwig S, Lang S, Thakur BK. Challenges in the Isolation and Proteomic Analysis of Cancer Exosomes-Implications for Translational Research. Proteomes. 2019;7(2):22.
73. Jang SC, Crescitelli R, Cvjetkovic A, Belgrano V, Olofsson Bagge R, Sundfeldt K, Ochiya T, Kalluri R, Lötvall J. Mitochondrial protein enriched extracellular vesicles discovered in human melanoma tissues can be detected in patient plasma. J Extracell Vesicles. 2019;8(1):1635420.
74. Jeppesen DK, Nawrocki A, Jensen SG, Thorsen K, Whitehead B, Howard KA, Dyrskjøt L, Ørntoft TF, Larsen MR, Ostenfeld MS. Quantitative proteomics of fractionated membrane and lumen exosome proteins from isogenic metastatic and nonmetastatic bladder cancer cells reveal differential expression of EMT factors. Proteomics. 2014;14(6):699-712.
75. Jonak ST, Liu Z, Liu J, Li T, D'Souza BV, Schiaffino JA, Oh S, Xie Y-H. Analyzing Bronchoalveolar Fluid Derived Small Extracellular Vesicles Using Single-Vesicle SERS for Non-Small Cell Lung Cancer Detection. Sens. Diagn. 2023;2:90–99.
76. Joshi RN, Stadler C, Lehmann R, Lehtiö J, Tegnér J, Schmidt A, Vesterlund M. TcellSubC: An Atlas of the Subcellular Proteome of Human T Cells. Front Immunol. 2019;10:2708.
77. Kalluri R, LeBleu VS. The biology, function, and biomedical applications of exosomes. Science. 2020;367(6478):eaau6977.
78. Kassem S, van der Pan K, de Jager AL, Naber BAE, de Laat IF, Louis A, van Dongen JJM, Teodosio C, Díez P. Proteomics for Low Cell Numbers: How to Optimize the Sample Preparation Workflow for Mass Spectrometry Analysis. J Proteome Res. 2021;20(9):4217-4230.
79. Kazimierczak U, Przybyla A, Smielowska M, Kolenda T, Mackiewicz A. Targeting the Hippo Pathway in Cutaneous Melanoma. Cells. 2024;13(12):1062.
80. Ke W, Afonin KA. Exosomes as natural delivery carriers for programmable therapeutic nucleic acid nanoparticles (NANPs). Adv Drug Deliv Rev. 2021;176:113835.

81. Kowal J, Arras G, Colombo M, Jouve M, Morath JP, Primdal-Bengtson B, Dingli F, Loew D, Tkach M, Théry C. Proteomic comparison defines novel markers to characterize heterogeneous populations of extracellular vesicle subtypes. Proc Natl Acad Sci U S A. 2016;113(8):E968-77.
82. Kulkarni YM, Chambers E, McGray AJ, Ware JS, Bramson JL, Klinke DJ 2nd. A quantitative systems approach to identify paracrine mechanisms that locally suppress immune response to Interleukin-12 in the B16 melanoma model. Integr Biol (Camb). 2012;4(8):925-36.
83. Kurian TK, Banik S, Gopal D, Chakrabarti S, Mazumder N. Elucidating Methods for Isolation and Quantification of Exosomes: A Review. Mol Biotechnol. 2021;63(4):249-266.
84. Lattmann E, Räss L, Tognetti M, Gómez JMM, Lapaire V, Bruderer R, Reiter L, Feng Y, Steinmetz LM, Levesque MP. Size-exclusion chromatography combined with DIA-MS enables deep proteome profiling of extracellular vesicles from melanoma plasma and serum. Cell Mol Life Sci. 2024;81(1):90.
85. Laulagnier K, Motta C, Hamdi S, Roy S, Fauvelle F, Pageaux JF, Kobayashi T, Salles JP, Perret B, Bonnerot C, Record M. Mast cell- and dendritic cell-derived exosomes display a specific lipid composition and an unusual membrane organization. Biochem J. 2004;380(Pt 1):161-71.
86. Leonardi GC, Falzone L, Salemi R, Zanghì A, Spandidos DA, Mccubrey JA, Candido S, Libra M. Cutaneous melanoma: From pathogenesis to therapy (Review). Int J Oncol. 2018; 52(4):1071-1080.
87. Li C, Kuai L, Cui R, Miao X. Melanogenesis and the Targeted Therapy of Melanoma. Biomolecules. 2022;12(12):1874.
88. Li J, Zhang Y, Dong PY, Yang GM, Gurunathan S. A comprehensive review on the composition, biogenesis, purification, and multifunctional role of exosome as delivery vehicles for cancer therapy. Biomed Pharmacother. 2023;165:115087.
89. Lin S, Yu Z, Chen D, Wang Z, Miao J, Li Q, Zhang D, Song J, Cui D. Progress in Microfluidics-Based Exosome Separation and Detection Technologies for Diagnostic Applications. Small. 2020;16(9):e1903916.
90. Liu H, Tian Y, Xue C, Niu Q, Chen C, Yan X. Analysis of extracellular vesicle DNA at the single-vesicle level by nano-flow cytometry. J Extracell Vesicles. 2022;11(4):e12206.
91. Liu YJ, Wang C. A review of the regulatory mechanisms of extracellular vesicles-mediated intercellular communication. Cell Commun Signal. 2023;21(1):77.
92. Liu Z, Du D, Zhang S. Tumor-derived exosomal miR-1247-3p promotes angiogenesis in bladder cancer by targeting FOXO1. Cancer Biol Ther. 2024;25(1):2290033.
93. Llorente A, Skotland T, Sylvänne T, Kauhanen D, Róg T, Orłowski A, Vattulainen I, Ekroos K, Sandvig K. Molecular lipidomics of exosomes released by PC-3 prostate cancer cells. Biochim Biophys Acta. 2013;1831(7):1302-9.
94. Lobasso S, Tanzarella P, Mannavola F, Tucci M, Silvestris F, Felici C, Ingrosso C, Corcelli A, Lopalco P. A Lipidomic Approach to Identify Potential Biomarkers in Exosomes From Melanoma Cells With Different Metastatic Potential. Front Physiol. 2021;12:748895.

95. Long GV, Swetter SM, Menzies AM, Gershenwald JE, Scolyer RA. Cutaneous melanoma. Lancet. 2023; 402(10400):485-502. Ludwig N, Gillespie DG, Reichert TE, Jackson EK, Whiteside TL. Purine Metabolites in Tumor-Derived Exosomes May Facilitate Immune Escape of Head and Neck Squamous Cell Carcinoma. Cancers (Basel). 2020;12(6):1602.
96. Ludwig N, Gillespie DG, Reichert TE, Jackson EK, Whiteside TL. Purine Metabolites in Tumor-Derived Exosomes May Facilitate Immune Escape of Head and Neck Squamous Cell Carcinoma. Cancers (Basel). 2020;12(6):1602.
97. Ludwig N, Rao A, Sandlesh P, Yerneni SS, Swain AD, Bullock KM, Hansen KM, Zhang X, Jaman E, Allen J, Krueger K, Hong CS, Banks WA, Whiteside TL, Amankulor NM. Characterization of systemic immunosuppression by IDH mutant glioma small extracellular vesicles. Neuro Oncol. 2022;24(2):197-209.
98. Ludwig N, Whiteside TL, Reichert TE. Challenges in Exosome Isolation and Analysis in Health and Disease. Int J Mol Sci. 2019;20(19):4684
99. Luga V, Zhang L, Viloria-Petit AM, Ogunjimi AA, Inanlou MR, Chiu E, Buchanan M, Hosein AN, Basik M, Wrana JL. Exosomes mediate stromal mobilization of autocrine Wnt-PCP signaling in breast cancer cell migration. Cell. 2012;151(7):1542-56.
100. Markovic SN, Erickson LA, Rao RD, Weenig RH, Pockaj BA, Bardia A, Vachon CM, Schild SE, McWilliams RR, Hand JL, Laman SD, Kottschade LA, Maples WJ, Pittelkow MR, Pulido JS, Cameron JD, Creagan ET; Melanoma Study Group of the Mayo Clinic Cancer Center. Malignant melanoma in the 21st century, part 1: epidemiology, risk factors, screening, prevention, and diagnosis. Mayo Clin Proc. 2007; 82(3):364-80.
101. Martínez-Lorenzo MJ, Anel A, Alava MA, Piñeiro A, Naval J, Lasierra P, Larrad L. The human melanoma cell line MelJuSo secretes bioactive FasL and APO2L/TRAIL on the surface of microvesicles. Possible contribution to tumor counterattack. Exp Cell Res. 2004;295(2):315-29.
102. Marvin DL, Dijkstra J, Zulfiqar RM, Vermeulen M, Ten Dijke P, Ritsma L. TGF-β Type I Receptor Signaling in Melanoma Liver Metastases Increases Metastatic Outgrowth. Int J Mol Sci. 2023;24(10):8676
103. Mashouri L, Yousefi H, Aref AR, Ahadi AM, Molaei F, Alahari SK. Exosomes: composition, biogenesis, and mechanisms in cancer metastasis and drug resistance. Mol Cancer. 2019;18(1):75.
104. Mathieu M, Martin-Jaular L, Lavieu G, Lavieu G, Théry C. Specificities of secretion and uptake of exosomes and other extracellular vesicles for cell-to-cell communication. Nature Cell Biology. 2019;21(1):9-17.
105. Matsumoto A, Takahashi Y, Nishikawa M, Sano K, Morishita M, Charoenviriyakul C, Saji H, Takakura Y. Accelerated growth of B16BL6 tumor in mice through efficient uptake of their own exosomes by B16BL6 cells. Cancer Sci. 2017;108(9):1803-1810.
106. Melo SA, Luecke LB, Kahlert C, Fernandez AF, Gammon ST, Kaye J, LeBleu VS, Mittendorf EA, Weitz J, Rahbari N, Reissfelder C, Pilarsky C, Fraga MF, Piwnica-Worms D, Kalluri R. Glypican-1 identifies cancer exosomes and detects early

pancreatic cancer. Nature. 2015;523(7559):177-82. Erratum in: Nature. 2022 Oct;610(7932):E15-E17.
107. Meng X, Müller V, Milde-Langosch K, Trillsch F, Pantel K, Schwarzenbach H. Diagnostic and prognostic relevance of circulating exosomal miR-373, miR-200a, miR-200b and miR-200c in patients with epithelial ovarian cancer. Oncotarget. 2016;7(13):16923-35.
108. Meng X, Pan J, Sun S, Gong Z. Circulating exosomes and their cargos in blood as novel biomarkers for cancer. Transl Cancer Res 2018;7(Suppl 2):S226-S242.
109. Miao X, Wu X, You W, He K, Chen C, Pathak JL, Zhang Q. Tailoring of apoptotic bodies for diagnostic and therapeutic applications: advances, challenges, and prospects. J Transl Med. 2024;22(1):810.
110. Mincheva-Nilsson L, Baranov V. Cancer exosomes and NKG2D receptor-ligand interactions: impairing NKG2D-mediated cytotoxicity and anti-tumour immune surveillance. Semin Cancer Biol. 2014;28:24-30.
111. Mizutani K., Terazawa R., Kameyama K., Kato T., Horie K., Tsuchiya T., Seike K., Ehara H., Fujita Y., Kawakami K., et al. Isolation of prostate cancer-related exosomes. Anticancer Res. 2014;34:3419–3423.
112. Möbius W, Ohno-Iwashita Y, van Donselaar EG, Oorschot VM, Shimada Y, Fujimoto T, Heijnen HF, Geuze HJ, Slot JW. Immunoelectron microscopic localization of cholesterol using biotinylated and non-cytolytic perfringolysin O. J Histochem Cytochem. 2002;50(1):43-55
113. Mondal SK, Whiteside TL. Immunoaffinity-Based Isolation of Melanoma Cell-Derived and T Cell-Derived Exosomes from Plasma of Melanoma Patients. Methods Mol Biol. 2021;2265:305-321.
114. Monteforte A, Lam B, Sherman MB, Henderson K, Sligar AD, Spencer A, Tang B, Dunn AK, Baker AB. * Glioblastoma Exosomes for Therapeutic Angiogenesis in Peripheral Ischemia. Tissue Eng Part A. 2017;23(21-22):1251-1261.
115. Motwani J, Eccles MR. Genetic and Genomic Pathways of Melanoma Development, Invasion and Metastasis. Genes (Basel). 2021;12(10):1543.
116. Mu C, Zhang X, Wang L, Xu A, Ahmed KA, Pang X, Chibbar R, Freywald A, Huang J, Zhu Y, Xiang J. Enhanced suppression of polyclonal CD8+25+ regulatory T cells via exosomal arming of antigen-specific peptide/MHC complexes. J Leukoc Biol. 2017;101(5):1221-1231.
117. Nieuwland R, Siljander PR. A beginner's guide to study extracellular vesicles in human blood plasma and serum. J Extracell Vesicles. 2024;13(1):e12400
118. O'Brien K, Ughetto S, Mahjoum S, Nair AV, Breakefield XO. Uptake, functionality, and re-release of extracellular vesicle-encapsulated cargo. Cell Rep. 2022;39(2):110651.
119. Palomar-Alonso N, Lee M, Kim M. Exosomes: Membrane-associated proteins, challenges and perspectives. Biochem Biophys Rep. 2023;37:101599.
120. Paluncic J, Kovacevic Z, Jansson PJ, Kalinowski D, Merlot AM, Huang ML, Lok HC, Sahni S, Lane DJ, Richardson DR. Roads to melanoma: Key pathways and emerging players in melanoma progression and oncogenic signaling. Biochim Biophys Acta. 2016;1863(4):770-84.

121. Pampena R., Kyrgidis A., Lallas A., Moscarella E., Argenziano G., Longo C. A meta-analysis of nevus-associated melanoma: Prevalence and practical implications. J. Am. Acad. Dermatol. 2017;77:938–945.e4.
122. Paolillo M, Schinelli S. Integrins and Exosomes, a Dangerous Liaison in Cancer Progression. Cancers (Basel). 2017 ;9(8):95.
123. Peinado H, Alečković M, Lavotshkin S, Matei I, Costa-Silva B, Moreno-Bueno G, Hergueta-Redondo M, Williams C, García-Santos G, Ghajar C, Nitadori-Hoshino A, Hoffman C, Badal K, Garcia BA, Callahan MK, Yuan J, Martins VR, Skog J, Kaplan RN, Brady MS, Wolchok JD, Chapman PB, Kang Y, Bromberg J, Lyden D. Melanoma exosomes educate bone marrow progenitor cells toward a pro-metastatic phenotype through MET. Nat Med. 2012;18(6):883-91.
124. Phuyal S, Skotland T, Hessvik NP, Simolin H, Øverbye A, Brech A, Parton RG, Ekroos K, Sandvig K, Llorente A. The ether lipid precursor hexadecylglycerol stimulates the release and changes the composition of exosomes derived from PC-3 cells. J Biol Chem. 2015;290(7):4225-37.
125. Pietrowska M, Zebrowska A, Gawin M, Marczak L, Sharma P, Mondal S, Mika J, Polańska J, Ferrone S, Kirkwood JM, Widlak P, Whiteside TL. Proteomic profile of melanoma cell-derived small extracellular vesicles in patients' plasma: a potential correlate of melanoma progression. J Extracell Vesicles. 2021;10(4):e12063.
126. Price MA, Colvin Wanshura LE, Yang J, Carlson J, Xiang B, Li G, Ferrone S, Dudek AZ, Turley EA, McCarthy JB. CSPG4, a potential therapeutic target, facilitates malignant progression of melanoma. Pigment Cell Melanoma Res. 2011;24(6):1148-57.
127. Pust S, Brech A, Wegner CS, Stenmark H, Haglund K. Vesicle-mediated transport of ALIX and ESCRT-III to the intercellular bridge during cytokinesis. Cell Mol Life Sci. 2023;80(8):235.
128. Qiu S, Xie L, Lu C, Gu C, Xia Y, Lv J, Xuan Z, Fang L, Yang J, Zhang L, Li Z, Wang W, Xu H, Li B, Xu Z. Gastric cancer-derived exosomal miR-519a-3p promotes liver metastasis by inducing intrahepatic M2-like macrophage-mediated angiogenesis. J Exp Clin Cancer Res. 2022;41(1):296
129. Qiu X, Campos Y, van de Vlekkert D, Gomero E, Tanwar AC, Kalathur R, Weesner JA, Bongiovanni A, Demmers J, d'Azzo A. Distinct functions of dimeric and monomeric scaffold protein Alix in regulating F-actin assembly and loading of exosomal cargo. J Biol Chem. 2022;298(10):102425.
130. Quiralte M, Barquín A, Yagüe Fernández M, Navarro P, Grazioso TP, Sevillano E, Rodriguez Moreno JF, Balarezo-Saldivar A, Peinado H, Izquierdo E, et al. Proteomic Profiles of Peritoneal-Derived Small Extracellular Vesicles Correlate with Outcome in Ovarian Cancer Patients. J. Clin. Investig. 2024;134:e176161.
131. Raimondo S, Pucci M, Alessandro R, Fontana S. Extracellular Vesicles and Tumor-Immune Escape: Biological Functions and Clinical Perspectives. Int J Mol Sci. 2020;21(7):2286.
132. Rappsilber J, Ishihama Y, Mann M. Stop and go extraction tips for matrix-assisted laser desorption/ionization, nanoelectrospray, and LC/MS sample pretreatment in proteomics. Anal Chem. 2003;75(3):663-70.

133. Rashid S, Shaughnessy M, Tsao H. Melanoma classification and management in the era of molecular medicine. Dermatol Clin. 2023;41(1):49-63.
134. Ren X, Lin S, Guan F, Kang H. Glycosylation Targeting: A Paradigm Shift in Cancer Immunotherapy. Int J Biol Sci 2024; 20(7):2607-2621.
135. Richards KE, Zeleniak AE, Fishel ML, Wu J, Littlepage LE, Hill R. Cancer-associated fibroblast exosomes regulate survival and proliferation of pancreatic cancer cells. Oncogene. 2017;36(13):1770-1778.
136. Ricklefs FL, Alayo Q, Krenzlin H, Mahmoud AB, Speranza MC, Nakashima H, Hayes JL, Lee K, Balaj L, Passaro C, Rooj AK, Krasemann S, Carter BS, Chen CC, Steed T, Treiber J, Rodig S, Yang K, Nakano I, Lee H, Weissleder R, Breakefield XO, Godlewski J, Westphal M, Lamszus K, Freeman GJ, Bronisz A, Lawler SE, Chiocca EA. Immune evasion mediated by PD-L1 on glioblastoma-derived extracellular vesicles. Sci Adv. 2018;4(3):eaar2766.
137. Rodríguez-Cerdeira C, Molares-Vila A, Carnero-Gregorio M, Corbalán-Rivas A. Recent advances in melanoma research via "omics" platforms. J Proteomics. 2018;188:152-166.
138. Rutkowski P, Wysocki PJ, Kozak K, Nasierowska-Guttmejer A, Jeziorski A, Wysocki WM, Kalinka E, Świtaj T, Kamińska-Winciorek G, Czarnecka AM, Koseła-Paterczyk H, Cybulska-Stopa B, Wiśniewski P, Szumera-Ciećkiewicz A, Zdzienicki M, Ziobro M, Fijuth J, Kawecki A, Tysarowski A, Romanowska-Dixon B, Markiewicz A, Dedecjus M, Kubiatowski T, Dolecki K, Tchórzewska-Korba H, Rudnicka L, Owczarek W, Krzakowski M. Expert recommendations on diagnostic-therapeutic management of melanoma patients. Oncol Clin Pract 2022;18(6):357-392.
139. Sabatke B, Rossi IV, Sana A, Bonato LB, Ramirez MI. Extracellular vesicles biogenesis and uptake concepts: A comprehensive guide to studying host-pathogen communication. Mol Microbiol. 2024;122(5):613-629
140. Saginala K, Barsouk A, Aluru JS, Rawla P, Barsouk A. Epidemiology of Melanoma. Med Sci (Basel). 2021;9(4):63
141. Sakai-Kato K, Yoshida K, Takechi-Haraya Y, Izutsu KI. Physicochemical Characterization of Liposomes That Mimic the Lipid Composition of Exosomes for Effective Intracellular Trafficking. Langmuir. 2020;36(42):12735-12744.
142. Santavanond JP, Rutter SF, Atkin-Smith GK, Poon IKH. Apoptotic Bodies: Mechanism of Formation, Isolation and Functional Relevance. Subcell Biochem. 2021;97:61-88..
143. Sharma P, Diergaarde B, Ferrone S, Kirkwood JM, Whiteside TL. Melanoma cell-derived exosomes in plasma of melanoma patients suppress functions of immune effector cells. Sci Rep. 2020;10(1):92
144. Sharma P, Ludwig S, Muller L, Hong CS, Kirkwood JM, Ferrone S, Whiteside TL. Immunoaffinity-based isolation of melanoma cell-derived exosomes from plasma of patients with melanoma. J Extracell Vesicles. 2018;7(1):1435138.
145. Shi P, Liu Y, Yang H, Hu B. Breast cancer derived exosomes promoted angiogenesis of endothelial cells in microenvironment via circHIPK3/miR-124-3p/MTDH axis. Cell Signal. 2022;95:110338.

146. Shu S, Yang Y, Allen CL, Maguire O, Minderman H, Sen A, Ciesielski MJ, Collins KA, Bush PJ, Singh P, Wang X, Morgan M, Qu J, Bankert RB, Whiteside TL, Wu Y, Ernstoff MS. Metabolic reprogramming of stromal fibroblasts by melanoma exosome microRNA favours a pre-metastatic microenvironment. Sci Rep. 2018;8(1):12905.
147. Singh A, Anang V, Kumari K, Kottarath SK, Verma C. Role of lymphocytes, macrophages and immune receptors in suppression of tumor immunity. Prog Mol Biol Transl Sci. 2023;194:269-310.
148. Singh S, Paul D, Nath V, A R. Exosomes: current knowledge and future perspectives. Tissue Barriers. 2024;12(2):2232248.
149. Skarmoutsou E, Bevelacqua V, D' Amico F, Russo A, Spandidos DA, Scalisi A, Malaponte G, Guarneri C. FOXP3 expression is modulated by TGF-β1/NOTCH1 pathway in human melanoma. Int J Mol Med. 2018;42(1):392-404
150. Skoczylas Ł, Gawin M, Fochtman D, Widłak P, Whiteside TL, Pietrowska M. Immune capture and protein profiling of small extracellular vesicles from human plasma. Proteomics. 2024;24(11):e2300180.
151. Skotland T, Hessvik NP, Sandvig K, Llorente A. Exosomal lipid composition and the role of ether lipids and phosphoinositides in exosome biology. J Lipid Res. 2019;60(1):9-18.
152. Skotland T, Llorente A, Sandvig K. Lipids in Extracellular Vesicles: What Can Be Learned about Membrane Structure and Function? Cold Spring Harb Perspect Biol. 2023;15(8):a041415.
153. Skotland T, Sandvig K, Llorente A. Lipids in exosomes: Current knowledge and the way forward. Prog Lipid Res. 2017;66:30-41.
154. Smolarz M, Pietrowska M, Matysiak N, Mielańczyk Ł, Widłak P. Proteome Profiling of Exosomes Purified from a Small Amount of Human Serum: The Problem of Co-Purified Serum Components. Proteomes. 2019;7(2):18.
155. Soura E, Eliades PJ, Shannon K, Stratigos AJ, Tsao H. Hereditary melanoma: Update on syndromes and management: Genetics of familial atypical multiple mole melanoma syndrome. J Am Acad Dermatol. 2016; 74(3):395-407; quiz 408-10.
156. Strauss K, Goebel C, Runz H, Mobius W, Weiss S, Feussner I, et al. Exosome secretion ameliorates lysosomal storage of cholesterol in Niemann-Pick type C disease. J Biol Chem. 2010;285(34):26279–88.
157. Szczepanski MJ, Szajnik M, Welsh A, Whiteside TL, Boyiadzis M. Blast-derived microvesicles in sera from patients with acute myeloid leukemia suppress natural killer cell function via membrane-associated transforming growth factor-beta1. Haematologica. 2011;96(9):1302-9.
158. Szklarczyk, D. , Gable, A. L. , Lyon, D. , Junge, A. , Wyder, S. , Huerta-Cepas, J. , Simonovic, M. , Doncheva, N. T. , Morris, J. H. , Bork, P. , Jensen, L. J. , Mering, C. V. (2019). STRING v11: protein-protein association networks with increased coverage, supporting functional discovery in genome-wide experimental datasets. Nucleic Acids Research 47(D1), D607-D613.

159. Takahashi Y, Nishikawa M, Shinotsuka H, Matsui Y, Ohara S, Imai T, Takakura Y. Visualization and in vivo tracking of the exosomes of murine melanoma B16-BL6 cells in mice after intravenous injection. J Biotechnol. 2013 May 20;165(2):77-84.
160. Tang M, Diao J, Gu H, Khatri I, Zhao J, Cattral MS. Toll-like Receptor 2 Activation Promotes Tumor Dendritic Cell Dysfunction by Regulating IL-6 and IL-10 Receptor Signaling. Cell Rep. 2015;13(12):2851-64.
161. Tao SC, Guo SC, Zhang CQ. Platelet-derived Extracellular Vesicles: An Emerging Therapeutic Approach. Int J Biol Sci. 2017;13(7):828-834.
162. Teixido C, Castillo P, Martinez-Vila C, Arance A, Alos L. Molecular Markers and Targets in Melanoma. Cells. 2021;10(9):2320.
163. Tengler L, Tiedtke M, Schütz J, Bieback K, Uhlig S, Theodoraki M-N, Nitschke K, Worst TS, Seiz E, Scherl C, et al. Optimization of Extracellular Vesicles Preparation from Saliva of Head and Neck Cancer Patients. Sci. Rep. 2024;14:946.
164. Theodoraki MN, Hoffmann TK, Whiteside TL. Separation of plasma-derived exosomes into CD3(+) and CD3(-) fractions allows for association of immune cell and tumour cell markers with disease activity in HNSCC patients. Clin Exp Immunol. 2018;192(3):271-283.
165. Theodoraki MN, Yerneni SS, Hoffmann TK, Gooding WE, Whiteside TL. Clinical Significance of PD-L1+ Exosomes in Plasma of Head and Neck Cancer Patients. Clin Cancer Res. 2018;24(4):896-905.
166. Théry C, Witwer KW, Aikawa E, Alcaraz MJ, Anderson JD, Andriantsitohaina R, Antoniou A, Arab T, Archer F, Atkin-Smith GK, Ayre DC, Bach JM, Bachurski D, Baharvand H, Balaj L, Baldacchino S, Bauer NN, Baxter AA, Bebawy M, Beckham C, Bedina Zavec A, Benmoussa A, Berardi AC, Bergese P, Bielska E, Blenkiron C, Bobis-Wozowicz S, Boilard E, Boireau W, Bongiovanni A, Borràs FE, Bosch S, Boulanger CM, Breakefield X, Breglio AM, Brennan MÁ, Brigstock DR, Brisson A, Broekman ML, Bromberg JF, Bryl-Górecka P, Buch S, Buck AH, Burger D, Busatto S, Buschmann D, Bussolati B, Buzás EI, Byrd JB, Camussi G, Carter DR, Caruso S, Chamley LW, Chang YT, Chen C, Chen S, Cheng L, Chin AR, Clayton A, Clerici SP, Cocks A, Cocucci E, Coffey RJ, Cordeiro-da-Silva A, Couch Y, Coumans FA, Coyle B, Crescitelli R, Criado MF, D'Souza-Schorey C, Das S, Datta Chaudhuri A, de Candia P, De Santana EF, De Wever O, Del Portillo HA, Demaret T, Deville S, Devitt A, Dhondt B, Di Vizio D, Dieterich LC, Dolo V, Dominguez Rubio AP, Dominici M, Dourado MR, Driedonks TA, Duarte FV, Duncan HM, Eichenberger RM, Ekström K, El Andaloussi S, Elie-Caille C, Erdbrügger U, Falcón-Pérez JM, Fatima F, Fish JE, Flores-Bellver M, Försönits A, Frelet-Barrand A, Fricke F, Fuhrmann G, Gabrielsson S, Gámez-Valero A, Gardiner C, Gärtner K, Gaudin R, Gho YS, Giebel B, Gilbert C, Gimona M, Giusti I, Goberdhan DC, Görgens A, Gorski SM, Greening DW, Gross JC, Gualerzi A, Gupta GN, Gustafson D, Handberg A, Haraszti RA, Harrison P, Hegyesi H, Hendrix A, Hill AF, Hochberg FH, Hoffmann KF, Holder B, Holthofer H, Hosseinkhani B, Hu G, Huang Y, Huber V, Hunt S, Ibrahim AG, Ikezu T, Inal JM, Isin M, Ivanova A, Jackson HK, Jacobsen S, Jay SM, Jayachandran M, Jenster G, Jiang L, Johnson SM, Jones JC, Jong A, Jovanovic-Talisman T, Jung S, Kalluri R, Kano SI, Kaur S, Kawamura Y, Keller ET, Khamari D, Khomyakova E, Khvorova A, Kierulf P, Kim KP, Kislinger T, Klingeborn M, Klinke DJ

2nd, Kornek M, Kosanović MM, Kovács ÁF, Krämer-Albers EM, Krasemann S, Krause M, Kurochkin IV, Kusuma GD, Kuypers S, Laitinen S, Langevin SM, Languino LR, Lannigan J, Lässer C, Laurent LC, Lavieu G, Lázaro-Ibáñez E, Le Lay S, Lee MS, Lee YXF, Lemos DS, Lenassi M, Leszczynska A, Li IT, Liao K, Libregts SF, Ligeti E, Lim R, Lim SK, Linē A, Linnemannstöns K, Llorente A, Lombard CA, Lorenowicz MJ, Lörincz ÁM, Lötvall J, Lovett J, Lowry MC, Loyer X, Lu Q, Lukomska B, Lunavat TR, Maas SL, Malhi H, Marcilla A, Mariani J, Mariscal J, Martens-Uzunova ES, Martin-Jaular L, Martinez MC, Martins VR, Mathieu M, Mathivanan S, Maugeri M, McGinnis LK, McVey MJ, Meckes DG Jr, Meehan KL, Mertens I, Minciacchi VR, Möller A, Møller Jørgensen M, Morales-Kastresana A, Morhayim J, Mullier F, Muraca M, Musante L, Mussack V, Muth DC, Myburgh KH, Najrana T, Nawaz M, Nazarenko I, Nejsum P, Neri C, Neri T, Nieuwland R, Nimrichter L, Nolan JP, Nolte-'t Hoen EN, Noren Hooten N, O'Driscoll L, O'Grady T, O'Loghlen A, Ochiya T, Olivier M, Ortiz A, Ortiz LA, Osteikoetxea X, Østergaard O, Ostrowski M, Park J, Pegtel DM, Peinado H, Perut F, Pfaffl MW, Phinney DG, Pieters BC, Pink RC, Pisetsky DS, Pogge von Strandmann E, Polakovicova I, Poon IK, Powell BH, Prada I, Pulliam L, Quesenberry P, Radeghieri A, Raffai RL, Raimondo S, Rak J, Ramirez MI, Raposo G, Rayyan MS, Regev-Rudzki N, Ricklefs FL, Robbins PD, Roberts DD, Rodrigues SC, Rohde E, Rome S, Rouschop KM, Rughetti A, Russell AE, Saá P, Sahoo S, Salas-Huenuleo E, Sánchez C, Saugstad JA, Saul MJ, Schiffelers RM, Schneider R, Schøyen TH, Scott A, Shahaj E, Sharma S, Shatnyeva O, Shekari F, Shelke GV, Shetty AK, Shiba K, Siljander PR, Silva AM, Skowronek A, Snyder OL 2nd, Soares RP, Sódar BW, Soekmadji C, Sotillo J, Stahl PD, Stoorvogel W, Stott SL, Strasser EF, Swift S, Tahara H, Tewari M, Timms K, Tiwari S, Tixeira R, Tkach M, Toh WS, Tomasini R, Torrecilhas AC, Tosar JP, Toxavidis V, Urbanelli L, Vader P, van Balkom BW, van der Grein SG, Van Deun J, van Herwijnen MJ, Van Keuren-Jensen K, van Niel G, van Royen ME, van Wijnen AJ, Vasconcelos MH, Vechetti IJ Jr, Veit TD, Vella LJ, Velot É, Verweij FJ, Vestad B, Viñas JL, Visnovitz T, Vukman KV, Wahlgren J, Watson DC, Wauben MH, Weaver A, Webber JP, Weber V, Wehman AM, Weiss DJ, Welsh JA, Wendt S, Wheelock AM, Wiener Z, Witte L, Wolfram J, Xagorari A, Xander P, Xu J, Yan X, Yáñez-Mó M, Yin H, Yuana Y, Zappulli V, Zarubova J, Žėkas V, Zhang JY, Zhao Z, Zheng L, Zheutlin AR, Zickler AM, Zimmermann P, Zivkovic AM, Zocco D, Zuba-Surma EK. Minimal information for studies of extracellular vesicles 2018 (MISEV2018): a position statement of the International Society for Extracellular Vesicles and update of the MISEV2014 guidelines. J Extracell Vesicles. 2018;7(1):1535750.

167. Tímár J, Ladányi A. Molecular Pathology of Skin Melanoma: Epidemiology, Differential Diagnostics, Prognosis and Therapy Prediction. Int J Mol Sci. 2022;23(10):5384.

168. Tung KH, Ernstoff MS, Allen C, Shu S. A Review of Exosomes and their Role in The Tumor Microenvironment and Host-Tumor "Macroenvironment". J Immunol Sci. 2019;3(1):4-8.

169. Turay D, Khan S, Diaz Osterman CJ, Curtis MP, Khaira B, Neidigh JW, Mirshahidi S, Casiano CA, Wall NR. Proteomic Profiling of Serum-Derived Exosomes from Ethnically Diverse Prostate Cancer Patients. Cancer Invest. 2016;34(1):1-11.

170. van Niel G, Carter DRF, Clayton A, Lambert DW, Raposo G, Vader P. Challenges and directions in studying cell-cell communication by extracellular vesicles. Nat Rev Mol Cell Biol. 2022;23(5):369-382
171. Vignard V, Labbé M, Marec N, André-Grégoire G, Jouand N, Fonteneau JF, Labarrière N, Fradin D. MicroRNAs in Tumor Exosomes Drive Immune Escape in Melanoma. Cancer Immunol Res. 2020;8(2):255-267.
172. Wang H, Lin Y, Chen R, Zhu Y, Wang H, Li S, Yu L, Zhang K, Liu Y, Jing T, Sun F. Human Seminal Extracellular Vesicles Enhance Endometrial Receptivity Through Leukemia Inhibitory Factor. Endocrinology. 2024;165(5):bqae035.
173. Wang S, Tang L, Lin J, Shen Z, Yao Y, Wang W, Tao S, Gu C, Ma J, Xie Y, Liu Y. ABCB5 promotes melanoma metastasis through enhancing NF-κB p65 protein stability. Biochem Biophys Res Commun. 2017;492(1):18-26.
174. Wehner MR, Chren MM, Nameth D, Choudhry A, Gaskins M, Nead KT, Boscardin WJ, Linos E. International prevalence of indoor tanning: A systematic review and meta-analysis. JAMA Dermatol. 2014;150:390–400.
175. Wei D, Zhan W, Gao Y, Huang L, Gong R, Wang W, Zhang R, Wu Y, Gao S, Kang T. RAB31 marks and controls an ESCRT-independent exosome pathway. Cell Res. 2021;31(2):157-177.
176. Welsh JA, Goberdhan DCI, O'Driscoll L, Buzas EI, Blenkiron C, Bussolati B, Cai H, Di Vizio D, Driedonks TAP, Erdbrügger U, Falcon-Perez JM, Fu QL, Hill AF, Lenassi M, Lim SK, Mahoney MG, Mohanty S, Möller A, Nieuwland R, Ochiya T, Sahoo S, Torrecilhas AC, Zheng L, Zijlstra A, Abuelreich S, Bagabas R, Bergese P, Bridges EM, Brucale M, Burger D, Carney RP, Cocucci E, Crescitelli R, Hanser E, Harris AL, Haughey NJ, Hendrix A, Ivanov AR, Jovanovic-Talisman T, Kruh-Garcia NA, Ku'ulei-Lyn Faustino V, Kyburz D, Lässer C, Lennon KM, Lötvall J, Maddox AL, Martens-Uzunova ES, Mizenko RR, Newman LA, Ridolfi A, Rohde E, Rojalin T, Rowland A, Saftics A, Sandau US, Saugstad JA, Shekari F, Swift S, Ter-Ovanesyan D, Tosar JP, Useckaite Z, Valle F, Varga Z, van der Pol E, van Herwijnen MJC, Wauben MHM, Wehman AM, Williams S, Zendrini A, Zimmerman AJ; MISEV Consortium; Théry C, Witwer KW. Minimal information for studies of extracellular vesicles (MISEV2023): From basic to advanced approaches. J Extracell Vesicles. 2024;(2):e12404.
177. Whiteside TL, Diergaarde B, Hong CS. Tumor-Derived Exosomes (TEX) and Their Role in Immuno-Oncology. Int J Mol Sci. 2021;22(12):6234.
178. Whiteside TL. Biology of extracellular vesicles and the potential of tumor-derived vesicles for subverting immunotherapy of cancer. J Immunother Cancer. 2025;13(1):e010376.
179. Whiteside TL. Evaluating tumor cell- and T cell-derived extracellular vesicles as potential biomarkers of cancer and immune cell competence. Expert Rev Mol Diagn. 2023;23(2):109-122
180. Whiteside TL. The role of tumor-derived exosomes in epithelial mesenchymal transition (EMT). Transl Cancer Res. 2017;6(Suppl 1):S90-S92
181. Whiteside TL. Tumor-derived Exosomes and Antitumor Immunity. J Immunol. 2024;213(7):923-931.

182. Whiteside TL. Tumor-Derived Exosomes and Their Role in Cancer Progression. Adv Clin Chem. 2016;74:103-41.
183. Wieckowski EU, Visus C, Szajnik M, Szczepanski MJ, Storkus WJ, Whiteside TL. Tumor-derived microvesicles promote regulatory T cell expansion and induce apoptosis in tumor-reactive activated CD8+ T lymphocytes. J Immunol. 2009;183(6):3720-30.
184. Wilczak M, Surman M, PRZYBYŁO M. Melanoma-derived extracellular vesicles transfer proangiogenic factors. Oncol Res. 2025;33(2):245-262.
185. Wiśniewski JR, Gaugaz FZ. Fast and sensitive total protein and Peptide assays for proteomic analysis. Anal Chem. 2015;87(8):4110-6.
186. Wiśniewski JR, Zougman A, Nagaraj N, Mann M. Universal sample preparation method for proteome analysis. Nat Methods. 2009;6(5):359-62.
187. Witwer KW, Théry C. Extracellular vesicles or exosomes? On primacy, precision, and popularity influencing a choice of nomenclature. J Extracell Vesicles. 2019;8(1):1648167.
188. Wu Y, Deng W, McGinley EC, Klinke DJ 2nd. Melanoma exosomes deliver a complex biological payload that upregulates PTPN11 to suppress T lymphocyte function. Pigment Cell Melanoma Res. 2017;30(2):203-218.
189. Wubbolts R, Leckie RS, Veenhuizen PT, Schwarzmann G, Möbius W, Hoernschemeyer J, Slot JW, Geuze HJ, Stoorvogel W. Proteomic and biochemical analyses of human B cell-derived exosomes. Potential implications for their function and multivesicular body formation. J Biol Chem. 2003 Mar;278(13):10963-72.
190. Xiao D, Barry S, Kmetz D, Egger M, Pan J, Rai SN, Qu J, McMasters KM, Hao H. Melanoma cell-derived exosomes promote epithelial-mesenchymal transition in primary melanocytes through paracrine/autocrine signaling in the tumor microenvironment. Cancer Lett. 2016;376(2):318-27.
191. Xie D, Qian B, Li X. Nucleic acids and proteins carried by exosomes from various sources: Potential role in liver diseases. Front Physiol. 2022;13:957036.
192. Xu R, Greening DW, Zhu HJ, Takahashi N, Simpson RJ. Extracellular vesicle isolation and characterization: toward clinical application. J Clin Invest. 2016;126(4):1152-62.
193. Yáñez-Mó M, Siljander PR, Andreu Z, Zavec AB, Borràs FE, Buzas EI, Buzas K, Casal E, Cappello F, Carvalho J, Colás E, Cordeiro-da Silva A, Fais S, Falcon-Perez JM, Ghobrial IM, Giebel B, Gimona M, Graner M, Gursel I, Gursel M, Heegaard NH, Hendrix A, Kierulf P, Kokubun K, Kosanovic M, Kralj-Iglic V, Krämer-Albers EM, Laitinen S, Lässer C, Lener T, Ligeti E, Linē A, Lipps G, Llorente A, Lötvall J, Manček-Keber M, Marcilla A, Mittelbrunn M, Nazarenko I, Nolte-'t Hoen EN, Nyman TA, O'Driscoll L, Olivan M, Oliveira C, Pállinger É, Del Portillo HA, Reventós J, Rigau M, Rohde E, Sammar M, Sánchez-Madrid F, Santarém N, Schallmoser K, Ostenfeld MS, Stoorvogel W, Stukelj R, Van der Grein SG, Vasconcelos MH, Wauben MH, De Wever O. Biological properties of extracellular vesicles and their physiological functions. J Extracell Vesicles. 2015;4:27066.

194. Yang CH, Yue J, Pfeffer SR, Handorf CR, Pfeffer LM. MicroRNA miR-21 regulates the metastatic behavior of B16 melanoma cells. J Biol Chem. 2011;286(45):39172-8.
195. Zarovni N, Corrado A, Guazzi P, Zocco D, Lari E, Radano G, Muhhina J, Fondelli C, Gavrilova J, Chiesi A. Integrated isolation and quantitative analysis of exosome shuttled proteins and nucleic acids using immunocapture approaches. Methods. 2015;87:46-58.
196. Zebrowska A, Jelonek K, Mondal S, Gawin M, Mrowiec K, Widłak P, Whiteside T, Pietrowska M. Proteomic and Metabolomic Profiles of T Cell-Derived Exosomes Isolated from Human Plasma. Cells. 2022;11(12):1965.
197. Zebrowska A, Skowronek A, Wojakowska A, Widlak P, Pietrowska M. Metabolome of Exosomes: Focus on Vesicles Released by Cancer Cells and Present in Human Body Fluids. Int J Mol Sci. 2019;20(14):3461.
198. Zebrowska A, Widlak P, Whiteside T, Pietrowska M. Signaling of Tumor-Derived sEV Impacts Melanoma Progression. Int J Mol Sci. 2020;21(14):5066.
199. Zeng Z, Li Y, Pan Y, Lan X, Song F, Sun J, Zhou K, Liu X, Ren X, Wang F, Hu J, Zhu X, Yang W, Liao W, Li G, Ding Y, Liang L. Cancer-derived exosomal miR-25-3p promotes pre-metastatic niche formation by inducing vascular permeability and angiogenesis. Nat Commun. 2018;9(1):5395.
200. Zhang Q, Peng C. Cancer-associated fibroblasts regulate the biological behavior of cancer cells and stroma in gastric cancer. Oncol Lett. 2018;15(1):691-698.
201. Zhang Y, Liu Y, Liu H, Tang WH. Exosomes: biogenesis, biologic function and clinical potential. Cell Biosci. 2019;9:19.
202. Zhao H, Yang L, Baddour J, Achreja A, Bernard V, Moss T, Marini JC, Tudawe T, Seviour EG, San Lucas FA, Alvarez H, Gupta S, Maiti SN, Cooper L, Peehl D, Ram PT, Maitra A, Nagrath D. Tumor microenvironment derived exosomes pleiotropically modulate cancer cell metabolism. Elife. 2016;5:e10250.
203. Zhao XP, Wang M, Song Y, Song K, Yan TL, Wang L, Liu K, Shang ZJ. Membrane microvesicles as mediators for melanoma-fibroblasts communication: roles of the VCAM-1/VLA-4 axis and the ERK1/2 signal pathway. Cancer Lett. 2015;360(2):125-33.
204. Zhou J, Yang Y, Wang W, Zhang Y, Chen Z, Hao C, Zhang J. Melanoma-released exosomes directly activate the mitochondrial apoptotic pathway of CD4+ T cells through their microRNA cargo. Exp Cell Res. 2018;371(2):364-371.
205. Zhou X, Yan T, Huang C, Xu Z, Wang L, Jiang E, Wang H, Chen Y, Liu K, Shao Z, Shang Z. Melanoma cell-secreted exosomal miR-155-5p induce proangiogenic switch of cancer-associated fibroblasts via SOCS1/JAK2/STAT3 signaling pathway. J Exp Clin Cancer Res. 2018;37(1):242.
206. Zhuang G, Wu X, Jiang Z, Kasman I, Yao J, Guan Y, Oeh J, Modrusan Z, Bais C, Sampath D, Ferrara N. Tumour-secreted miR-9 promotes endothelial cell migration and angiogenesis by activating the JAK-STAT pathway. EMBO J. 2012;31(17):3513-23.
207. Zocchi L, Lontano A, Merli M, Dika E, Nagore E, Quaglino P, Puig S, Ribero S. Familial Melanoma and Susceptibility Genes: A Review of the Most Common

Clinical and Dermoscopic Phenotypic Aspect, Associated Malignancies and Practical Tips for Management. J Clin Med. 2021; 10(16):3760.

208. Zugazagoitia J, Gupta S, Liu Y, Fuhrman K, Gettinger S, Herbst RS, Schalper KA, Rimm DL. Biomarkers Associated with Beneficial PD-1 Checkpoint Blockade in Non-Small Cell Lung Cancer (NSCLC) Identified Using High-Plex Digital Spatial Profiling. Clin Cancer Res. 2020;26(16):4360-4368.

8. SCIENTIFIC ACHIEVEMENTS

Publications:

1. **Zebrowska A**, Skowronek A, Wojakowska A, Widlak P, Pietrowska M. Metabolome of Exosomes: Focus on Vesicles Released by Cancer Cells and Present in Human Body Fluids. Int J Mol Sci. 2019 Jul 14;20(14):3461. doi: 10.3390/ijms20143461. PMID: 31337156; PMCID: PMC6678201.

2. **Zebrowska A**, Widlak P, Whiteside T, Pietrowska M. Signaling of Tumor-Derived sEV Impacts Melanoma Progression. Int J Mol Sci. 2020 Jul 17;21(14):5066. doi: 10.3390/ijms21145066. PMID: 32709086; PMCID: PMC7404104.

3. Wojakowska A, **Zebrowska A**, Skowronek A, Rutkowski T, Polanski K, Widlak P, Marczak L, Pietrowska M. Metabolic Profiles of Whole Serum and Serum-Derived Exosomes Are Different in Head and Neck Cancer Patients Treated by Radiotherapy. J Pers Med. 2020 Nov 13;10(4):229. doi: 10.3390/jpm10040229. PMID: 33203021; PMCID: PMC7711528.

4. Pietrowska M, **Zebrowska A**, Gawin M, Marczak L, Sharma P, Mondal S, Mika J, Polańska J, Ferrone S, Kirkwood JM, Widlak P, Whiteside TL. Proteomic profile of melanoma cell-derived small extracellular vesicles in patients' plasma: a potential correlate of melanoma progression. J Extracell Vesicles. 2021 Feb;10(4):e12063. doi: 10.1002/jev2.12063. Epub 2021 Feb 11. PMID: 33613873; PMCID: PMC7876545.

5. **Zebrowska A**, Jelonek K, Mondal S, Gawin M, Mrowiec K, Widłak P, Whiteside T, Pietrowska M. Proteomic and Metabolomic Profiles of T Cell-Derived Exosomes Isolated from Human Plasma. Cells. 2022 Jun 18;11(12):1965. doi: 10.3390/cells11121965. PMID: 35741093; PMCID: PMC9222142.

Conferences:

1. **XXVII Gliwice Scientific Meetings**, Gliwice (Poland), 21-22.11.2024: poster presentation entitled “Distinct proteomic profiles of T cell-derived small extracellular vesicles from plasma of melanoma patients and healthy donors”, **Zebrowska A**, Mika J, Widlak P, Mondal S, Gawin M, Najjar Y, Polanska J, Whiteside T, Pietrowska M.

2. **XI Śląskie Spotkania Naukowe** [11th Silesian Scientific Meetings], 17-19.05.2024: oral presentation entitled „Proteom małych pęcherzyków zewnątrzkomórkowych uwalnianych z limfocytów T i wyizolowanych z osocza pacjentów z rozpoznaniem czerniaka i zdrowych dawców" **Zebrowska A**, Mika J, Gawin M, Widlak P, Whiteside T, Pietrowska M
3. **8th Warsaw conference on Perspectives of Molecular Oncology**, Warszawa (Poland), 7-8.09.2023, poster presentation entitled "Proteomic profiles of T cell-derived small extracellular vesicles isolated from human plasma", **Zebrowska A**, Mondal S, Gawin M, Mika J, Polańska J, Widłak P, Whiteside T, Pietrowska M, second place in the best poster competition during the poster session
4. **XXVI Gliwice Scientific Meetings**, Gliwice (Poland), 18-19.11.2022, oral presentation entitled "Proteomic and metabolomics profiles of T cell-derived exoxomes isolated from human plasma", **Zebrowska A**, Jelonek K, Mondal S, Gawin M, Mrowiec K, Widłak P, Whiteside T, Pietrowska M
5. **ISEV 2021 Annual Meeting**, Virtual Event, 18-21.05.2021, poster presentation entitled "Proteomics of small extracellular vesicles produced by non-malignant cells in plasma of healthy donors and cancer patients", **Zebrowska A**, Gawin M, Ponge L, Widłak P, Mondal S, Ferrone S, Whiteside TL, Pietrowska M, Abstract Book: e12083, Journal of Extracellular Vesicles Vol. 10, Issue S1, page: 240, PS17.07
6. **5th Warsaw Conference on Perspectives of Molecular Oncology: Molecular Immunology of Cancer**, Warszawa (Poland), 23-24.09.2020, poster presentation entitled "Proteomic profile of tumor-derived exosomes in plasma of melanoma patients", **Zebrowska A**, Gawin M, Marczak Ł, Sharma P, Mika J, Polańska P, Widlak P, Whiteside T, Pietrowska M
7. **5th Warsaw Conference on Perspectives of Molecular Oncology: Molecular Immunology of Cancer**, Warszawa (Poland), 23-24.09.2020, poster presentation entitled "GC-MS-based metabolomic profiling of serum and exosomes isolated from head and neck cancer patients after radiotherapy", Wojakowska A, Marczak Ł, **Zebrowska A**, Skowronek A, Rutkowski T, Widlak P, Pietrowska M
8. **VII Śląskie Spotkania Naukowe** [7th Silesian Scientific Meetings], On-line Event, 29-30.05.2020, presentation entitled "Metoda immunowychwytywania w ocenie

molekularnego profilu subpopulacji egzosomów GSPG4+ uwalnianych przez komórki czerniaka" [Immunocapture method for assessing the molecular profile of GSPG4+ exosome subpopulations released by melanoma cells], **Zebrowska A**, Gawin M, Marczak Ł, Sharma P, Mika J, Polańska J, Ferrone S, Kirkwood J, Widłak P, Whiteside T, Pietrowska M

9. **13th Central and Eastern European Proteomic Conference (13th CEEPC)**, Ustroń (Poland), 23-25.09.2019, oral presentation entitled "Challenges in analysis of metabolome of serum exosomes", **Żebrowska A**, Skowronek A, Rutkowski T, Widłak P, Pietrowska M, Wojakowska A, Marczak Ł
10. **IV Spotkania z Onkologią Molekularną i Translacyjną** [4th Molecular and Translational Oncology Meetings], Warszawa (Poland), 04-05.04.2019, poster presentation entitled "Proteomic profiles of melanoma-derived exosomes (MTEX) from the plasma of melanoma patients – a preliminary study", **Zebrowska A**, Gawin M, Marczak Ł, Sharma P, Widłak P, Whiteside T, Pietrowska M
11. **11th International Conference of Contemporary Oncology**, Poznań (Poland), 13-15.03.2019, poster presentation entitled "Proteomic profiles of melanoma-derived exosomes (MTEX) from the plasma of melanoma patients – a preliminary study", **Zebrowska A**, Gawin M, Marczak Ł, Sharma P, Widlak P, Whiteside TL, Pietrowska M, Abstract Book: Współczesna Onkologia, 2019, 23, Suppl. 1, p. 23.

Grants:

1. Project title: The role of PDCD6IP protein from plasma exosomes in progression of melanoma [Rola białka PDCD6IP z egzosomów osocza w progresji czerniaka], National Science Centre, Poland, OPUS 23, 2022/45/B/NZ5/03510, Principal Investigator: Monika Pietrowska

2. Project title: Molecular profiling of tumor-derived exosomes in plasma of patients with melanoma [Molekularny profil egzosomów wydzielanych przez komórki nowotworowe w osoczu pacjentów z rozpoznaniem czerniaka], National Science Centre, Poland, HARMONIA 8, 2016/22/M/NZ5/00667, Principal Investigator: Monika Pietrowska

9. APPENDIX

1. **Zebrowska A**, Skowronek A, Wojakowska A, Widlak P, Pietrowska M. Metabolome of Exosomes: Focus on Vesicles Released by Cancer Cells and Present in Human Body Fluids. Int J Mol Sci. 2019 Jul 14;20(14):3461. doi: 10.3390/ijms20143461. PMID: 31337156; PMCID: PMC6678201.

2. **Zebrowska A**, Widlak P, Whiteside T, Pietrowska M. Signaling of Tumor-Derived sEV Impacts Melanoma Progression. Int J Mol Sci. 2020 Jul 17;21(14):5066. doi: 10.3390/ijms21145066. PMID: 32709086; PMCID: PMC7404104.

3. Wojakowska A, **Zebrowska A**, Skowronek A, Rutkowski T, Polanski K, Widlak P, Marczak L, Pietrowska M. Metabolic Profiles of Whole Serum and Serum-Derived Exosomes Are Different in Head and Neck Cancer Patients Treated by Radiotherapy. J Pers Med. 2020 Nov 13;10(4):229. doi: 10.3390/jpm10040229. PMID: 33203021; PMCID: PMC7711528.

4. Pietrowska M, **Zebrowska A**, Gawin M, Marczak L, Sharma P, Mondal S, Mika J, Polańska J, Ferrone S, Kirkwood JM, Widlak P, Whiteside TL. Proteomic profile of melanoma cell-derived small extracellular vesicles in patients' plasma: a potential correlate of melanoma progression. J Extracell Vesicles. 2021 Feb;10(4):e12063. doi: 10.1002/jev2.12063. Epub 2021 Feb 11. PMID: 33613873; PMCID: PMC7876545.

5. **Zebrowska A**, Jelonek K, Mondal S, Gawin M, Mrowiec K, Widłak P, Whiteside T, Pietrowska M. Proteomic and Metabolomic Profiles of T Cell-Derived Exosomes Isolated from Human Plasma. Cells. 2022 Jun 18;11(12):1965. doi: 10.3390/cells11121965. PMID: 35741093; PMCID: PMC9222142.

International Journal of
Molecular Sciences

MDPI

Review

Metabolome of Exosomes: Focus on Vesicles Released by Cancer Cells and Present in Human Body Fluids

Aneta Zebrowska [1], Agata Skowronek [1], Anna Wojakowska [2], Piotr Widlak [1] and Monika Pietrowska [1,*]

1 Maria Sklodowska-Curie Institute—Oncology Center, Gliwice Branch, 44-100 Gliwice, Poland
2 Institute of Bioorganic Chemistry, Polish Academy of Sciences, 44-100 Poznan, Poland
* Correspondence: monika.pietrowska@io.gliwice.pl; Tel.: +48-32-278-9627

Received: 18 June 2019; Accepted: 11 July 2019; Published: 14 July 2019

Abstract: Exosomes and other classes of extracellular vesicles (EVs) have gained interest due to their role in cell-to-cell communication. Knowledge of the molecular content of EVs may provide important information on features of parental cells and mechanisms of cross-talk between cells. To study functions of EVs it is essential to know their composition, that includes proteins, nucleic acids, and other classes biomolecules. The metabolome, set of molecules the most directly related to the cell phenotype, is the least researched component of EVs. However, the metabolome of EVs circulating in human blood and other bio-fluids is of particular interest because of its potential diagnostic value in cancer and other health conditions. On the other hand, the metabolome of EVs released to culture media in controlled conditions in vitro could shed light on important aspects of communication between cells in model systems. This paper summarizes the most common approaches implemented in EV metabolomics and integrates currently available data on the composition of the metabolome of EVs obtained in different models with particular focus on human body fluids and cancer cells.

Keywords: extracellular vesicles; exosomes; lipids; liquid biopsy; mass spectrometry; metabolomics; metabolites

1. Introduction

Exosomes (EX) are membranous virus-sized (30–150 nm) structures belonging to the group of extracellular vesicles (EVs). This class of vesicles derives exclusively from the inward budding of the endosomal membrane to form the multivesicular body, which fuses with the plasma membrane to release exosomes to the extracellular space [1–3]. EVs are a heterogeneous group of vesicles, that in addition to exosomes, include two other major classes: microvesicles (also termed ectosomes) and apoptotic bodies [1,4,5]. Though the classification of EVs based on their biogenesis and cellular origin has been well established in the scientific community, the currently available and commonly used techniques of their isolation do not provide efficient separation of individual classes. Therefore "simplified" nomenclature is accepted nowadays, like small EVs (i.e., <200 nm) and medium/large EVs (>200 nm) [6]. The small EVs class is apparently enriched in exosomes but could also contain a fraction of smaller microvesicles formed by budding of the plasma membrane. In this review term "exosomes" is used afterward for simplicity, yet because of abovementioned limitations of methods used for purification and specification of vesicles that were implemented in quoted papers this should be used read rather as "small EVs"; terms exosomes and (small) EVs are used interchangeably thereafter.

Exosomes are released by many various cell types, including red blood cells, B cells, T cells, mast cells, platelets, endothelial cells, fibroblasts, adipocytes, epithelial cells, muscle, dendritic cells, and tumor cells. Their presence in the extracellular medium (in vitro) and in body fluids (in vivo) is confirmed repeatedly. Exosomes, among others, were found in blood, urine, saliva, breasts milk,

ascites effusions, nasal secretions, tears, amniotic, synovial, lymphatic, cerebrospinal, and seminal fluids [7–19]. Numerous investigations revealed an important role of these vesicles in intercellular communication under both normal and pathological conditions. Exosomes could reach recipient cells in the local environment (paracrine mode) or could be transported to distant tissues via the circulation system (endocrine mode) [8,10,14,20–24]. What is more, recent evidence has shown that in pathological conditions the number of exosomes is significantly increasing comparing to healthy donors. Data showing a high number of these vesicles in bio-fluids of patients with ovarian, prostate, lung, colorectal, and gastric cancers, and acute myeloid leukemia, are available in the literature [25–32]. Moreover, the essential role of exosomes in cancer biology as key mediators of a cross-talk between cancer cells and the immune system cells was revealed, pointing out their crucial involvement in a metastatic cascade [22,23,33–38]. Therefore, exosomes are a potential source of tumor biomarkers (e.g., tumor-specific proteins or miRNA) [20,26–32,39–41].

The exosomal cargo consists of selected molecules located inside these vesicles or associated with their membrane [4]. However, the majority of available studies addressed mainly exosomal proteins and RNAs. Metabolites, which are also a part of the exosomal cargo, have been given less attention, so far. Metabolites are defined as (low molecular) end products or intermediates of chemical reactions occurring in the organism. They are varied in terms of a chemical structure and, as a consequence, polarity, lipophilicity, and stability. Classification of metabolites is based on functional groups of molecules. Low-molecular-weight metabolites (LMWMs; size < 900 Da) include alcohols, amides, amino acids, carboxylic acids, and sugars [42]. The second group, often considered as a separate field of analysis, represented by lipids and their derivatives has their own classification, which was comprehensively described by Fahy et al. [43]. As metabolites are representing the intermediate or the end point of any cellular process, they can show phenotype printout of organism state. Therefore, important clinical information on disease stage and response to treatment can be achieved from monitoring metabolic changes in patient's bio-fluids like blood (whole blood, plasma, or serum), urine, saliva, synovial and cerebrospinal fluid, and semen [44–46]. Rising interest in exosome metabolome has been initiated by studies aimed at determination of lipids in membranes of exosomes derived from different cells [7,47–49]. Afterward, metabolomics approaches were applied to blood-derived [50,51] and urinary-derived exosomes [52,53], revealing a complex set of molecules. Nevertheless, knowledge of metabolome of exosomes, especially derived from bio-fluids, which have a high clinical value, remains rather limited. Here we aim to summarize the current status of this particular field of metabolomics.

2. Methods Used in Studies Oriented on the Metabolome of Exosomes

2.1. Exosomes Isolation and Characterization

Both bio-fluids and cell culture medium contain exosomes and could be used for their purification. However, it is important to note that at the same time these specimens contain circulating cells, cell debris, and other classes of extracellular vesicles. Multiple techniques have been used to isolate exosomes from complex mixtures [54–56]. Currently, available approaches utilize differences in chemical and physical properties of vesicles in regard to other components of biofluids. Ultracentrifugation (UC), density gradient centrifugation, ultrafiltration (UF), or precipitation are commonly used techniques of exosomes purification that are based on differences in sedimentation and density of different classes of particles [55,57,58]. However, these techniques are recently replaced by approaches based on size exclusion chromatography (SEC) or a combination of SEC with (ultra)centrifugation [54,59–61]. Although this method offers advantages for proteomic studies, it has limitations in studies on lipidome because Sepharose CL-4B, the popular SEC matrix (fractionation range of 70–40,000 kDa), may not provide good resolution of (very) small EVs from lipoproteins. Therefore, to enhance the selectivity of exosome capture it is recommended to use immune-affinity techniques (IA), e.g., immunomagnetic beads [62] or nanoplasmon-enhanced scattering (nPES) [63], which are based on immobilized antibodies against specific antigens present in their membranes. For more detailed information on exosomes' separation techniques

authors recommend referring to another review on this issue [64]. The application of abovementioned techniques allows separation of exosomes (small EVs) from "soluble" contaminants and larger vesicles/cell debris. However, the separation of different fractions of exosomes remains a more challenging issue. For example, when tumor-derived exosomes (TEX) circulating in the blood are of particular interest their separation from non-TEX exosomes requires knowledge of specific tumor markers [65].

Taking into account heterogeneity of extracellular vesicles and the necessity of distinguishing them from other objects/vesicles present in body fluids or culture mediums the very important issue is the characterization of isolated vesicles. There are a few commonly used techniques to confirm what type of EVs contain the sample of interest. Biochemical and immune-based methods include Western blotting (WB), flow cytometry (FC), and immunosorbent assays (ISAs), which enables characterization of their molecular content. The size and shape of EVs could be determined by electron microscopy (EM) imaging, atomic force microscopy (AFM), nanoparticle tracking analysis (NTA), photon correlation spectroscopy (PCS), and tunable resistive pulse sensing (tRPS). Limitations and advantages of these methods were summarized by Oeyen et al. [66] and Hartjes et al. [67]. However, it is important to note that none of the abovementioned methods itself is able to cover all needs of vesicle characterization. This is why it is recommended to combine biochemical (molecular) EVs analysis with a high-resolution imaging and other technique revealing the size of analyzed vesicles [6,67].

2.2. MS-Based Techniques in Metabolomics Studies

Aforementioned techniques of exosome isolation do not provide complete and absolute removal of "contaminating" components, hence analytical methods enabling discrimination between similar molecules in complex mixtures are required. On the other hand, purification procedures entail an inevitable reduction in exosomes yield and affect the concentration of metabolites, which requires very sensitive methods. The selection of the analytical approach is dictated by the complexity of the analyzed sample and chemical properties of desired compounds. A large diversity of metabolites present in a typical biological sample is the reason why available techniques cannot cover all metabolites in a "single run." Currently, the most suitable approaches for rapid screening and high-throughput analyses of a broad set of low-concentrated metabolites are tools based on chromatography coupled with mass spectrometry (MS). Therefore, in our paper, we focused on the analysis of metabolic profiles of exosomes using MS technique. This approach offers quantitative identification of hundreds or even thousands of metabolites in the sample. MS-based analyses are widely used for fingerprinting and profiling of metabolites [68,69], but can also be applied to study only a selected class of compounds in the targeted analysis [70]. However, many different analytical techniques based on a combination of chromatography and mass spectrometry exist that could be selected depending on the physical and chemical properties of metabolites of interest. Major types of such techniques are listed in Table 1.

Table 1. Selected mass spectrometry (MS)-based techniques applied for metabolomics.

Technique	Abbreviation	Application	References
Gas chromatography-mass spectrometry	GC-MS	Selective method for measuring volatile, thermally stable LMWMs. Requires derivatization of non-volatile LMWMs. Allows the highest sensitivity (in range of pmol–nmol).	[71,72]
Liquid chromatography-mass spectrometry	LC-MS	Measurement of both lipophilic and amphiphilic metabolites with use of different columns on the same device. Covers broad set of metabolites by measuring in negative and positive ion modes.	[73,74]
Thin layer chromatography-mass spectrometry	TLC-MS	An alternative method to direct matrix-assisted laser desorption ionization (MALDI) desorption of sample in lipidomics. Provides glycosphingolipids (GSL) and phospholipids (PL) separation and allows to categorize them into classes.	[75]

There are two critical elements of any mass spectrometer that determine its applicability for analysis of different compounds: type of ionization and type of mass analyzer. First of all, the capability of identification and quantification of metabolites strongly depends on the ionization process. If labile fragments are present in the structure of an analyte, they can break away from the parental molecule and be ionized as its fragment. The higher fragmentation, the more possible it is to find the unique fragment and identify an unknown compound. This very important criterion is met by electron impact (EI) ionization used in GC-MS analysis of LMWMs and by electrospray ionization (ESI) used in LC-MS/MS for lipids. However, two other ionization types, atmospheric pressure chemical ionization (APCI) and matrix-assisted laser desorption ionization (MALDI), could be also used. APCI is suitable for LMWMs which have a relatively stable structure when exposed to high temperature for vaporization [76], while MALDI for non-volatile, large molecules, for example, lipids [75]. Ionization of the analyte molecules is followed by selection and separation of ions by mass analyzers. There are several types of mass analyzers characterized by different mass accuracy and mass resolution used in metabolomics. In metabolome profiling, as well as in targeted analysis, isomeric and isobaric compounds (molecules having the same m/z) can occur and are usually difficult to separate on chromatography columns. Analyzers with high mass accuracy and resolution power bring the opportunity to resolve the mixture of such molecules. Isomeric and isobaric LMWM can be well separated on GC-EI-MS with single or triple quadrupole, but in lipidomics, much higher resolution power is required (m/z accuracy $\leq$ 5 ppm) [77]. This condition can be fulfilled by using time of flight analyzer (TOF), Fourier-transform ion cyclotron, or ion traps (linear and two-dimension). Ion traps, like Linear Trap Quadrupole (LTQ)-Orbitrap, are also very useful for multiple reaction monitoring (MRM) of metabolite ions chosen in targeted analyses [78]. However, despite all these improvements, the information about lipid subclass is frequently missed. This issue can be addressed using ion mobility spectrometry (IMS) which cope with stereomeric diversity of metabolites [79].

GC-MS is frequently considered a 'gold standard' in quantitative metabolomics due to its high sensitivity [68]. However, the application of GC-MS is limited to volatile and thermally stable molecules. To increase the number of analytes that could be targeted by GC-MS, chemical derivatization is required. In this strategy, silylation of hydroxyl and primary amine groups along with oximation of carbonyl groups results in reduced polarity and increased volatility of analytes [74,80]. GC-MS is suitable for analysis of LMWMs from different classes, including sugars, carboxylic acids, amino acids, alcohols, and amines. Lipids cannot be analyzed comprehensively with this technique as they have different chemical features (higher molecular weight, polar, and non-volatile). The information on lipids in a wide range of masses can be achieved by LC-MS [81,82]. The advantage of LC-MS is that it can also be preceded by derivatization to increase signals of low-abundant and poorly ionizing metabolites, such as thiol compounds [83]. Recently, thin layer chromatography coupled with MS has been proposed as an alternative tool in lipidomics but only for separation and detection of lipids with $m/z > 500$ [75]. However, this technique provides data for lipid classes identification without precise information on subclasses, which is the bottleneck in lipidomics. Each MS-based technique has its advantages but also limitations. MS-coupled systems can be modified to overcome some technical obstacles. Therefore, different analytical approaches based on MS should be taken into consideration in studies that address the metabolome of exosomes; these approaches are schematically illustrated in Figure 1.

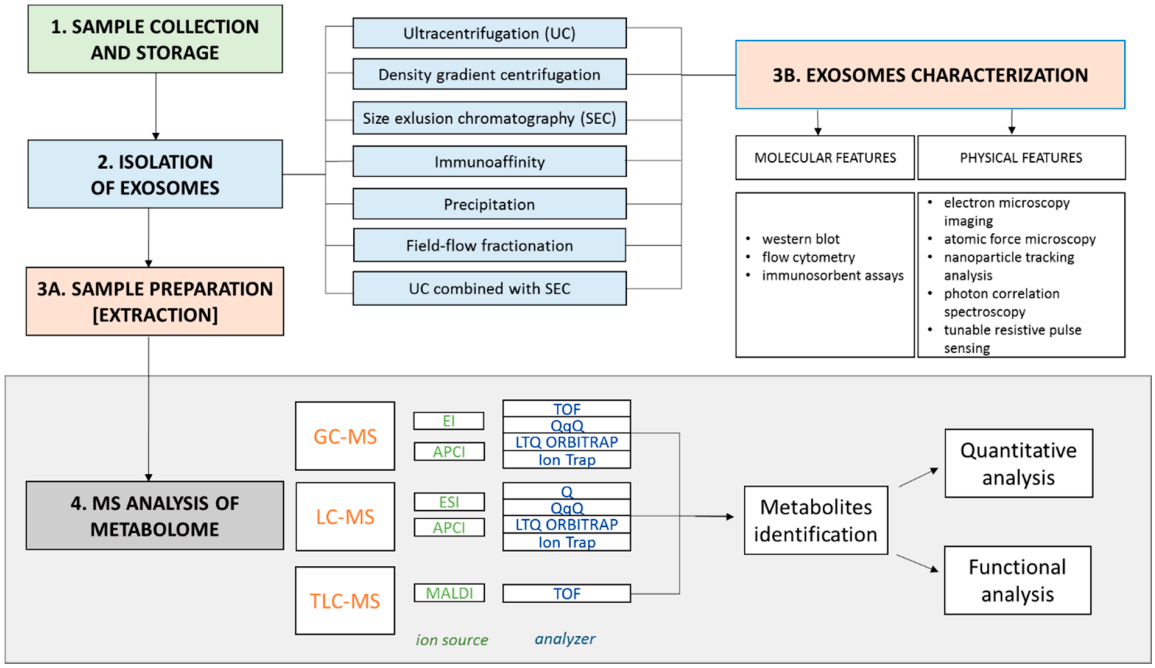

Figure 1. Different analytical approaches combining chromatography and mass spectrometry that could be implemented in studies on exosomes' (small extracellular vesicles (EVs)) metabolome.

3. Metabolites Present in Exosomes—Results of Metabolomics Studies

Although the general profile of blood (serum and plasma) or urine metabolites has been investigated with promising results in many studies [84–87], metabolomics of exosomes is a new approach and knowledge of metabolites present in extracellular vesicles has started to accumulate in a few recent years. A large part of relevant studies took under investigation exosomes (small EVs) derived from the cell culture medium, while the ones addressing vesicles derived from body fluids are less represented. Based on these studies it has been established that exosomes contain different classes of both low-molecular-weight compounds (small molecules) and lipids. Most of the analyses are focused on EVs lipidome and report detection and quantification of different classes of lipids, including glycerolipids (GL), glycerophospholipids (GP), sphingolipids (SP), sterol lipids (ST), prenol lipids (PR), and fatty acids (FA) [7,11,47,52,88–97]. Part of the studies showed a similarity between the lipid content of EVs and the composition of their parental cells' membranes, while others reveal disparities in proportions of specific membrane components. Moreover, the available data indicated marked differences in lipid composition of EVs derived from different cells (e.g., ceramide enrichment in EVs produced by tumor cells, but its absence in EVs from RBCs) [7,47,88,95]. Much fewer papers addressed a complete set of metabolites present in EVs and showed that their metabolome contains not only lipids, but also organic acids, amino acids, sugars and their conjugates, nucleotides and nucleosides, cyclic alcohols, carnitines, aromatic compounds, and vitamins [50,51,98–100]. The selection of available literature in the area of EV metabolome is listed below (Table 2).

Table 2. Review on metabolomics studies oriented on the composition of small EVs from different sources.

Cell Type/Body Fluid	Method of EVs Purification and Characterization	MS Approach	Detected Groups of Metabolites	Ref.
Human dendritic cells and RBL-2H3 mast cells	UC/EM	HPLC-MS	lipids (FA, GL, GP, SP, ST)	[7]
Seminal fluid: vasectomized men	UC + SEC/NTA, Cryo-EM, WB	APCI-HPLC-MS	lipids (GP, SP, ST)	[11]
Human B cells (RN HLA-DR15$^+$)	UC + SEC/EM, WB	Q-TOF TLC-MS; MALDI-TOF-TLC-MS	lipids (FA, GL, GP, SP, ST)	[48]
PANC1 cancer cell line; human plasma: endometrioid adenocarcinoma patients and healthy controls	UC/NTA, WB	UPLC-ESI-Q-TOF-MS	lipids (FA, GP, SP, ST, PR), carboxylic acids, amino acids, peptides, sugars, cyclic alcohols, nucleotides, and nucleosides	[50]
Human urine: prostate cancer patients and healthy controls	UC/NTA, EM, WB	QqQ ESI LC-MS	lipids (GL, GP, SP, ST)	[89]
Human urine: prostate cancer patients and healthy controls	FFF/TEM, WB	nUPLC-ESI-MS	lipids (GL, GP, SP, ST)	[52]
Human urine: renal carcinoma patients and healthy controls	UC/WB	microLC Q-TOF MS	lipids (GP, SP)	[90]
PC-3 cell line (prostate cancer)	UC/EM, WB	QqQ ESI LC-MS; UHPLC-MS	lipids (FA, GL, GP, SP, ST)	[91]
PC3, DU145, VCaP, LNCaP, C4–2, and RWPE-1 cell lines (prostate cancer)	UC/TEM, WB	UPLC-MS	lipids (GL, GP, SP, ST)	[92]
LIM1215 cell line (colorectal cancer)	UC/TEM, WB	nESI-LC-MS; HCD-MS/MS	lipids (FA, GL, GP, SP, ST)	[93]
FEMX-I cell line (melanoma)	DC + IA/NTA, WB, FM	ESI-LC-MS/MS	lipids (GL, GP, SP)	[94]
U87, Huh7, and hMSCs cell lines (glioblastoma and hepatocellular carcinoma)	UC/NTA, EM, WB	TripleTOF LC-MS/MS	lipids (FA, GL, GP, SP, ST, PR)	[95]
Normal mesenchymal stromal cells (SD-hMSC)	UC/NTA, TEM, IEM, WB	HPLC-MS/MS; LC-MS; SFC-MS	lipids (GL, GP, SP), carboxylic acids	[96]
Syncytiotrophoblast cells (preeclampsia or history of recurrent miscarriage and healthy controls)	UC/NTA, EM	APCI-HPLC-MS/MS; ESI-LC-MS MRM	lipids (GP, SP, ST)	[97]
Human serum: pancreatic cancer patients (before and after CT)	UC/TEM, WB	CIL nLC-MS	lipids (FA, GL, GP, ST), carboxylic acids, amino acids, peptides, biogenic amines, nucleotides, and nucleosides	[51]
Human plasma and urine: prostate cancer patients (before and after prostatectomy) and healthy controls	UC/NTA, EM, WB	TQ-S-UPLC-MS	carboxylic acids, amino acids, sugars, carnitines, biogenic amines, vitamins, nucleotides, and nucleosides	[98]
Human urine: prostate cancer patients and benign prostate hyperplasia patients	UC/NTA, cryo-EM, WB	UHPLC-MS	lipids (FA, GL, GP, SP, ST), amino acids, carnitines, vitamins, nucleotides, and nucleosides	[99]
PCa hCAFs, CAF-35, CAF-19, BxPC3, and MiaPaCa-2 cell lines (prostate cancer and pancreatic cancer)	UC/NTA, FM, WB	GC-MS; UPLC-MS	FA, carboxylic acids, amino acids	[100]

Abbreviations: methods of EVs purification: UC—ultracentrifugation, SEC—size-exclusion chromatography, DC—differential centrifugation, IA—immune-affinity techniques, FFF—field-flow fractionation; methods of EVs characterization: NTA—nanoparticle tracking analysis, EM—electron microscopy, TEM—transmission electron microscopy, IEM—immuno-electron microscopy, FM—fluorescence inverted microscope, WB—Western blotting; lipid classes: FA—fatty acids, GL—glycerolipids, GP—glycerophospholipids, SP—sphingophospholipids, ST—sterol lipids, PR—prenol lipids.

3.1. Analysis of Metabolome in Small EVs Derived from Cell Culture Medium in Vitro

Exosomes play an essential role in communication between cancer cells and their microenvironment, which is visible also at the level of their metabolome. Zhao et al. [100] showed that exosomes released by cancer cells and cancer-associated fibroblasts (CAFs) participate in the regulation of cancer cells metabolism. Downregulation of mitochondrial activity and increased glucose uptake and glycolysis was

observed in PC3 cancer cells cultured in the presence of EVs derived from CAFs from prostate cancer (PCa) patients. Increased level of pyruvate and lactate was correlated with a reduced level of α-ketoglutarate, fumarate, malate, and glutamate, which confirmed that EVs derived from CAFs stimulated the Warburg effect in recipient cancer cells. Moreover, these authors revealed high levels of different amino acids, carboxylic acids, and fatty acids in EVs released by different types of CAFs, and postulated that EVs act as carriers of metabolites enabling intensification of cancer cell metabolism [100]. Similarly, the presence of lactic and glutamic acids in EVs released by serum deprived mesenchymal stromal cells supported a potential role of EVs in the regulation of glucose metabolism [96]. Therefore, EVs released to culture media by specific cell types in vitro are an interesting model to study mechanisms related to the regulation of cancer cell metabolism.

The complete composition of different classes of metabolites in EVs purified from cell culture media was performed for PANC1 cells derived from pancreatic cancer. This analysis showed that major components of EVs metabolome are main components of membranes: glycerophospholipids and sphingolipids (they comprised 56% of detected compounds), fatty acids esters, amides and alcohols (14%), nucleotides and derivatives (7%), amino acids (6%), and eicosanoids, steroids and prenols (5%). Sugars, cyclic alcohols, aromatic compounds, and organic acids were also found, but less represented [50]. Other studies on metabolites detected in EVs purified from culture media focused on their lipid profile. Llorente et al. [91] compared lipidome of EVs and parental PC3 cells; there were 217 and 250 lipids detected, respectively, with 190 species common for both types of samples. The study showed enrichment of EVs in cholesterol, sphingomyelins, glycosphingolipids, and phosphatidylserines [91]. Hosseini-Beheshti et al. [92] performed an analysis of lipid content of EVs and parental cells for six different prostate cell lines. In general, they observed differences between cells and their EVs in the relative abundance of glycerophospholipids (average content 86.3% and 65.1%, respectively) and sphingolipids (9.6% and 30.2%, respectively). Moreover, cells derived from prostate cancer contain significantly less cholesterol than cells from benign prostate (RWPE-1), while the average cholesterol content of EVs derived from PCa cells was three times higher than EVs derived from RWPE-1 cells [92]. Increased level of sphingolipids and cholesterol in cancer-derived EVs was confirmed in other models. Lydic et al. [93] revealed a higher concentration of sphingomyelins, phosphatidylserines, and cholesterol in EVs derived from colorectal cancer cell line LIM1215 while compared to parental cells. There were different proportions of glycerophospholipids (91.5% vs. 68.3%), sphingolipids (5.3% vs. 22.7%), sterol lipids (1.9% vs. 4.3%), and glycerolipids (1.4% vs. 4.8%) in parental cells and their EVs, respectively [93]. Elevated levels of sphingolipids, phosphatidylserines, phosphatidylethanolamines, and phosphatidylglycerols, while decreased levels of phosphatidylcholines were observed in EVs derived from melanoma FEMX-I cells [94]. Sphingomyelin, ceramides, glycolipids, free fatty acids, phosphatidylserines, and cholesterol were enriched in EVs releases by glioblastoma cells (U87), hepatocellular carcinoma cells (Huh7) and bone marrow-derived MSCs [95]. The high abundance of sphingomyelins and ceramides was observed also in EVs released by serum-deprived MSCs [96], while sphingomyelin and cholesterol enrichment was found in EVs derived from rat mast cells (RBL-2H3 cells) [7], and human B-cells (RN HLA-DR15$^+$ cells) [48]. Therefore, the increased level of sphingomyelins and cholesterol, and the decreased level of glycerophospholipids (especially phosphatidylcholines) appeared a general feature of EVs when compared to the lipid composition of their parental cells.

3.2. Composition of The Metabolome in Small EVs Derived from Body Fluids In Vivo

The metabolome and lipidome of EVs derived from blood and urine are the most often investigated in this field of research. Studies based on different LC-MS approaches revealed that the major class of lipids detected in plasma-derived EVs (pEVs) and urine-derived EVs (uEVs) comprised of glycerophospholipids and sphingolipids, i.e., major components of membranes. Moreover, the metabolome contained fatty acids and amino acids, steroids, prenols and eicosanoids, peptides and peptide conjugates, nucleotides, nucleosides and their derivatives, as well as less abundant

sugars, alcohols, amino acids, and carboxylic acids [50,51,98,99]. Nevertheless, all these classes of metabolites present in EVs derived from human bio-fluids have high importance as a potential source of disease biomarkers.

Several metabolome-oriented studies addressed the composition of EVs derived from the urine of patients with genitourinary malignancies. Puhka et al. [98] studied metabolome of EVs derived from urine and plasma of prostate cancer (PCa) patients and detected 102 metabolites in uEV and 111 metabolites in pEV samples. There were 11 metabolites specific for uEV (creatinine, l-cystathionine, gamma-glutamylcysteine, guanidynoacetic acid, 4-hydroxyproline, kynurenic acid, glucuronate, pantothenic acid, 4-pyridoxic acid, 1-methylhistamine, trimethylamine N-oxide), and five metabolites specific for pEV (kynurenine, lysine, threonine, tryptophan, cytidine). Moreover, several metabolites showed markedly different abundances between uEV and pEV. This is noteworthy that this work revealed differences in uEV metabolome content between cancer patients before prostatectomy and after prostatectomy, as well as between untreated cancer patients and control group. There were four metabolites with a lower level in the pre-prostatectomy group: adenosine, glucuronate, isobutyryl-L-carnitine, and D-ribose 5-phosphate. The largest difference was noted for glucuronate (20-fold difference) between untreated cancer patients and treated patients combined with a control group [98]. Another study of a complete metabolome profile of EVs derived from the urine of prostate cancer patients and patients with benign prostate hyperplasia (BPH) was reported by Clos-Garcia et al. [99]. There were 248 metabolites detected out of which 76 showed significant differences between BPH and PCa patients. Moreover, there were five molecules, namely ceramides Cer (d18:1/16:0), Cer (d18:1/20:0), Cer (d18:1/22:0), PC (30:0), and acylcarnitine AC (18:0) expressed differentially between two subgroups of PCa patients (stages 2 and 3) [99]. Another two studies addressed the lipid content of EVs derived from the urine of PCa patients. One of them identified 36 lipid species and revealed that few of them, including lactosylceramide LacCer (d18:1/16:0), phosphatidylserine PS (18:1/18:1), and PS (16:0–18:1), showed markedly different levels between uEV from cancer patients and healthy controls [89]. Yet another study identified 286 lipids in uEV from PCa patients and healthy controls and showed that several classes of lipids (except for diacylglycerol, triacylglycerol, and cholesterol esters) were more abundant in uEV of cancer patients [52]. Lipid profile of uEV was analyzed also in a group of patients with renal carcinoma, which showed several differences between cancer patients and healthy controls [90]. A few studies addressed the metabolome composition of EVs derived from the blood of patients with other malignancies. There were about 1950 metabolites detected in EVs derived from serum of patients with pancreatic cancer (PANC). The analysis revealed several metabolites, including alanyl-histidine, 6-dimethyl-aminopurine, leucylproline, and methionine sulfoxide, whose abundances differentiated samples collected before and after chemotherapy [51]. The comparison of a metabolic profile of EVs derived from plasma of patients with endometrioid adenocarcinoma and healthy controls also revealed several discriminatory compounds [50]. Very few metabolome-oriented studies addressed EVs present in other human bio-specimens and related to not cancer health conditions. Brouwers et al. investigated a lipid profile of EVs derived from the seminal fluid of vasectomized men [11]. A lipid profile of EVs derived from placental syncytiotrophoblast of pregnant women was analyzed by Baig et al. [97]. The study revealed several EV lipids whose levels differentiated women with preeclampsia or history of recurrent miscarriages from women with a healthy pregnancy.

4. Conclusions

Extracellular vesicles—their composition, biology, and role in the pathophysiological processes—are extensively studied. However, the variability of data available in the literature is mostly concentrated on their proteome and transcriptome (miRNome in particular). Studies on the metabolic profile of exosomes are the youngest part of this area. Nevertheless, from the practical and clinical point of view, metabolomics of exosomes derived from human bio-fluids is the most appropriable because the metabolome of these vesicles is a potential goldmine of disease biomarkers. Unfortunately, despite a promising start of metabolomics of exosomes derived from in vitro cell models, much less information

is available concerning the metabolome of body fluids-derived vesicles. Results available in literature until now give the first input into this knowledge, but they still need to be extended and validated.

It is also important to understand the future challenges of exosome metabolome studies. The relevant analytical pipeline should consist of separation techniques for efficient and specific exosomes purification, instrumental analysis for a sensitive and specific measurement of metabolites, and adequate data processing. The concerns of all studies with EVs are standardization and improvement of methods of isolation and distinguishing of EV subpopulations. Additionally, one of the concerns of exosomes derived from body fluids is the reduction of contamination from lipoproteins and "soluble" compounds. Another important issue addressed to metabolomics of exosomes is the detection of low abundant metabolites that could be solved with targeted MS analyses if relevant compounds were identified in the source material and their transitions (ions specific for the precursor and the product of each metabolite) are known. For identification of metabolites present in bio-fluids, Human Metabolome Database (HMDB) [101] is a very useful tool. Unfortunately, identification of exosomal metabolites based on currently available databases dedicated for extracellular vesicles is less feasible. Open access databases for exosome small metabolites (EVpedia) and lipids (EVpedia, ExoCarta) do not offer comprehensive information that could be compared to the knowledge of exosome proteins and RNAs.

One should admit the lack of widely accepted gold standard of exosome metabolome analysis at present. Diversity of exosome sources, isolation methods, and analytical techniques together with a limited amount of research performed, foreclose the possibility of rational and well-balanced comparison of available metabolomics approaches. Although, based on recently published data and own research we could recommend two strategies. A combination of SEC with UC or UF might be particularly suitable for in vitro studies, where an amount of material for EV isolation is not a limiting factor; a specific mass spectrometry approach (e.g., type of spectrometer) is not a critical factor. Another situation concerns work with actual clinical samples, where available amount of material for exosome isolation might be a limiting factor. In that case we recommend implementation of a highly efficient one-step method for exosome isolation (e.g., based on SEC) and targeted MS approach for analysis of pre-selected metabolites. Nevertheless, implemented methodology has to be optimized and tailored to the needs of specific research models.

Nonetheless, the knowledge on metabolites carried by exosomes, especially those produced by cancer cells, accumulates constantly. Therefore, it may soon provide valuable information on the phenotype of cancer cells and provide new biomarkers for disease detection, monitoring, and prognosis.

Funding: This study was funded by the National Science Centre, Poland, Grant 2013/11/B/NZ7/01512 (to M.P.), Grant 2017/27/B/NZ7/01833 (to P.W.) and Grant 2017/26/D/NZ2/00964 (to A.W.).

Conflicts of Interest: The authors declare no conflict of interest.

Abbreviations

EVs	Extracellular Vesicles
EX	Exosomes
LMWMs	Low-Molecular-Weight Metabolites
MV	Microvesicles
UC	Ultracentrifugation
SEC	Size exclusion chromatography
DC	Differential centrifugation
UF	Ultrafiltration
IA	Immune-affinity techniques
nPES	Nanoplasmon-enhanced scattering
TEX	Tumor-derived Exosomes
FFF	Field-flow fractionation
WB	Western blotting

FC	Flow cytometry
ISAs	Immunosorbent assays
EM	Electron microscopy imaging
AFM	Atomic force microscopy
NTA	Nanoparticle tracking analysis
PCS	Photon correlation spectroscopy
tRPS	Tunable resistive pulse sensing
MS	Mass Spectrometry
GC	Gas chromatography
LC	Liquid chromatography
UPLC	Ultra Performance Liquid Chromatography
TLC	Thin Layer Chromatography
MALDI	Matrix Assisted Laser Desorption Ionization
EI	Electron Impact
ESI	Electrospray Ionization
APCI	Atmospheric Pressure Chemical Ionization
TOF	Time-Of-Flight
Q	Quadrupole
QqQ/QQQ	Triple Quadrupole
LTQ	Linear Trap Quadrupole
GL	Glycerolipids
GP	Glycerophospholipids
GSL	Glycosphingolipids
PL	Phospholipids
SP	Sphingolipids
ST	Sterol lipids
PR	Prenol lipids
FA	Fatty Acids
RBS	Red blood cells
CAFs	Cancer-associated fibroblasts
PCa	Prostate Cancer
PANC	Pancreatic cancer
uEV	Urine derived extracellular vesicles
pEV	Plasma derived extracellular vesicles
TAG	Triacylglyceroles
Cer	Ceramides
PS	Phosphatidylserine
HMDB	Human Metabolome Database

References

1. Minciacchi, V.R.R.; Freeman, M.R.; Di Vizio, D. Extracellular Vesicles in Cancer: Exosomes, Microvesicles and the Emerging Role of Large Oncosomes. *Semin. Cell Dev. Biol.* **2015**, *40*, 41–51. [CrossRef] [PubMed]
2. Février, B.; Raposo, G. Exosomes: Endosomal-derived vesicles shipping extracellular messages. *Curr. Opin. Cell Biol.* **2014**, *16*, 415–421. [CrossRef] [PubMed]
3. Recordi, M. Intercellular communication by exosomes in placenta: A possible role in cell fusion? *Placenta* **2014**, *35*, 297–302. [CrossRef] [PubMed]
4. György, B.; Szabó, T.G.; Pásztói, M.; Pál, Z.; Misják, P.; Aradi, B.; László, V.; Pállinger, E.; Pap, E.; Kittel, A.; et al. Membrane vesicles, current state-of-the-art: Emerging role of extracellular vesicles. *Cell Mol. Life Sci.* **2011**, *68*, 2667–2688. [CrossRef] [PubMed]
5. Van Niel, G.; D'Angelo, G.; Raposo, G. Shedding light on the cell biology of extracellular vesicles. *Nat. Rev. Mol. Cell Biol.* **2018**, *19*, 213–228. [CrossRef]

6. Théry, C.; Witwer, K.W.; Aikawa, E.; Alcaraz, M.J.; Anderson, J.D.; Andriantsitohaina, R.; Antoniou, A.; Arab, T.; Archer, T.; Atkin-Smith, G.K.; et al. Minimal information for studies of extracellular vesicles 2018 (MISEV2018): A position statement of the International Society for Extracellular Vesicles and update of the MISEV2014 guidelines. *J. Extracell. Vesicles* **2019**, *8*, 1535750.
7. Laulagnier, K.; Motta, C.; Hamdi, S.; Roy, S.; Fauvelle, F.; Pageaux, J.F.; Kobayashi, T.; Salles, J.-P.; Perret, B.; Bonnerot, C.; et al. Mast cell- and dendritic cell-derived exosomes display a specific lipid composition and an unusual membrane organization. *Biochem. J.* **2004**, *380*, 161–171. [CrossRef] [PubMed]
8. Vlassov, A.V.; Magdaleno, S.; Setterquist, R.; Conrad, R. Exosomes: Current knowledge of their composition, biological functions, and diagnostic and therapeutic potentials. *Biochim. Biophys. Acta* **2012**, *1820*, 940–948. [CrossRef] [PubMed]
9. Romancino, D.P.; Paterniti, G.; Campos, Y.; De Luca, A.; Di Felice, V.; d'Azzo, A.; Bongiovanni, A. Identification and characterization of the nano-sized vesicles released by muscle cells. *FEBS Lett.* **2013**, *587*, 1379–1384. [CrossRef] [PubMed]
10. Yáñez-Mó, M.; Siljander, P.R.; Andreu, Z.; Zavec, A.B.; Borràs, F.E.; Buzas, E.I.; Buzas, K.; Casal, E.; Cappello, F.; Carvalho, J.; et al. Biological properties of extracellular vesicles and their physiological functions. *J. Extracell. Vesicles* **2015**, *4*, 27066. [CrossRef] [PubMed]
11. Brouwers, J.F.; Aalberts, M.; Jansen, J.W.; van Niel, G.; Wauben, M.H.; Stout, T.A.; Helms, J.B.; Stoorvogel, W. Distinct lipid compositions of two types of human prostasomes. *Proteomics* **2013**, *13*, 1660–1666. [CrossRef] [PubMed]
12. Chiasserini, D.; van Weering, J.R.; Piersma, S.R.; Pham, T.V.; Malekzadeh, A.; Teunissen, C.E.; de Wit, H.; Jiménez, C.R. Proteomic analysis of cerebrospinal fluid extracellular vesicles: A comprehensive dataset. *J. Proteom.* **2014**, *106*, 191–204. [CrossRef] [PubMed]
13. Saunderson, S.C.; Dunn, A.C.; Crocker, P.R.; McLellan, A.D. CD169 mediates the capture of exosomes in spleen and lymph node. *Blood* **2014**, *123*, 208–216. [CrossRef] [PubMed]
14. Keller, S.; König, A.K.; Marmé, F.; Runz, S.; Wolterink, S.; Koensgen, D.; Mustea, A.; Sehouli, J.; Altevogt, P. Systemic presence and tumor-growth promoting effect of ovarian carcinoma released exosomes. *Cancer Lett.* **2009**, *278*, 73–81. [CrossRef] [PubMed]
15. Runz, S.; Keller, S.; Rupp, C.; Stoeck, A.; Issa, Y.; Koensgen, D.; Mustea, A.; Sehouli, J.; Kristiansen, G.; Altevogt, P. Malignant ascites-derived exosomes of ovarian carcinoma patients contain CD24 and EpCAM. *Gynecol. Oncol.* **2007**, *107*, 563–571. [CrossRef] [PubMed]
16. Wu, G.; Yang, G.; Zhang, R. Altered microRNA Expression Profiles of Extracellular Vesicles in Nasal Mucus From Patients With Allergic Rhinitis. *Allergy Asthma Immunol. Res.* **2015**, *7*, 449–457. [CrossRef] [PubMed]
17. Grigor'eva, A.E.; Tamkovich, S.N.; Eremina, A.V.; Tupikin, A.E.; Kabilov, M.R.; Chernykh, V.V.; Vlassov, V.V.; Laktionov, P.P.; Ryabchikova, E.I. Exosomes in tears of healthy individuals: Isolation, identification, and characterization. *Biochem. Moscow. Suppl. Ser. B* **2016**, *10*, 165. [CrossRef]
18. Dixon, C.L.; Sheller-Miller, S.; Saade, G.R.; Fortunato, S.J.; Lai, A.; Palma, C.; Guanzon, D.; Salomon, C.; Menon, R. Amniotic Fluid Exosome Proteomic Profile Exhibits Unique Pathways of Term and Preterm Labor. *Endocrinology* **2018**, *159*, 2229–2240. [CrossRef]
19. Yu, J.; Lin, Y.; Xiong, X.; Li, K.; Yao, Z.; Dong, H.; Jiang, Z.; Yu, D.; Yeung, S.J.; Zhang, H. Detection of Exosomal PD-L1 RNA in Saliva of Patients With Periodontitis. *Front. Genet.* **2019**, *10*, 202. [CrossRef]
20. Xie, C.; Ji, N.; Tang, Z.; Li, J.; Chen, Q. The role of extracellular vesicles from different origin in the microenvironment of head and neck cancers. *Mol. Cancer* **2019**, *18*, 83. [CrossRef]
21. Milasan, A.; Tessandier, N.; Tan, S.; Brisson, A.; Boilard, E.; Martel, C. Extracellular vesicles are present in mouse lymph and their level differs in atherosclerosis. *J. Extracell. Vesicles* **2016**, *5*, 31427. [CrossRef] [PubMed]
22. Ludwig, A.K.; Giebel, B. Exosomes: Small vesicles participating in intercellular communication. *Int. J. Biochem. Cell Biol.* **2012**, *44*, 11–15. [CrossRef] [PubMed]
23. Mathivanan, S.; Ji, H.; Simpson, R.J. Exosomes: Extracellular organelles important in intercellular communication. *J. Proteom.* **2010**, *73*, 1907–1920. [CrossRef] [PubMed]
24. Greening, D.W.; Gopal, S.K.; Xu, R.; Simpson, R.J.; Chen, W. Exosomes and their roles in immune regulation and cancer. *Semin. Cell Dev. Biol.* **2015**, *40*, 72–81. [CrossRef] [PubMed]

25. Shender, V.O.; Pavlyukov, M.S.; Ziganshin, R.H.; Arapidi, G.P.; Kovalchuk, S.I.; Anikanov, N.A.; Altukhov, I.A.; Alexeev, D.G.; Butenko, I.O.; Shavarda, A.L.; et al. Proteome-metabolome profiling of ovarian cancer ascites reveals novel components involved in intercellular communication. *Mol. Cell. Proteom.* **2014**, *13*, 3558–3571. [CrossRef]
26. Duijvesz, D.; Versluis, C.Y.; van der Fels, C.A.; Vredenbregt-van den Berg, M.S.; Leivo, J.; Peltola, M.T.; Bangma, C.H.; Pettersson, K.S.; Jenster, G. Immuno-based detection of extracellular vesicles in urine as diagnostic marker for prostate cancer. *Int. J. Cancer* **2015**, *137*, 2869–2878. [CrossRef] [PubMed]
27. Mitchell, P.J.; Welton, J.; Staffurth, J.; Court, J.; Mason, M.D.; Tabi, Z.; Clayton, A. Can urinary exosomes act as treatment response markers in prostate cancer? *J. Transl. Med.* **2009**, *7*, 4. [CrossRef]
28. Rabinowits, G.; Gercel-Taylor, C.; Day, J.M.; Taylor, D.D.; Kloecker, G.H. Exosomal microRNA: A diagnostic marker for lung cancer. *Clin. Lung Cancer* **2009**, *10*, 42–46. [CrossRef]
29. Silva, J.; Garcia, V.; Rodriguez, M.; Compte, M.; Cisneros, E.; Veguillas, P.; Garcia, J.M.; Dominguez, G.; Campos-Martin, Y.; Cuevas, J.; et al. Analysis of exosome release and its prognostic value in human colorectal cancer. *Genes Chromosomes Cancer* **2012**, *51*, 409–418. [CrossRef]
30. Szczepanski, M.J.; Szajnik, M.; Welsh, A.; Whiteside, T.L.; Boyiadzis, M. Blast-derived microvesicles in sera from patients with acute myeloid leukemia suppress natural killer cell function via membrane-associated transforming growth factor-beta1. *Haematologica* **2011**, *96*, 1302–1309. [CrossRef]
31. Szajnik, M.; Derbis, M.; Lach, M.; Patalas, P.; Michalak, M.; Drzewiecka, H.; Szpurek, D.; Nowakowski, A.; Spaczynski, M.; Baranowski, W.; et al. Exosomes in Plasma of Patients with Ovarian Carcinoma: Potential Biomarkers of Tumor Progression and Response to Therapy. *Gynecol. Obstet. (Sunnyvale)* **2013**, *4*, 003.
32. Baran, J.; Baj-Krzyworzeka, M.; Weglarczyk, K.; Szatanek, R.; Zembala, M.; Barbasz, J.; Czupryna, A.; Szczepanik, A.; Zembala, M. Circulating tumour-derived microvesicles in plasma of gastric cancer patients. *Cancer Immunol. Immunother.* **2010**, *59*, 841–850. [CrossRef] [PubMed]
33. Fujita, Y.; Yoshioka, Y.; Ochiya, T. Extracellular vesicle transfer of cancer pathogenic components. *Cancer Sci.* **2016**, *107*, 385–390. [CrossRef] [PubMed]
34. Chaput, N.; Théry, C. Exosomes: Immune properties and potential clinical implementations. *Semin. Immunopathol.* **2011**, *33*, 419–440. [CrossRef] [PubMed]
35. Hyenne, V.; Lefebvre, O.; Goetz, J.G. Going live with tumor exosomes and microvesicles. *Cell Adhes. Migr.* **2017**, *11*, 173–186. [CrossRef] [PubMed]
36. Becker, A.; Thakur, B.K.; Weiss, J.M.; Kim, H.S.; Peinado, H.; Lyden, D. Extracellular Vesicles in Cancer: Cell-to-Cell Mediators of Metastasis. *Cancer Cell.* **2016**, *30*, 836–848. [CrossRef] [PubMed]
37. Naito, Y.; Yoshioka, Y.; Yamamoto, Y.; Ochiya, T. How cancer cells dictate their microenvironment: Present roles of extracellular vesicles. *Cell Mol. Life Sci.* **2017**, *74*, 697–713. [CrossRef]
38. Spugnini, E.P.; Logozzi, M.; Di Raimo, R.; Mizzoni, D.; Fais, S. A Role of Tumor-Released Exosomes in Paracrine Dissemination and Metastasis. *Int. J. Mol Sci.* **2018**, *19*, 3968. [CrossRef]
39. Guan, M.; Chen, X.; Ma, Y.; Tang, L.; Guan, L.; Ren, X.; Yu, B.; Zhang, W.; Su, B. MDA-9 and GRP78 as potential diagnostic biomarkers for early detection of melanoma metastasis. *Tumor Biol.* **2015**, *36*, 2973–2982. [CrossRef]
40. Taylor, D.D.; Gercel-Taylor, C. MicroRNA signatures of tumor-derived exosomes as diagnostic biomarkers of ovarian cancer. *Gynecol. Oncol.* **2008**, *110*, 13–21. [CrossRef]
41. Melo, S.A.; Luecke, L.B.; Kahlert, C.; Fernandez, A.F.; Gammon, S.T.; Kaye, J.; LeBleu, V.S.; Mittendorf, E.A.; Weitz, J.; Rahbari, N.; et al. Glypican-1 identifies cancer exosomes and detects early pancreatic cancer. *Nature* **2015**, *523*, 177–182. [CrossRef] [PubMed]
42. Hadacek, F.; Bachmann, G. Low-molecular-weight metabolite systems chemistry. *Front. Environ. Sci.* **2015**, *3*, 1–21. [CrossRef]
43. Fahy, E.; Cotter, D.; Sud, M.; Subramaniam, S. Lipid classification, structures and tools. *Biochim. Biophys. Acta-Mol. Cell Biol. Lipids* **2011**, *1811*, 637–647. [CrossRef] [PubMed]
44. Zhang, A.; Sun, H.; Wang, X. Serum metabolomics as a novel diagnostic approach for disease: A systematic review. *Anal. Bioanal. Chem.* **2012**, *404*, 1239–1245. [CrossRef] [PubMed]
45. Zhang, A.; Sun, H.; Wang, P.; Han, Y.; Wang, X. Recent and potential developments of biofluid analyses in metabolomics. *J. Proteom.* **2012**, *75*, 1079–1088. [CrossRef] [PubMed]
46. Sharma, A.; Khatun, Z.; Shiras, A. Tumor exosomes: Cellular postmen of cancer diagnosis and personalized therapy. *Nanomedicine* **2016**, *11*, 421–437. [CrossRef]

47. Subra, C.; Laulagnier, K.; Perret, B.; Record, M. Exosome lipidomics unravels lipid sorting at the level of multivesicular bodies. *Biochimie* **2007**, *89*, 205–212. [CrossRef]
48. Wubbolts, R.; Leckie, R.S.; Veenhuizen, P.T.; Schwarzmann, G.; Mobius, W.; Hoernschemeyer, J.; Slot, J.W.; Geuze, H.J.; Stoorvogel, W. Proteomic and biochemical analyses of human B-cell-derived exosomes. Potential implications for their function and multivesicular body formation. *J. Biol. Chem.* **2003**, *278*, 10963–10972. [CrossRef]
49. Subra, C.; Grand, D.; Laulagnier, K.; Stella, A.; Lambeau, G.; Paillasse, M.; De Medina, P.; Monsarrat, B.; Perret, B.; Silvente-Poirot, S.; et al. Exosomes account for vesicle-mediated transcellular transport of activatable phospholipases and prostaglandins. *J. Lipid Res.* **2010**, *51*, 2105–2120. [CrossRef]
50. Altadill, T.; Campoy, I.; Lanau, L.; Gill, K.; Rigau, M.; Gil-Moreno, A.; Reventos, J.; Byers, S.; Colas, E.; Cheema, A.K. Enabling metabolomics based biomarker discovery studies using molecular phenotyping of exosome-like vesicles. *PLoS ONE* **2016**, *11*, e0151339. [CrossRef]
51. Luo, X.; An, M.; Cuneo, K.C.; Lubman, D.M.; Li, L. High-Performance Chemical Isotope Labeling Liquid Chromatography Mass Spectrometry for Exosome Metabolomics. *Anal. Chem.* **2018**, *90*, 8314–8319. [CrossRef] [PubMed]
52. Yang, J.S.; Lee, J.C.; Byeon, S.K.; Rha, K.H.; Moon, M.H. Size Dependent Lipidomic Analysis of Urinary Exosomes from Patients with Prostate Cancer by Flow Field-Flow Fractionation and Nanoflow Liquid Chromatography-Tandem Mass Spectrometry. *Anal. Chem.* **2017**, *89*, 2488–2497. [CrossRef] [PubMed]
53. Kumari, S.; Singh, A. Urinary Exosomal Lipidomics Reveals Markers for Diabetic Nephropathy. *Curr. Metabol.* **2018**, *6*, 131–139. [CrossRef]
54. De Menezes-Neto, A.; Sáez, M.J.; Lozano-Ramos, I.; Segui-Barber, J.; Martin-Jaular, L.; Ullate, J.M.E.; Fernandez-Becerra, C.; Borrás, F.E.; Del Portillo, H.A. Size-exclusion chromatography as a stand-alone methodology identifies novel markers in mass spectrometry analyses of plasma-derived vesicles from healthy individuals. *J. Extracell. Vesicles* **2015**, *4*, 10. [CrossRef] [PubMed]
55. Lobb, R.J.; Becker, M.; Wen Wen, S.; Wong, C.S.F.; Wiegmans, A.P.; Leimgruber, A.; Möller, A. Optimized exosome isolation protocol for cell culture supernatant and human plasma. *J. Extracell. Vesicles* **2015**, *4*, 27031. [CrossRef] [PubMed]
56. Tang, Y.T.; Huang, Y.Y.; Zheng, L.; Qin, S.H.; Xu, X.P.; An, T.X.; Xu, Y.; Wu, Y.S.; Hu, X.M.; Ping, B.H.; et al. Comparison of isolation methods of exosomes and exosomal RNA from cell culture medium and serum. *Int. J. Mol. Med.* **2017**, *40*, 834–844. [CrossRef] [PubMed]
57. Rekker, K.; Saare, M.; Roost, A.M.; Kubo, A.L.; Zarovni, N.; Chiesi, A.; Salumets, A.; Peters, M. Comparison of serum exosome isolation methods for microRNA profiling. *Clin. Biochem.* **2014**, *47*, 135–138. [CrossRef]
58. Yu, L.L.; Zhu, L.; Liu, J.X.; Jiang, F.; Ni, W.K.; Qu, L.S.; Ni, R.Z.; Lu, C.H.; Xiao, M.B. A Comparison of Traditional and Novel Methods for the Separation of Exosomes from Human Samples. *BioMed Res. Int.* **2018**, *2018*, 3634563. [CrossRef]
59. Muller, L.; MHong, C.S.; Stolz, D.B.; Watkins, S.C.; Whiteside, T.L. Isolation of biologically-active exosomes from human plasma. *J. Immunol. Methods* **2014**, *411*, 55–65. [CrossRef]
60. Hong, C.S.; Funk, S.; Muller, L.; Boyiadzis, M.; Whiteside, T.L. Isolation of biologically active and morphologically intact exosomes from plasma of patients with cancer. *J. Extracell. Vesicles* **2016**, *5*, 29289. [CrossRef]
61. Benedikter, B.J.; Bouwman, F.G.; Vajen, T.; Heinzmann, A.C.A.; Grauls, G.; Mariman, E.C.; Wouters, E.F.M.; Savelkoul, P.H.; Lopez-Iglesias, C.; Koenen, R.R.; et al. Ultrafiltration combined with size exclusion chromatography efficiently isolates extracellular vesicles from cell culture media for compositional and functional studies. *Sci. Rep.* **2017**, *7*, 15297. [CrossRef] [PubMed]
62. Tauro, B.J.; Greening, D.W.; Mathias, R.A.; Ji, H.; Mathivanan, S.; Scott, A.M.; Simpson, R.J. Comparison of ultracentrifugation, density gradient separation, and immunoaffinity capture methods for isolating human colon cancer cell line LIM1863-derived exosomes. *Methods* **2012**, *56*, 293–304. [CrossRef]
63. Liang, K.; Liu, F.; Fan, J.; Sun, D.; Liu, C.; Lion, C.J.; Bernard, D.W.; Li, Y.; Yokoi, K.; Katz, M.H.; et al. Nanoplasmonic quantification of tumour-derived extracellular vesicles in plasma microsamples for diagnosis and treatment monitoring. *Nature Biomed. Eng.* **2017**, *1*, 21. [CrossRef] [PubMed]
64. Abramowicz, A.; Widlak, P.; Pietrowska, M. Proteomic analysis of exosomal cargo: The challenge of high purity vesicle isolation. *Mol. Biosyst.* **2016**, *12*, 1407–1419. [CrossRef]

65. Sharma, P.; Ludwig, S.; Muller, L.; Hong, C.S.; Kirkwood, J.M.; Ferrone, S.; Whiteside, T.L. Immunoaffinity-based isolation of melanoma cell-derived exosomes from plasma of patients with melanoma. *J. Extracell. Vesicles* **2018**, *7*, 1435138. [CrossRef] [PubMed]
66. Oeyen, E.; Van Mol, K.; Baggerman, G.; Willems, H.; Boonen, K.; Rolfo, C.; Pauwels, P.; Jacobs, A.; Schildermans, K.; Cho, W.C.; et al. Ultrafiltration and size exclusion chromatography combined with asymmetrical-flow field-flow fractionation for the isolation and characterisation of extracellular vesicles from urine. *J. Extracell. Vesicles* **2018**, *7*, 1490143. [CrossRef] [PubMed]
67. Hartjes, T.A.; Mytnyk, S.; Jenster, G.W.; van Steijn, V.; van Royen, M.E. Extracellular Vesicle Quantification and Characterization: Common Methods and Emerging Approaches. *Bioengineering (Basel)* **2019**, *6*, 7. [CrossRef]
68. Vallejo, M.; García, A.; Tuñón, J.; García-Martínez, D.; Angulo, S.; Martin-Ventura, J.L.; Blanco-Colio, L.M.; Almeida, P.; Egido, J.; Barbas, C. Plasma fingerprinting with GC-MS in acute coronary syndrome. *Anal. Bioanal. Chem.* **2009**, *394*, 1517–1524. [CrossRef]
69. Rojo, D.; Barbas, C.; Rupérez, F.J. LC-MS metabolomics of polar compounds. *Bioanalysis* **2012**, *4*, 1235–1243. [CrossRef]
70. Villas-Bôas, S.G.; Mas, S.; Åkesson, M.; Smedsgaard, J.; Nielsen, J. Mass spectrometry in metabolome analysis. *Mass Spectrom. Rev.* **2005**, *24*, 613–646. [CrossRef]
71. Fanos, V.; Caboni, P.; Corsello, G.; Stronati, M.; Gazzolo, D.; Noto, A.; Lussu, M.; Dessì, A.; Giuffrè, M.; Lacerenza, S.; et al. Urinary (1)H-NMR and GC-MS metabolomics predicts early and late onset neonatal sepsis. *Early Hum. Dev.* **2014**, *90* (Suppl. 1), 78–83. [CrossRef]
72. Goodacre, R.; Vaidyanathan, S.; Dunn, W.B.; Harrigan, G.G.; Kell, D.B. Metabolomics by numbers: Acquiring and understanding global metabolite data. *Trends Biotechnol.* **2004**, *22*, 245–252. [CrossRef] [PubMed]
73. Yang, Y.; Cruickshank, C.; Armstrong, M.; Mahaffey, S.; Reisdorph, R.; Reisdorph, N. New sample preparation approach for mass spectrometry-based profiling of plasma results in improved coverage of metabolome. *J. Chromatogr. A* **2013**, *1300*, 217–226. [CrossRef] [PubMed]
74. Dunn, W.B.; Ellis, D.I. Metabolomics: Current analytical platforms and methodologies. *TrAC Trends Anal. Chem.* **2005**, *24*, 285–294.
75. Köfeler, H.C.; Fauland, A.; Rechberger, G.N.; Trötzmüller, M. Mass spectrometry based lipidomics: An overview of technological platforms. *Metabolites* **2012**, *2*, 19–38. [CrossRef]
76. Kostiainen, R.; Kauppila, T.J. Effect of eluent on the ionization process in liquid chromatography-mass spectrometry. *J. Chromatogr. A* **2009**, *1216*, 685–699. [CrossRef]
77. Koulman, A.; Woffendin, G.; Narayana, V.K.; Welchman, H.; Crone, C.; Volmer, D.A. High-resolution extracted ion chromatography, a new tool for metabolomics and lipidomics using a second-generation orbitrap mass spectrometer. *Rapid Commun. Mass Spectrom.* **2009**, *23*, 1411–1418. [CrossRef]
78. Roberts, L.D.; Souza, A.L.; Gerszten, R.E.; Clish, C.B. Targeted metabolomics. *Curr. Protoc. Mol. Biol.* **2012**, *1* (Suppl. 98), 1–34. [CrossRef]
79. Kanu, A.B.; Dwivedi, P.; Tam, M.; Matz, L.; Hill, H.H., Jr. Ion mobility-mass spectrometry. *J. Mass Spectrom.* **2008**, *43*, 1–22. [CrossRef]
80. Halket, J.M.; Waterman, D.; Przyborowska, A.M.; Patel, R.K.P.; Fraser, P.D.; Bramley, P.M. Chemical derivatization and mass spectral libraries in metabolic profiling by GC/MS and LC/MS/MS. *J. Exp. Bot.* **2005**, *56*, 219–243. [CrossRef]
81. Cajka, T.; Fiehn, O. Comprehensive analysis of lipids in biological systems by liquid chromatography-mass spectrometry. *TrAC Trends Anal. Chem.* **2014**, *61*, 192–206. [CrossRef] [PubMed]
82. Quehenberger, O.; Armando, A.M.; Brown, A.H.; Milne, S.B.; Myers, D.S.; Merrill, A.H.; Bandyopadhyay, S.; Jones, K.N.; Kelly, S.; Shaner, R.L.; et al. Lipidomics reveals a remarkable diversity of lipids in human plasma. *J. Lipid Res.* **2010**, *51*, 3299–3305. [CrossRef] [PubMed]
83. Lu, W.; Bennett, B.D.; Rabinowitz, J.D. Analytical strategies for LC-MS-based targeted metabolomics. *J. Chromatogr. B Anal. Technol. Biomed. Life Sci.* **2008**, *871*, 236–242. [CrossRef] [PubMed]
84. Spratlin, J.L.; Serkova, N.J.; Eckhardt, S.G. Clinical applications of metabolomics in oncology: A review. *Clin. Cancer Res.* **2009**, *15*, 431–440. [CrossRef] [PubMed]
85. Rockel, J.S.; Kapoor, M. The Metabolome and Osteoarthritis: Possible Contributions to Symptoms and Pathology. *Metabolites* **2018**, *8*, 92. [CrossRef] [PubMed]
86. Erben, V.; Bhardwaj, M.; Schrotz-King, P.; Brenner, H. Metabolomics Biomarkers for Detection of Colorectal Neoplasms: A Systematic Review. *Cancers (Basel)* **2018**, *10*, 246. [CrossRef] [PubMed]

87. Jelonek, K.; Roś, M.; Pietrowska, M.; Widłak, P. Cancer biomarkers and mass spectrometry-based analyses of phospholipids in body fluids. *Clin. Lipidol.* **2013**, *8*, 137–150. [CrossRef]
88. Lauren, E.; Tigistu-Sahle, F.; Valkonen, S.; Westberg, M.; Valkeajarvi, A.; Eronen, J.; Siljander, P.; Pettila, V.; Kakela, R.; Laitinen, S.; et al. Phospholipid composition of packed red blood cells and that of extracellular vesicles show a high resemblance and stability during storage. *Biochim. Biophys. Acta* **2018**, *1863*, 1–8. [CrossRef]
89. Skotland, T.; Ekroos, K.; Kauhanen, D.; Simolin, H.; Seierstad, T.; Berge, V.; Sandvig, K.; Llorente, A. Molecular lipid species in urinary exosomes as potential prostate cancer biomarkers. *Eur. J. Cancer* **2017**, *70*, 122–132. [CrossRef]
90. Del Boccio, P.; Raimondo, F.; Pieragostino, D.; Morosi, L.; Cozzi, G.; Sacchetta, P.; Magni, F.; Pitto, M.; Urbani, A. A hyphenated microLC-Q-TOF-MS platform for exosomal lipidomics investigations: Application to RCC urinary exosomes. *Electrophoresis* **2012**, *33*, 686–696. [CrossRef]
91. Llorente, A.; Skotland, T.; Sylvänne, T.; Kauhanen, D.; Róg, T.; Orłowski, A.; Vattulainen, I.; Ekroos, K.; Sandvig, K. Molecular lipidomics of exosomes released by PC-3 prostate cancer cells. *Biochim. Biophys. Acta* **2013**, *1831*, 1302–1309. [CrossRef] [PubMed]
92. Hosseini-Beheshti, E.; Pham, S.; Adomat, H.; Li, N.; Tomlinson Guns, E.S. Exosomes as biomarker enriched microvesicles: Characterization of exosomal proteins derived from a panel of prostate cell lines with distinct AR phenotypes. *Mol. Cell. Proteom.* **2012**, *11*, 863–885. [CrossRef] [PubMed]
93. Lydic, T.A.; Townsend, S.; Adda, C.G.; Collins, C.; Mathivanan, S.; Reid, G.E. Rapid and comprehensive 'shotgun' lipidome profiling of colorectal cancer cell derived exosomes. *Methods* **2015**, *87*, 83–95. [CrossRef] [PubMed]
94. Rappa, G.; Mercapide, J.; Anzanello, F.; Pope, R.M.; Lorico, A. Biochemical and biological characterization of exosomes containing prominin-1/CD133. *Mol. Cancer* **2013**, *12*, 62. [CrossRef] [PubMed]
95. Haraszti, R.A.; Didiot, M.C.; Sapp, E.; Leszyk, J.; Shaffer, S.A.; Rockwell, H.E.; Gao, F.; Narain, N.R.; DiFiglia, M.; Kiebish, M.A.; et al. High-resolution proteomic and lipidomic analysis of exosomes and microvesicles from different cell sources. *J. Extracell. Vesicles* **2016**, *5*, 32570. [CrossRef] [PubMed]
96. Vallabhaneni, K.C.; Penfornis, P.; Dhule, S.; Guillonneau, F.; Adams, K.V.; Mo, Y.Y.; Xu, R.; Liu, Y.; Watabe, K.; Vemuri, M.C.; et al. Extracellular vesicles from bone marrow mesenchymal stem/stromal cells transport tumor regulatory microRNA, proteins, and metabolites. *Oncotarget* **2015**, *6*, 4953–4967. [CrossRef]
97. Baig, S.; Lim, J.Y.; Fernandis, A.Z.; Wenk, M.R.; Kale, A.; Su, L.L.; Biswas, A.; Vasoo, S.; Shui, G.; Choolani, M. Lipidomic analysis of human placental syncytiotrophoblast microvesicles in adverse pregnancy outcomes. *Placenta* **2013**, *34*, 436–442. [CrossRef]
98. Puhka, M.; Takatalo, M.; Nordberg, M.E.; Valkonen, S.; Nandania, J.; Aatonen, M.; Yliperttula, M.; Laitinen, S.; Velagapudi, V.; Mirtti, T.; et al. Metabolomic Profiling of Extracellular Vesicles and Alternative Normalization Methods Reveal Enriched Metabolites and Strategies to Study Prostate Cancer-Related Changes. *Theranostics* **2017**, *7*, 3824–3841. [CrossRef]
99. Clos-Garcia, M.; Loizaga-Iriarte, A.; Zuñiga-Garcia, P.; Sánchez-Mosquera, P.; Rosa Cortazar, A.; González, E.; Torrano, V.; Alonso, C.; Pérez-Cormenzana, M.; Ugalde-Olano, A.; et al. Metabolic alterations in urine extracellular vesicles are associated to prostate cancer pathogenesis and progression. *J. Extracell. Vesicles* **2018**, *7*, 1470442. [CrossRef]
100. Zhao, H.; Yang, L.; Baddour, J.; Achreja, A.; Bernard, V.; Moss, T.; Marini, J.C.; Tudawe, T.; Seviour, E.G.; San Lucas, F.A.; et al. Tumor microenvironment derived exosomes pleiotropically modulate cancer cell metabolism. *eLife* **2016**, *5*, e10250. [CrossRef]
101. Wishart, D.S.; Feunang, Y.D.; Marcu, A.; Guo, A.C.; Liang, K.; Vázquez-Fresno, R.; Sajed, T.; Johnson, D.; Li, C.; Karu, N.; et al. HMDB 4.0: The human metabolome database for 2018. *Nucleic Acids Res.* **2018**, *46*, D608–D617. [CrossRef] [PubMed]

International Journal of
Molecular Sciences

MDPI

Review

Signaling of Tumor-Derived sEV Impacts Melanoma Progression

Aneta Zebrowska [1], Piotr Widlak [1], Theresa Whiteside [2,3] and Monika Pietrowska [1,*]

[1] Maria Sklodowska-Curie National Research Institute of Oncology, Gliwice Branch, 44-100 Gliwice, Poland; aneta7zebrowska@gmail.com (A.Z.); piotr.widlak@io.gliwice.pl (P.W.)
[2] UPMC Hillman Cancer Center, University of Pittsburgh, Pittsburgh, PA 15213, USA; whitesidetl@upmc.edu
[3] Department of Pathology, University of Pittsburgh School of Medicine Pittsburgh, Pittsburgh, PA 15261, USA
* Correspondence: monika.pietrowska@io.gliwice.pl; Tel.: +48-32-278-9627

Received: 30 June 2020; Accepted: 15 July 2020; Published: 17 July 2020

Abstract: Small extracellular vesicles (sEV or exosomes) are nanovesicles (30–150 nm) released both in vivo and in vitro by most cell types. Tumor cells produce sEV called TEX and disperse them throughout all body fluids. TEX contain a cargo of proteins, lipids, and RNA that is similar but not identical to that of the "parent" producer cell (i.e., the cargo of exosomes released by melanoma cells is similar but not identical to exosomes released by melanocytes), possibly due to selective endosomal packaging. TEX and their role in cancer biology have been intensively investigated largely due to the possibility that TEX might serve as key component of a "liquid tumor biopsy." TEX are also involved in the crosstalk between cancer and immune cells and play a key role in the suppression of anti-tumor immune responses, thus contributing to the tumor progression. Most of the available information about the TEX molecular composition and functions has been gained using sEV isolated from supernatants of cancer cell lines. However, newer data linking plasma levels of TEX with cancer progression have focused attention on TEX in the patients' peripheral circulation as potential biomarkers of cancer diagnosis, development, activity, and response to therapy. Here, we consider the molecular cargo and functions of TEX as potential biomarkers of one of the most fatal malignancies—melanoma. Studies of TEX in plasma of patients with melanoma offer the possibility of an in-depth understanding of the melanoma biology and response to immune therapies. This review features melanoma cell-derived exosomes (MTEX) with special emphasis on exosome-mediated signaling between melanoma cells and the host immune system.

Keywords: small extracellular vesicles (sEV); tumor-derived exosomes (TEX); melanoma cell-derived exosomes (MTEX); proteomics; tumor microenvironment; biomarkers

1. Introduction

Small extracellular vesicles (sEV), also known as exosomes (EX), are virus-size (30–150 nm) membrane-bound vesicles released by different cell types under both normal and pathological conditions. They represent a subset of the heterogeneous group of extracellular vesicles (EV) that in addition to sEV include larger (250–1000 nm) microvesicles (MV, ectosomes) and the largest (>1000 nm) apoptotic bodies (AB). EV vary in size, biogenesis, release mechanisms, and biochemical properties. sEV or exosomes are formed in the endosomal network as intraluminal vesicles (ILV) within the multivesicular bodies (MVB) and are released to the extracellular space when MVBs fuse with the cellular plasma membrane. In contrast, MV are produced by outward budding ("blebbing") of the plasma membrane, while apoptotic bodies are released when cells undergo the programmed cell death [1–7]. At present, inconsistency in the EV nomenclature exists causing much confusion in the field, which extends to the methodology for sEV isolation and characterization. Currently, the most

common vesicle isolation methods, including ultracentrifugation, do not adequately discriminate between various EV subsets. To ease confusion, a simplified nomenclature has been recently adopted in the literature that distinguishes small EV (i.e., <200 nm) and medium/large EV (>200 nm). The class of small EV consists mostly of exosomes, yet other types of EV, e.g., small MV, could also copurify with this fraction [8–11]. In this review, the terms "exosomes" (EX) and (small) extracellular vesicles (sEV) are used interchangeably for simplicity and to stay in line with the recent guidelines from International Society for Extracellular Vesicles (ISEV) [8].

Among various subsets of EV in body fluids of cancer patients, tumor-derived exosomes, called TEX, have attracted much attention as major mediators of intercellular communication in the tumor microenvironment (TME) and as potentially promising diagnostic, prognostic, and predictive biomarkers in cancer and other diseases. The knowledge of the molecular profiles and biology of TEX offers the possibility of a deeper understanding of pathological processes involved in cancer development and may provide important clinical information about disease activity and response to treatment. Today, TEX are considered as prime candidates for a liquid tumor biopsy, and much effort is being invested in validation of this concept. In this review, we summarize recent insights into the biology and composition of melanoma cell-derived exosomes (MTEX) and provide an up-to-date account of their pleiotropic role in melanoma progression and response to anti-melanoma therapies.

2. General Characteristics of sEV

sEV are produced and released by various cell types, including hematopoietic cells and a broad variety of normal or malignant tissue cells [5,7,12,13]. sEV can be isolated from supernatants of cultured cells or diverse body fluids, including blood, urine, saliva, breast milk, ascites effusions, bile, tears, nasal secretions, amniotic, synovial, cerebrospinal, lymphatic, and seminal fluids [5,7,10,14–23]. The molecular content of sEV is of special interest, as it reflects the nature of parental cells. sEV originating from different cell types share their general features, such as the structure of the bilayer lipid–protein membrane and key molecular components. Their molecular cargo consists of proteins (including cytoskeletal proteins, transmembrane proteins, tetraspanins, heat shock proteins, adhesion proteins, enzymes, immunocompetent proteins e.g., death receptor ligands: tumor necrosis factor ligand (FasL, CD95L or CD178) or TNF-related apoptosis-inducing ligand (TRAIL), check-point receptor ligands such as: programmed death-ligand 1 (PD-L1), inhibitory cytokines such as: interleukin 10 (IL-10), IL-6, TNF-α, IL-1β, and TGF-β1, prostaglandin E2, major histocompatibility molecules MHC-I and II, and tumor-associated antigens), nucleic acids (including DNA, RNA, miRNA, non-coding RNA), lipids, and low-molecular-weight metabolites (including alcohols, amides, amino acids, carboxylic acids, sugars). Proteomic analysis of exosome cargos revealed that some proteins are typical for most of these vesicles (including proteins such as Rab2, Rab7, flotillin, and annexin; cytoskeletal proteins, including actin, myosin, tubulin; or heat shock proteins, such as Hsc70 and Hsc90). Tetraspanins, such as CD9, CD63, CD81, CD83, along with housekeeping proteins, ALIX (programmed cell death 6-interacting protein) and TSG101 (tumor susceptibility gene 101 protein), are widely considered as exosome markers. However, in addition to the "common" set of components, sEV of different cellular origins may also carry proteins that are cell-type specific [8–12,24]. It has been shown in many studies that the molecular profile of TEX is distinct from that of sEV derived from non-malignant cells such as dendritic cells (DC), T cells, and others [6,7,11–13,25]. However, it should be noted that the discrimination of TEX from other types of sEV in patients' plasma using, e.g., tetraspanins as sEV-specific markers has been limited and currently, separation of TEX from total sEV in plasma has not been readily available or reliably performed.

sEV circulating in body fluids represent a complex mixture of vesicles released by many different cell types. The majority of studies of TEX present in body fluids of cancer patients are based on analyzes performed with a mixture of sEV derived from different normal or pathological cells. Separation of TEX from this mixture remains a challenge due to the lack of universal cancer-specific antigens that could be targeted for TEX isolation. Nevertheless, a few studies that used specific membrane markers

for isolation of TEX from body fluids have been reported. Chondroitin sulfate proteoglycan 4 (CSPG4) was used for separation of melanoma-derived TEX, referred to as MTEX, from vesicles released by non-malignant cells [26–28]. Glypican 1 (GPC1) was used to isolate TEX from plasma of patients with pancreatic cancer [29], and prostate-specific membrane antigen (PSMA) was used to isolate TEX from plasma of prostate cancer patients [30]. CD34 antigen, a unique marker of AML blasts, was used to isolate TEX from the plasma of patients with acute myeloid leukemia [31]. Moreover, MAGE3/6 antigen was used to identify TEX present in sera of patients with melanoma or head and neck squamous cell carcinoma (HNSCC) [25]. In contrast to plasma-derived sEV, TEX isolated from supernatants of cancer cell lines are putatively homogenous. These TEX derived from tumor cell lines are an excellent in vitro model for investigations of interactions of TEX with other cells. In fact, much of what is known about TEX signaling, uptake by responder cells, and reprogramming in TME is derived from in vitro and in vivo studies of TEX isolated from supernatants of tumor cell lines.

sEV have gained interest due to their essential role in "normal" intercellular signaling and communication, which impact the physiological balance and homeostasis as well as disease progression. [1,6,32–36]. Importantly, sEV can modulate the phenotype/functions of recipient cells, even those located in distant organs [2,3,35–38]. Moreover, the role of TEX in cancer progression has been reported for many cancer types, including ovarian, prostate, breast, lung, colorectal and gastric cancers, melanoma, and acute myeloid leukemia [26,37–44]. TEX are being intensively investigated because they play a key role in the reorganization of the TME, remodeling functions of the cells residing in the TME, and enhancing their contribution to tumorigenesis, metastasis, cancer immune escape, as well as resistance to cancer treatment [34,44–54]. The potential role of TEX in cancer biology is schematically illustrated in Figure 1. A better understanding of the mechanisms underlying TEX-mediated reprogramming of normal cells in TME is expected to be clinically significant, leading to improved cancer diagnosis/prognosis and treatment. In addition, TEX are considered to be an attractive source of cancer biomarkers.

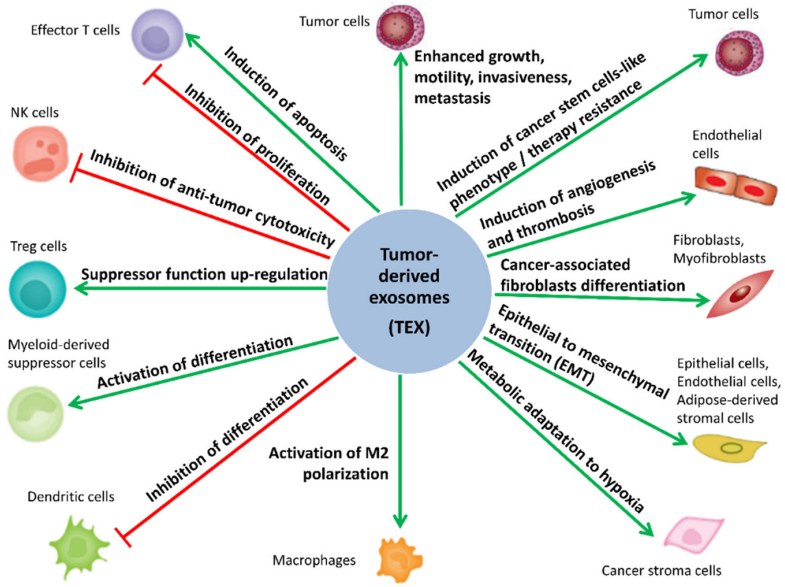

Figure 1. Role of tumor-derived small extracellular vesicles (sEV) (TEX) in cancer biology. Tumor-derived exosomes (TEX) are involved in intercellular signaling and communication between tumor cells and non-malignant cells residing in the tumor microenvironment. TEX reprogram these cells to acquire functions favoring tumor growth and metastasis. TEX-induced changes include enhancing cancer immune escape, remodeling of the tumor stroma, molecular and metabolic reprogramming, and promotion of angiogenesis. Green arrows indicate the processes stimulated by TEX. Red lines with blunt ends indicate processes inhibited by TEX.

3. General Features of Melanoma

Melanoma is the most aggressive skin cancer whose incidence has been increasing worldwide. Melanoma prognosis is generally poor, as it has a high potential for vascular invasion, metastasis, and recurrence [55–57]. Primary melanomas detected in an early stage and completely removed surgically show favorable outcome, with 5-year disease-specific survival rates of 99% [58]. However, melanoma cells tend to metastasize to distant sites, most often to lungs and brain, while evading the host immune system. Hence, the survival rate dramatically decreases when the cancer metastasizes, and 1-year survival rate drops to 35%–62% [57,59], while 5-year survival rate drops to 25% [58]. Currently, surgery is the treatment of choice for patients with cutaneous melanoma, and the adjuvant treatment scheme is usually tailored individually. Melanoma is sensitive to immune checkpoint inhibitors, such as anti-CTLA4 (anti-cytotoxic T-lymphocyte-associated protein 4 or anti-CD 152) and anti-PD1 (anti-programmed cell death protein 1 or anti-CD279) monoclonal antibodies (mAb), and to small-molecule targeted drugs, such as serine/threonine-protein kinase B-Raf (BRAF) or mitogen-activated protein kinase (MEK) inhibitors. Hence, different treatment schemes, including radiotherapy and/or adjuvant treatments with anti-BRAF/MEK inhibitors and anti-PD-1 mAb are currently used, depending on the patient's clinical situation [60]. Despite these novel combinatorial therapies, tumor escape from the immune control and development of primary or acquired therapy resistance that occurs in about half of melanoma patients remain the major therapeutic barrier [61–63]. Melanoma cells communicate with other cells present in the TME, including components of the immune system, via melanoma cell-derived exosomes (MTEX). Hence, in-depth knowledge of MTEX composition and function is expected to bring better understanding of the mechanisms determining the response of melanoma to treatments.

4. The Molecular Cargo of MTEX

4.1. The Proteome of MTEX

Recently, studies of proteomic profiles of cancer-derived sEV have been much intensified [64–67]. However, only limited data are available about the proteome of melanoma-derived TEX. A great part of the available literature focuses on in vitro studies with TEX isolated from supernatants of various melanoma cell lines [68–73]. Ex vivo studies performed with TEX isolated from the blood of melanoma patients are rare [74]. It is important to emphasize that only sEV derived from melanoma cell lines are "pure" MTEX, as those present in the plasma will be mixtures of sEV derived from many different cells. The available studies of MTEX have utilized different proteomic approaches. Most of them are based on shotgun LC-MS/MS strategies (i.e., tryptic digestion of proteins, followed by nano HPLC-MS/MS analysis of the resulting peptides), while others are based on LC-MS/MS analysis of proteins separated by 1D or 2D SDS-PAGE [75]. Currently available proteomic studies demonstrate differences in protein profiles of MTEX in comparison to melanocyte-derived sEV [68,69]. In addition, MTEX derived from melanoma cell lines with a different tumorigenic potential appeared to have distinct proteomic profiles [70]. Moreover, proteomic analysis of sEV present in the plasma of melanoma patients and healthy donors showed clear differences and revealed increased levels of TYRP2, VLA-4, and HSP70 in patients' samples [74]. However, the knowledge of the proteome in TEX produced by melanoma cells remains rather limited, and the available data are difficult to compare because they represent distinct experimental models. A summary of data on proteomics profiling of MTEX released by melanoma cell lines is presented in Table 1.

Table 1. Proteomics Profiling of Melanoma Cell-Derived Exosomes (MTEX) Released in Vitro by Melanoma Cell Lines.

Cell Line	Method of MTEX Purification and Characterization	MS Approach	Major Findings	Ref.
MeWo, SK-MEL-28 (human)	UC/TEM, WB, 1D/2D SDS-PAGE	MALDI-TOF MS/MS	A few proteins identified in MTEX for the first time: prostaglandin regulatory-like protein (PGRL), p120 catenin, syntaxin-binding proteins 1 and 2, septin 2 (Nedd5), ezrin, radixin, tryptophan/aspartic acid (WD) repeat-containing protein 1	[68]
A375 (human)	UC/TEM, NTA, WB	LC-MS/MS	Different sets of proteins present in MTEX and melanocyte-derived EV, including annexin A1, HAPLN1, GRP78, endoplasmin precursor (gp 96), TUBA1B, PYGB), ferritin, heavy polypeptide 1 (MTEX-upregulated), annexin A2, syntenin-1, MFGE8, OXCT (MTEX-downregulated)	[69]
MNT-1, G1, 501 mel, SKMEL28, Daju, A375M, 1205Lu (human)	UC+SEC/WB, TEM, NTA	nanoLC-MS/MS	Different sets of proteins present in MTEX from nontumorigenic, tumorigenic, and metastatic cell lines, including EGFR, PTK2/FAK1, EPHB2, SRC, LGALS1/LEG1, LGALS3/LEG3, NT5E/5NTD-CD73, NRAS, KIT, MCAM/MUC18, MET specific for metastatic cell lines	[70]
B16-F1 (murine)	UC+SEC/CEM, DLS, IA-FCM	uHPLC-MS	10 most abundant proteins: CD81, CD9, histones (H2A, H2B, H3.1, H4), heat shock proteins (HSPA5/GRP78, HSC71), syntetin-1	[71]
B16-F10 (murine)	UC+SEC, UF+SEC/TEM, NTA, WB	nanoLC-MS/MS	Different sets of proteins identified in low- and high-density MTEX, including ACTN4 and CCNY enriched in LD-MTEX and EPHA2 enriched in HD-MTEX	[72]
Mel501 (human)	UC+SEC/WB, CM	RPLC-MS/MS	Different sets of proteins identified in MTEX released in neutral and acidic environment (pH 6.7 and 6.0, respectively), including HRAS, NRAS, TIMP3, HSP90AB1, HSP90B1, HSPAIL, HSPA5, GANAB, gelsolin, and cofilin upregulated in acidic conditions.	[73]

Abbreviations: methods of EX purification: UC—ultracentrifugation, UF—ultrafiltration, SEC—size-exclusion chromatography; methods of EX characterization: NTA—nanoparticle tracking analysis, DLS—dynamic light scattering, TEM—transmission electron microscopy, CEM—cryo-electron microscopy, CM—confocal microscopy, WB—Western blotting.

4.2. Micro RNA Component of MTEX

Micro RNAs are small (19–25 nucleotides) non-coding RNAs that play an important role as regulators of cell differentiation, metabolism, proliferation, or innate and adaptive immunity [76–78]. Micro RNA profiles of TEX differ from miRNA profiles of their donor cancer cells as well as from profiles of sEV released by normal cells [78–81]. The majority of available works report miRNA signatures of pure MTEX released in vitro by melanoma cell lines [69,82–90]. Moreover, a few studies addressed miRNA composition of sEV derived from serum/plasma of melanoma patients [82,91–94]. Similar to proteomics data, few consistencies were observed among these studies due to different models applied. Nevertheless, there were 6 MTEX-upregulated miRNA species reported in more than one study: miR-494 [82,83], let-7c [69,84], miR-690 [84,85], miR-17 [84,91], and miR-494 [82,83], while miR-125b was reported to be downregulated in MTEX or sEV from plasma of melanoma patients [83,92]. Noteworthy, all the above mentioned miRs are known to be involved in cancer cell invasion, migration, and proliferation as well as in inflammatory processes linked to tumorigenesis and cancer progression [82–86,91,92].

Xiao et al. showed significant differences in miRNA content of exosomes isolated from normal melanocytes and malignant cell lines (HEMa-LP and A375), respectively [69]. In this study, 130 miRNAs were upregulated and 98 miRNAs downregulated in MTEX versus melanocyte-derived EX. The majority of differently expressed miRNAs were associated with tumor aggressiveness, including fifteen miRNAs

known to be associated with melanoma metastasis: miR-138, miR-125b, miR-130a, miR-34a, miR-196a, miR-199a-3p, miR-25, miR-27a, miR-200b, miR-23b, miR-146a, miR-613, miR-205, miR-149, let-7c [69]. Another study reported enrichment of miRNA-494, which is known for its high metastatic potential, in MTEX released by A375 cells. A series of functional experiments performed by Li et al. demonstrated that intercellular transport of miR-494 in MTEX was responsible for melanoma metastasis [82]. Blocking of exosomal transfer of miR-494 by a knockdown (KO) of Rab27a induced cellular apoptosis and inhibited tumor growth and metastasis in vitro and in human xenografts [82].

Another analysis of the miRs upregulated in sEV of patients with metastatic melanoma (miR-17-5p, miR-19a-3p, miR-149-5p, miR-21, and miR-126-3p) focused on discovery of putative targets of these miRNAs [91]. Among their targets were genes associated with skin response to UV irradiation, genes coding the tumor protein p53 (TP53)/retinoblastoma protein (RB1) and genes related to the TGF-β/SMAD pathway. Upregulation of miRNAs controlling TP53/RB1 activation and the TGF-β/SMAD signaling pathway might play an important role in melanoma progression, as the TGFβ/SMAD pathway regulates the G1/S checkpoint in normal melanocytes [91]. Moreover, miR-17 was identified as a potential oncomiR not only in melanoma but also in other malignancies [93,94]. Association of miR-19a upregulation with increased melanoma invasiveness was confirmed by Levy et al. [95]. Upregulation of miR-21 and miR-19a is associated with increased proliferation, low apoptosis, invasiveness, and high metastatic potential, as reported for various human tumor cells [96,97], while KO of miR-21 in B16 melanoma cells reduced their metastatic potential [98,99]. The oncogenic properties of miR-21 may be a result of down-regulation of the tumor suppressors: PTEN, PDCD4 and the antiproliferative protein BTG2. In addition, miR-21 induced the IFN pathway with protumorigenic effects [98,99]. High abundance of another oncomiR—miR-1246 was detected in MTEX isolated from patient-derived melanoma cell lines, namely, DMBC9, -10, -11, and -12 [83,100]. Many other studies have confirmed its high concentration in sEV from the plasma of patients with various cancers, including melanoma [101,102]. The overexpression of miR-222 in MTEX and cells is also associated with tumor initiation, differentiation, increased cell motility, and invasion, as well as cancer progression [87]. MiR-222 inhibits anti-neoplastic functions of p27, CDKN1B, and c-Fos by down-modulation of their gene expression, reduces apoptosis, and allows proliferation by induction of the PI3K/AKT pathway [89]. Müller et al. showed the importance of let-7a in melanoma development [103]. Let-7a regulates the expression of integrin β-3, the promotor of melanoma progression. The loss of let-7a expression in MTEX derived from 8 different melanoma cell lines resulted in higher integrin β-3 levels in melanoma cells, enhancing their migratory and invasive potential [103]. Finally, let-7a was detected in serum EX as a factor differentiating stage I melanoma patients from non-melanoma subjects [104]. Altogether, the literature supports the key role played by miRs transferred by melanoma-associated TEX in oncogenesis and melanoma metastasis.

In addition to microRNA, MTEX contain mRNA transcripts of genes expressed in melanoma. Sets of mRNAs with different abundance in MTEX and in melanosome-derived exosomes were identified, including 945 transcripts associated with cancer and 364 associated with dermatological diseases [69]. Among upregulated transcripts there was DNA topoisomerase I (TOP1), which is known to be associated with aggressive, advanced tumors and poor prognosis in melanoma [69,105]. Among downregulated transcripts there were ATP-binding cassette, sub-family B, member 5 (ABCB5), which activates the NF-κB pathway enhancing p65 protein stability [106] and is also known to be closely co-regulated with melanoma tumor antigen p97 (tumor growth regulator—melanotransferrin, MTf) [107], and TYRP1 encoding tyrosinase-related protein 1, which is considered as an inhibitor of TYRP1-dependent miR-16 mediating tumor suppression [108,109].

5. Biological Activity of MTEX

The multi-level contribution of MTEX to tumorigenesis accounts for activation of biological processes enabling cancer immune evasion, as well as molecular and metabolic remodeling of tumor micro- and macro-environment, favoring cancer growth and metastasis. The in-depth knowledge of the pleiotropic role of MTEX in the natural history of melanoma has a great potential clinical

application in the disease diagnosis, treatment design, and prognosis of patient's outcomes. MTEX are involved in a plethora of functions involved in initiation, progression, and metastasis of tumors, which is schematically depicted in Figure 2 (according to [26,37,73,74,83–150]). The most essential functions of MTEX are addressed more specifically in the following sub-chapters.

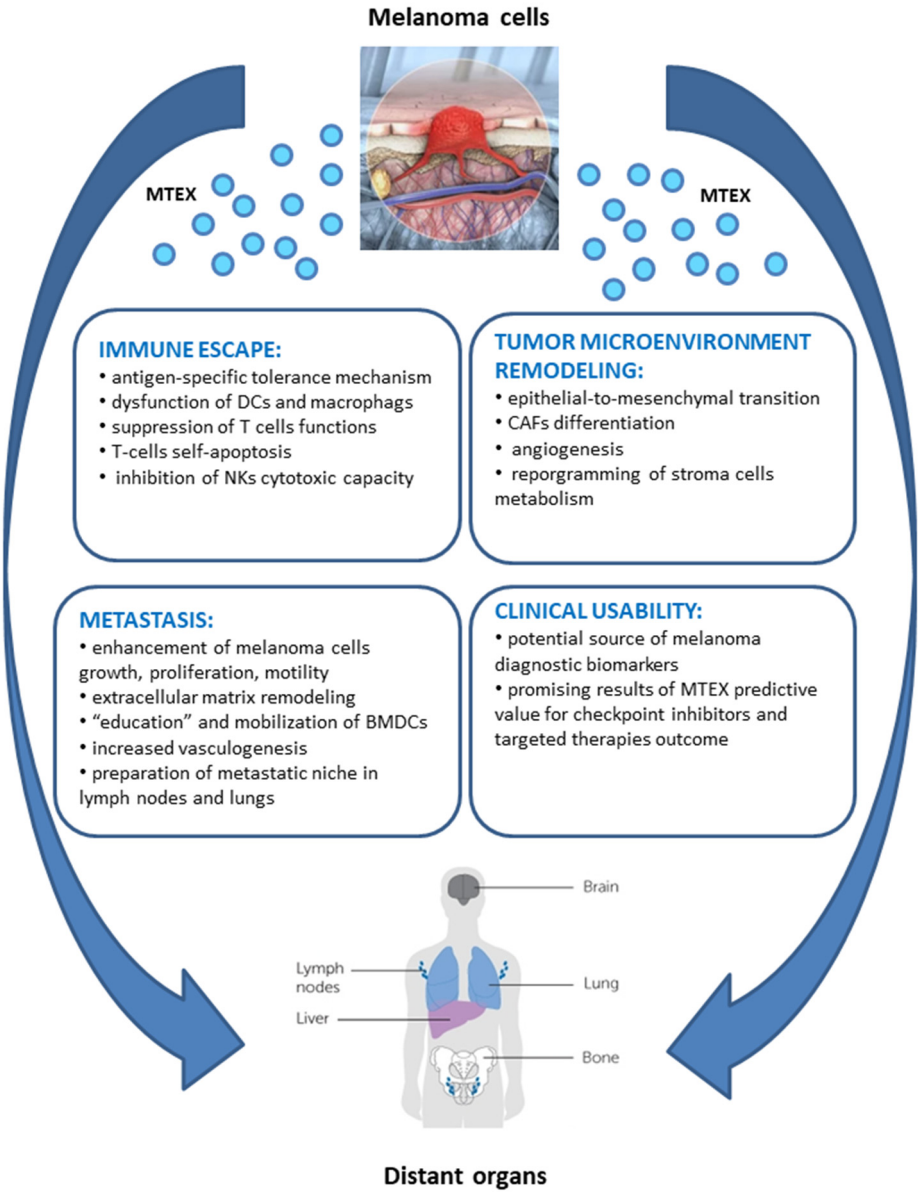

Figure 2. Pleiotropic effect of MTEX on melanoma biology.

5.1. MTEX Participate in the Reprogramming of Immune Cells

Growth and progression of cancer involve the escape from the immune surveillance as the sine qua non condition. Emerging evidence supports the idea that MTEX are involved in facilitating tumor escape from the host immune system [33,44,47,49,110–117]. However, in most of the studies reported in this context, melanoma cell lines were used as a source of MTEX. Düchler et al. showed that cancer-induced immunosuppression was mediated by MTEX, and involved an antigen-specific mechanism [118]. The authors provided evidence that MTEX transferred MHC class I receptor proteins from cancer cells to the surface of antigen-presenting cells (APC). At the same time, CD86 and CD40 (co-stimulatory molecules required for differentiation and proliferation of T cells) were down-regulated, while the production of immunosuppressive cytokine IL-6 was induced. Collaboration of TGF-β transported by

MTEX was also demonstrated in this process. The authors hypothesized that MTEX-mediated transfer of the combination of TAA-derived peptide-MHC complexes with immunosuppressive cytokines was a part of antigen-specific tolerance induction enabling melanoma immune escape [118]. The mechanism of melanoma immune escape is also related to the suppression of T cell functions. This can be attributed to an increased level of PD-L1 in MTEX. This immunosuppression is driven by the interaction between PD-L1 carried by MTEX and PD-1 receptors on $CD8^+$ T cells, leading to inhibition of T-cell functions [111,119]. MTEX are also enriched in Fas ligand (FasL) and APO2 ligand (APO2L)/TRAIL, both known as inducing factors of T cell-apoptosis [120]. Another possible mechanism for the suppression of T cell function by MTEX is through the upregulation of PTPN11 protein, which was found to negatively regulate interferon, IL-2, and T cell receptor signaling pathways [121]. Wu et al. confirmed that B16F0-derived MTEX are enriched with Ptpn11 mRNA and can increase PTPN11 dose-dependently in recipient cells. In addition to upregulating PTPN11 in lymphocytes, MTEX derived from B16F0 locally suppressed responses of cells to IL-12 (anti-tumor immunity enhancer) via inhibition of IL12RB2 expression in primary $CD8^+$ T cells. These inhibitory mechanisms of the immune cell response to IL-12 are complemented by B16F0 release of the Wnt-inducible signaling protein 1 (WISP1) that blocks T cell response to IL-12 [121,122]. Furthermore, the cargo of MTEX might alter mitochondrial respiration of cytotoxic T cells and up-regulate genes associated with the Notch signaling pathway [84]. Immunosuppressive activity of MTEX depends on their ligands that engage the T cell receptor (TCR) and IL-2 receptor (IL-2R). Recent studies showed that MTEX inhibited signaling and proliferation of activated primary $CD8^+$ T cells, inducing their apoptosis [25,32,90]. Furthermore, MTEX significantly promoted conversion of CD4(+) T cells to CD4(+)CD25(+)FOXP3(+) T regulatory cells (Treg) enhancing their suppressor functions [25]. Vignard et al. additionally confirmed decreased TCR signaling in T cells as a result of the enrichment in miRNAs regulating TCR signaling and TNF-α secretion (miR-3187-3p, miR-498, miR-122, miR149, miR-181a/b) in MTEX [90].

Accumulating evidence reveals that TNF is negatively regulated by miR-21. This may explain the effects of miR-21 on cell proliferation, migration, invasion, and transformation associated with excessive miR-21 levels in MTEX. Moreover, some results suggest that TNF can promote miR-21 biogenesis [123] as well as the turnover of PDCD4 in macrophages [124]. Yang et al. also showed that increased levels of miR-21 associated with a decreased level of TNF were consistent with elevated IL-10 protein expression and increased Arg1 macrophage expression, which could explain poor immune responses against cancer cells [98]. On the other hand, Fabri et al. reported that miR-21 which was found to be enriched in MTEX might also act as a ligand by binding to receptors of the Toll-like receptor (TLR) family members, murine TLR7, and human TLR8, in immune cells. Triggering the TLR-mediated prometastatic inflammatory response in responder cells might promote tumor growth and metastasis [125].

Stimulation of $TLR2^+$ DC by tumor-derived TLR2 ligands was reported to drive inhibitory signals leading to dysfunctional activity of DC in murine melanoma [126]. Modulation of immune response by MTEX was confirmed by Zhou et al. [85]. They observed that B16-derived MTEX induced apoptosis of $CD4^+$ T cells in vitro and promoted the growth of tumor cells implanted in mice. The opposite results were reported by blocking MTEX release (disrupting the expression of Rab27a), thus confirming the proposed mechanism. Further, they showed that B16-derived MTEX induced activation of caspase-3, caspase-7, and caspase-9, reducing the level of anti-apoptotic proteins, such as BCL-2, BCL-xL, and MCL-1 in $CD4^+$ T cells [85]. MTEX can also alter the functions of natural killer (NK) cells. They were found to modulate the tumor immune responses by inhibiting the cytotoxic activity of NKs and downregulating the expression of NKG2D, NKp30, NKP46, and NKG2C proteins on the surface of NK cells [26,42,127].

5.2. MTEX Participate in the Reprogramming of TME

TME plays a major role in cancer growth and evolution. Diverse cells such as fibroblasts, endothelial, epithelial, and mesenchymal cells or immune cells present in the TME might

be reprogrammed by MTEX to favor tumor growth [45,56]. Accumulating data provide evidence that MTEX promote epithelial-to-mesenchymal transition (EMT), which promotes metastasis [46,48,55,57,128]. The mitogen-activated protein kinase (MAPK) signaling pathway is activated during the MTEX-mediated EMT, with the involvement of Let-7i, a miRNA modulator of EMT [104]. Furthermore, acquisition of the EMT-like phenotype is enforced by expression of other key regulators of EMT induction, including ZEB2 and Snail 2 [119,129]. Upregulation of ZEB2 and Snail 2 in primary melanocytes after co-culture with MTEX was confirmed by Xiao et al. This process was accompanied by decreased expression of E-cadherin and increased expression of vimentin [104]. The interplay between MTEX and myeloid stem cells (MSCs) induce the emergence of a tumor-like phenotype with PD-1 and mTOR overexpression in naïve MSCs in vitro and fast tumor progression in vivo [119]. Interaction networks build basing on genes overexpressed in recipient cells upon co-incubation with MTEX identified a variety of other exosomal molecules, apart from PD-1 and mTOR, which might affect tumor progressions, such as MET, Ras, RAF1, Mek, ERK1/2, MITF, BCL2, PI3K, Akt, KIT, JAK STAT3, or ETS1 [119].

MTEX transform fibroblasts into proangiogenic cancer-associated fibroblasts (CAF) in vitro and in vivo. CAF are known to support development of pre-cancerous micro- and macro-environments [86,130,131]. Zhao et al. discovered that incubation of MTEX with fibroblasts resulted in a significant increase of VCAM-1 expression, and this enhancement was even stronger when EX were derived from highly metastatic melanoma cells [131]. Overexpression of miR-155 in MTEX was found to be the trigger factor for the proangiogenic switch of fibroblasts into CAF [86]. MTEX-mediated delivery of miR-155 to fibroblasts suppressed expression of cytokine signaling 1 (SOCS1), that activates the JAK2/STAT3 signaling pathway which, in turn, regulates the expression of proangiogenic factors. Elevated expression of vascular endothelial growth factor A (VEGFa), fibroblast growth factor 2 (FGF2), and matrix metalloproteinase 9 (MMP9) in fibroblasts after incubation with MTEX was confirmed in this study [86]. Shu et al. also reported the presence of exosomal miR-155 and miR-210 across six melanoma cell lines [89] and showed that miRNA cargo of MTEX was capable of reprogramming the metabolism of human adult dermal fibroblasts (HADF). In this study, miR-155 upregulated glucose metabolism (i.e., increased glycolysis), while miR-210 decreased oxidative phosphorylation under non-hypoxic conditions. Exposure of HADF to MTEX resulted in upregulated aerobic glycolysis and downregulated oxidative phosphorylation in stromal fibroblasts, with consequently increasing extracellular acidification [89]. Furthermore, the acidic environment led to upregulation of over 50% of exosomal proteins involved in cancer progression in MTEX derived from the primary non-tumorigenic MEL501 cell line [73]. The upregulated proteins were associated with focal adhesion, actin cytoskeleton regulation, leukocyte trans-endothelial migration, regulation and modification of cell morphology, HSP family proteins, proteoglycans related to cancer, small GTPase mediated signal transduction, and epidermal growth factor receptor (EGFR) signaling pathways [73]. This shows that MTEX are important contributors to changes in the TME that are responsible for creating favorable conditions for the pre-metastatic niche. On the one hand accelerated aerobic glycolysis ensures more effective energy production, but on the other hand, the acidic microenvironment drives immune suppression and creates a pro-metastatic environment [73,89,132].

The pro-angiogenic effects of MTEX are well-documented. MTEX cargos are enriched in pro-angiogenic cytokines, including IL-1α, FGF, GCS-F, TNFα, leptin, TGFα, and VEGF [107]. MTEX also mediate the transfer of miR-9 from melanoma to endothelial cells (EC), which triggers the JAK-STAT pathway and enhances the migratory propensity of vascular cells as well as the formation of a tumor-supporting vascular net [133]. Additionally, it was reported that increased WNT5A signaling, which is known to promote melanoma metastasis, induced a Ca^{2+}-dependent release of exosomes containing the pro-angiogenic VEGF and MMP2 factors in melanoma cells [134].

5.3. MTEX Can Modulate Tumor Progression and Invasiveness

In general, TEX may induce tumor growth in vitro and in vivo [135,136]. It was reported that B16BL6-derived MTEX induced proliferation and inhibited apoptosis of murine melanoma B16BL6 cells, while inhibition of MTEX release by the N-Smase inhibitor suppressed melanoma growth. Noteworthy, the uptake of MTEX resulted in increased levels of cyclin D1, p-Akt (cell proliferation-related proteins), Bcl-2 (survival-related protein), and decreased level of Bax (apoptosis-related proteins) [137]. Peinado et al. reported that the oncoprotein MET selectively enriched in MTEX released by metastatic melanoma cells promoted the tumorigenic potential of melanoma [74]. Pre-conditioning of bone marrow (BM) with MTEX obtained from a highly metastatic melanoma B16-F10 cell line promoted mobilization of bone marrow-derived cells (BMDC), increasing tumor vasculogenesis, invasion, and metastasis. Comparative analysis of the protein content in MTEX from highly metastatic and poorly metastatic melanoma cells confirmed MET signaling as the principal mediator of BM progenitor cell "education". Pre-treatment of BM cells with B16-F10 MTEX resulted in HGF-induced S6 and ERK phosphorylation compared to non-treated controls. Effectors of MET-mediated BM progenitor cell mobilization, i.e., S6-kinase (mTOR pathway) and ERK (MAPK pathway), are known mediators of HGF/MET signaling. Further, the metastatic spread and organotropism of highly metastatic B16-F10 primary tumors were reduced by the BM of mice "educated" with the low-metastatic B16-F1 MTEX that lacked the MET receptor. These data suggested that non-metastatic MTEX might educate the BM and prevent metastatic disease, a finding that is worth further exploration. Finally, it was confirmed that MET expression was elevated in sEV circulating in the plasma of patients with metastatic melanoma [74]. Additionally, influence of metabotropic glutamate receptor 1 (GRM1) expressed on melanoma cells was tested for cell migration and invasiveness [138]. This neuronal receptor induces in vitro melanocytic transformation and spontaneous malignant melanoma development in vivo. Moreover, modulation (decrease) of GRM1 expression results in a decrease in both cell proliferation in vitro and tumor progression in vivo. Isola et al. verified a hypothesis that exosomes released by a GRM1-positive (metastatic) cell line made GRM1-negative (non-metastatic) cells acquire features characteristic for GRM1-positive cells, i.e., to migrate, invade, form colonies, and exhibit anchorage-independent cell growth. They found that acquiring these features was not connected with expression of this receptor on GRM1-negative cells. Another aspect of the potential role of MTEX in tumorigenesis is analysis of specific RAB genes involved in sEV secretion (RAB1A, RAB5B, RAB7, RAB27A) [74]. Rab27a is a regulator of protein trafficking and melanoma proliferation [139]. Reduced expression of Rab27a resulted in decreased sEV production, and in decreased release of pro-angiogenic factors (PlGF-2, osteopontin, and PDGF-AA) from tumor cells, interfering with BMDC mobilization and tumor invasiveness [74]. These results are in line with the latest findings of Guo and colleagues [140], who reported that the GTPase RAB27A was overexpressed in melanoma patients and correlated with poor patient survival. A loss of RAB27A expression in melanoma cell lines blocked invasion and cell motility in vitro, and spontaneous metastasis in vivo. Furthermore, RAB27A-expressing MTEX promoted the invasion phenotype of melanoma cells in contrast to MTEX without RAB27A [140]. All in all, these results suggest that RAB27A promotes the biogenesis of a distinct pro-invasive MTEX subpopulation [74,140].

MTEX are also involved in preparation of metastatic niche for melanoma in lymph nodes and lungs and in reprogramming of innate osteotropism of melanoma cells [74,141,142]. MTEX from a highly-metastatic B16-F10 cell line promoted lymph nodes (LN) metastasis in mice [142] and were detected after 24h in the interstitium of the lung, BM, liver, and spleen (organotropic sites for B16-F10 metastasis), but not in the circulatory system [74]. Several genes responsible for the recruitment of melanoma cells (stabilin 1, ephrin receptor β4, and αv integrin), extracellular matrix remodeling (Mapk14, uPA, laminin 5, Col 18α1, G-α13, p38), vascular growth (TNF-α, TNF-αip2, VEGF-B, HIF-1α, Thbs1) [142], and effectors of pre-metastatic niche formation such as S100A8, S100A9 [74] were upregulated by B16-F10 MTEX. The osteotropism of melanoma cells is related to the activation of the SDF-1/CXCR4/CXCR7 axis. MTEX were found to promote osteotropism of not-osteotropic melanoma

cells (SK-Mel28, WM266) in vitro through membrane CXCR7 up-regulation. Thus, MTEX were found to contribute to bone metastasis in melanoma [141].

6. MTEX as Potential Clinical Biomarkers

MTEX present in body fluids of melanoma patients are a promising source of prognostic biomarkers as a new type of so-called liquid biopsy. Alegre et al. performed an analysis of the established melanoma biomarkers such as: MIA, S100B, and tyrosinase-related protein 2 (TYRP2) in sEV isolated from sera of stage IV melanoma patients, patients with no evidence of disease (NED), and healthy donors (HD) [37]. The levels of MIA and S100B were significantly higher in melanoma patients in comparison to HD and NED patients. Furthermore, patients with high EV concentration of MIA had shorter median survival compared to those with lower MIA levels (4 versus 11 months; $p < 0.05$). Hence, the data suggest the potential diagnostic and prognostic utility of MIA in plasma sEV [37]. Levels of MIA, along with growth/differentiation factor 15 precursor protein (GDF15) showed a significant increase in the whole secretome of uveal melanoma versus non-malignant cells [143], which was in line with the results of Alegre et al. [37]. Tenga et al. showed that miR-532-5p and miR-106b present in serum sEV could be used for classification of melanoma patients, including differentiation of patients with metastatic and non-metastatic disease and stage I-II patients from stage III-IV patients [144]. In addition, miR-17, miR-19a, miR-21, miR-126, and miR-149 were found to be expressed at significantly higher levels in patients with metastatic sporadic melanoma compared to familial melanoma patients or healthy controls [91]. On the other hand, levels of miR-125b in sEV were significantly lower in patients with advanced melanoma compared with disease-free patients with melanoma and healthy controls, while there was no statistical difference in the miR-125b levels between patients and controls when analyzing serum samples [92].

Melanoma is sensitive to immune checkpoint inhibitors (such as anti-CTLA4 and anti-PD1 monoclonal antibodies) and small-molecule targeted drugs (such as BRAF inhibitors and MEK inhibitors). However, many patients with melanoma fail to respond to these therapies, and the mechanisms of resistance to a therapy are not understood [61–63,145,146]. The accumulating data suggest the importance of MTEX in understanding these mechanisms and the role of MTEX as predictive biomarkers of response to immune therapies and outcome [55–57,147]. Higher levels of miR-497-5p in circulating sEV during MAPKi-based therapy of cutaneous metastatic melanoma patients (with BRAFV600 mutations) were significantly correlated with progression-free survival (hazard ratio of 0.27) [147]. Increased level of miR-497-5p was also associated with prolonged post-recurrence survival in resected metastases from patients with metastatic III (lymph nodes) and metastatic IV cutaneous malignant melanoma (CMM) [148]. Treatment with vemurafenib and dabrafenib induced miR-211-5p up-regulation in melanoma-derived EV, both in vitro and in vivo, thus promoting survival in parent melanoma cells despite a down-regulation of pERK1/2 by BRAF inhibitors [146]. What is more, transfection of miR-211 in low-expressing miR-211–5p melanoma cells resulted in enhanced proliferation of melanoma cells. What is more, 100-fold increase in miR-211–5p expression in vemurafenib-treated miR-211-5p-transfected cells was found with no reduction of cells proliferation upon BRAF inhibitor treatment. These findings suggest that miR-211-5p up-regulation upon vemurafenib treatment allows these cells to survive and grow into a population of cells that have reduced sensitivity to vemurafenib. Going further, inhibition of miR-211-5p in a vemurafenib resistant cell line decreased cell proliferation. The outcome of the study of Lunavat et al. leads to better understanding of possible mechanisms of acquiring by patients' resistance to the BRAF inhibitors treatment by showing that miR-211-5p can reduce the sensitivity to vemurafenib treatment in melanoma cells by regulating cellular proliferation. [146]. Another group of "new drugs" used in the treatment of melanoma are immune checkpoint inhibitors. Anti-PD-1 antibodies are frequently used in melanoma treatment to rejuvenate anti-tumor immunity, and in the majority of patients the response is durable, yet not all melanoma patients respond to this therapy [60,149]. Chen et al. reported positive correlation between exosomal-PD-L1 (Exo-PD-L1) level and IFN-γ, both in vitro using melanoma cell lines and

in vivo in patients with metastatic melanoma [111]. Upregulation of PD-L1 by IFN-γ in metastatic melanoma leads to functional suppression of CD8+ T effector cells enabling melanoma growth and metastasis. In part, this explains low response rate to anti-PD-1 therapy (pembrolizumab). The level of circulating Exo-PD-L1 distinguished clinical responders from non-responders to pembrolizumab treatment. Since the level of exosomal PD-L1 was altered early during the anti-PD-1 therapy, the authors suggest that it might be an indicator of response to treatment [111]. A recent paper by Cordonnier et al. describes monitoring of circulating Exo-PD-L1 in melanoma patients treated with immune checkpoint inhibitors and BRAF/MEK inhibitors. This prospective clinical study confirmed a significantly higher level of Exo-PD-L1 in plasma of melanoma patients compared to soluble PD-L1 and demonstrated that the level of Exo-PD-L1 inversely correlated with patients' response to therapy [150]. The results of this clinical study provide a rationale for monitoring Exo-PD-L1 level as a potential predictor of the melanoma patients' response to treatment and outcome [150].

Clinical relevance of MTEX-based biomarkers is currently limited by the necessity of separation of MTEX from other fractions of sEV circulating in body fluids. Recently, however, the anti-CSPG4 mAb was used for the separation of MTEX and sEV produced by normal tissue from the plasma of melanoma patients [26–28]. $CSPG4^+$ MTEX captured from the plasma of melanoma patients are highly enriched in melanoma-associated antigens (MAA) in comparison to CSPG4(-) non-MTEX, including CSPG4, TYRP2, MelanA, Gp100, VLA4. Moreover, several immunostimulatory (CD40, CD40L, CD80, OX40, OX40L) and immunosuppressive (PDL-1, CD39, CD73, FasL, LAP-TGFβ, TRAIL, CTLA-4) proteins were enriched in MTEX compared to sEV purified from plasma of healthy donors [26,28]. Noteworthy, looking at individual differences among proteins in the cargo of MTEX and non-MTEX, significant correlations with disease activity were observed for both fractions of vesicles. For example, non-MTEX ability to induce apoptosis of T cells positively correlated with the disease stage [28]. The obtained data suggest that features of both MTEX and non-MTEX, as well as individual MTEX/total sEV ratios, might be useful for monitoring melanoma progression [26,28]. In addition to CSPG4, other melanoma-specific or enhanced proteins might also be considered as potential markers of MTEX. This includes several melanoma-associated antigens (MAA-4, MAA-B2, and melanoma antigen recognized by T-cells) found in MTEX released by 7 different melanoma cell lines with various phenotypic features (non-tumorigenic, tumorigenic, metastatic) [70]. Moreover, several other cancer-related proteins (NRAS, Src, c-Met, c-Kit, EGFR, MCAM, annexin A1, HAPLN1, LGALS1, GALS3, NT5E, and PMEL) were detected in MTEX originating from various melanoma cell lines [69,70]. Therefore, several candidates for MTEX-markers are known that could be used for the immune capture of MTEX circulating in the body fluids of melanoma patients. Hence, the emerging concept of MTEX-based biomarkers of melanoma will meet the necessary methodological support in the nearest future.

7. Future Directions

Although the number of publications reporting on sEV in melanoma is growing exponentially, the resulting knowledge remains limited. Most likely, this is due to several factors that impede research of sEV. First, no uniformly accepted nomenclature for EV has been established, creating havoc in the definition of investigated EV. Further, no standardized procedures for the isolation of different EV types exist, leading to differences in contamination levels and co-isolation of various vesicles. The criteria and methods of EV characterization are also not clear and seem to change as we progress in the understanding of the EV heterogeneity. Despite the recommendations updated yearly by the International Society of Extracellular Vesicles (ISEV), published papers often provide incomplete data creating further confusion. The emerging view of the complex biology of EV requires strict criteria for the definition of phenotypes, genotypes, and functions of participating EV. Specifically, in a large body of available data on melanoma-associated sEV in body fluids, their origin is often unclear. Until recently, melanoma cell lines had been the only reliable source of MTEX. However, research performed with vesicles produced by cell lines does not adequately reflect interactions taking place in body fluids or tissues. Separation of MTEX from plasma by immune capture allowed for a more relevant evaluation

of their characteristics and functions in disease and comparisons of data between individual patients. While this represents considerable progress, ex vivo analysis of MTEX also provides only a limited view of their biological agenda in the TME and the periphery. In vivo studies of MTEX in murine models of melanoma are critical for the translation of signaling mediated by MTEX in vitro to cells, tissues, and organs in animals. Correlative studies of MTEX and clinical endpoints in melanoma progression, resistance, or response to therapies are growing in numbers and the concept of MTEX as a liquid tumor biopsy is slowly crystallizing. Understanding of multicellular MTEX-mediated signaling and their reprogramming activities in the TME opens a way for the use of MTEX-induced changes as yet another biomarker of disease activity. The next step is to develop and implement reliable means for the isolation and molecular characterization of MTEX from body fluids and tissues of patients with melanoma. At present, these methods are in the discovery stage, and the emerging results are promising not only due to successful subsetting of sEV into MTEX and non-MTEX, but also because of evidence that mechanistic and functional studies of MTEX can yield new and previously unsuspected information. For example, the ability of MTEX to simultaneously deliver to recipient cells multiple and often contradictory, i.e., suppressive vs. stimulatory signals have alerted us to the possibility of regulatory functions MTEX might exercise in vivo. Similarly, the realization that MTEX utilize surface proteins as well as miRs to transmit signals to recipient cells alerts us to ask why these two signaling pathways co-exist and how they impact the biology. As melanoma biomarkers, MTEX might provide a more reliable diagnostic, prognostic, or outcome data than total sEV isolated from body fluids. Future validation studies encompassing all aspects of MTEX isolation, characterization, and signaling will be necessary to move the field forward and translate current knowledge to clinically applicable strategies and methods. In this respect, antibody-based microarrays, multiparameter quantitative flow cytometry, and targeted proteomics are emerging as the tools applicable to serial monitoring of MTEX in body fluids of patients with melanoma. The future will likely see numerous such studies performed as part of clinical trials designed to validate the roles of MTEX in the biology of melanoma.

Author Contributions: All authors have read and agree to the published version of the manuscript. A.Z.—conception and drafting the article; P.W. and T.W.—critical revision of the article; M.P.—design and revision of the manuscript, funding and final approval of the version to be published.

Funding: This study was funded by the National Science Centre, Poland, Grant 2016/22/M/NZ5/00667 (to A.Z., M.P. and T.W.).

Conflicts of Interest: The authors declare no conflict of interest. The funders had no role in the design of the study; in the collection, analyses, or interpretation of data; in the writing of the manuscript, or in the decision to publish the results.

Abbreviations

AB	apoptotic bodies
APC	antigen presenting cells
BM	bone marrow
BMDC	bone marrow derived cells
CAF	cancer-associated fibroblasts
CEM	cryo-electron microscopy
CM	confocal microscopy
DC	differential centrifugation
DC	dendritic cells
DLS	dynamic light scattering
EC	endothelial cells
EMT	epithelial-to-mesenchymal transition
EV	extracellular vesicles
EX	exosomes
HADF	human adult dermal fibroblasts

IA-FCM	immune-affinity flow cytometry
KO	knockdown
MAA	melanoma associated antigens
mAb	monoclonal antibodies
MSC	myeloid stem cells
MTEX	melanoma cell-derived exosomes
MV	microvesicles
MVB	multivesicular bodies
NTA	nanoparticle tracking analysis
SEC	size-exclusion chromatography
SEM	scanning electron microscopy
sEV	small extracellular vesicles
TEM	transmission electron microscopy
TEX	tumor-derived exosomes
TME	tumor microenvironment
UC	ultracentrifugation
UF	ultrafiltration
WB	western blotting

References

1. Kalluri, R.; LeBleu, V.S. The biology, function, and biomedical applications of exosomes. *Science* **2020**, *367*, eaau6977. [CrossRef] [PubMed]
2. Willms, E.; Cabañas, C.; Mäger, I.; Wood, M.J.A.; Vader, P. Extracellular Vesicle Heterogeneity: Subpopulations, Isolation Techniques, and Diverse Functions in Cancer Progression. *Front. Immunol.* **2018**, *9*, 738. [CrossRef] [PubMed]
3. van Niel, G.; D'Angelo, G.; Raposo, G. Shedding light on the cell biology of extracellular vesicles. *Nat. Rev. Mol. Cell Biol.* **2018**, *19*, 213–228. [CrossRef]
4. Zaborowski, M.P.; Balaj, L.; Breakefield, X.O.; Lai, C.P. Extracellular Vesicles: Composition, Biological Relevance, and Methods of Study. *Bioscience* **2015**, *65*, 783–797. [CrossRef] [PubMed]
5. Yáñez-Mó, M.; Siljander, P.R.; Andreu, Z.; Zavec, A.B.; Borràs, F.E.; Buzas, E.I.; Buzas, K.; Casal, E.; Cappello, F.; Carvalho, J.; et al. Biological properties of extracellular vesicles and their physiological functions. *J. Extracell. Vesicles* **2015**, *4*, 27066. [CrossRef]
6. Minciacchi, V.R.; Freeman, M.R.; Di Vizio, D. Extracellular Vesicles in Cancer: Exosomes, Microvesicles and the Emerging Role of Large Oncosomes. *Semin. Cell Dev. Biol.* **2015**, *40*, 41–51. [CrossRef]
7. György, B.; Szabó, T.G.; Pásztói, M.; Pál, Z.; Misják, P.; Aradi, B.; László, V.; Pállinger, E.; Pap, E.; Kittel, A.; et al. Membrane vesicles, current state-of-the-art: Emerging role of extracellular vesicles. *Cell. Mol. Life Sci.* **2011**, *68*, 2667–2688. [CrossRef]
8. Théry, C.; Witwer, K.W.; Aikawa, E.; Alcaraz, M.J.; Anderson, J.D.; Andriansitohaina, R.; Antoniou, A.; Arab, T.; Archer, F.; Atkin-Smith, G.K.; et al. Minimal information for studies of extracellular vesicles 2018 (MISEV2018): A position statement of the International Society for Extracellular Vesicles and update of the MISEV2014 guidelines. *J. Extracell. Vesicles* **2019**, *8*, 1535750. [CrossRef]
9. Kowal, J.; Arras, G.; Colombo, M.; Jouve, M.; Morath, P.J.; Primdal-Bengtson, B.; Dingli, F.; Leow, D.; Tkach, M.; Théry, C. Proteomic comparison defines novel markers to characterize heterogeneous populations of extracellular vesicle subtypes. *Proc. Natl. Acad. Sci. USA* **2016**, *113*, 968–977. [CrossRef]
10. Abramowicz, A.; Widlak, P.; Pietrowska, M. Proteomic analysis of exosomal cargo: The challenge of high purity vesicle isolation. *Mol. Biosyst.* **2016**, *12*, 1407–1419. [CrossRef]
11. Gurunathan, S.; Kang, M.H.; Jeyaraj, M.; Qasim, M.; Kim, J.H. Review of the Isolation, Characterization, Biological Function, and Multifarious Therapeutic Approaches of Exosomes. *Cells* **2019**, *8*, 307. [CrossRef]
12. Zebrowska, A.; Skowronek, A.; Wojakowska, A.; Widlak, P.; Pietrowska, M. Metabolome of Exosomes: Focus on Vesicles Released by Cancer Cells and Present in Human Body Fluids. *Int. J. Mol. Sci.* **2019**, *20*, 3461. [CrossRef] [PubMed]
13. Théry, C.; Ostrowski, M.; Segura, E. Membrane vesicles as conveyors of immune responses. *Nat. Rev. Immunol.* **2009**, *9*, 581–593. [CrossRef]

14. Dixon, C.L.; Sheller-Miller, S.; Saade, G.R.; Fortunato, S.J.; Lai, A.; Palma, C.; Guanzon, D.; Salomon, C.; Menon, R. Amniotic Fluid Exosome Proteomic Profile Exhibits Unique Pathways of Term and Preterm Labor. *Endocrinology* **2018**, *159*, 2229–2240. [CrossRef]
15. Yu, J.; Lin, Y.; Xiong, X.; Li, K.; Yao, Z.; Dong, H.; Jiang, Z.; Yu, D.; Yeung, S.J.; Zhang, H. Detection of Exosomal PD-L1 RNA in Saliva of Patients With Periodontitis. *Front. Genet.* **2019**, *10*, 202. [CrossRef]
16. Grigor'eva, A.E.; Tamkovich, S.N.; Eremina, A.V.; Tupikin, A.E.; Kabilov, M.R.; Chernykh, V.V.; Vlassov, V.V.; Laktionov, P.P.; Ryabchikova, E.I. Exosomes in tears of healthy individuals: Isolation, identification, and characterization. *Biochem. Moscow Suppl. Ser. B* **2016**, *10*, 165. [CrossRef]
17. Wu, G.; Yang, G.; Zhang, R. Altered microRNA Expression Profiles of Extracellular Vesicles in Nasal Mucus From Patients With Allergic Rhinitis. *Allergy Asthma Immunol. Res.* **2015**, *7*, 449–457. [CrossRef]
18. Saunderson, S.C.; Dunn, A.C.; Crocker, P.R.; McLellan, A.D. CD169 mediates the capture of exosomes in spleen and lymph node. *Blood* **2014**, *123*, 208–216. [CrossRef] [PubMed]
19. Chiasserini, D.; van Weering, J.R.; Piersma, S.R.; Pham, T.V.; Malekzadeh, A.; Teunissen, C.E.; de Wit, H.; Jiménez, C.R. Proteomic analysis of cerebrospinal fluid extracellular vesicles: A comprehensive dataset. *J. Proteom.* **2014**, *106*, 191–204. [CrossRef]
20. Romancino, D.P.; Paterniti, G.; Campos, Y.; De Luca, A.; Di Felice, V.; d'Azzo, A.; Bongiovanni, A. Identification and characterization of the nano-sized vesicles released by muscle cells. *FEBS Lett.* **2013**, *587*, 1379–1384. [CrossRef]
21. Masyuk, A.I.; Huang, B.Q.; Ward, C.J.; Gradilone, S.A.; Banales, J.M.; Masyuk, T.V.; Radtke, B.; Splinter, P.L.; LaRusso, N.F. Biliary exosomes influence cholangiocyte regulatory mechanisms and proliferation through interaction with primary cilia. *Am. J. Physiol. Gastrointest. Liver Physiol.* **2010**, *299*, G990–G999. [CrossRef] [PubMed]
22. Runz, S.; Keller, S.; Rupp, C.; Stoeck, A.; Issa, Y.; Koensgen, D.; Mustea, A.; Sehouli, J.; Kristiansen, G.; Altevogt, P. Malignant ascites-derived exosomes of ovarian carcinoma patients contain CD24 and EpCAM. *Gynecol. Oncol.* **2007**, *107*, 563–571. [CrossRef] [PubMed]
23. Admyre, C.; Johansson, S.M.; Qazi, K.R.; Filén, J.J.; Lahesmaa, R.; Norman, M.; Neve, E.P.; Scheynius, A.; Gabrielsson, S. Exosomes with immune modulatory features are present in human breast milk. *J. Immunol.* **2007**, *179*, 1969–1978. [CrossRef]
24. Andreau, Z.; Yanez-Mo, M. Tetraspanins in extracellular vesicle formation and function. *Front. Immunol.* **2014**, *5*, 442. [CrossRef]
25. Wieckowski, E.U.; Visus, C.; Szajnik, M.; Szczepanski, M.J.; Storkus, W.J.; Whiteside, T.L. Tumor-Derived Microvesicles Promote Regulatory T Cell Expansion and Induce Apoptosis in Tumor-Reactive Activated CD8+ T Lymphocytes. *J. Immunol.* **2009**, *183*, 3720–3730. [CrossRef]
26. Sharma, P.; Diergaarde, B.; Ferrone, S.; Kirkwood, J.M.; Whietside, T.L. Melanoma cell-derived exosomes in plasma of melanoma patients suppress functions of immune effector cells. *Sci. Rep.* **2020**, *10*, 92. [CrossRef]
27. Ferrone, S.; Whiteside, T.L. Targeting CSPG4 for isolation of melanoma cell-derived exosomes from body fluids. *HNO* **2020**, *68*, 100–105. [CrossRef]
28. Sharma, P.; Ludwig, S.; Muller, L.; Hong, C.S.; Kirkwood, J.M.; Ferrone, S.; Whiteside, T.L. Immunoaffinity-based isolation of melanoma cell-derived exosomes from plasma of patients with melanoma. *J. Extracell. Vesicles* **2018**, *7*, 1435138. [CrossRef]
29. Melo, S.A.; Luecke, L.B.; Kahlert, C.; Fernandez, A.F.; Gammon, S.T.; Kaye, J.; LeBleu, V.S.; Mittendorf, E.A.; Weitz, J.; Rahbari, N.; et al. Glypican-1 identifies cancer exosomes and detects early pancreatic cancer. *Nature* **2015**, *523*, 177–182. [CrossRef]
30. Mizutani, K.; Terazawa, R.; Kameyama, K.; Kato, T.; Horie, K.; Tsuchiya, T.; Seike, K.; Ehara, H.; Fujita, Y.; Kawakami, K.; et al. Isolation of prostate cancer-related exosomes. *Anticancer Res.* **2014**, *34*, 3419–3423.
31. Hong, C.S.; Muller, L.; Boyiadzis, M.; Whiteside, T.L. Isolation and characterization of CD34+ blast-derived exosomes in acute myeloid leukemia. *PLoS ONE* **2014**, *9*, e103310. [CrossRef]
32. Raimondo, S.; Pucci, M.; Alessandro, R.; Fontana, S. Extracellular Vesicles and Tumor-Immune Escape: Biological Functions and Clinical Perspectives. *Int. J. Mol. Sci.* **2020**, *21*, 2286. [CrossRef] [PubMed]
33. Whiteside, T.L. Exosomes in Cancer: Another Mechanism of Tumor-Induced Immune Suppression. In *Tumor Immune Microenvironment in Cancer Progression and Cancer Therapy*; Kalinski, P., Ed.; Springer: Cham, Switzerland, 2017; Volume 1036, pp. 81–89. [CrossRef]

34. Whiteside, T.L. Tumor-Derived Exosomes and Their Role in Cancer Progression. *Adv. Clin. Chem.* **2016**, *74*, 103–141. [CrossRef] [PubMed]
35. Meldolesi, J. Exosomes and Ectosomes in Intercellular Communication. *Curr. Biol.* **2018**, *28*, R435–R444. [CrossRef]
36. Ludwig, A.K.; Giebel, B. Exosomes: Small vesicles participating in intercellular communication. *Int. J. Biochem. Cell Biol.* **2012**, *44*, 11–15. [CrossRef] [PubMed]
37. Alegre, E.; Zubiri, L.; Perez-Gracia, J.L.; González-Cao, M.; Soria, L.; Martín-Algarra, S.; González, A. Circulating melanoma exosomes as diagnostic and prognosis biomarkers. *Clin. Chim. Acta* **2016**, *454*, 28–32. [CrossRef] [PubMed]
38. Whiteside, T.L. The potential of tumor-derived exosomes for noninvasive cancer monitoring. *Expert Rev. Mol. Diagn.* **2015**, *15*, 1293–1310. [CrossRef] [PubMed]
39. Duijvesz, D.; Versluis, C.Y.; van der Fels, C.A.; Vredenbregt-van den Berg, M.S.; Leivo, J.; Peltola, M.T.; Bangma, C.H.; Pettersson, K.S.; Jenster, G. Immuno-based detection of extracellular vesicles in urine as diagnostic marker for prostate cancer. *Int. J. Cancer* **2015**, *137*, 2869–2878. [CrossRef]
40. Szajnik, M.; Derbis, M.; Lach, M.; Patalas, P.; Michalak, M.; Drzewiecka, H.; Szpurek, D.; Nowakowski, A.; Spaczynski, M.; Baranowski, W.; et al. Exosomes in Plasma of Patients with Ovarian Carcinoma: Potential Biomarkers of Tumor Progression and Response to Therapy. *Gynecol. Obstet.* **2013**, *4*, 003. [CrossRef]
41. Silva, J.; Garcia, V.; Rodriguez, M.; Compte, M.; Cisneros, E.; Veguillas, P.; Garcia, J.M.; Dominguez, G.; Campos-Martin, Y.; Cuevas, J.; et al. Analysis of exosome release and its prognostic value in human colorectal cancer. *Genes Chromosomes Cancer* **2012**, *51*, 409–418. [CrossRef]
42. Szczepanski, M.J.; Szajnik, M.; Welsh, A.; Whiteside, T.L.; Boyiadzis, M. Blast-derived microvesicles in sera from patients with acute myeloid leukemia suppress natural killer cell function via membrane-associated transforming growth factor-beta1. *Haematologica* **2011**, *96*, 1302–1309. [CrossRef] [PubMed]
43. Baran, J.; Baj-Krzyworzeka, M.; Weglarczyk, K.; Szatanek, R.; Zembala, M.; Barbasz, J.; Czupryna, A.; Szczepanik, A.; Zembala, M. Circulating tumour-derived microvesicles in plasma of gastric cancer patients. *Cancer Immunol. Immunother.* **2010**, *59*, 841–850. [CrossRef] [PubMed]
44. Zhang, L.; Yu, D. Exosomes in cancer development, metastasis, and immunity. *Biochim. Biophys. Acta Rev. Cancer* **2019**, *1871*, 455–468. [CrossRef] [PubMed]
45. Mashouri, L.; Yousefi, H.; Aref, A.R.; Ahadi, A.M.; Molaei, F.; Alahari, S.K. Exosomes: Composition, biogenesis, and mechanisms in cancer metastasis and drug resistance. *Mol. Cancer* **2019**, *18*, 75. [CrossRef]
46. Tung, K.H.; Ernstoff, M.S.; Allen, C.; Shu, S. A Review of Exosomes and their Role in The Tumor Microenvironment and Host-Tumor "Macroenvironment". *J. Immunol. Sci.* **2019**, *3*, 4–8. [CrossRef]
47. Wang, T.; Nasser, M.I.; Shen, J.; Qu, S.; He, Q.; Zhao, M. Functions of Exosomes in the Triangular Relationship between the Tumor, Inflammation, and Immunity in the Tumor Microenvironment. *J. Immunol. Res.* **2019**, *2019*, 4197829. [CrossRef]
48. Syn, N.; Wang, L.; Sethi, G.; Thiery, J.P.; Goh, B.C. Exosome-Mediated Metastasis: From Epithelial-Mesenchymal Transition to Escape from Immunosurveillance. *Trends Pharmacol. Sci.* **2016**, *37*, 606–617. [CrossRef]
49. Whiteside, T.L. Exosomes and tumor-mediated immune suppression. *J. Clin. Investig.* **2016**, *126*, 1216–1223. [CrossRef]
50. Whiteside, T.L. The role of tumor-derived exosomes in epithelial mesenchymal transition (EMT). *Transl. Cancer Res.* **2017**, *6*, S90–S92. [CrossRef]
51. Ludwig, N.; Yerneni, S.S.; Razzo, B.M.; Whiteside, T.L. Exosomes from HNSCC Promote Angiogenesis through Reprogramming of Endothelial Cells. *Mol. Cancer Res.* **2018**, *16*, 1798–1808. [CrossRef] [PubMed]
52. Barros, F.M.; Carneiro, F.; Machado, J.C.; Melo, S.A. Exosomes and Immune Response in Cancer: Friends or Foes? *Front. Immunol.* **2018**, *9*, 730. [CrossRef] [PubMed]
53. Czernek, L.; Düchler, M. Functions of Cancer-Derived Extracellular Vesicles in Immunosuppression. *Arch. Immunol. Ther. Exp.* **2017**, *65*, 311–323. [CrossRef] [PubMed]
54. Whiteside, T.L. Immune modulation of T-cell and NK (natural killer) cell activities by TEX (tumour-derived exosomes). *Biochem. Soc. Trans.* **2013**, *41*, 245–251. [CrossRef] [PubMed]
55. Tucci, M.; Mannavola, F.; Passarelli, A.; Stucci, L.S.; Cives, M.; Silvestris, F. Exosomes in melanoma: A role in tumor progression, metastasis and impaired immune system activity. *Oncotarget* **2018**, *9*, 20826–20837. [CrossRef]

56. Tucci, M.; Passarelli, A.; Mannavola, F.; Felici, C.; Stucci, L.S.; Cives, M.; Silvestris, F. Immune System Evasion as Hallmark of Melanoma Progression: The Role of Dendritic Cells. *Front. Oncol.* **2019**, *9*, 1148. [CrossRef]
57. Isola, A.L.; Eddy, K.; Chen, S. Biology, Therapy and Implications of Tumor Exosomes in the Progression of Melanoma. *Cancers* **2016**, *8*, 110. [CrossRef]
58. Siegel, R.L.; Miller, K.D.; Jemal, A. Cancer statistics, 2020. *CA Cancer J. Clin.* **2020**, *70*, 7–30. [CrossRef]
59. Osella-Abate, S.; Ribero, S.; Sanlorenzo, M.; Maule, M.M.; Richiardi, L.; Merletti, F.; Tomasini, C.; Marra, E.; Macripò, G.; Fierro, M.T.; et al. Risk factors related to late metastases in 1,372 melanoma patients disease free more than 10 years. *Int. J. Cancer* **2015**, *136*, 2453–2457. [CrossRef]
60. Rutkowski, P.; Wysocki, P.J.; Nasierowska-Guttmejer, A.; Jeziorski, A.; Wysocki, W.M.; Kalinka-Warzocha, E.; Świtaj, T.; Kozak, K.; Kamińska-Winciorek, G.; Czarnecka, A.M.; et al. Cutaneous melanomas. *Oncol. Clin. Pract.* **2019**, *15*, 1–19. [CrossRef]
61. Weiss, S.A.; Wolchok, J.D.; Sznol, M. Immunotherapy of Melanoma: Facts and Hopes. *Clin. Cancer Res.* **2019**, *25*, 5191–5201. [CrossRef]
62. Fujimura, T.; Fujisawa, Y.; Kambayashi, Y.; Aiba, S. Significance of BRAF Kinase Inhibitors for Melanoma Treatment: From Bench to Bedside. *Cancers* **2019**, *11*, 1342. [CrossRef] [PubMed]
63. Pasquali, S.; Hadjinicolaou, A.V.; Chiarion Sileni, V.; Rossi, C.R.; Mocellin, S. Systemic treatments for metastatic cutaneous melanoma. *Cochrane Database Syst. Rev.* **2018**, *2*, CD011123. [CrossRef] [PubMed]
64. Sun, Y.; Huo, C.; Qiao, Z.; Shang, Z.; Uzzaman, A.; Liu, S.; Jiang, X.; Fan, L.Y.; Ji, L.; Guan, X.; et al. Comparative Proteomic Analysis of Exosomes and Microvesicles in Human Saliva for Lung Cancer. *J. Proteome Res.* **2018**, *17*, 1101–1107. [CrossRef] [PubMed]
65. Luo, D.; Zhan, S.; Xia, W.; Huang, L.; Ge, W.; Wang, T. Proteomics study of serum exosomes from papillary thyroid cancer patients. *Endocr. Relat. Cancer* **2018**, *25*, 879–891. [CrossRef]
66. Gangoda, L.; Liem, M.; Ang, C.S.; Keerthikumar, S.; Adda, C.G.; Parker, B.S.; Mathivanan, S. Proteomic Profiling of Exosomes Secreted by Breast Cancer Cells with Varying Metastatic Potential. *Proteomics* **2017**, *17*, 23–24. [CrossRef]
67. Ludwig, S.; Marczak, L.; Sharma, P.; Abramowicz, A.; Gawin, M.; Widlak, P.; Whiteside, T.L.; Pietrowska, M. Proteomes of exosomes from HPV(+) or HPV(−) head and neck cancer cells: Differential enrichment in immunoregulatory proteins. *Oncoimmunology* **2019**, *8*, 1593808. [CrossRef]
68. Mears, R.; Craven, R.A.; Hanrahan, S.; Totty, N.; Upton, C.; Young, S.L.; Patel, P.; Selby, P.J.; Banks, R.E. Proteomic analysis of melanoma-derived exosomes by two-dimensional polyacrylamide gel electrophoresis and mass spectrometry. *Proteomics* **2004**, *4*, 4019–4031. [CrossRef] [PubMed]
69. Xiao, D.; Ohlendorf, J.; Chen, Y.; Taylor, D.D.; Rai, S.N.; Waigel, S.; Zacharias, W.; Hao, H.; McMasters, K.M. Identifying mRNA, microRNA and protein profiles of melanoma exosomes. *PLoS ONE* **2012**, *7*, e46874. [CrossRef]
70. Lazar, I.; Clement, E.; Ducoux-Petit, M.; Denat, L.; Soldan, V.; Dauvillier, S.; Balor, S.; Burlet-Schiltz, O.; Larue, L.; Muller, C.; et al. Proteome characterization of melanoma exosomes reveals a specific signature for metastatic cell lines. *Pigment Cell Melanoma Res.* **2015**, *28*, 464–475. [CrossRef]
71. Muhsin-Sharafaldine, M.R.; Saunderson, S.C.; Dunn, A.C.; Faed, J.M.; Kleffmann, T.; McLellan, A.D. Procoagulant and immunogenic properties of melanoma exosomes, microvesicles and apoptotic vesicles. *Oncotarget* **2016**, *7*, 56279–56294. [CrossRef]
72. Willms, E.; Johansson, H.J.; Mäger, I.; Lee, Y.; Blomberg, K.E.; Sadik, M.; Alaarg, A.; Smith, C.I.; Lehtiö, J.; El Andaloussi, S.; et al. Cells release subpopulations of exosomes with distinct molecular and biological properties. *Sci. Rep.* **2016**, *6*, 22519. [CrossRef] [PubMed]
73. Boussadia, Z.; Lamberti, J.; Mattei, F.; Pizzi, E.; Puglisi, R.; Zanetti, C.; Pasquini, L.; Fratini, F.; Fantozzi, L.; Felicetti, F.; et al. Acidic microenvironment plays a key role in human melanoma progression through a sustained exosome mediated transfer of clinically relevant metastatic molecules. *J. Exp. Clin. Cancer Res.* **2018**, *37*, 245. [CrossRef] [PubMed]
74. Peinado, H.; Alečković, M.; Lavotshkin, S.; Matei, I.; Costa-Silva, B.; Moreno-Bueno, G.; Hergueta-Redondo, M.; Williams, C.; García-Santos, G.; Ghajar, C.; et al. Melanoma exosomes educate bone marrow progenitor cells toward a pro-metastatic phenotype through MET. *Nat. Med.* **2012**, *18*, 883–891. [CrossRef] [PubMed]
75. Surman, M.; Stępień, E.; Przybyło, M. Melanoma-Derived Extracellular Vesicles: Focus on Their Proteome. *Proteomes* **2019**, *7*, 21. [CrossRef]
76. Kalluri, R. The biology and function of exosomes in cancer. *J. Clin. Investig.* **2016**, *126*, 1208–1215. [CrossRef]

77. Tsitsiou, E.; Lindsay, M.A. microRNAs and the immune response. *Trends Immunol.* **2008**, *29*, 343–351. [CrossRef]
78. Salehi, M.; Sharifi, M. Exosomal miRNAs as novel cancer biomarkers: Challenges and opportunities. *J. Cell. Physiol.* **2018**, *233*, 6370–6380. [CrossRef]
79. Sun, Z.; Shi, K.; Yang, S.; Liu, J.; Zhou, Q.; Wang, G.; Song, J.; Li, Z.; Zhang, Z.; Yuan, W. Effect of exosomal miRNA on cancer biology and clinical applications. *Mol. Cancer* **2018**, *17*, 147. [CrossRef]
80. Hessvik, N.P.; Phuyal, S.; Brech, A.; Sandvig, K.; Llorente, A. Profiling of microRNAs in exosomes released from PC-3 prostate cancer cells. *Biochim. Biophys. Acta* **2012**, *1819*, 1154–1163. [CrossRef]
81. Gajos-Michniewicz, A.; Duechler, M.; Czyz, M. MiRNA in melanoma-derived exosomes. *Cancer Lett.* **2014**, *347*, 29–37. [CrossRef]
82. Li, J.; Chen, J.; Wang, S.; Li, P.; Zheng, C.; Zhou, X.; Tao, Y.; Chen, X.; Sun, L.; Wang, A.; et al. Blockage of transferred exosome-shuttled miR-494 inhibits melanoma growth and metastasis. *J. Cell. Physiol.* **2019**, *234*, 15763–15774. [CrossRef] [PubMed]
83. Wozniak, M.; Peczek, L.; Czernek, L.; Düchler, M. Analysis of the miRNA Profiles of Melanoma Exosomes Derived Under Normoxic and Hypoxic Culture Conditions. *Anticancer Res.* **2017**, *37*, 6779–6789. [CrossRef] [PubMed]
84. Bland, C.L.; Byrne-Hoffman, C.N.; Fernandez, A.; Rellick, S.L.; Deng, W.; Klinke, D.J., 2nd. Exosomes derived from B16F0 melanoma cells alter the transcriptome of cytotoxic T cells that impacts mitochondrial respiration. *FEBS J.* **2018**, *285*, 1033–1050. [CrossRef] [PubMed]
85. Zhou, J.; Yang, Y.; Wang, W.; Zhang, Y.; Chen, Z.; Hao, C.; Zhang, J. Melanoma-released exosomes directly activate the mitochondrial apoptotic pathway of CD4+ T cells through their microRNA cargo. *Exp. Cell Res.* **2018**, *371*, 364–371. [CrossRef]
86. Zhou, X.; Yan, T.; Huang, C.; Xu, Z.; Wang, L.; Jiang, E.; Wang, H.; Chen, Y.; Liu, K.; Shao, Z.; et al. Melanoma cell-secreted exosomal miR-155-5p induce proangiogenic switch of cancer-associated fibroblasts via SOCS1/JAK2/STAT3 signaling pathway. *J. Exp. Clin. Cancer Res.* **2018**, *37*, 242. [CrossRef]
87. Felicetti, F.; De Feo, A.; Coscia, C.; Puglisi, R.; Pedini, F.; Pasquini, L.; Bellenghi, M.; Errico, M.C.; Pagani, E.; Carè, A. Exosome-mediated transfer of miR-222 is sufficient to increase tumor malignancy in melanoma. *J. Transl. Med.* **2016**, *1*, 56. [CrossRef]
88. Chen, L.; Karisma, V.W.; Liu, H.; Zhong, L. MicroRNA-300: A Transcellular Mediator in Exosome Regulates Melanoma Progression. *Front. Oncol.* **2019**, *9*, 1005. [CrossRef]
89. Shu, S.L.; Yang, Y.; Allen, C.L.; Maguire, O.; Minderman, H.; Sen, A.; Ciesielski, M.J.; Collins, K.A.; Bush, P.J.; Singh, P.; et al. Metabolic reprogramming of stromal fibroblasts by melanoma exosome microRNA favours a pre-metastatic microenvironment. *Sci. Rep.* **2018**, *8*, 12905. [CrossRef]
90. Vignard, V.; Labbé, M.; Marec, N.; André-Grégoire, G.; Jouand, N.; Fonteneau, J.F.; Labarrière, N.; Fradin, D. MicroRNAs in Tumor Exosomes Drive Immune Escape in Melanoma. *Cancer Immunol. Res.* **2020**, *8*, 255–267. [CrossRef]
91. Pfeffer, S.R.; Grossmann, K.F.; Cassidy, P.B.; Yang, C.H.; Fan, M.; Kopelovich, L.; Leachman, S.A.; Pfeffer, L.M. Detection of Exosomal miRNAs in the Plasma of Melanoma Patients. *J. Clin. Med.* **2015**, *4*, 2012–2027. [CrossRef]
92. Alegre, E.; Sanmamed, M.F.; Rodriguez, C.; Carranza, O.; Martín-Algarra, S.; González, A. Study of circulating microRNA-125b levels in serum exosomes in advanced melanoma. *Arch. Pathol. Lab. Med.* **2014**, *138*, 828–832. [CrossRef] [PubMed]
93. Greenberg, E.; Hershkovitz, L.; Itzhaki, O.; Hajdu, S.; Nemlich, Y.; Ortenberg, R.; Gefen, N.; Edry, L.; Modai, S.; Keisari, Y.; et al. Regulation of cancer aggressive features in melanoma cells by microRNAs. *PLoS ONE* **2011**, *6*, e18936. [CrossRef] [PubMed]
94. Rao, E.; Jiang, C.; Ji, M.; Huang, X.; Iqbal, J.; Lenz, G.; Wright, G.; Staudt, L.M.; Zhao, Y.; McKeithan, T.W.; et al. The miRNA-17 approximately 92 cluster mediates chemoresistance and enhances tumor growth in mantle cell lymphoma via pi3k/akt pathway activation. *Leukemia* **2012**, *26*, 1064–1072. [CrossRef] [PubMed]
95. Levy, C.; Khaled, M.; Iliopoulos, D.; Janas, M.M.; Schubert, S.; Pinner, S.; Chen, P.H.; Li, S.; Fletcher, A.L.; Yokoyama, S.; et al. Intronic miR-211 assumes the tumor suppressive function of its host gene in melanoma. *Mol. Cell* **2010**, *40*, 841–849. [CrossRef]
96. Si, M.L.; Zhu, S.; Wu, H.; Lu, Z.; Wu, F.; Mo, Y.Y. MiR-21-mediated tumor growth. *Oncogene* **2007**, *26*, 2799–2803. [CrossRef]

97. Zhu, S.; Wu, H.; Wu, F.; Nie, D.; Sheng, S.; Mo, Y.Y. MicroRNA-21 targets tumor suppressor genes in invasion and metastasis. *Cell Res.* **2008**, *18*, 350–359. [CrossRef]
98. Yang, C.H.; Yue, J.; Pfeffer, S.R.; Handorf, C.R.; Pfeffer, L.M. MicroRNA miR-21 regulates the metastatic behavior of b16 melanoma cells. *J. Biol. Chem.* **2011**, *286*, 39172–39178. [CrossRef] [PubMed]
99. Yang, C.H.; Yue, J.; Fan, M.; Pfeffer, L.M. IFN induces miR-21 through a signal transducer and activator of transcription 3-dependent pathway as a suppressive negative feedback on IFN-induced apoptosis. *Cancer Res.* **2010**, *70*, 8108–8116. [CrossRef] [PubMed]
100. Xu, Y.F.; Hannafon, B.N.; Khatri, U.; Gin, A.; Ding, W.Q. The origin of exosomal miR-1246 in human cancer cells. *RNA Biol.* **2019**, *16*, 770–784. [CrossRef]
101. Bhagirath, D.; Yang, T.L.; Bucay, N.; Sekhon, K.; Majid, S.; Shahryari, V.; Dahiya, R.; Tanaka, Y.; Saini, S. microRNA-1246 Is an Exosomal Biomarker for Aggressive Prostate Cancer. *Cancer Res.* **2018**, *78*, 1833–1844. [CrossRef]
102. Felicetti, F.; Errico, M.C.; Bottero, L.; Segnalini, P.; Stoppacciaro, A.; Biffoni, M.; Felli, N.; Mattia, G.; Petrini, M.; Colombo, M.P.; et al. The promyelocytic leukemia zinc finger-microRNA-221/-222 pathway controls melanoma progression through multiple oncogenic mechanisms. *Cancer Res.* **2008**, *68*, 2745–2754. [CrossRef]
103. Müller, D.; Bosserhoff, A. Integrin β3 expression is regulated by let-7a miRNA in malignant melanoma. *Oncogene* **2008**, *27*, 6698–6706. [CrossRef]
104. Xiao, D.; Barry, S.; Kmetz, D.; Egger, M.; Pan, J.; Rai, S.N.; Qu, J.; McMasters, K.M.; Hao, H. Melanoma cell-derived exosomes promote epithelial-mesenchymal transition in primary melanocytes through paracrine/autocrine signaling in the tumor microenvironment. *Cancer Lett.* **2016**, *376*, 318–327. [CrossRef] [PubMed]
105. Ryan, D.; Rafferty, M.; Hegarty, S.; O'Leary, P.; Faller, W.; Gremel, G.; Bergqvist, M.; Agnarsdottir, M.; Strömberg, S.; Kampf, C.; et al. Topoisomerase I amplification in melanoma is associated with more advanced tumours and poor prognosis. *Pigment Cell Melanoma Res.* **2010**, *23*, 542–553. [CrossRef] [PubMed]
106. Wang, S.; Tang, L.; Lin, J.; Shen, Z.; Yao, Y.; Wang, W.; Tao, S.; Gu, C.; Ma, J.; Xie, Y.; et al. ABCB5 promotes melanoma metastasis through enhancing NF-κB p65 protein stability. *Biochem. Biophys. Res. Commun.* **2017**, *492*, 18–26. [CrossRef] [PubMed]
107. Suryo Rahmanto, Y.; Dunn, L.; Richardson, D. The melanoma tumor antigen, melanotransferrin (p97): A 25-year hallmark—From iron metabolism to tumorigenesis. *Oncogene* **2007**, *26*, 6113–6124. [CrossRef] [PubMed]
108. Soengas, M.; Hernando, E. TYRP1 mRNA goes fishing for miRNAs in melanoma. *Nat. Cell Biol.* **2017**, *19*, 1311–1312. [CrossRef]
109. Gilot, D.; Migault, M.; Bachelot, L.; Journé, F.; Rogiers, A.; Donnou-Fournet, E.; Mogha, A.; Mouchet, N.; Pinel-Marie, M.L.; Mari, B.; et al. A non-coding function of TYRP1 mRNA promotes melanoma growth. *Nat. Cell Biol.* **2017**, *19*, 1348–1357. [CrossRef] [PubMed]
110. Li, X.; Wang, Y.; Wang, Q.; Liu, Y.; Bao, W.; Wu, S. Exosomes in cancer: Small transporters with big functions. *Cancer Lett.* **2018**, *435*, 55–65. [CrossRef]
111. Chen, G.; Huang, A.C.; Zhang, W.; Zhang, G.; Wu, M.; Xu, W.; Yu, Z.; Yang, J.; Wang, B.; Sun, H.; et al. Exosomal PD-L1 contributes to immunosuppression and is associated with anti-PD-1 response. *Nature* **2018**, *560*, 382–386. [CrossRef]
112. Kaiser, J. Malignant messengers. *Science* **2016**, *352*, 164–166. [CrossRef] [PubMed]
113. Chen, D.S.; Mellman, I. Elements of cancer immunity and the cancer-immune set point. *Nature* **2017**, *541*, 321–330. [CrossRef]
114. Muller, L.; Mitsuhashi, M.; Simms, P.; Gooding, W.E.; Whiteside, T.L. Tumor-derived exosomes regulate expression of immune function-related genes in human T cell subsets. *Sci. Rep.* **2016**, *6*, 20254. [CrossRef]
115. Bergmann, C.; Strauss, L.; Wang, Y.; Szczepanski, M.J.; Lang, S.; Johnson, J.T.; Whiteside, T.L. T regulatory Type 1 cells (Tr1) in squamous cell carcinoma of the head and neck: Mechanisms of suppression and expansion in advanced disease. *Clin. Cancer Res.* **2008**, *14*, 3706–3715. [CrossRef]
116. Clayton, A.; Al-Taei, S.; Webber, J.; Mason, M.D.; Tabi, Z. Cancer exosomes express CD39 and CD73, which suppress T cells through adenosine production. *J. Immunol.* **2011**, *187*, 676–683. [CrossRef] [PubMed]

117. Szajnik, M.; Czystowska, M.; Szczepanski, M.J.; Mandapathil, M.; Whiteside, T.L. Tumor-derived microvesicles induce, expand and up-regulate biological activities of human regulatory T cells (Treg). *PLoS ONE* **2010**, *5*, e11469. [CrossRef] [PubMed]
118. Düchler, M.; Czernek, L.; Peczek, L.; Cypryk, W.; Sztiller-Sikorska, M.; Czyz, M. Melanoma-Derived Extracellular Vesicles Bear the Potential for the Induction of Antigen-Specific Tolerance. *Cells* **2019**, *8*, 665. [CrossRef]
119. Gyukity-Sebestyén, E.; Harmati, M.; Dobra, G.; Németh, I.B.; Mihály, J.; Zvara, Á.; Hunyadi-Gulyás, É.; Katona, R.; Nagy, I.; Horváth, P.; et al. Melanoma-Derived Exosomes Induce PD-1 Overexpression and Tumor Progression via Mesenchymal Stem Cell Oncogenic Reprogramming. *Front. Immunol.* **2019**, *10*, 2459. [CrossRef]
120. Martínez-Lorenzo, M.J.; Anel, A.; Alava, M.A.; Piñeiro, A.; Naval, J.; Lasierra, P.; Larrad, L. The human melanoma cell line MelJuSo secretes bioactive FasL and APO2L/TRAIL on the surface of microvesicles. Possible contribution to tumor counterattack. *Exp. Cell Res.* **2004**, *295*, 315–329. [CrossRef]
121. Wu, Y.; Deng, W.; McGinley, E.C.; Klinke, D.J., 2nd. Melanoma exosomes deliver a complex biological payload that upregulates PTPN11 to suppress T lymphocyte function. *Pigment Cell Melanoma Res.* **2017**, *30*, 203–218. [CrossRef]
122. Kulkarni, Y.M.; Chambers, E.; McGray, A.J.R.; Ware, J.S.; Bramson, J.L.; Klinke, D.J. A quantitative systems approach to identify paracrine mechanisms that locally suppress immune response to Interleukin-12 in the B16 melanoma model. *Integr. Biol.* **2012**, *4*, 925–936. [CrossRef] [PubMed]
123. Cottonham, C.L.; Kaneko, S.; Xu, L. miR-21 and miR-31 converge on TIAM1 to regulate migration and invasion of colon carcinoma cells. *J. Biol. Chem.* **2010**, *285*, 35293–35302. [CrossRef]
124. Yasuda, M.; Schmid, T.; Rubsamen, D.; Colburn, N.H.; Irie, K.; Murakami, A. Downregulation of programmed cell death 4 by inflammatory conditions contributes to the generation of the tumor promoting microenvironment. *Mol. Carcinog.* **2010**, *49*, 837–848. [CrossRef] [PubMed]
125. Fabbri, M.; Paone, A.; Calore, F.; Galli, R.; Gaudio, E.; Santhanam, R.; Lovat, F.; Fadda, P.; Mao, C.; Nuovo, G.J.; et al. MicroRNAs bind to Toll-like receptors to induce prometastatic inflammatory response. *Proc. Natl. Acad. Sci. USA* **2012**, *109*, E2110–E2116. [CrossRef] [PubMed]
126. Tang, M.; Diao, J.; Gu, H.; Khatri, I.; Zhao, J.; Cattral, M.S. Toll-like Receptor 2 Activation Promotes Tumor Dendritic Cell Dysfunction by Regulating IL-6 and IL-10 Receptor Signaling. *Cell Rep.* **2015**, *13*, 2851–2864. [CrossRef]
127. Ashiru, O.; Boutet, P.; Fernández-Messina, L.; Agüera-González, S.; Skepper, J.N.; Valés-Gómez, M.; Reyburn, H.T. Natural killer cell cytotoxicity is suppressed by exposure to the human NKG2D ligand MICA*008 that is shed by tumor cells in exosomes. *Cancer Res.* **2010**, *70*, 481–489. [CrossRef] [PubMed]
128. Guo, Y.; Ji, X.; Liu, J.; Fan, D.; Zhou, Q.; Chen, C.; Wang, W.; Wang, G.; Wang, H.; Yuan, W.; et al. Effects of exosomes on pre-metastatic niche formation in tumors. *Mol. Cancer* **2019**, *18*, 39. [CrossRef]
129. Caramel, J.; Papadogeorgakis, E.; Hill, L.; Browne, G.J.; Richard, G.G.; Wierinckx, A.; Saldanha, G.; Osborne, J.; Hutchinson, P.; Tse, G.; et al. A switch in the expression of embryonic EMT-inducers drives the development of malignant melanoma. *Cancer Cell.* **2013**, *24*, 466–480. [CrossRef]
130. Hu, T.; Hu, J. Melanoma-derived exosomes induce reprogramming fibroblasts into cancer-associated fibroblasts via Gm26809 delivery. *Cell Cycle* **2019**, *18*, 3085–3094. [CrossRef]
131. Zhao, X.-P.; Wang, M.; Song, Y.; Song, K.; Yan, T.L.; Wang, L.; Li, K.; Shang, Z.J. Membrane microvesicles as mediators for melanoma-fibroblasts communication: Roles of the VCAM-1/VLA-4 axis and the ERK1/2 signal pathway. *Cancer Lett.* **2015**, *360*, 125–133. [CrossRef]
132. Hood, J.; Pan, H.; Lanza, G.; Wickline, S.A. Paracrine induction of endothelium by tumor exosomes. *Lab. Investig.* **2009**, *89*, 1317–1328. [CrossRef] [PubMed]
133. Zhuang, G.; Wu, X.; Jiang, Z.; Kasman, I.; Yao, J.; Guan, Y.; Oeh, J.; Modrusan, Z.; Bais, C.; Sampath, D.; et al. Tumour-secreted miR-9 promotes endothelial cell migration and angiogenesis by activating the JAK-STAT pathway. *EMBO J.* **2012**, *31*, 3513–3523. [CrossRef] [PubMed]
134. Ekström, E.J.; Bergenfelz, C.; von Bülow, V.; Serifler, F.; Carlemalm, E.; Jönsson, G.; Andersson, T.; Leandersson, K. WNT5A induces release of exosomes containing pro-angiogenic and immunosuppressive factors from malignant melanoma cells. *Mol. Cancer* **2014**, *13*, 88. [CrossRef] [PubMed]

135. Sento, S.; Sasabe, E.; Yamamoto, T. Application of a persistent heparin treatment inhibits the malignant potential of oral squamous carcinoma cells induced by tumor cell-derived exosomes. *PLoS ONE* **2016**, *11*, e0148454. [CrossRef]
136. Hazan-Halevy, I.; Rosenblum, D.; Weinstein, S.; Bairey, O.; Raanani, P.; Peer, D. Cell-specific uptake of mantle cell lymphoma-derived exosomes by malignant and non-malignant B-lymphocytes. *Cancer Lett.* **2015**, *364*, 59–69. [CrossRef] [PubMed]
137. Matsumoto, A.; Takahashi, Y.; Nishikawa, M.; Sano, K.; Morishita, M.; Charoenviriyakul, C.; Saji, H.; Takakura, Y. Accelerated growth of B16BL6 tumor in mice through efficient uptake of their own exosomes by B16BL6 cells. *Cancer Sci.* **2017**, *108*, 1803–1810. [CrossRef]
138. Isola, A.L.; Eddy, K.; Zembrzuski, K.; Goydos, J.S.; Chen, S. Exosomes released by metabotropic glutamate receptor 1 (GRM1) expressing melanoma cells increase cell migration and invasiveness. *Oncotarget* **2018**, *9*, 1187–1199. [CrossRef]
139. Ostrowski, M.; Carmo, N.B.; Krumeich, S.; Fanget, I.; Raposo, G.; Savina, A.; Moita, C.F.; Schauer, K.; Hume, A.N.; Freitas, R.P.; et al. Rab27a and Rab27b control different steps of the exosome secretion pathway. *Nat. Cell Biol.* **2009**, *12*, 19–30. [CrossRef] [PubMed]
140. Guo, D.; Lui, G.Y.L.; Lai, S.L.; Wilmott, J.S.; Tikoo, S.; Jackett, L.A.; Quek, C.; Brown, D.L.; Sharp, D.M.; Kwan, R.Y.Q.; et al. RAB27A promotes melanoma cell invasion and metastasis via regulation of pro-invasive exosomes. *Int. J. Cancer* **2019**, *144*, 3070–3085. [CrossRef]
141. Mannavola, F.; Tucci, M.; Felici, C.; Passarelli, A.; D'Oronzo, S.; Silvestris, F. Tumor-derived exosomes promote the in vitro osteotropism of melanoma cells by activating the SDF-1/CXCR4/CXCR7 axis. *J. Transl. Med.* **2019**, *17*, 230. [CrossRef] [PubMed]
142. Hood, J.L.; San, R.S.; Wickline, S.A. Exosomes released by melanoma cells prepare sentinel lymph nodes for tumor metastasis. *Cancer Res.* **2011**, *71*, 3792–3801. [CrossRef] [PubMed]
143. Angi, M.; Kalirai, H.; Prendergast, S.; Simpson, D.; Hammond, D.E.; Madigan, M.C.; Beynon, R.J.; Coupland, S.E. In-depth proteomic profiling of the uveal melanoma secretome. *Oncotarget* **2016**, *7*, 49623–49635. [CrossRef] [PubMed]
144. Tengda, L.; Shuping, L.; Mingli, G.; Jie, G.; Yun, L.; Weiwei, Z.; Anmei, D. Serum exosomal microRNAs as potent circulating biomarkers for melanoma. *Melanoma Res.* **2018**, *28*, 295–303. [CrossRef] [PubMed]
145. Larkin, J.; Ascierto, P.A.; Dréno, B.; Atkinson, V.; Liszkay, G.; Maio, M.; Mandalà, M.; Demidov, L.; Stroyakovskiy, D.; Thomas, L.; et al. Combined vemurafenib and cobimetinib in BRAF-mutated melanoma. *N. Engl. J. Med.* **2014**, *371*, 1867–1876. [CrossRef]
146. Lunavat, T.R.; Cheng, L.; Einarsdottir, B.O.; Olofsson Bagge, R.; Veppil Muralidharan, S.; Sharples, R.A.; Lässer, C.; Gho, Y.S.; Hill, A.F.; Nilsson, J.A.; et al. BRAFV600 inhibition alters the microRNA cargo in the vesicular secretome of malignant melanoma cells. *Proc. Natl. Acad. Sci. USA* **2017**, *114*, E5930–E5939. [CrossRef]
147. Svedman, F.C.; Lohcharoenkal, W.; Bottai, M.; Brage, S.E.; Sonkoly, E.; Hansson, J.; Pivarcsi, A.; Eriksson, H. Extracellular microvesicle microRNAs as predictive biomarkers for targeted therapy in metastastic cutaneous malignant melanoma. *PLoS ONE* **2018**, *13*, e0206942. [CrossRef]
148. Segura, M.F.; Belitskaya-Lévy, I.; Rose, A.E.; Zakrzewski, J.; Gaziel, A.; Hanniford, D.; Darvishian, F.; Berman, R.S.; Shapiro, R.L.; Pavlick, A.C.; et al. Melanoma MicroRNA signature predicts post-recurrence survival. *Clin. Cancer Res.* **2010**, *16*, 1577–1586. [CrossRef]
149. Ribas, A.; Hamid, O.; Daud, A.; Hodi, F.S.; Wolchok, J.D.; Kefford, R.; Joshua, A.M.; Patnaik, A.; Hwu, W.I.; Weber, J.S.; et al. Association of Pembrolizumab With Tumor Response and Survival Among Patients With Advanced Melanoma. *JAMA* **2016**, *315*, 1600–1609. [CrossRef]
150. Cordonnier, M.; Nardin, C.; Chanteloup, G.; Derangere, V.; Algros, M.P.; Arnould, L.; Garrido, C.; Aubin, F.; Gobbo, J. Tracking the evolution of circulating exosomal-PD-L1 to monitor melanoma patients. *J. Extracell. Vesicles* **2020**, *9*, 1. [CrossRef]

Journal of *Personalized Medicine*

MDPI

Article

Metabolic Profiles of Whole Serum and Serum-Derived Exosomes Are Different in Head and Neck Cancer Patients Treated by Radiotherapy

Anna Wojakowska [1,†], Aneta Zebrowska [2,†], Agata Skowronek [2], Tomasz Rutkowski [2], Krzysztof Polanski [3], Piotr Widlak [2], Lukasz Marczak [1,*] and Monika Pietrowska [2,*]

1 Institute of Bioorganic Chemistry Polish Academy of Sciences, 61-704 Poznan, Poland; astasz@ibch.poznan.pl
2 Maria Sklodowska-Curie National Research Institute of Oncology, Gliwice Branch, 44-101 Gliwice, Poland; aneta7zebrowska@gmail.com (A.Z.); agata.w2012@gmail.com (A.S.); Tomasz.Rutkowski@io.gliwice.pl (T.R.); Piotr.Widlak@io.gliwice.pl (P.W.)
3 Wellcome Sanger Institute, Wellcome Genome Campus, Hinxton, Cambridgeshire CB10 1SA, UK; kp9@sanger.ac.uk
* Correspondence: lukasmar@ibch.poznan.pl (L.M.); Monika.Pietrowska@io.gliwice.pl (M.P.)
† These authors contributed equally.

Received: 15 October 2020; Accepted: 13 November 2020; Published: 13 November 2020

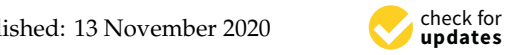

Abstract: Background: In general, the serum metabolome reflects the patient's body response to both disease state and implemented treatment. Though serum-derived exosomes are an emerging type of liquid biopsy, the metabolite content of these vesicles remains under researched. The aim of this pilot study was to compare the metabolite profiles of the whole serum and serum-derived exosomes in the context of differences between cancer patients and healthy controls as well as patients' response to radiotherapy (RT). Methods: Serum samples were collected from 10 healthy volunteers and 10 patients with head and neck cancer before and after RT. Metabolites extracted from serum and exosomes were analyzed by the gas chromatography–mass spectrometry (GC–MS). Results: An untargeted GC–MS-based approach identified 182 and 46 metabolites in serum and exosomes, respectively. Metabolites that differentiated cancer and control samples, either serum or exosomes, were associated with energy metabolism. Serum metabolites affected by RT were associated with the metabolism of amino acids, sugars, lipids, and nucleotides. Conclusions: cancer-related features of energy metabolism could be detected in both types of specimens. On the other hand, in contrast to RT-induced changes observed in serum metabolome, this pilot study did not reveal a specific radiation-related pattern of exosome metabolites.

Keywords: head and neck cancer; exosomes; serum; radiotherapy; metabolomics; GC/MS

1. Introduction

Head and neck cancer (HNC) is the sixth most common malignancy worldwide. The incidence of HNC exceeds half a million annually and accounts for approximately 6% of all cancer cases worldwide [1,2]. Although over the last decade we have observed an improvement in the treatment of HNC, there is still a need for new biomarkers of this type of cancer because, since the tumor location and classical staging remain the major criteria of the treatment selection, and molecular heterogeneity of HNC [3]. Radiotherapy (RT), used either alone or in combination with other treatment modalities (surgery, chemotherapy, or immunotherapy) is the major modality in the HNC treatment. The major benefit of RT is a well established local control of the tumor. However, ionizing radiation induces damage to the adjacent healthy tissues, which is reflected at the systemic level in body fluids [4–7]. Hence, detection in the patient's blood of a molecular fingerprint of the body's response to the treatment

is another important aspect of HNC diagnostics, which could potentially enable the monitoring and prediction of radiation toxicity.

Various types of "omics" studies (genomics, transcriptomics, proteomics, metabolomics) using different sources of samples (blood, urine, saliva, tissues) uncovered molecules and genes of potential use as clinical biomarkers [8,9]. Cancer cells' metabolism differs from one of the healthy cells and it is considered as the closest footprint of a cancer phenotype. This is why metabolomics studies are among the fastest-growing areas of cancer research in recent decades. Recent studies revealed disparities in the metabolite profile between diseased and normal states as well as between miscellaneous types of cancer or various stages of the disease. Therefore, altered metabolic pathways in various cancer systems might be used to identify biomarkers in terms of diagnosis, prognosis, or treatment schedule choice [10,11]. The NMR-based metabolomics study revealed an increased level of glucose, ketone bodies, ornithine, asparagine, and 2-hydroxybutyrate while decreased levels of citric acid cycle (TCA cycle) intermediates (citrate, succinate, and formate), lactate, alanine, and other gluconeogenic amino acids in the sera of patients with HNC [12]. Another GC/MS-based metabolomic analysis of serum and tissues of HNC patients revealed different metabolite profiles in patients with different treatment outcomes. In patients with disease relapse, the serum levels of metabolites related to the glycolytic pathway (especially glucose, ribose, fructose) were higher while serum levels of amino acids (lysine and trans-4-hydroxy-L-proline) were lower than in samples of patients without disease relapse [13]. Hence, one could conclude that the altered energy metabolism, mostly the switch from the TCA cycle to aerobic glycolysis known as the Warburg effect, is characteristic for patients with HNC [12–15]. Moreover, a few studies addressed therapy-induced changes in metabolic profiles of HNC, revealing compounds whose levels were associated with the treatment escalation (e.g., of the radiation dose during radiotherapy) or the intensity of treatment toxicity [16–18]. However, the knowledge about molecular mechanisms involved in radiation-induced changes of the patient's metabolome remains limited.

In the present study, the GC/MS approach was applied to profile the serum metabolites of HNC patients who underwent RT to uncover the metabolome changes induced by radiation. Furthermore, we included in the study another emerging biospecimen—exosomes circulating in patients' blood. Exosomes are virus-sized (50–150 nm) vesicles of endosomal origin released by the majority of cell types, either normal and cancerous [19]. Exosomes and other classes of extracellular vesicles (EVs) play an essential role in cancer biology, being the key mediators of communication between cells [20,21]. EVs present in the blood and other biofluids represent an interesting type of so-called liquid biopsy, which is an emerging source of potential biomarkers with applicability in treatment personalization [22,23]. There is a growing evidence for the increased level of EVs in the biofluids of cancer patients as well as the radiation-induced enhancement of exosome secretion [24,25]. Even though literature data support the important role of transcriptome and proteome content of cancer-related EVs, much less is known about their metabolome component [20]. Similarly, the data regarding radiation-induced changes in the EVs' cargo refer mainly to its transcriptome and proteome [26,27]. Hence, through searching for cancer-related and RT-induced changes in the serum metabolome of HNC patients, we aimed to address the metabolite profiles of serum-derived EVs.

2. Materials and Methods

2.1. Samples Collection

Ten patients with squamous cell carcinoma located in pharynx regions (6 males and 4 females, aged between 49 and 71 years) treated by the continuous accelerated irradiation (CAIR) scheme with a daily fraction dose of 1.8 Gy to the total dose of 64–72 Gy were included in the study. Blood samples were collected before RT (cancer pre-treatment sample A) and one month after the end of RT (cancer post-treatment sample B). The control group constituted of ten age- and sex-matched healthy volunteers (control sample C). This study was approved by the appropriate local Ethics Committee (NRIO; approval no. 1/2016) and all participants provided informed consent indicating their conscious

and voluntary participation. 5 milliliters of blood was collected into an anticoagulant-free tube (Becton Dickinson, Franklin Lakes, NJ, USA; 367955), incubated for 30 min at 20 °C then centrifuged at 1000× *g* for 10 min at 4 °C. The serum (supernatant) was transferred to clean tubes stored at −80 °C until analysis.

2.2. Exosomes Isolation and Characterization

The method for the isolation of exosomes from small amounts of serum was established and optimized in our laboratory as described previously [28]. Briefly, exosomes were isolated from serum (500 µL) by differential centrifugation (1000× *g* and 10,000× *g* for 10 and 30 min, respectively, at 4 °C) and filtration through a 0.22 µm filter followed by the size exclusion chromatography (SEC). SEC was performed using hand-packed columns (BioRad) filled with 10 mL of Sepharose CL-2B (GE Healthcare), conditioned previously with phosphate buffer saline (PBS). Consecutive fractions (500 µL each) were collected and characterized for EV enrichment (fraction #8 was used for further analyses). The size of vesicles in the SEC fractions was evaluated by the dynamic light scattering (DLS) using Zetasizer Nano-ZS90 instrument (Malvern Instruments, Malvern, UK) and by transmission electron microscopy. Exosome markers CD63 and CD81 were analyzed by Western blots as reported in detail elsewhere [28]. The concentration of proteins in the analyzed samples was assessed using the PierceTM BCA Protein Assay kit (Thermo Fisher Scientific, Waltham, MA, USA; 23225) according to the manufacturer's instructions.

2.3. Metabolite Extraction

Two-hundred microliters of 80% MeOH was added to 25 µL of serum sample. In the case of exosomes, 2 mL of 100% MeOH was added to 500 µL of the selected SEC fraction. The mixture was vortexed and centrifuged for 5 min followed by sonication for 10 min. The mixture was placed at −20 °C for 20 min and after that centrifuged for 10 min at 23,000× *g* at 4 °C. The supernatant was transferred to a new tube and evaporated in a SpeedVac concentrator (CentriVap Concentrator, Labconco, USA). The dried extract was then derivatized with 25 µL of methoxyamine hydrochloride in pyridine (20 mg/mL) at 37 °C for 90 min with agitation. The second step of derivatization was performed by adding 40 µL of MSTFA (*N*-Trimethylsilyl-*N*-methyl trifluoroacetamide) and incubation at 37 °C for 30 min with agitation. Samples were subjected to GC/MS analysis directly after derivatization.

2.4. GC–MS Analysis

The GS/MS analysis was performed using TRACE 1310 gas chromatograph connected with TSQ8000 triple-quad mass spectrometer (Thermo Scientific, Waltham, Massachusetts, USA). A DB-5MS bonded-phase fused-silica capillary column (30 m length, 0.25 mm inner diameter, 0.25 µm film thickness) (J&W Scientific Co., Folsom, California, USA) was used for separation. The GC oven temperature gradient was as follows: 70 °C for 2 min, followed by 10 °C/min up to 300 °C (10 min), 2 min at 70 °C, raised by 8 °C/min to 300 °C and held for 16 min at 300 °C. For sample injection, a PTV (Programmable Temperature Vaporization) injector was used in a range of 60–250 °C, transfer line temperature was set to 250 °C, and source to 250 °C. Spectra were recorded in m/z range of 50–850 in EI+ mode with an electron energy of 70 eV. Raw MS-data were converted to abf format and analyzed using MSDial software package v. 3.96. To eliminate the retention time (Rt) shift and to determine the retention indexes (RI) for each compound, the alkane series mixture (C-10 to C-36) was injected into the GC/MS system. Identified artifacts (alkanes, column bleed, plasticizers, MSTFA, and reagents) were excluded from further analyses. Obtained normalized (using total ion current (TIC) approach) results were then exported to Excel for pre-formatting and then used for statistical analyses.

2.5. Statistical and Chemometric Analyses

Differences between independent samples were assessed using the T-test, Welch test, or U-Mann–Whitney test, dependent on the normality and homoscedasticity of data (assessed via the

Shapiro–Wilk test and Levene test, respectively). For paired samples, the paired *t*-test or Wilcoxon test were used based on the normality of the difference distribution. In each case, the Benjamini–Hochberg protocol was used for the false discovery rate (FDR) correction. However, due to the small sample size, none of the differences remained significant after the FDR correction. Hence, the effect size analysis was employed to overcome this problem [29]. For independent samples, the rank-biserial coefficient of correlation (RBCC; an effect size equivalent of the U-Mann–Whitney test) was applied; the effect sizes ≥ 0.3 and ≥ 0.5 were considered medium and high, respectively [30]. For paired samples, the paired *t*-test derived Cohen's d effect size was applied; the effect sizes ≥ 0.5 and ≥ 0.8 were considered medium and high, respectively [31]. Principal component analysis (PCA) and hierarchical cluster analysis (HCA) based on the Euclidean distance method were performed to illustrate general similarities between samples. Metabolic pathways were associated with differentiating compounds that showed high and medium effect sizes using the quantitative enrichment analysis on the MetaboAnalyst platform (https://www.metaboanalyst.ca/MetaboAnalyst/ModuleView.xhtml). Obtained enriched pathways and their connections together with statistical information were further analyzed in Cytoscape. The DyNet addon was used to compare two networks and find interacting nodes [32]; the fold enrichment and significance of enrichment (FDR) were coded by the size and color of nodes, respectively.

3. Results

Extracellular vesicles (EVs) isolated from serum by size exclusion chromatography were characterized by their size and the presence of specific biomarkers. The SEC fraction #8 was enriched in vesicles, in which size was estimated in a range between 50 and 150 nm by the DLS measurement (with the maximum at 100–120 nm) (Figure 1A). The size of the isolated vesicles was confirmed by transmission electron microscopy (TEM) (Figure 1B). Furthermore, the presence of exosome biomarkers, tetraspanins CD63, and CD81, was confirmed in the same fraction by Western blot analysis (the same proteins remained undetected in the whole serum) (Figure 1C). Considering their specific size and the presence of exosome-specific biomarkers, vesicles present in the analyzed fraction were called exosomes for simplicity, yet other subpopulations of the small EVs could be present in this fraction.

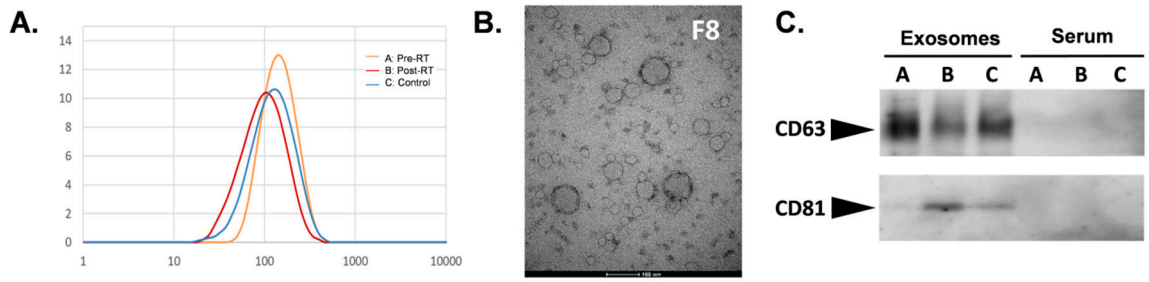

Figure 1. Characterization of serum-derived exosomes. Analysis of the size of vesicles in the size exclusion chromatography (SEC) fraction #8 by the dynamic light scattering (**A**) and transmission electron microscopy (**B**). (**C**) Western blot analysis of CD63 and CD81 in whole serum and serum-derived exosomes (fraction #8) for the three groups of samples (**A**: pre-radiotherapy (RT), **B**: post-RT, **C**: control).

The GC–MS-based approach was used to profile the metabolites in the whole serum and the corresponding serum-derived exosomes of HNC patients, in either pre-treatment (A) and post-treatment (B) samples, or samples of matched healthy controls (C). In general, the untargeted approach allowed to identify 182 metabolites in serum samples and 46 metabolites in exosome samples, of which 33 metabolites overlapped; the complete list of 195 identified compounds is presented in Supplementary Table S1. Figure 2 illustrates the distribution of different classes of small metabolites identified by GC–MS in serum and serum-derived exosome samples. Among the most abundant classes of metabolites common for serum and exosomes were fatty acids, sugar alcohols, and carboxylic acids (22%, 15%, and 12% of all identified compounds, respectively). It is noteworthy that amino acids

that were the largest group of metabolites in serum samples that were markedly less frequent in exosome samples (21% vs. 7% of all identified compounds, respectively, which corresponded to 40 and 3 compounds). All identified metabolites were used to perform the unsupervised clustering of samples. The metabolite composition of the whole serum enabled the relatively good separation of all three groups of samples using either the principal component analysis (Figure 3A) or the hierarchical cluster analysis (Figure 4A). Interestingly, control samples C were more similar to cancer pre-treatment samples A than to cancer post-treatment samples B, which indicated the additional putative treatment-related differential component. In contrast, neither the PCA or the HCA type of analysis allowed the separation of corresponding groups when samples of serum-derived exosomes were analyzed (Figures 3B and 4B).

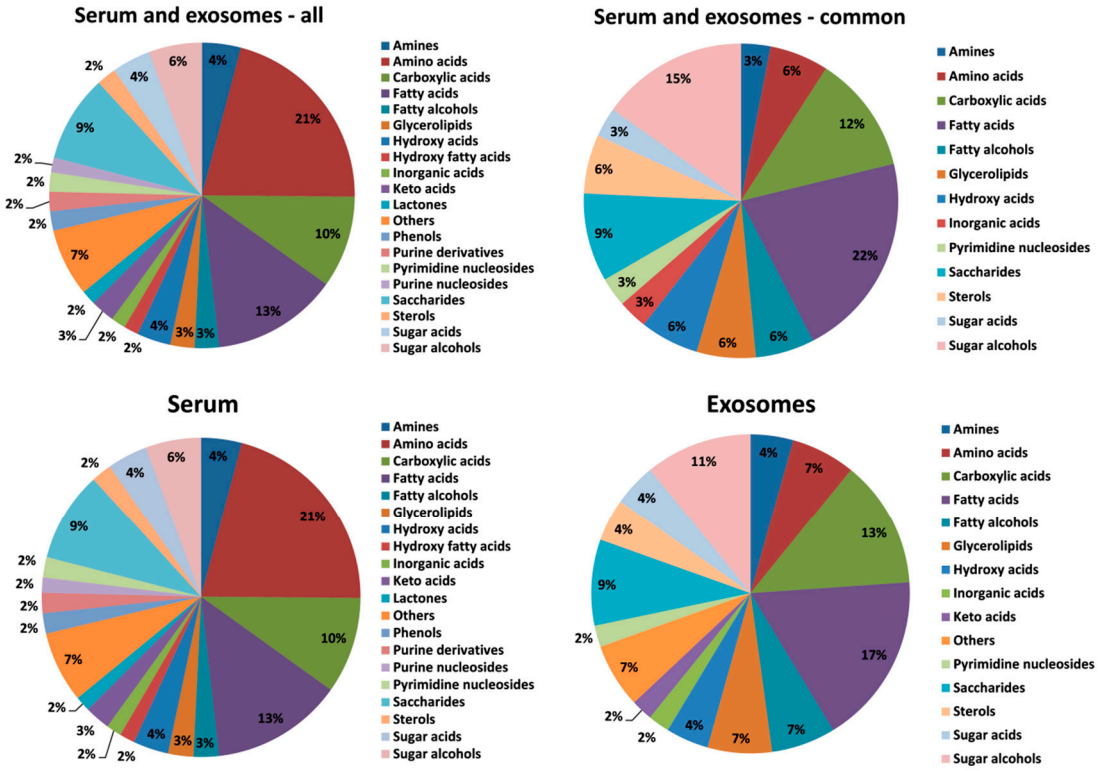

Figure 2. The relative contribution of different classes of metabolites present in serum and serum-derived exosomes (metabolites detected in all types of analyzed samples were considered).

In the next step, we detected specific metabolites for which abundances were significantly different between groups. First, we looked for compounds that differentiated cancer patients (pre-treatment samples A) from healthy individuals (control samples C). There were 27 compounds for which serum levels were markedly different (large effect size; RBCC effect size ≥ 0.5) between control and cancer samples. These included 12 upregulated metabolites (four amino acids, four fatty acids, two purines, one glycerolipid, and lactose) and 15 downregulated metabolites (three carboxylic acids, three purines, three sugars, two fatty acids, serotonin, acetyl-hexosamine, isoleucine, and phosphate) in cancer samples, listed in Table 1. Furthermore, there were 18 cancer-upregulated and 38 cancer-downregulated compounds where differences showed a medium effect size (RBCC effect size ≥ 0.3) (Supplementary Table S1). On the other hand, there were only a few compounds whose abundance was significantly different in serum-derived exosomes from healthy controls and cancer patients. 1-Hexadecanol was markedly upregulated while citric acid, 4-hydroxybenzoic acid, and propylene glycol were markedly downregulated (large effect size) in exosomes from cancer patients (Table 1). Moreover, there were seven metabolites where differences showed no medium effect size, including myo-inositol, linoleic acid, succinic acid, and glyceric acid downregulated in

cancer samples (Supplementary Table S1). Metabolites for which levels were different between control and cancer samples (either a large effect size or medium effect size) were annotated with their corresponding metabolic pathways. Interestingly, the overrepresented pathways associated with metabolites discriminating cancer patients and healthy controls (i.e., cancer-specific pattern) in both whole serum and serum-derived exosome samples included ones involved in energy production (citric acid cycle, Warburg effect, pyruvate metabolism, mitochondrial electron transport chain) and inositol metabolism. Pathways associated specifically with serum metabolites included the metabolism of amino acids, sugars, and lipids. On the other hand, pathways associated with metabolites specific for serum-derived exosomes included the oxidation of fatty acids and ketone body metabolism (Figure 5A).

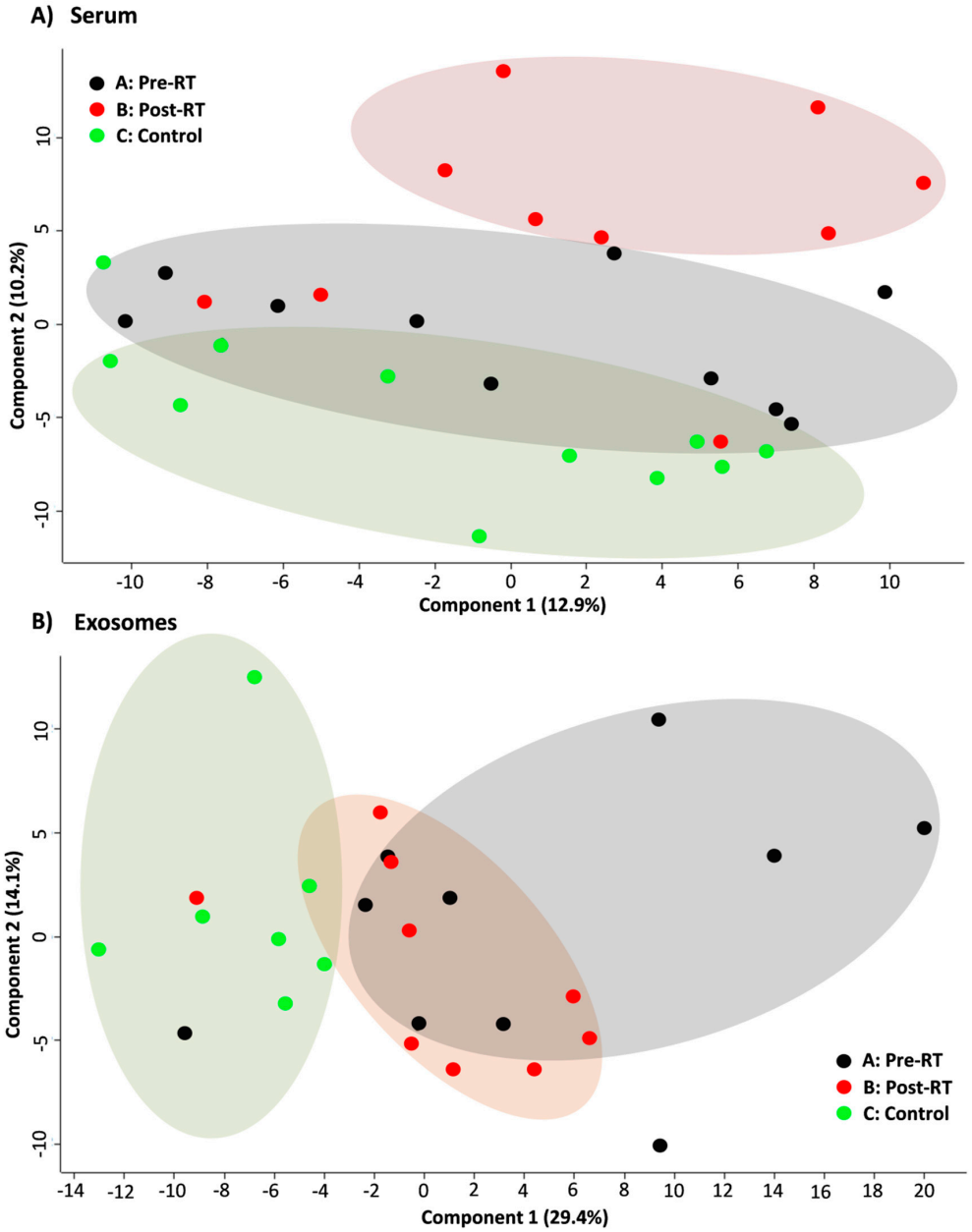

Figure 3. PCA score plots showing the clustering of cancer pre-RT samples A, cancer post-RT samples B, and control samples C. Shown are two the first components responsible for 23.1% of the variability of the serum samples (panel **A**) and 43.5% of the variability for the exosome samples (panel **B**).

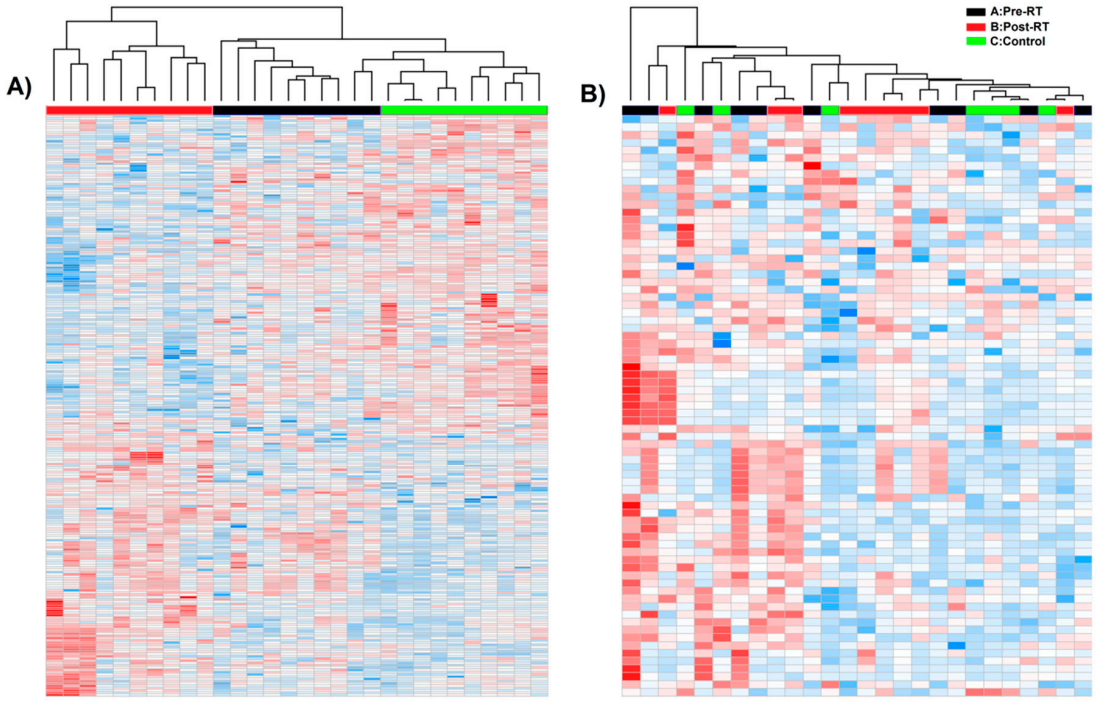

Figure 4. Hierarchical cluster analysis of cancer pre-RT samples A, cancer post-RT samples B, and control samples C. Shown are separate dendrograms for serum samples (panel **A**) and exosome samples (panel **B**).

Then, we looked for metabolites with an abundance that was different in serum and serum-derived exosomes of cancer patients between pre-RT samples A and post-RT samples B, to allow the detection of changes related to radiotherapy. There were 12 compounds with serum levels that were markedly different (large effect size; Cohen's d effect size ≥ 0.8) between pre-RT and post-RT cancer samples. These included four metabolites that were upregulated (including hypotaurine and serotonin) and eight metabolites that were downregulated in post-RT serum samples, listed in Table 2. Furthermore, there were 29 RT-upregulated and 12 RT-downregulated compounds where differences showed a medium effect size (Cohen's d effect size ≥ 0.5) (Supplementary Table S1). In marked contrast, only two metabolites detected in serum-derived exosomes (glycerol and cholesterol) showed reduced levels (medium effect size) in post-RT samples. Finally, metabolites with an abundance different in the pre-RT and post-RT samples (either large effect size or medium effect size) were annotated with their corresponding metabolic pathways. Over represented pathways associated with metabolites with serum level affected by RT included those involved in the metabolism of different classes of compounds (amino acids, sugars, nucleotides, lipids, and biogenic amines), which indicated multifaceted effects of radiation on the serum metabolome profile (Figure 5B).

Table 1. Metabolites that differentiated cancer patients and healthy individuals. Listed are compounds where differences between head and neck cancer (HNC) patients (samples A) and healthy controls (samples C) showed a large effect size (RBCC effect size ≥ 0.5).

Metabolite Name	Class	Mean Abundance in Cancer (Samples A)	Mean Abundance in Control (Samples C)	Significance of Differences between Control and Cancer (RBCC Effect Size)
		Serum Metabolites		
		Upregulated in Cancer		
Myristic acid	Fatty acids	3.90×10^{-3}	3.18×10^{-3}	0.82
Hypoxanthine	Purines	3.48×10^{-4}	1.46×10^{-4}	0.76
L-Glutamic acid	Amino acids	4.97×10^{-3}	2.34×10^{-3}	0.70
Xanthine	Purines	2.96×10^{-5}	2.01×10^{-5}	0.66
beta-Lactose	Saccharides	2.41×10^{-5}	9.82×10^{-6}	0.64
L-Serine	Amino acids	8.19×10^{-3}	6.07×10^{-3}	0.60
Oleic acid monoglyceride	Glycerolipids	2.41×10^{-5}	3.14×10^{-5}	0.60
O-Acetylserine	Amino acids	4.37×10^{-3}	3.60×10^{-3}	0.58
Eicosenoic acid	Fatty acids	3.61×10^{-5}	2.18×10^{-5}	0.58
Palmitoleic acid	Fatty acids	1.02×10^{-3}	3.12×10^{-4}	0.56
Oleamide	Fatty acids	6.71×10^{-5}	1.72×10^{-5}	0.54
L-Aspartic acid	Amino acids	2.02×10^{-3}	1.32×10^{-3}	0.52
		Downregulated in Cancer		
Inosine	Purines	4.55×10^{-5}	4.28×10^{-4}	−1.00
Salicylic acid	Carboxylic acids	6.74×10^{-6}	8.44×10^{-4}	−0.92
Adenosine	Purines	1.27×10^{-5}	5.74×10^{-5}	−0.89
2-Ethylhexanoic acid	Fatty acids	1.14×10^{-4}	2.51×10^{-4}	−0.74
Gentisic acid	Carboxylic acids	6.36×10^{-6}	1.56×10^{-5}	−0.64
D-Threitol	Sugar alcohols	2.01×10^{-4}	2.88×10^{-4}	−0.64
Oxalic acid	Carboxylic acids	2.08×10^{-2}	2.47×10^{-2}	−0.62
Paraxanthine	Purines	1.94×10^{-4}	4.26×10^{-4}	−0.62
Serotonin	Amines	5.43×10^{-5}	1.06×10^{-4}	−0.60
D-Ribose	Saccharides	1.50×10^{-4}	1.51×10^{-4}	−0.60
N-acetyl-d-hexosamine	Amines	6.21×10^{-5}	1.69×10^{-5}	−0.57
Nonanoic acid	Fatty acids	2.23×10^{-4}	2.67×10^{-4}	−0.56
D-Xylonic acid	Sugar acids	3.07×10^{-5}	4.48×10^{-5}	−0.56
Phosphate	Inorganic acids	1.40×10^{-2}	1.64×10^{-2}	−0.54
L-Isoleucine	Amino acids	2.69×10^{-3}	3.30×10^{-3}	−0.52
		Exosome Metabolites		
		Upregulated in Cancer		
1-Hexadecanol	Fatty alcohols	5.81×10^{-5}	3.12×10^{-5}	0.52
		Downregulated in Cancer		
4-Hydroxybenzoic acid	Carboxylic acids	8.05×10^{-7}	2.61×10^{-5}	−0.66
Citric acid	Carboxylic acids	8.58×10^{-6}	3.22×10^{-4}	−0.54
Propylene glycol	Others	2.89×10^{-5}	1.96×10^{-4}	−0.52

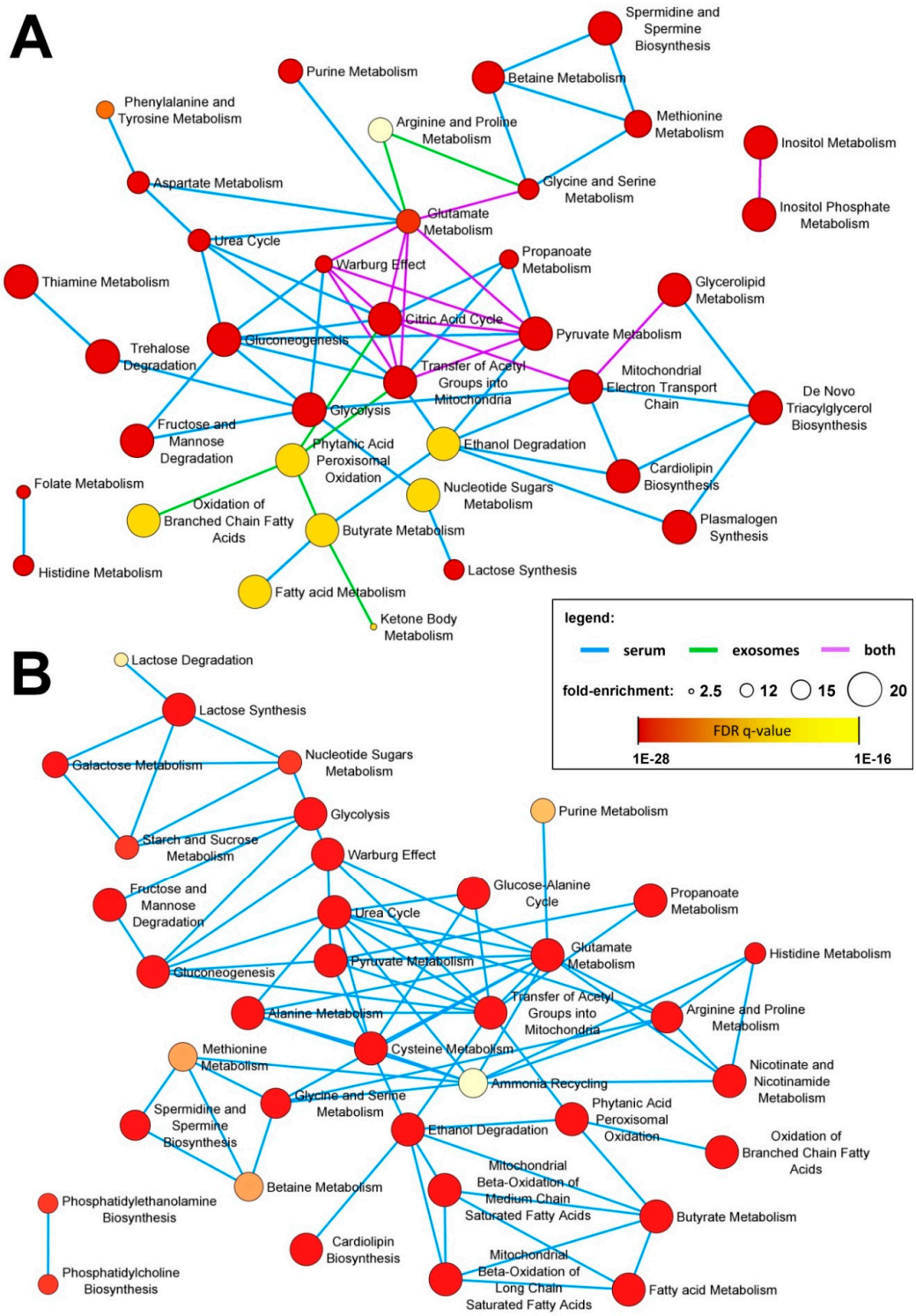

Figure 5. Metabolic pathways associated with specific subsets of compounds detected in the whole serum and serum-derived exosomes. Illustrated are over represented pathways associated with metabolites differentiating between cancer and control samples (panel **A**) and between pre-RT and post-RT samples (panel **B**); metabolites that showed large and medium effect size were included. The size of the network nodes corresponds to the pathway's fold-enrichment while the statistical significance of the over-representation is color coded.

Table 2. Metabolites that were affected by radiotherapy. Listed are compounds where differences between paired pre-RT (samples A) and post-RT (samples C) specimens showed a large effect size (Cohen's d effect size ≥ 0.8).

Metabolite Name	Class	Mean Abundance Pre-RT (Samples A)	Mean Abundance Post-RT (Samples B)	Significance of Differences between Pre-RT and Post-RT (Cohen's D Effect Size)
Serum Metabolites				
Upregulated by RT				
Hypotaurine	Others	6.48×10^{-5}	1.09×10^{-4}	−1.16
Glycerol-1-phosphate	Glycerolipids	1.03×10^{-4}	1.46×10^{-4}	−1.06
Oleamide	Fatty acids	6.71×10^{-5}	1.77×10^{-4}	−0.81
Serotonin	Amines	5.43×10^{-5}	6.71×10^{-5}	−0.81
Downregulated by RT				
1-Methylhistidine	Amino acids	1.13×10^{-4}	7.84×10^{-5}	0.96
Urea	Others	1.81×10^{-4}	4.76×10^{-2}	0.96
Quinic acid	Others	7.48×10^{-5}	5.60×10^{-5}	0.87
2-ketoglucose dimethylacetal	Hydroxy acids	1.68×10^{-4}	7.86×10^{-5}	0.85
4-Deoxyerythronic acid	Sugar acids	4.44×10^{-5}	2.77×10^{-5}	0.85
Galactosylglycerol	Glycerolipids	4.55×10^{-5}	1.69×10^{-5}	0.85
Gentisic acid	Carboxylic acids	6.36×10^{-6}	3.78×10^{-6}	0.85
D-Xylitol	Sugar alcohols	2.29×10^{-4}	1.49×10^{-4}	0.82

4. Discussion

Serum-derived exosomes, an emerging type of liquid biopsy, are a potential source of biomarkers. However, their metabolite compartment is less characterized compared to proteome or miRNome [20]. Here, we compared the metabolite profiles of whole human serum and serum-derived exosomes, and found significantly fewer compounds in the latter specimen. This difference could be caused by both a lower number of compounds present in vesicles per se (i.e., putatively lower molecular complexity) or their lower concentration, which hindered their detection by the method used in our approach. Hence, a direct comparison of metabolic pathways associated with compounds present in the whole serum and serum-derived vesicles could be compromised by this discrepancy. However, it has to be emphasized that the major metabolic hallmark of cancer—the modified energy metabolism could be detected in both specimens. In head and neck cancer, as in many other types of cancers, tumor cells can alter their energy metabolism by switching from the citric acid cycle (TCA cycle) to the aerobic glycolysis and oxidation of fatty acids as a backup mechanism for energy production [16], a phenomenon which is known as the Warburg effect [33]. Our study confirmed that metabolites associated with processes involved in energy metabolism, including glycolysis, gluconeogenesis, Warburg effect, TCA cycle, pyruvate metabolism, and mitochondrial electron transport chain showed different levels in samples of HNC patients and healthy controls. Importantly, features associated with this characteristic cancer phenotype were observed in both whole serum and serum-derived exosomes. Noteworthy, however, different types of cells and tissues, both cancerous and normal, release exosomes circulating in the blood and regulate the metabolome of the whole serum. Nevertheless, pathways associated with metabolites specific for serum-derived exosomes of cancer patients included oxidation of fatty acids and ketone body metabolism. The beta-oxidation of fatty acids and increased lipolysis, which is reflected as the accumulation of ketone bodies, was reported in HNC patients as a potential backup mechanism for energy production [12]. Previous studies reported that molecules involved in fatty acids transport and storage as well as lipolysis and fatty acids oxidation are enriched in EVs and suggested that fatty acid transport from cell to cell and across cell membranes could be mediated

by EVs [34,35]. Hence, a specific role of serum EVs in the transmission of mediators associated with cancer-related lipid metabolism deserves further attention.

Our study revealed that RT affected the serum levels of several amino acids, biogenic amines, sugars, nucleotides, lipids, and fatty acids, which mirrored potential RT-induced changes in a plethora of metabolic pathways ongoing in a patients' body. It is noteworthy that different radiation-related mechanisms might contribute to metabolic changes observed in samples collected one month after the end of RT, including toxicity induced by radiation in normal tissues and a reduced number of cancer cells. It was previously reported that the altered metabolism of amino acid plays an important role in the response of HNC patients to RT [36]. For example, Boguszewicz and co-workers [4] demonstrated that a decreased serum level of alanine, the main substrate for gluconeogenesis during fasting and cachexia, correlated with the acute radiation toxicity-associated weight loss in HNC patients undergoing RT. The whole-body response to irradiation frequently involves molecules associated with oxidative stress and inflammation [18]. Hence, it is noteworthy that hypotaurine, which is involved in protection against oxidative stress as an effect of RT [37], was significantly elevated in post-RT serum samples. Moreover, RT-induced changes in the serum level of phospholipids potentially associated with the inflammatory response and disruption of plasma membranes were previously reported in samples of HNC patients [38,39]. Here, we found that compounds associated with lipid metabolism (e.g., phosphatidylethanolamine and phosphatidylcholine biosynthesis) were affected in post-RT serum samples, which confirmed the general RT-related metabolic phenotype. Interestingly, very few RT-related changes were detected in the metabolic profile of serum-derived exosomes. This was in contrast to the significant radiation-induced changes observed at the level of the proteome [40] and miRNome [41] of exosomes released by HNC cells. Exosomes released by irradiated cells are known mediators of radiation bystander effect and other aspects of radiation-related cell-to-cell signaling [42]. Hence, the potential role of metabolites in exosomes-mediated radiation-related signaling should be addressed in further studies.

5. Conclusions

In this pilot study, we compared the metabolite profiles of the whole serum and serum-derived exosomes in healthy controls and patients treated with RT due to a head and neck cancer aiming to reveal cancer-related features (by the comparison of cancer and control samples) and RT-related features (by the comparison of cancer pre-RT and post-RT samples). We found that the metabolite profile of serum-derived exosomes is putatively less complex and consists of fewer components than that of the complete serum. However, cancer-related features of energy metabolism were detected in both types of specimens, which confirmed the feasibility of cancer biomarkers based on exosome metabolites. On the other hand, in contrast to RT-induced changes observed in serum metabolome, this pilot study did not reveal a specific pattern of radiotherapy-related changes in exosome metabolites. Hence, further metabolomics study with a larger cohort of individuals treated with RT is necessary to validate a hypothetical radiation signature of serum exosomes.

Supplementary Materials: The following are available online at http://www.mdpi.com/2075-4426/10/4/229/s1, Table S1: Metabolites identified in human serum and serum-derived exosomes.

Author Contributions: Conceptualization, M.P.; methodology, L.M.; formal analysis, L.M.; investigation, A.Z. and A.S.; resources, T.R.; data curation, A.W., L.M. and K.P.; writing—original draft preparation, A.W., A.Z.; writing—review and editing, P.W.; visualization, A.W. and L.M.; supervision, M.P. All authors have read and agreed to the published version of the manuscript.

Funding: This research was funded by the National Science Centre, Poland, grant no. 2015/17/B/NZ5/01387 (M.P., T.R., P.W.), 2016/22/M/NZ5/00667 (A.Z., A.S., M.P.), and 2017/26/D/NZ2/00964 (A.W., L.M.).

Conflicts of Interest: The authors declare no conflict of interest.

References

1. Gupta, B.; Johnson, N.W.; Kumar, N. Global epidemiology of head and neck cancers: A Continuing Challenge. *Oncology* **2016**, *91*, 13–23. [CrossRef]
2. Budach, V.; Tinhofer, I. Novel prognostic clinical factors and biomarkers for outcome prediction in head and neck cancer: A systematic review. *Lancet Oncol.* **2019**, *20*, e313–e326. [CrossRef]
3. Economopoulou, P.; de Bree, R.; Kotsantis, I.; Psyrri, A. Diagnostic tumor markers in head and neck squamous cell carcinoma (HNSCC) in the clinical setting. *Front. Oncol.* **2019**, *9*, 827. [CrossRef]
4. Boguszewicz, Ł.; Bieleń, A.; Mrochem-Kwarciak, J.; Skorupa, A.; Ciszek, M.; Heyda, A.; Wygoda, A.; Kotylak, A.; Składowski, K.; Sokół, M. NMR-based metabolomics in real-time monitoring of treatment induced toxicity and cachexia in head and neck cancer: A method for early detection of high risk patients. *Metabolomics* **2019**, *15*, 110. [CrossRef]
5. Baskar, R.; Lee, K.A.; Yeo, R.; Yeoh, K.W. Cancer and radiation therapy: Current advances and future directions. *Int. J. Med. Sci.* **2012**, *9*, 193–199. [CrossRef]
6. Darby, S.C.; Cutter, D.J.; Boerma, M.; Constine, L.S.; Fajardo, L.F.; Kodama, K.; Mabuchi, K.; Marks, L.B.; Mettler, F.A.; Pierce, L.J.; et al. Radiation-related heart disease: Current knowledge and future prospects. *Int. J. Radiat. Oncol. Biol. Phys.* **2010**, *76*, 656–665. [CrossRef]
7. Travis, L.B.; Ng, A.K.; Allan, J.M.; Pui, C.H.; Kennedy, A.R.; Xu, X.G.; Purdy, J.A.; Applegate, K.; Yahalom, J.; Constine, L.S.; et al. Second malignant neoplasms and cardiovascular disease following radiotherapy. *Health Phys.* **2014**, *106*, 229–246. [CrossRef]
8. Pinu, F.R.; Beale, D.J.; Paten, A.M.; Kouremenos, K.; Swarup, S.; Schirra, H.J.; Wishart, D. Systems biology and multi-omics integration: Viewpoints from the Metabolomics Research Community. *Metabolites* **2019**, *9*, 76. [CrossRef]
9. Wheelock, C.E.; Goss, V.M.; Balgoma, D.; Nicholas, B.; Brandsma, J.; Skipp, P.J.; Snowden, S.; Burg, D.; D'Amico, A.; Horvath, I.; et al. Application of 'omics technologies to biomarker discovery in inflammatory lung diseases. *Eur. Respir. J.* **2013**, *42*, 802–825. [CrossRef]
10. Patel, S.; Ahmed, S. Emerging field of metabolomics: Big promise for cancer biomarker identification and drug discovery. *J. Pharm. Biomed. Anal.* **2015**, *107*, 63–74. [CrossRef]
11. Armitage, E.G.; Barbas, C. Metabolomics in cancer biomarker discovery: Current trends and future perspectives. *J. Pharm. Biomed. Anal.* **2014**, *87*, 1–11. [CrossRef] [PubMed]
12. Tiziani, S.; Lopes, V.; Günther, U.L. Early stage diagnosis of oral cancer using 1H NMR-Based metabolomics1,2. *Neoplasia* **2009**, *11*, 269–276. [CrossRef] [PubMed]
13. Yonezawa, K.; Nishiumii, S.; Kitamoto-Matsuda, J.; Fujita, T.; Morimoto, K.; Yamashita, D.; Saito, M.; Otsuki, N.; Irino, Y.; Shinohara, M.; et al. Serum and tissue metabolomics of head and neck cancer. *Cancer Genom. Proteom.* **2013**, *10*, 233–238.
14. Hsieh, Y.T.; Chen, Y.F.; Lin, S.C.; Chang, K.W.; Li, W.C. Targeting cellular metabolism modulates head and neck oncogenesis. *Int. J. Mol. Sci.* **2019**, *20*, 3960. [CrossRef]
15. Kasiappan, R.; Kamarajan, P.; Kapila, Y.L. Metabolomics in head and neck cancer: A summary of findings. *Transl. Syst. Med. Oral. Dis.* **2019**, 119–135.
16. Shin, J.M.; Kamarajan, P.; Christopher Fenno, J.; Rickard, A.H.; Kapila, Y.L. Metabolomics of head and neck cancer: A mini-review. *Front. Physiol.* **2016**, *7*, 526. [CrossRef]
17. Rai, V.; Mukherjee, R.; Ghosh, A.K.; Routray, A.; Chakraborty, C. "Omics" in oral cancer: New approaches for biomarker discovery. *Arch. Oral Biol.* **2018**, *87*, 15–34. [CrossRef]
18. Jelonek, K.; Pietrowska, M.; Widlak, P. Systemic effects of ionizing radiation at the proteome and metabolome levels in the blood of cancer patients treated with radiotherapy: The influence of inflammation and radiation toxicity. *Int. J. Radiat. Biol.* **2017**, *93*, 683–696. [CrossRef]
19. Doyle, L.; Wang, M. Overview of extracellular vesicles, their origin, composition, purpose, and methods for exosome isolation and analysis. *Cells* **2019**, *8*, 727. [CrossRef]
20. Zebrowska, A.; Skowronek, A.; Wojakowska, A.; Widlak, P.; Pietrowska, M. Metabolome of exosomes: Focus on vesicles released by cancer cells and present in human body fluids. *Int. J. Mol. Sci.* **2019**, *20*, 3461. [CrossRef]

21. Tian, W.; Liu, S.; Li, B. Potential role of exosomes in cancer metastasis. *Biomed. Res. Int.* **2019**, *2019*, 4649705. [CrossRef] [PubMed]
22. Pang, B.; Zhu, Y.; Ni, J.; Thompson, J.; Malouf, D.; Bucci, J.; Graham, P.; Li, Y. Extracellular vesicles: The next generation of biomarkers for liquid biopsy-based prostate cancer diagnosis. *Theranostics* **2020**, *10*, 2309–2326. [CrossRef] [PubMed]
23. Marrugo-Ramírez, J.; Mir, M.; Samitier, J. Blood-based cancer biomarkers in liquid biopsy: A promising non-invasive alternative to tissue biopsy. *Int. J. Mol. Sci.* **2018**, *19*, 2877. [CrossRef] [PubMed]
24. Jelonek, K.; Widlak, P.; Pietrowska, M. The influence of ionizing radiation on exosome composition, secretion and intercellular communication. *Protein Pept. Lett.* **2016**, *23*, 656–663. [CrossRef]
25. Jabbari, N.; Nawaz, M.; Rezaie, J. Ionizing radiation increases the activity of exosomal secretory pathway in MCF-7 human breast cancer cells: A possible way to communicate resistance against radiotherapy. *Int. J. Mol. Sci.* **2019**, *20*, 3649. [CrossRef]
26. Zorrilla, S.R.; García, A.G.; Carrión, A.B.; Vila, P.G.; Martín, M.S.; Torreira, M.G.; Sayans, M.P. Exosomes in head and neck cancer. Updating and revisiting. *J. Enzyme Inhib. Med. Chem.* **2019**, *34*, 1641–1651. [CrossRef]
27. Xiao, C.; Song, F.; Zheng, Y.L.; Lv, J.; Wang, Q.F.; Xu, N. Exosomes in head and neck squamous cell carcinoma. *Front. Oncol.* **2019**, *9*, 894. [CrossRef]
28. Smolarz, M.; Pietrowska, M.; Matysiak, N.; Mielańczyk, Ł.; Widłak, P. Proteome profiling of exosomes purified from a small amount of human serum: The problem of co-purified serum components. *Proteomes* **2019**, *7*, 18. [CrossRef]
29. Sullivan, G.M.; Feinn, R. Using effect size—Or why the p value is not enough. *J. Grad. Med. Educ.* **2012**, *4*, 279–282. [CrossRef]
30. Cureton, E.E. Rank-biserial correlation. *Psychometrika* **1956**, *21*, 287–290. [CrossRef]
31. Rosenthal, R. Parametric measures of effect size. In *The Handbook of Research Synthesis*; Cooper, H., Hedges, L.V., Valentine, J.C., Eds.; Russell Sage Foundation: New York, NY, USA, 1994; pp. 231–244, References-Scientific Research Publishing; Available online: https://www.scirp.org/(S(351jmbntvnsjt1aadkposzje))/reference/ReferencesPapers.aspx?ReferenceID=1985786 (accessed on 13 July 2020).
32. Goenawan, I.H.; Bryan, K.; Lynn, D.J. DyNet: Visualization and analysis of dynamic molecular interaction networks. *Bioinformatics* **2016**, *32*, 2713–2715. [CrossRef] [PubMed]
33. Warburg, O. On the origin of cancer cells. *Science* **1956**, *123*, 309–314. [CrossRef] [PubMed]
34. Lazar, I.; Clement, E.; Attane, C.; Muller, C.; Nieto, L. Thematic review series: Exosomes and microvesicles: Lipids as key components of their biogenesis and functions: A new role for extracellular vesicles: How small vesicles can feed tumors' big appetite. *J. Lipid Res.* **2018**, *59*, 1793–1804. [CrossRef] [PubMed]
35. Record, M.; Carayon, K.; Poirot, M.; Silvente-Poirot, S. Exosomes as new vesicular lipid transporters involved in cell–cell communication and various pathophysiologies. *Biochim. Biophys. Acta Mol. Cell Biol. Lipids.* **2014**, *1841*, 108–120. [CrossRef]
36. Kim, E.J.; Lee, M.; Kim, D.Y.; Kim, K., II; Yi, J.Y. Mechanisms of energy metabolism in skeletal muscle mitochondria following radiation exposure. *Cells* **2019**, *8*, 950. [CrossRef]
37. Gossai, D.; Lau-Cam, C.A. The effects of taurine, taurine homologs and hypotaurine on cell and membrane antioxidative system alterations caused by type 2 diabetes in rat erythrocytes. *Adv. Exp. Med. Biol.* **2009**, *643*, 359–368.
38. Jelonek, K.; Pietrowska, M.; Ros, M.; Zagdanski, A.; Suchwalko, A.; Polanska, J.; Marczyk, M.; Rutkowski, T.; Skladowski, K.; Clench, M.R.; et al. Radiation-induced changes in serum lipidome of head and neck cancer patients. *Int. J. Mol. Sci.* **2014**, *15*, 6609–6624. [CrossRef]
39. Jelonek, K.; Krzywon, A.; Jablonska, P.; Slominska, E.M.; Smolenski, R.T.; Polanska, J.; Rutkowski, T.; Mrochem-Kwarciak, J.; Skladowski, K.; Widlak, P. Systemic effects of radiotherapy and concurrent chemo-radiotherapy in head and neck cancer patients—Comparison of serum metabolome profiles. *Metabolites* **2020**, *10*, 60. [CrossRef]
40. Abramowicz, A.; Wojakowska, A.; Marczak, L.; Lysek-Gladysinska, M.; Smolarz, M.; Story, M.D.; Polanska, J.; Widlak, P.; Pietrowska, M. Ionizing radiation affects the composition of the proteome of extracellular vesicles released by head-and-neck cancer cells in vitro. *J. Radiat. Res.* **2019**, *60*, 289–297. [CrossRef]

41. Abramowicz, A.; Łabaj, W.; Mika, J.; Szołtysek, K.; Ślęzak-Prochazka, I.; Mielańczyk, Ł.; Story, M.D.; Pietrowska, M.; Polański, A.; Widłak, P. MicroRNA profile of exosomes and parental cells is differently affected by ionizing radiation. *Radiat. Res.* **2020**, *194*, 133–142. [CrossRef]
42. Kumar Jella, K.; Rani, S.; O'Driscoll, L.; McClean, B.; Byrne, H.J.; Lyng, F.M. Exosomes are involved in mediating radiation induced bystander signaling in human keratinocyte cells. *Radiat. Res.* **2014**, *181*, 138–145. [CrossRef] [PubMed]

Received: 8 September 2020 | Revised: 7 December 2020 | Accepted: 12 January 2021

DOI: 10.1002/jev2.12063

RESEARCH ARTICLE

WILEY

Proteomic profile of melanoma cell-derived small extracellular vesicles in patients' plasma: a potential correlate of melanoma progression

Monika Pietrowska[1] | **Aneta Zebrowska**[1] | **Marta Gawin**[1] | **Lukasz Marczak**[2] | **Priyanka Sharma**[3] | **Sujan Mondal**[3] | **Justyna Mika**[5] | **Joanna Polańska**[5] | **Soldano Ferrone**[6] | **John M. Kirkwood**[3,7] | **Piotr Widlak**[1] | **Theresa L. Whiteside**[3,4]

[1] Maria Sklodowska-Curie National Research Institute of Oncology, Gliwice, Poland

[2] European Center for Bioinformatics and Genomics, Institute of Bioorganic Chemistry PAS, Poznan, Poland

[3] UPMC Hillman Cancer Center, University of Pittsburgh Cancer Institute, Pittsburgh, Pennsylvania, USA

[4] Department of Pathology, University of Pittsburgh School of Medicine, Pittsburgh, Pennsylvania, USA

[5] Department of Data Science and Engineering, Silesian University of Technology, Gliwice, Poland

[6] Department of Surgery, Harvard Medical School, Massachusetts General Hospital, Boston, Massachusetts, USA

[7] Department of Medicine, University of Pittsburgh School of Medicine, Pittsburgh, Pennsylvania, USA

Correspondence
Monika Pietrowska, Maria Sklodowska-Curie National Research Institute of Oncology, Wybrzeże Armii Krajowej 15, 44–102 Gliwice, Poland.
Email: monika.pietrowska@io.gliwice.pl
Theresa L. Whiteside, UPMC Hillman Cancer Center, University of Pittsburgh Cancer Institute, 5115 Centre Ave, Pittsburgh, Pittsburgh, PA 15232, USA.
Email: whitesidetl@upmc.edu

Funding information
Narodowym Centrum Nauki, Grant/Award Number: 2016/22/M/NZ5/00667; US National Institutes of Health, Grant/Award Numbers: R01-CA168628, U01-DE029759

Abstract

Molecular profiling of small extracellular vesicles (sEV) isolated from plasma of cancer patients emerges as promising strategy for biomarkers discovery. We investigated the proteomic profiles of sEV immunoselected using anti-CSPG4 antibodies from 15 melanoma patients' plasma. The proteomes of sEV separated into melanoma cell-derived (MTEX) and non-malignant cell-derived (NMTEX) were compared using high-resolution mass spectrometry. Paired analysis identified the MTEX-associated profile of 16 proteins that discriminated MTEX from NMETEX. We also identified the MTEX profile that discriminated between seven patients with no evidence of melanoma (NED) after therapy and eight with progressive disease (PD). Among 75 MTEX proteins overexpressed in PD patients, PDCD6IP (ALIX) had the highest discriminating value, while CNTN1 (contactin-1) was upregulated only in MTEX of NED patients. This is the first report documenting that proteomes of tumour-derived sEV in patients' plasma discriminate cancer from non-cancer and identify proteins with potential to serve as prognostic biomarkers in melanoma.

KEYWORDS
high-resolution mass spectrometry (HRMS), melanoma cell-derived exosomes (MTEX), proteomics, small extracellular vesicles (sEV), tumour-derived exosomes (TEX)

1 | INTRODUCTION

Melanoma is among the most aggressive and therapy-resistant human cancers. The epidemiology of melanoma is complex, and individual risk depends on the sun and other UV exposure, host genetic factors and their interactions (Shannan et al., 2016; Tripp et al., 2016). The successes of immunotherapy and targeted therapies have vastly changed the treatment and prognosis of melanoma in the last five years. Therapy with immune checkpoint inhibitors (ICIs) has induced long term responses and improved survival in a fraction of patients (Hodi et al., 2010). However, many patients still do not respond to ICIs for reasons that are not clear but are putatively related to the pre-existing tumour-induced immune suppression that is not overcome by ICIs. Tumour cell escape from the host immune system remains the major barrier to successful immunotherapy (Weiss et al., 2019). Numerous cellular and molecular mechanisms responsible for the dysregulation of tumour antigen-specific immune responses in patients with cancer have been identified and studied in the last two decades (Whiteside et al., 2016; Yaguchi & Kawakami, 2016). Among these mechanisms, interactions between cancer cells and the tumour microenvironment (TME) are considered to be critically important for tumour progression (Cai et al., 2018; Whiteside, 2014).

Extracellular vesicles (EV) have recently emerged as an intercellular communication system that mediates the molecular crosstalk between malignant and non-malignant cells in the TME (Maas et al., 2017; Whiteside, 2017). EV are highly heterogeneous and include different vesicle classes varying in size, mechanisms of biogenesis, and molecular cargos (Willms et al., 2018). Small virus-size EV (sEV) that originate from the endocytic compartment of cells are referred to as exosomes, while those produced by cancer cells are referred to as "tumour cell-derived exosomes" (TEX). EV are involved in many aspects of cell-to-cell communication, including interactions between cancer and immune cells (Whiteside, 2017). We and others have reported that TEX play a key role in tumour-induced suppression of immune effector cells and promote tumour growth by autocrine, juxtacrine, or paracrine mechanisms (Ruivo et al., 2017). It has been reported that the molecular content of exosomes mimics that of parent cells. Therefore, TEX could potentially serve as a "liquid biopsy" for non-invasive tumour diagnosis or the assessment of prognosis and are currently of special interest.

Several attempts to characterize EV derived from different types of cancer cells have been made, including studies of TEX derived from cultures of melanoma cell lines (Valenti et al., 2007; Wieckowski et al., 2009). However, only a few studies characterizing TEX among total EV isolated from the blood of melanoma patients have been reported, and these studies highlight the biomarker potential of TEX (Peinado et al., 2012; Sharma et al., 2018). For example, the analysis of exosomes isolated from plasma of patients with stage IV melanoma reported increased levels of vesicular TYRP2, VLA-4, and HSP70, while only TYRP2 levels were elevated in vesicles from the stage III disease when compared to healthy controls (Peinado et al., 2012). However, systematic proteomics analysis of sEV released in vivo from melanoma cells and isolated from the peripheral circulation of melanoma patients has not been reported so far.

The concept of a non-invasive "liquid biopsy" of cancer includes sEV in the patients' peripheral circulation. However, sEV are released into extracellular space by all cell types and, therefore, vesicles present in body fluids represent a heterogeneous mixture of different EV subpopulations. To demonstrate that TEX present in plasma (or other body fluids) of cancer patients can serve as a surrogate of tumour cells, it is necessary to separate TEX from vesicles produced by non-malignant cells. We have recently described an immunocapture-based method that separates melanoma cell-derived TEX (MTEX) from sEV produced by non-malignant cells (NMTEX) (Sharma et al., 2020). A pilot characterization of these exosome fractions using quantitative on-bead flow cytometry and functional assays showed that MTEX were strongly immunosuppressive, but their molecular characterization was limited to a few selected markers related to immune reactivity (Sharma et al., 2020). Here, we have extended the molecular characterization of MTEX present in the plasma of melanoma patients using a comprehensive proteomics approach that allows for a deeper and broader analysis of proteins in MTEX and a better understanding of their molecular and functional significance.

2 | MATERIALS AND METHODS

2.1 | Patients

Blood samples were obtained from patients with melanoma treated at the UPMC Hillman Cancer Center Melanoma Program Outpatient Clinic by John M. Kirkwood, MD, and colleagues. Blood samples were collected for research under the University of Pittsburgh IRB approval #970186. All blood donors signed an informed consent form. The study included specimens collected from 15 melanoma patients (the disease status and clinicopathological information for all patients are listed in the Table S1). In addition, we collected blood specimens from five consented healthy donors (HDs) (IRB approval #04-001) for proteomics analysis of total plasma exosomes. Blood samples were processed to separate plasma which was divided into aliquots and stored at −80°C until thawed and used for exosome isolation.

2.2 | Total plasma exosome isolation

Exosomes were isolated from plasma of patients with melanoma or HDs by the mini-SEC method optimized in our laboratory (Hong et al., 2016). Briefly, plasma samples stored at −80°C were thawed and centrifuged at 2000 x *g* for 10 min followed by another centrifugation at 10,000 x *g* for 30 min at 4°C. Samples were then ultra-filtered through 0.22 μm filters (EMD Millipore, Billerica, MA). An aliquot (1 ml) of plasma was loaded onto a 10 cm-long SEC column and 1 ml fractions were eluted with PBS. The void volume fraction #4 containing the majority of non-aggregated, morphologically intact sEV was collected and used for analyses. Transmission electron microscopy (TEM), the vesicle size range, particle numbers, and protein content of fraction #4 were determined. The phenotype of vesicles was evaluated as previously described (Ludwig et al., 2019, Ludwig et al., 2019). The sEV protein concentration was determined by the BCA method (Pierce Biotechnology, Rockford, CA) as per manufacturer's instructions. sEV were concentrated using Vivaspin 500 (100,000 MWCO, Sartorius, Göttingen, Germany).

2.3 | Immunoaffinity-based separation of MTEX and NMTEX

MTEX (melanoma-derived TEX) were separated from NMTEX using the immunoaffinity capture method as described by us earlier (Sharma et al., 2018; Sharma et al., 2020). Selection of the capture mAb, anti-CSPG4, was based on the extensive analysis of its specificity for chondroitin sulfate peptidoglycan 4 (CSPG4), which selectively recognizes an epitope overexpressed on most (>80%) melanoma cells and melanoma stem cells but is not detectable in normal tissues, except for pericytes as previosly reviewed (Campoli et al., 2010; Ferrone & Whiteside, 2020). Anti-CSPG4 mAbs (clones 763.64 or 225.28) were biotinylated using a one-step antibody biotinylation kit (Novus Biologicals) following the manufacturer's protocol. An aliquot of sEV (10 μg protein) from fraction #4 was used for immunocapture on biotin-labelled mAb-charged streptavidin magnetic beads. Briefly, sEV were incubated with biotin-labelled anti-CSPG4 mAb overnight, then 100 μl of Streptavidin-coated magnetic beads (washed twice with PBS) were added to the sEV-mAb complex and incubated overnight. The recovered beads-bound complexes were washed twice with PBS and re-suspended in 250 μl of PBS as the MTEX fraction. The beads-unbound material was stored as the NMTEX fraction. Detection of proteins in the MTEX and NMTEX cargo was performed by on-bead flow cytometry.

2.4 | Bead-assisted flow cytometry

For the analysis of proteins carried on the surface or in the lumen of the isolated sEV, only the non-immunocaptured total sEV and NMTEX subsets in solution could be used. MTEX captured on immunobeads could not be so tested. Aliquots of sEV (30 μg protein) were lysed using 1%Triton-X100 for 10 min. The resulting sEV lysates were co-incubated with 1 μl aliquots of aldehyde/sulfate latex beads (Thermo Fisher Scientific, #A37304, bead size 4 μm) for 1 h at room temperature with mild vortexing to load the lysate onto the beads. Then, the protein loaded beads were blocked with 2% (w/v) BSA for 1 h followed by washing with PBS. The beads were then incubated with primary antibodies (Anti-Alix, #MA5-32773, Thermo Fisher Scientific, clone JM85-31, 1:100; Anti-CSPG4, #AF2585, R&D Systems, clone LHM-2, 1:100) for 1 h. The beads were then washed and stained with PE-conjugated secondary antibody (1:100 dilution) for 30 min. Finally, the beads were washed with PBS and analysed by flow cytometry using Cytoflex S (Beckman Coulter).

2.5 | Sample preparation for MS

sEV samples (MTEX and NMTEX fractions or total plasma sEV from patients or HDs) were mixed with a lysis buffer containing 4% (w/v) SDS, 100 mM Tris/HCl pH 8.0, 0.1 M DTT (buffer to sample volumetric ratio of 1:9), then boiled for 10 min and subsequently subjected to Filter-Aided Sample Preparation (FASP) procedure (Wisniewski et al., 2009). Sequencing-grade modified trypsin (Promega) was used at the enzyme to protein ratio of 1:100 (w/w); 50 mM ammonium bicarbonate was employed as a digestion buffer then incubation in a wet chamber was performed for 18 h at 37°C. The collected tryptic peptides were subsequently purified on C18 StageTips, each prepared by stacking six layers of Empore™ Octadecyl C18 extraction disk (3 M, Maplewood, MN, USA) in a 0.2 ml pipette tip. Peptide purification was performed by three consecutive washes with 5% methanol, 0.1% TFA (centrifugation at 4000 × *g*, 5 min) followed by additional two washes with 0.1% TFA. Elution was done using 60% ACN, 0.1% TFA. Eluates with purified peptides were evaporated to dryness in a vacuum centrifuge, peptides were reconstituted in 20 μl of LC-MS grade water and subjected to peptide assay using tryptophan fluorescence method described by Wiśniewski and Gaugaz (Wisniewski & Gaugaz, 2015) (fluorescence measurement was conducted for the whole volume of each sample, i.e., 20 μl). After the measurement samples were acidified with TFA to achieve the final concentration of 0.1% (v/v) and subjected to LC-MS/MS analysis.

2.6 | Protein identification and quantitation by MS

The analysis was performed with the use of the Dionex UltiMate 3000 RSLC nanoLC System connected to the Q Exactive Plus Orbitrap mass spectrometer (Thermo Fisher Scientific). Peptides from each fraction (0.5 μg) were separated on a reverse-phase Acclaim PepMap RSLC nanoViper C18 column (75 μm × 25 cm, 2 μm granulation) using acetonitrile gradient (from 4 to 60%, in 0.1% formic acid) at 30°C and a flow rate of 300 nL/min (total run time: 180 min). The spectrometer was operated in data-dependent MS/MS mode with survey scans acquired at the resolution of 70,000 at m/z 200 in MS mode, and 17,500 at m/z 200 in MS2 mode. Spectra were recorded in the scanning range of 300–2000 m/z in the positive ion mode. Higher energy collisional dissociation (HCD) ion fragmentation was performed with normalized collision energies set to 25. Protein identification was performed using a reviewed Swiss-Prot human database (release 2018_11_30 containing 11 378 269 sequence entries) with a precision tolerance 10 ppm for peptide masses and 0.02 Da for the fragment ion masses. All raw data obtained for each dataset were imported into Protein Discoverer v.1.4 (Thermo Fisher Scientific) < Thermo raw files > for protein identification and quantification (Sequest engine was used for database searches). Protein was considered as positively identified if at least two peptides per protein were found by the search engine, and a peptide score reached the significance threshold FDR = 0.01 (assessed by the Percolator algorithm); a protein was further considered as "present" if detected in at least one sample of a given type. The abundance of identified proteins was estimated in Proteome Discoverer using Precursor Ions Area detector node, which calculates the abundance of a given protein based on average intensity of three most intensive distinct peptides for this protein, with further normalization to the total ion current (TIC).

2.7 | Western blots

sEV isolated from plasma, immunocaptured sEV or cell lysates (10 ug protein) were separated on 7–15% SDS/PAGE gels and transferred onto PVDF membrane (Millipore, Billerica, MA, USA) for western blot analysis. Membranes were incubated overnight at 4°C with antibodies specific for ALIX (PDCD6IP) (1:500, #2171S, Cell Signaling), Gelsolin (1:500, #MA5-34684, Thermo Fisher Scientific), Contactin-1 (1:250, #MAB9041, R&D Systems), and TSG101 (1:500, PA5-31260, Thermo Fisher). Next, the HRP-conjugated secondary antibody (1:10,000, Pierce, Thermo Fisher) was added for 1 h at room temperature (RT) and blots were developed with ECL detection reagents (GE Healthcare Biosciences, Pittsburgh, PA, USA). The intensities of the bands on exposed films were quantified using Image J software (NIH, USA).

2.8 | Statistical analysis

Immunoglobulins were filtered from further analysis. To define proteins distinguishing MTEX from NMTEX, the set of identified proteins was split into two groups depending on the number of patients with observed measurements. The first group included proteins with non-zero measurements observed for at least eight of 15 patients for MTEX or NMTEX samples. These proteins were analysed with the use of a non-parametric one-sided paired Wilcoxon test, testing the hypothesis of higher median protein abundance in MTEX samples when compared to NMTEX samples. The rank-biserial coefficient of correlation (RBCC) for the Wilcoxon test (Kerby, 2014) was calculated as a measure of the effect size. The second group included the remaining proteins. These proteins were analysed regarding their presence-absence status in each sample. The McNemar test for related measurements was applied with the support of Cohen's g for proportions as a measure of the effect size (Cohen & Hillsdale, 1988). *P*-value for protein selection equal to 0.05 was considered the significance threshold (a functional analysis served as an additional false discovery verification). To define a panel of proteins discriminating melanoma patients with progressive disease (PD) from those with no evident/stable disease (NED/SD), U Mann-Whitney test with corresponding Wendt effect size r_U (Wendt, 1972) was applied to the MTEX-NMTEX difference levels. In the case of effect size measured by rank-biserial coefficients of correlation (both RBCC and r_U), the critical value for the large effect was set to 0.5. Cohen's g for proportions of at least 0.25 were interpreted as indicating the large effect (Cohen & Hillsdale, 1988). The effect size quantification was done for the absolute values of the relevant statistics. Large effect size values indicate differences with a very high level of confidence. Next, the decision tree classifier with five fold cross-validation was applied to find the protein signature differentiating melanoma patients with PD from those with NED/SD. A set of classifiers was constructed in a stepwise procedure to rank the proteins according to their informativeness.

2.9 | Bioinformatics analysis

A list of genes corresponding to differentially expressed proteins was used to search for enriched Gene Ontology terms and Reactome pathways by Fisher test. Bioconductor packages ReactomePA (Yu & He, 2016) and clusterProfiler (Yu et al., 2012) were used. To minimize false discoveries, terms and pathways with at least three and at most 600 genes assigned to them were

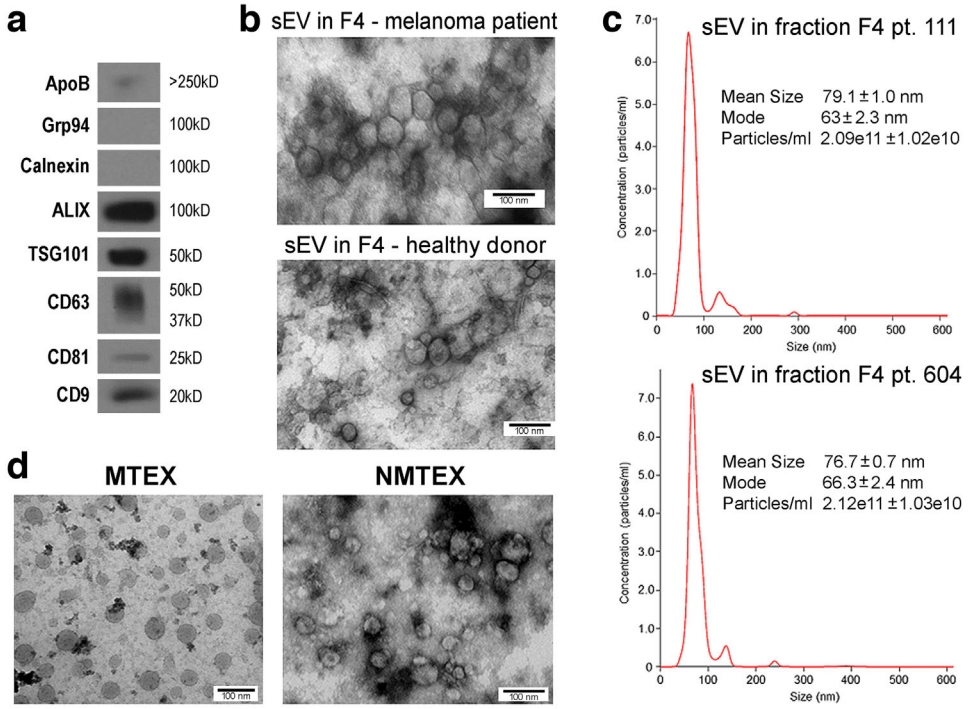

FIGURE 1 Characterization of sEV isolated from plasma. Panel a – western blot characterization of exosome markers in sEV collected in fraction #4 as described in Materials and Methods. Panel b – a TEM image of sEV in fraction #4 obtained from plasma of a melanoma patient or healthy donor. Panel c – NanoSight profiles of EVs in fraction #4 of two patients with melanoma. Panel d – TEM of MTEX detached from anti-CSPG4 mAbs on beads and NMTEX that remain in suspension following immune capture

tested only. The whole human genome served as a reference for the enrichment analysis of all proteins present in MTEX. For the remaining enrichment analyses, genes corresponding to all identified proteins (i.e., 573 proteins) served as a reference. FDR for tested GO terms and Reactome pathways was estimated with the Storey method. The threshold for q-value was set at 0.05. String-db database (Szklarczyk et al., 2019) was used to predict relations between chosen proteins.

2.10 | Data storage and availability

The HRMS-based proteomic data have been deposited to the ProteomeXchange Consortium via the PRIDE (https://www.ebi.ac.uk/pride) (Deutsch et al., 2020; Perez-Riverol et al., 2019) partner repository with the dataset identifier PXD021285 and PXD022867.

3 | RESULTS

3.1 | Characteristics of sEV isolated from plasma of melanoma patients or healthy donors

In this study, sEV isolation by SEC was performed using pre-cleared, ultrafiltered plasma specimens of 15 patients with metastatic melanoma. EVs collected in fraction #4 were used for immunocapture of MTEX as previously reported (Sharma et al., 2018; Sharma et al., 2020). Figure 1a shows western blots of isolated EVs in fraction #4 which carry ALIX, TSG101 and tetraspanins, CD63, CD81 and CD9, but not cytoplasmic proteins such as calnexin or Grp94. The content of ApoB is minimal. Figure 1b illustrates TEM images of EVs in fraction #4 isolated from plasma of a patient with melanoma or from plasma of a healthy donor (HD) indicating comparable vesicular morphology and size. Figure 1c shows representative NanoSight profiles for EVs in fraction #4 for two melanoma patients. The size (~80 nm), vesicular morphology by TME and endosomal origin in WBs suggest that these EVs fit in the category of small EVs and are designated as "**sEV**" in this study.

The sEV in fraction #4 of all 15 patients carried different relative levels of the CSPG4 epitope on the vesicle surface by quantitative on-bead flow cytometry performed as previously described (Sharma et al., 2018; Sharma et al., 2020) and as

presented in Figure S1. These sEV were separated into MTEX and NMTEX by immune capture using anti-CSPG4 mAb. Figure 1d shows representative TEM images of MTEX and NMTEX obtained by immune capture. MTEX, which were detached from anti-CSPG4 mAb on beads by a brief exposure to pH 2.5 buffer followed by neutralization, appear as slightly larger and "cleaner" vesicles. The MTEX and NMTEX separated by immune capture were used for paired comparative proteomic analysis. The total plasma sEV of five HDs underwent the same proteomic analysis. However, as HDs do not have MTEX, the available data do not contribute to the paired MTEX/NMTEX analysis and, therefore, are not shown. Nevertheless, preliminary proteomic analysis of HD's EVs in fraction #4 showed that 282 proteins were shared with NMTEX, while 75 proteins were upregulated in NMTEX. These data suggest that the proteomic profiles of NMTEX and sEV isolated from plasma of HDs are partly distinct, and that the biological significance of these differences deserves to be independently evaluated in future studies.

3.2 | Proteins detected in MTEX

The levels of total sEV protein (TEP) varied between melanoma patients from 54 to 92 μg/ml plasma (Table S1). Importantly, the average TEP level at 63 μg/ml for patients with non-evident or stable disease (NED/SD; $n = 7$) at the time of blood draw was lower than that for melanoma patients with progressive disease (PD; $n = 8$) at 78 μg/ml ($P < 0.02$). The ratios of MTEX/TEP varied, ranging from 0.32 to 0.75, while those for MTEX/NMTEX varied from 0.48 to 3.05 (Table S1), and these ratios did not reflect disease activity. Noteworthy, as documented in Figure S2, MTEX were enriched in melanoma-associated antigens (MAAs), including CSPG4, Melan A, Gp100 and VLA4, while the corresponding NMTEX samples were negative, confirming our previously reported data (Sharma et al., 2020).

Paired MTEX and NMTEX samples of 15 patients were analysed using a shotgun proteomics approach based on the high-resolution mass spectrometry (HRMS). This approach allowed for the identification of about 800 proteins. Further analyses identified 573 proteins encoded by the unique genes (immunoglobulins and putative uncharacterized proteins were excluded). The complete list of proteins identified and quantified in 30 exosome specimens (15 MTEX + 15 NMTEX) is presented in Table S2, while the abundance values for each protein in the analysed samples are presented as a heatmap in Figure S3. Interestingly, this heatmap indicates that in eight patients with PD, the level of many proteins was substantially higher than that in seven patients with NED/SD. This was especially striking for patients 7, 8, 9, and 10 as listed in Table S1.

3.3 | Proteome components characteristic for MTEX

To identify proteins with significantly upregulated levels in MTEX, that is, proteins which levels discriminated MTEX and NMTEX, the ratios of individual protein levels in MTEX and NMTEX were determined for each patient. There were 384 proteins detected in the samples obtained from more than half of the included patients (8/15; representing the "continuous" mode of the statistical testing). These included 62 proteins that were upregulated in MTEX (P-value > 0.05 and RBCC ≥ 0.5; Table S2). Furthermore, when the remaining 189 proteins were subjected to the binary mode of analysis (i.e., using the absent/present algorithm), there were 11 additional proteins that were found to be upregulated in MTEX (P-value > 0.05 and Cohen g ≥ 0.5; Table S2). Hence, 73 protein species (62+11) in the patients' plasma represented a subset of proteins upregulated in MTEX compared to NMTEX. Next, to identify proteins with levels that were markedly lower in MTEX than in NMTEX, effect size values were considered. Because all MTEX-upregulated proteins showed large effect size, the same threshold was required to call MTEX-downregulated proteins. Consequently, 77 proteins were classified as downregulated in MTEX (effect size ≤ -0.5; Table S2). The Venn diagram in Figure 1a shows that 496 sEV proteins were detected in MTEX, including 73 proteins that were markedly upregulated and 77 proteins that were significantly downregulated.

Among the 73 proteins that were significantly increased in abundance in MTEX, we were especially interested in those known to be involved in cancer progression as well as those proteins that were detected in more than 8/15 MTEX samples we examined. Figure 2b lists sixteen such proteins: AHCY, LDHA, GSN, NOTCH2, THBS1, UBA52, TLN1, PGK1, SERPINF2, WDR1, CSGP4, MSN, SLC1A4, YWHAE, TSG101, and RAP1B. Differences in levels of these proteins in paired MTEX and NMTEX samples of individual patients are presented. Furthermore, two additional proteins, PLOD1 and PROM1, that were detected only in a smaller proportion of melanoma specimens (and thus exemplify proteins in the characteristic absent/present mode) are illustrated in Figure 2c. The group of 16 selected MTEX proteins discriminated MTEX from NMTEX and could potentially be useful in differential analysis of plasma sEV in patients with melanoma. Noteworthy, the CSPG4 antigen used for the MTEX immunocapture was detected by LC-MS/MS in all MTEX specimens, and its median upregulation compared to NMTEX was about 19-fold. In addition to CSPG4, a few MTEX-upregulated proteins identified by LC-MS/MS, including PDCD6IP (ALIX), Gelsolin (GSN), and contactin-1 (CNTN1) were further analysed by the immune-based methods, which confirmed their reduced levels in NMTEX (Figure S4).

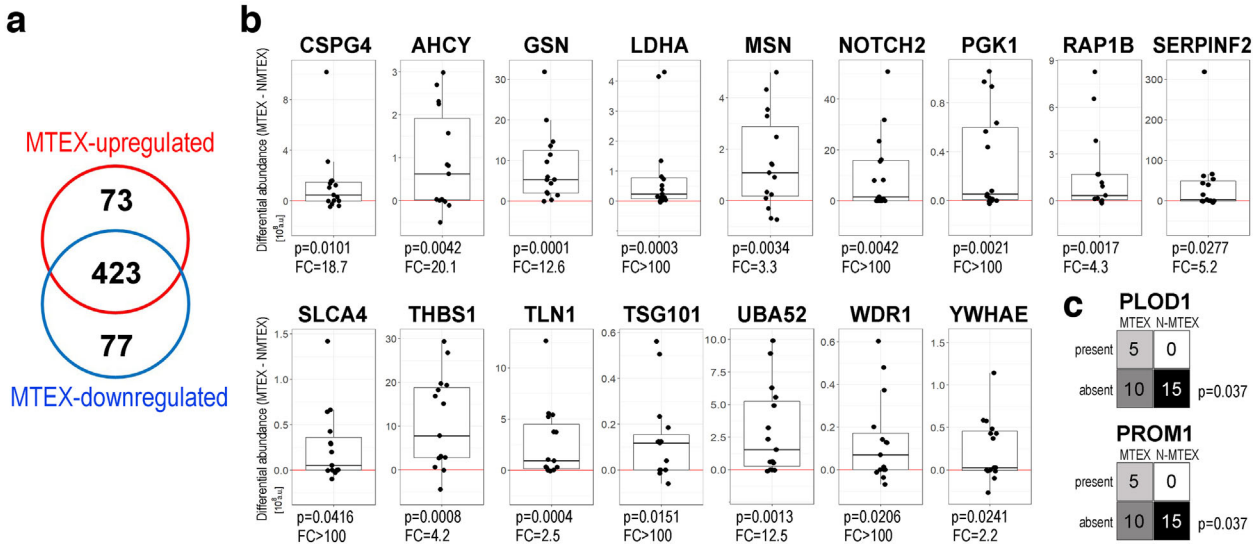

FIGURE 2 MTEX proteins found to have significantly upregulated levels relative to NMTEX. Panel a – the Venn diagram showing numbers of proteins upregulated or downregulated in MTEX. Panel b – individual differences in the protein levels between paired samples of MTEX and NMTEX; boxplots show median, upper and lower quartile, maximum and minimum (dots represent individual patients; the red line represents no difference between MTEX and NMTEX, FC – average fold-change). Panel c – PLOD1 and PROM 1 are shown as examples of the present/absent status analysis of proteins in paired samples of MTEX and NMTEX

3.4 | Biological functions associated with proteins characteristic for MTEX

To identify biological pathways associated with the proteins detected in MTEX, the analysis of gene ontology was performed after their annotation with the coding genes. First, pathways associated with 496 proteins abundant in MTEX (i.e., excluding 77 proteins downregulated in MTEX) were analysed, using the whole human genome as the reference. There were numerous significantly overrepresented GO terms associated with proteins present in MTEX listed in Table S3. These included "extracellular structure organization" (81 proteins), "wound healing" (87 proteins), "regulation of vesicle-mediated transport" (54 proteins), "acute inflammatory response" (44 proteins), and "protein activation cascade" (46 proteins). Moreover, 39 MTEX proteins were associated with the GO term "melanosome" (GO:0042470), out of 106 proteins listed in the human genome reference.

Next, the more specific analysis of gene ontologies was performed for the 73 proteins upregulated in MTEX (the list of 573 detected proteins was used as the reference). There were 393 GO terms associated with MTEX-upregulated proteins that were overrepresented ($P < 0.05$), yet only the establishment of cell polarity (GO:0030010) remained statistically significant after the multiple testing correction ($q < 0.05$; Table S4). The analysis of functional interactions between the MTEX-upregulated proteins was performed using the Reactome database (Jassal et al., 2020). This analysis enabled detection of 36 pathways that were significantly enriched ($P < 0.05$; see Table S5). Of these 36 pathways, twelve remained statistically significant after the FDR correction ($q < 0.05$); these were pathways involved in signal transduction, cell cycle progression, cell adhesion, and protein glycosylation. These overrepresented pathways and their corresponding protein components detected in MTEX are presented in Figure 3.

Furthermore, to illustrate possible interactions among all 73 proteins upregulated in MTEX, an additional analysis was performed using the String-db database (Szklarczyk et al., 2019). Potential interactions among these proteins are presented in Figure 4. The most numerous GO term associated with these proteins was "response to stimulus" (43 proteins), while connected molecular functions "signaling receptor binding" and "nucleotide binding" were attributed to 23 and 19 proteins, respectively. In aggregate, the above-presented data indicated that MTEX-associated proteins are mainly involved in signal transduction. Moreover, there were 28 proteins associated with the term "immune system process", which suggested that many MTEX-associated proteins mediate immune regulatory functions (all above-mentioned terms were statistically overrepresented, although the whole human genome was used as a reference in the String-db database, which made the statistical testing less reliable).

In addition to the "unsupervised" analysis of processes associated with the proteins upregulated in MTEX as described above, we specifically searched for proteins known to be expressed in melanoma. Taking advantage of the TCGA database (The TCGA Research Network), we confirmed that transcripts for the vast majority of MTEX-upregulated proteins were listed in the TCGA melanoma database (Table S6). Further, more than half of MTEX-upregulated proteins (38 out of 73) were present at high or moderate levels in melanoma tissues according to immunohistopathology data available in the Protein Atlas (Table S6) (The Human Protein Atlas). Moreover, 10 of MTEX-upregulated proteins are present in the melanosome (GO:0042470). There were also 28 MTEX-upregulated proteins associated with immune-related functions (GO:0002376), several of which are not expressed

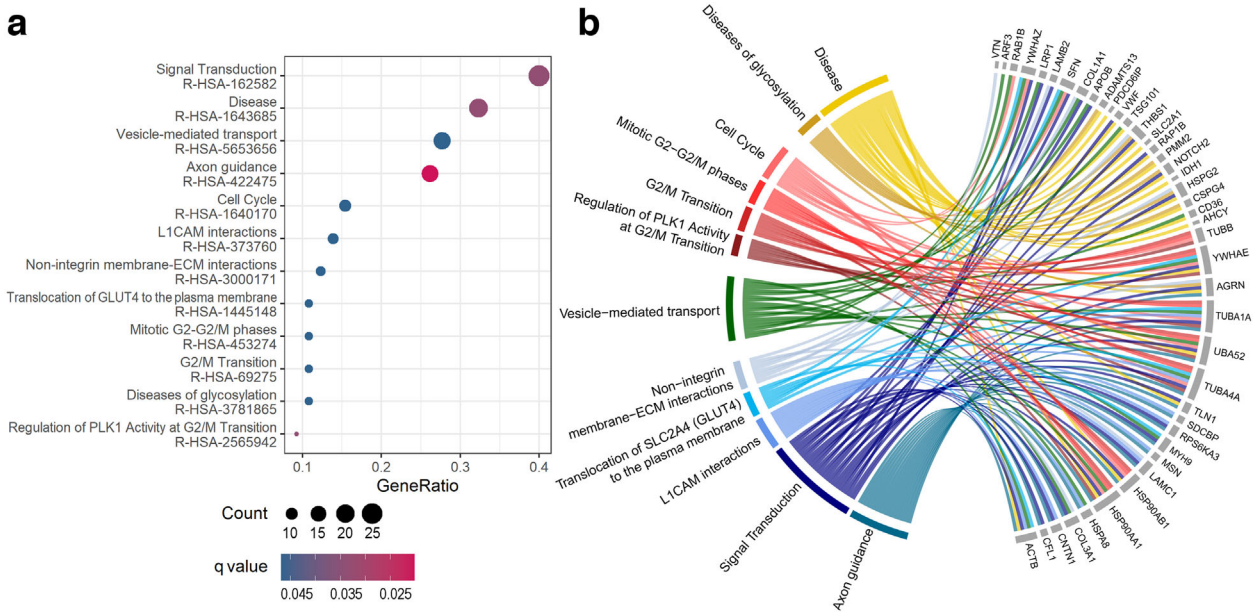

FIGURE 3 Reactome pathways analysis. Panel a shows a dot-plot with significantly enriched Reactome pathways ($q < 0.05$) coloured by FDR. GeneRatio on x-axis refers to the ratio of the number of differentially expressed genes in a pathway (Count) to the number of all differentially expressed genes ($n = 73$). The size of each dot corresponds to the number of differentially expressed genes in a pathway. Panel b shows a network of genes linked to the Reactome pathway terms

in melanoma tissues listed in the Protein Atlas (Table S6). Nevertheless, some of these upregulated proteins are known to possess immunoregulatory activity in melanoma (e.g., contactin1, fibulin, isocitrate dehydrogenase).

3.5 | MTEX proteins discriminate patients with progressing melanoma (PD) from those with no evident or stable disease (NED/SD) after therapy

Among 15 patients with metastatic melanoma (MM) donating plasma for this study, seven patients had NED/SD and eight had PD at the time of the blood draw for sEV recovery. All patients were previously treated for MM. To determine whether MTEX could confirm disease activity, the MTEX protein contents of the two patient groups were compared (see the heat map in Figure S3). We detected 83 proteins in MTEX that significantly differed in the two patient groups. There were 75 proteins whose differential (MTEX-NMTEX) level was markedly higher in MTEX from patients with PD than in patients with NED/SD (Table S2), including 12 proteins with significantly upregulated MTEX relative to NMTEX, namely: PDCD6IP, HSP90AB1, ITIH3, MSN, THBS1, TUBB, UBA52, F10, PLOD1, RPS6KA3, SGCE, ADAMTS13 (the data for eight of these proteins are shown in Figure 5a). On the other hand, there were eight proteins with a significantly lower level in MTEX from patients with PD than in those with NED/SD. The data for three of these proteins, including CNTM1 (contactin1, the only protein consistently upregulated in MTEX of NED/SD patients), are shown in Figure 5b.

Among the 12 MTEX-upregulated proteins with higher expression in PD patients, PDCD6IP (ALIX, ALG 2-interacting protein X) discriminated best ($P = 0.0003$) between the two groups of melanoma patients (Figure 5c). Remarkably, the level of this protein alone was sufficient to allow for errorless discrimination of seven patients with NED/SD from eight patients with PD. In contrast, any discrimination attempts using a decision tree classifier based on the level of the remaining 11 proteins generated data with less discriminating power. Despite the small size of the patient groups, the data suggest that PDC6IP alone can serve as a potentially reliable biomarker able to discriminate melanoma patients with a different disease status. Furthermore, increased levels of CNTM1 in MTEX of NED/SD patients and its absence in MTEX of patients with PD identified another potential indicator of disease activity. Also, the absence of TGF-β1 in MTEX of NED/SD patients was a significant discriminator of the two patient groups that together with the absence of CNTM1 in MTEX of patients with PD enhanced the prognostic value of this differential proteomic analysis.

A search for biological activities associated with 83 MTEX proteins (75+8) differentially expressed in the two groups of melanoma patients identified nine Reactome pathways at $P < 0.05$; yet none of them remained statistically significant after the multiple testing correction); see Table S7. The enriched pathways included processes involved in an extracellular matrix organization (15 proteins), metabolism (20 proteins, including nine proteins involved in the metabolism of carbohydrates), and cellular

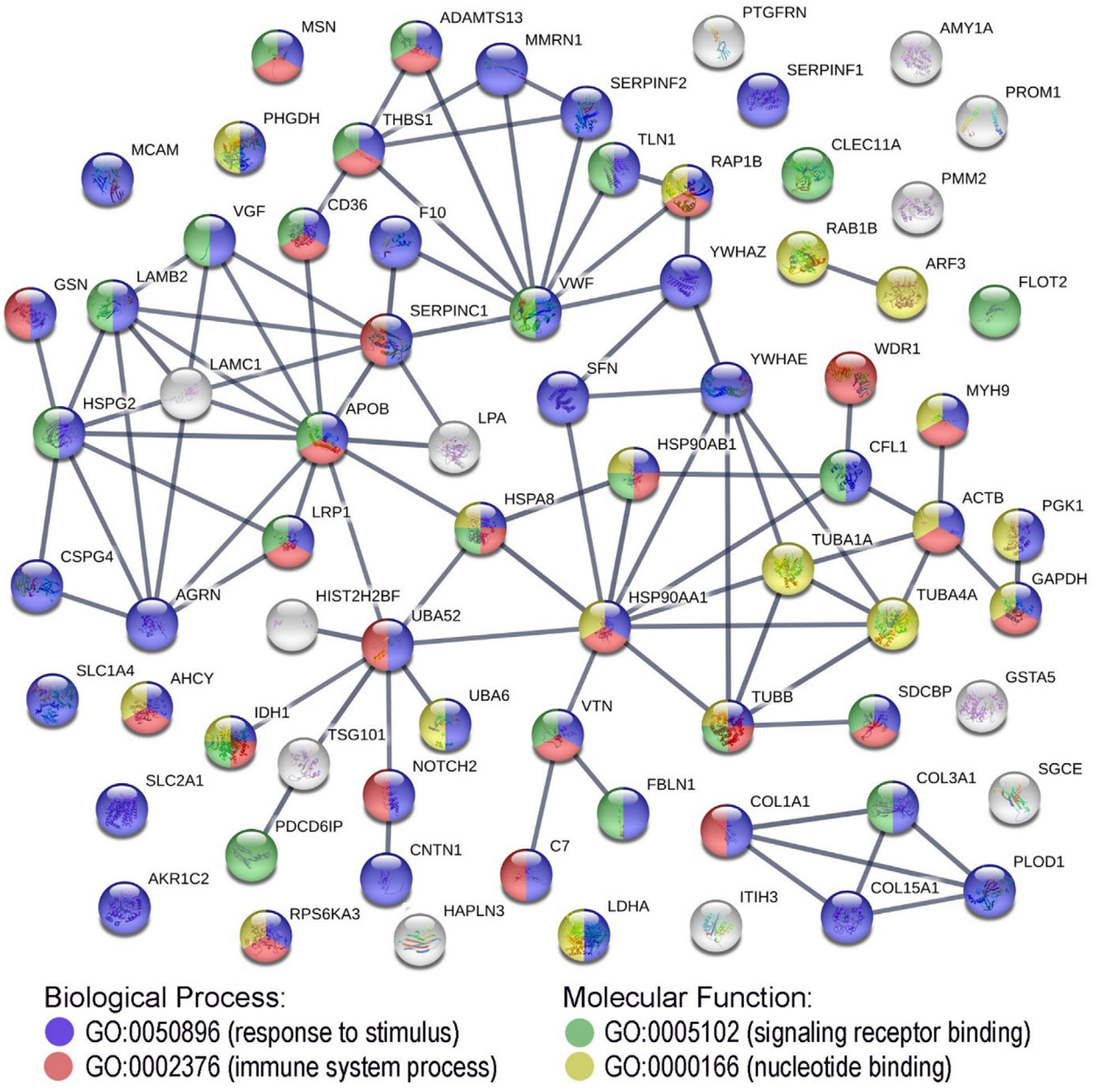

FIGURE 4 An interaction map for proteins found to be upregulated in MTEX. Proteins associated with the four selected GO terms are colour-coded

responses to stress (8 proteins). Moreover, there were 24 proteins involved in the immune system among them. The network of MTEX proteins characteristic for melanoma patients with a progressing disease (PD) is illustrated in Figure 6. Based on correlation analysis between PDC6IP and 83 MTEX proteins differentiating melanoma patients with PD from those with NED/SD, we found four proteins that strongly ($r_u > 0.7$, $P < 0.005$) associated with PDC6IP, namely HSP90AB1, PFN1, TUBB, and TUBB1 (Figure S5).

4 | DISCUSSION

The search for biomarkers of melanoma progression and response to therapy including recent genomics or other "omics" approaches has led to the discovery of numerous promising proteins (reviewed in (Gowda et al., 2020; Rodriguez-Cerdeira et al., 2018)). However, none of these potential biomarkers have been validated so far, and only soluble lactic dehydrogenase (sLDH) remains as the protein that correlates with the disease burden in some patients with metastatic melanoma (Byström et al., 2017). Recent attempts at establishing correlations between levels of sLDH and any specific molecular, immunological or metabolic

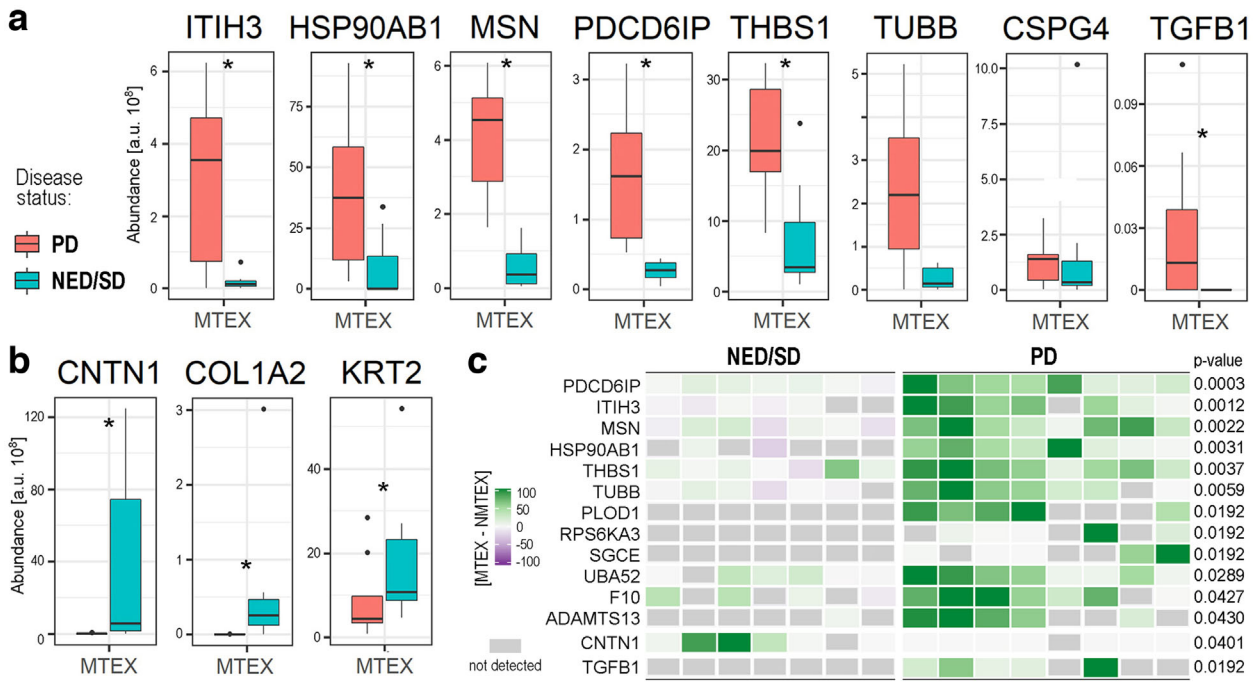

FIGURE 5 sEV-associated proteins that were present at a significantly different level in MTEX isolated from plasma of melanoma patients with PD relative to MTEX isolated from plasma of melanoma patients with NED/SD. Panel a – MTEX proteins with significantly higher levels in patients with PD. Panel b – MTEX proteins with significantly higher levels in patients with NED/SD. Boxplots show median, upper and lower quartile, maximum, and minimum; dots represent outliers. The statistical significance of differences between patient subgroups ($P < 0.05$) is marked with asterisks. Panel c – A heat map presenting the differential (MTEX-NMTEX) protein levels in individual melanoma patients with NED/SD ($n = 7$) or PD ($n = 8$). Twelve proteins found to be upregulated in MTEX of melanoma patients with PD are listed. Moreover, the levels of CNTN1 and TGFβ1 are presented in the corresponding samples. The relative levels of the listed proteins is colour-coded where gray boxes represent not detected proteins; *P*-values represent the significance of the difference between patients' subgroups of the differential (MTEX-NMTEX) value

phenotypes, including immune cell infiltrate in the tumour, point mutations, DNA copy number, promoter methylation, RNA expression or protein expression in melanoma metastases have been not been successful (Gowda et al., 2020). Therefore, the search for biomarkers predictive of response to immune therapies remains an unmet clinical urgent need. sEV have emerged as a new potentially diagnostic/prognostic tool in melanoma. Factors known to be involved in angiogenesis, immune suppression, modification of stroma, capture of cancer cells in lymph nodes and tumour cell progression have been identified in sEV from the plasma of melanoma patients by us and others (Alegre et al., 2016; Gowda et al., 2020; Hood, 2019; Sharma et al., 2020). Several previous studies suggested that the use of EV, especially tumour cell-derived sEV (TEX), might be a more promising approach to the discovery and development of melanoma-associated biomarkers than strategies dependent on conventional tumour tissue examination or on measuring levels of soluble factors in patients' plasma (Byström et al., 2017; Rodriguez-Cerdeira et al., 2018; The TCGA Research Network).

Most of the earlier studies with melanoma cell-derived TEX were performed using EV derived from melanoma cell lines. The most comprehensive proteomics profiling of EV proteins released by a panel of melanoma cell lines (1205Lu, 501MEL, A375M, Daju, G1, MNT-1, SK-MEL-28) identified 917 proteins in total, with each cell line representing subsets of between 486 and 632 of these proteins (Lazar et al., 2015). A quarter of the identified proteins were common among the cell lines (e.g., ESCRT proteins, CD9, CD63, CD81, small GTP-binding proteins, annexins, cytoskeletal, and motor proteins). There were 22 proteins specific for MTEX from non-tumorigenic cell lines, 29 proteins specific for MTEX from tumorigenic cell lines, and 112 proteins unique of MTEX from metastatic cell lines. Proteins unique of MTEX from metastatic cell lines included EGFR, EPHB2, KIT, LGALS1/LEG1, LGALS3/LEG3, MCAM/MUC18, MET, NRAS, NT5E/5NTD/CD73, PTK2/FAK1, and SRC (Lazar et al., 2015). More recently, plasma sEV carrying PD-L1 (EXO-PD-L1) have been used for monitoring melanoma patients treated with ICIs (Chen et al., 2018; Cordonnier et al., 2020). In agreement with correlative data reported for other solid tumours, the latter studies in melanoma showed that tracking changes in circulating levels of EXO-PD-L1 was associated with disease activity and progression (Ricklefs et al., 2018; Theodoraki et al., 2018) and predicted response to immune therapy (Chen et al., 2018; Cordonnier et al., 2020). While these results place EXO-PD-L1 in a category of promising biomarkers for melanoma and other cancer types, the tumour origin of EXO-PD-L1 remains speculative, as they were not validated TEX and might have largely originated from non-malignant PD-L1+ cells.

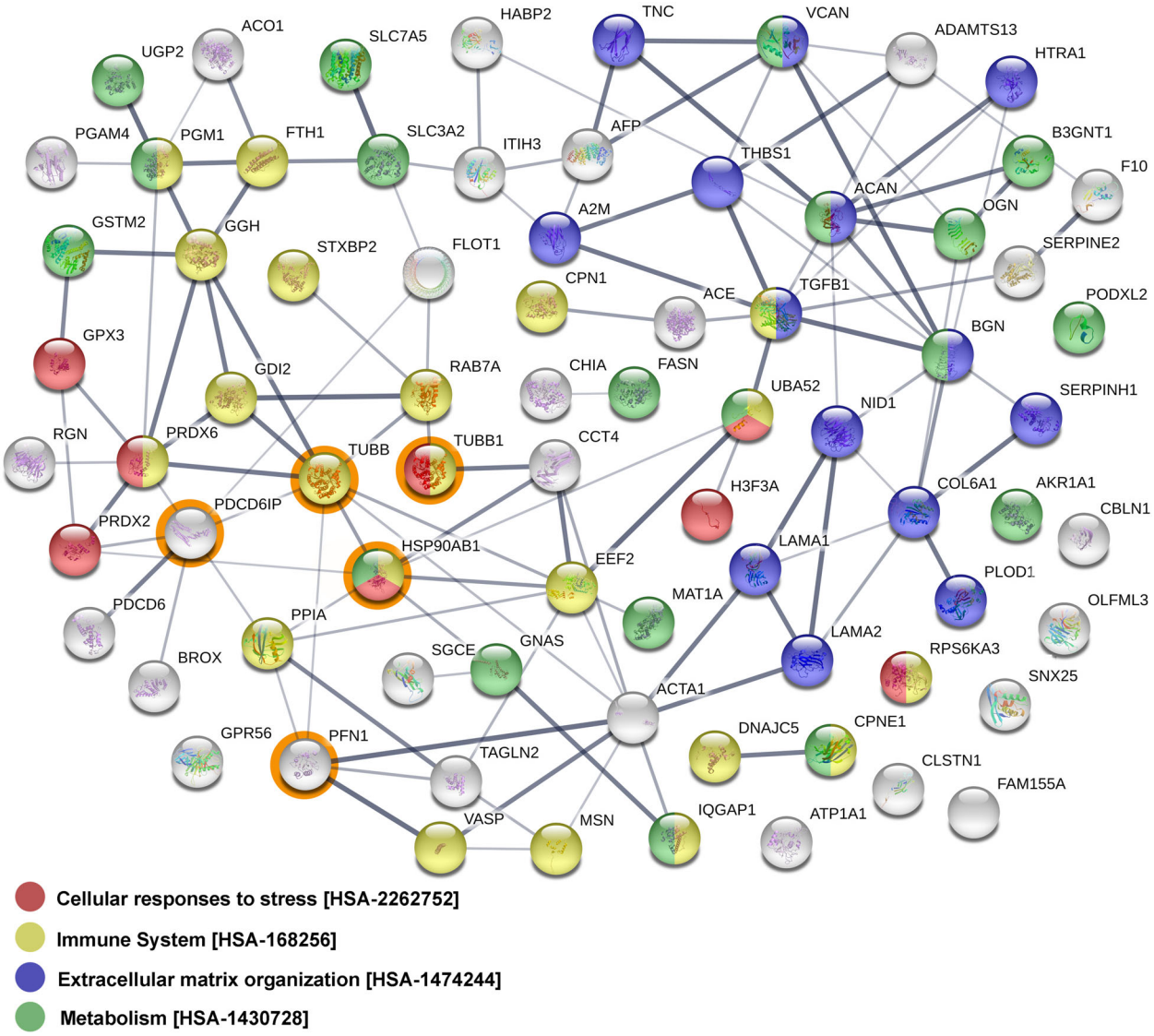

FIGURE 6 The network of potential interactions between MTEX proteins found to be overexpressed in patients with PD but not in patients with NED/SD. The four proteins (HSP90AB1, PFN1, TUBB, and TUBB1) strongly associated with PDCD6IP (ALIX) are circled in orange

The objective of the present study was to determine whether MTEX obtained from plasma of patients with melanoma have the potential to serve as a non-invasive liquid biopsy able to predict disease progression or response to therapy. The rationale for the current approach of comparing proteomic profiles of MTEX and NMTEX was based on an assumption that MTEX will serve as a more specific liquid biopsy of the tumour than total plasma sEV. Taking advantage of the previously developed immune capture of MTEX using anti-CSPG4 mAbs (Sharma et al., 2018; Sharma et al., 2020), we separated MTEX from vesicles derived from non-malignant cells (NMTEX) (Sharma et al., 2020). To evaluate MTEX as a potential liquid tumour biopsy, the LC-MS/MS analysis of the protein cargos in paired MTEX and NMTEX was performed. The expectation, based in part on our earlier flow-cytometry-based analysis of MTEX and NMTEX (Sharma et al., 2020), was that a panel of proteins uniquely and consistently identifiable in MTEX would provide the signature for MTEX in support of their role as surrogates of melanoma progression or response to therapy.

We first determined that HRMS of paired MTEX and NMTEX specimens of randomly selected patients with metastatic melanoma (MM) identified a set of 73 proteins specific or overexpressed in MTEX. Based on our previous study, where the separation of MTEX from NMTEX showed clinical relevance (Sharma et al., 2020), we expected that the identified 73 proteins might be useful in discriminating MTEX from NMTEX. We selected a group of 16/73 MTEX proteins to serve as an "MTEX differentiating panel". The selection was based on the criteria that included the known role of each protein in cancer progression, the presence of each protein in at least 8/15 MTEX examined, the known association with exosome membranes, and the inclusion in the Exocarta database (Keerthikumar et al., 2016). The protein-associated pathways identified by GO analysis in the group of 73

proteins upregulated in MTEX showed interesting functional features. In agreement with our previously reported data (Sharma et al., 2020), MTEX were predominantly enriched in proteins engaged in signalling pathways and immunoregulatory activity. The previously reported functional distinction between MTEX and NMTEX using flow cytometry and immune response results (Sharma et al., 2020) was thus confirmed by HRMS of separated MTEX and NMTEX.

Perhaps more importantly, this study also identified a set of MTEX proteins, including ADAMTS13, CNTN1, F10, HSP90AB1, ITIH3, MSN, PDCD6IP, PLOD1, RPS6KA3, SGCE, THBS1, TUBB, and UBA52, whose levels discriminated patients with MM who had PD from those who were NED/SD after therapy. This set of proteins enabled us to propose the hypothetical MTEX-based "prognostic signature". Even with a very small number of MM patients in each group, it was possible to show that the 83 proteins differentially expressed in MTEX included those associated with the ECM organization, metabolism, responses to stress, and immune regulation. This finding suggests that MTEX have a protein profile that reflects melanoma progression and outcome. Interestingly, a recently reported proteomic analysis of EVs from exudative serome obtained after lymphadenectomy in patients with melanoma by Peinado's group also showed enrichment in proteins correlating with or recapitulating melanoma progression (García-Silva et al., 2019).

Remarkably, despite the small patient numbers in each cohort, PDCD6IP (ALIX) emerged as the protein with the greatest power for discriminating melanoma patients with PD from patients with NED/SD. PDCD6IP (Programmed cell death 6-interacting protein also known as ALIX, ALG2 interacting protein X, AIPI, KIAA1375) is a multifunctional protein involved in endocytosis, multivesicular body (MVB) biogenesis, membrane repair, cytokinesis, apoptosis and maintenance of tight junction integrity (Monypenny et al., 2018; Odorizzi, 2006). ALIX/PDCD6IP is best known as a component of the endosomal-sorting complex required for transport (ESCRT) (Henne et al., 2011) involved in the concentration and sorting of cargo proteins directed to the MVB for incorporation into intraluminal vesicles (ILVs). More recent studies report that ALIX/PDCD6IP plays a role in tumour cell apoptosis and proliferation, regulates tumour-mediated immunosuppression and controls PD-L1 expression (García-Silva et al., 2019). We found that 4/83 proteins differentiating PD from NED/SD patients strongly correlated with ALIX/PDCD6IP; these are HSP90AB1 (heat shock protein 90), TUBB (β-tubulin), TUBB1 (Tubulin β1 chain) and PFN1 (profilin1). These proteins interact directly with each other, putatively forming the functional network. Moreover, CNTN1, a cell adhesion protein and a member of the immunoglobulin superfamily known to be expressed in melanoma (Deutsch et al., 2020; Jassal et al., 2020), was highly upregulated in MTEX of some patients with NED/SD and was not detectable in MTEX of PD patients. In contrast, TGF-β1, which was not detected in MTEX of NED/SD patients, was overexpressed in MTEX of patients with PD.

Hence, the molecular signature of MTEX consisting of PDCD6IP/ALIX, 4 correlated proteins (HSP90AB1, TUBB, TUBB1, and PFN1) highly expressed in MTEX of patients with PD, plus CNTN1 and TGF-β1 with differential distribution in MTEX of PD vs NED/SD patients may have prognostic significance in melanoma. Importantly, all these proteins have been reported to play a key role in melanoma progression and metastasis (Bracalente et al., 2016; Subramanian et al., 2004). In aggregate, our data indicate that the protein cargo of MTEX reflects the content of tumour cells, might serve as a liquid tumour biopsy and, upon further validation, it has a potential to become a surrogate of melanoma progression.

ACKNOWLEDGEMENTS

The research leading to these results has received funding from the National Science Centre, Poland, grant 2016/22/M/NZ5/00667 (to M.P., A.Z., and J.M.), and US National Institutes of Health grants R01-CA168628 and U01-DE029759 (to T.L.W.). J.P. was supported through the National Science Centre, Poland, grant 2015/19/B/ST6/01736, J.M.K was supported through National Institutes of Health grant SPORE CA19173.

ORCID

Monika Pietrowska https://orcid.org/0000-0001-9317-7822
Marta Gawin https://orcid.org/0000-0002-2834-5129
Lukasz Marczak https://orcid.org/0000-0001-8602-0077
Joanna Polańska https://orcid.org/0000-0001-8004-9864
Soldano Ferrone https://orcid.org/0000-0003-2900-8834
Piotr Widlak https://orcid.org/0000-0001-5099-4726
Theresa L. Whiteside https://orcid.org/0000-0001-7316-6181

REFERENCES

Alegre, E., Zubiri, L., Perez-Gracia, J. L., González-Cao, M., Soria, L., Martín-Algarra, S., & González, A. (2016). Circulating melanoma exosomes as diagnostic and prognosis biomarkers. *Clinica Chimica Acta 454*, 28-32.

Bracalente, C., Ibañez, I. L., Berenstein, A., Notcovich, C., Cerda, M. B., Klamt, F., Chernomoretz, A., & Durán, H. (2016). Reprogramming human A375 amelanotic melanoma cells by catalase overexpression: Upregulation of antioxidant genes correlates with regression of melanoma malignancy and with malignant progression when downregulated. *Oncotarget 7*(27), 41154-41171.

Byström, S., Fredolini, C., Edqvist, P. H., Nyaiesh, E. N., Drobin, K., Uhlén, M., Bergqvist, M., Pontén, F., & Schwenk, J. M. (2017). Affinity proteomics exploration of melanoma identifies proteins in serum with associations to T-stage and recurrence. *Translational Oncology 10*(3), 385-395.

Cai, L., Michelakos, T., Yamada, T., Fan, S., Wang, X., Schwab, J. H., Ferrone, C. R., & Ferrone, S. (2018). Defective HLA class I antigen processing machinery in cancer. *Cancer Immunology, Immunotherapy 67*(6), 999-1009.

Campoli, M., Ferrone, S., & Wang, X. (2010). Functional and clinical relevance of chondroitin sulfate proteoglycan 4. *Advances in Cancer Research 109*, 73-121.

Chen, G., Huang, A. C., Zhang, W., Zhang, G., Wu, M., Xu, W., Yu, Z., Yang, J., Wang, B., Sun, H., Xia, H., Man, Q., Zhong, W., Antelo, L. F., Wu, B., Xiong, X., Liu, X., Guan, L., Li, T., … Guo, W. (2018). Exosomal PD-L1 contributes to immunosuppression and is associated with anti-PD-1 response. *Nature 560*(7718), 382-386.

Cohen, J. (1988). *Statistical power analysis for the behavioral sciences*. Hillsdale, N.J: L. Erlbaum Associates.

Cordonnier, M., Nardin, C., Chanteloup, G., Derangere, V., Algros, M. P., Arnould, L., Garrido, C., Aubin, F., & Gobbo, J. (2020). Tracking the evolution of circulating exosomal-PD-L1 to monitor melanoma patients. *Journal of Extracellular Vesicles 9*(1):1710899.

Deutsch, E. W., Bandeira, N., Sharma, V., Perez-Riverol, Y., Carver, J. J., Kundu, D. J., García-Seisdedos, D., Jarnuczak, A. F., Hewapathirana, S., Pullman, B. S., Wertz, J., Sun, Z., Kawano, S., Okuda, S., Watanabe, Y., Hermjakob, H., MacLean, B., MacCoss, M. J., Zhu, Y., … Vizcaíno, J. A. (2020). The ProteomeXchange consortium in 2020: enabling 'big data' approaches in proteomics, *Nucleic Acids Res 48*(D1), D1145-D1152.

Ferrone, S., & Whiteside, T. L. (2020). Targeting CSPG4 for isolation of melanoma cell-derived exosomes from body fluids. *HNO 68*(2), 100-105.

Szklarczyk, D., Gable, A. L., Lyon, D., Junge, A., Wyder, S., Huerta-Cepas, J., Simonovic, M., Doncheva, N. T., Morris, J. H., Bork, P., Jensen, L. J., Mering, C. V. (2019). STRING v11: protein-protein association networks with increased coverage, supporting functional discovery in genome-wide experimental datasets. *Nucleic Acids Research 47*(D1), D607-D613.

García-Silva, S., Benito-Martín, A., Sánchez-Redondo, S., Hernández-Barranco, A., Ximénez-Embún, P., Nogués, L., Mazariegos, M. S., Brinkmann, K., Amor López, A., Meyer, L., Rodríguez, C., García-Martín, C., Boskovic, J., Letón, R., Montero, C., Robledo, M., Santambrogio, L., Sue Brady, M., Szumera-Ciećkiewicz, A., … Peinado, H. (2019). Use of extracellular vesicles from lymphatic drainage as surrogate markers of melanoma progression and BRAF (V600E) mutation. *Journal of Experimental Medicine 216*(5), 1061-1070.

Gowda, R., Robertson, B. M., Iyer, S., Barry, J., Dinavahi, S. S., & Robertson, G. P. (2020). The role of exosomes in metastasis and progression of melanoma. *Cancer Treatment Reviews 85*:101975.

Henne, W. M., Buchkovich, N. J., & Emr, S. D. (2011). The ESCRT pathway. *Developmental Cell 21*(1), 77-91.

Hong, C. S., Funk, S., Muller, L., Boyiadzis, M., & Whiteside, T. L. (2016). Isolation of biologically active and morphologically intact exosomes from plasma of patients with cancer. *Journal of Extracellular Vesicles 5*:29289.

Hood, J. L. (2019). Natural melanoma-derived extracellular vesicles. *Seminars in Cancer Biology 59*, 251-265.

Jassal, B., Matthews, L., Viteri, G., Gong, C., Lorente, P., Fabregat, A., Sidiropoulos, K., Cook, J., Gillespie, M., Haw, R., Loney, F., May, B., Milacic, M., Rothfels, K., Sevilla, C., Shamovsky, V., Shorser, S., Varusai, T., Weiser, J., … D'Eustachio, P. (2020). The reactome pathway knowledgebase. *Nucleic Acids Research 48*(D1), D498-D503.

Keerthikumar, S., Chisanga, D., Ariyaratne, D., Al Saffar, H., Anand, S., Zhao, K., Samuel, M., Pathan, M., Jois, M., Chilamkurti, N., Gangoda, L., & Mathivanan, S. (2016). ExoCarta: a web-based compendium of exosomal cargo. *Journal of Molecular Biology 428*(4), 688-692.

Kerby, D. S. (2014). The simple difference formula: an approach to teaching nonparametric correlation. *Comprehensive Psychology 3*(1).

Lazar, I., Clement, E., Ducoux-Petit, M., Denat, L., Soldan, V., Dauvillier, S., Balor, S., Burlet-Schiltz, O., Larue, L., Muller, C., & Nieto, L. (2015). Proteome characterization of melanoma exosomes reveals a specific signature for metastatic cell lines. *Pigment Cell & Melanoma Research 28*(4), 464-475.

Ludwig, N., Hong, C. S., Ludwig, S., Azambuja, J. H., Sharma, P., Theodoraki, M. N., & Whiteside, T. L. (2019). Isolation and analysis of tumor-derived exosomes. *Current Protocols in Immunology 127*(1):e91.

Ludwig, N., Razzo, B. M., Yerneni, S. S., & Whiteside, T. L. (2019). Optimization of cell culture conditions for exosome isolation using mini-size exclusion chromatography (mini-SEC). *Experimental Cell Research 378*(2), 149-157.

Maas, S. L. N., Breakefield, X. O., & Weaver, A. M. (2017). Extracellular vesicles: unique intercellular delivery vehicles. *Trends in Cell Biology 27*(3), 172-188.

Monypenny, J., Milewicz, H., Flores-Borja, F., Weitsman, G., Cheung, A., Chowdhury, R., Burgoyne, T., Arulappu, A., Lawler, K., Barber, P. R., Vicencio, J. M., Keppler, M., Wulaningsih, W., Davidson, S. M., Fraternali, F., Woodman, N., Turmaine, M., Gillett, C., Franz, D., … Ng, T. (2018). ALIX regulates tumor-Mediated immunosuppression by controlling EGFR activity and PD-L1 presentation. *Cell reports 24*(3), 630-641.

Hodi, F. S., O'Day, S. J., McDermott, D. F., Weber, R. W., Sosman, J. A., Haanen, J. B., Gonzalez, R., Robert, C., Schadendorf, D., Hassel, J. C., Akerley, W., van den Eertwegh, A. J., Lutzky, J., Lorigan, P., Vaubel, J. M., Linette, G. P., Hogg, D., Ottensmeier, C. H., Lebbé, C., … Urba, W. J. (2010). Improved survival with ipilimumab in patients with metastatic melanoma. *New England Journal of Medicine 363*(8), 711-723.

Odorizzi, G. (2006). The multiple personalities of Alix. *Journal of Cell Science 119*(Pt 15), 3025-3032.

Peinado, H., Alečković, M., Lavotshkin, S., Matei, I., Costa-Silva, B., Moreno-Bueno, G., Hergueta-Redondo, M., Williams, C., García-Santos, G., Ghajar, C., Nitadori-Hoshino, A., Hoffman, C., Badal, K., Garcia, B. A., Callahan, M. K., Yuan, J., Martins, V. R., Skog, J., Kaplan, R. N., … Lyden, D. (2012). Melanoma exosomes educate bone marrow progenitor cells toward a pro-metastatic phenotype through MET. *Nature Medicine 18*(6), 883-891.

Perez-Riverol, Y., Csordas, A., Bai, J., Bernal-Llinares, M., Hewapathirana, S., Kundu, D. J., Inuganti, A., Griss, J., Mayer, G., Eisenacher, M., Pérez, E., Uszkoreit, J., Pfeuffer, J., Sachsenberg, T., Yilmaz, S., Tiwary, S., Cox, J., Audain, E., Walzer, M., … Vizcaíno, J. A (2019). The PRIDE database and related tools and resources in 2019: improving support for quantification data. *Nucleic Acids Research 47*(D1), D442-D450.

Ricklefs, F. L., Alayo, Q., Krenzlin, H., Mahmoud, A. B., Speranza, M. C., Nakashima, H., Hayes, J. L., Lee, K., Balaj, L., Passaro, C., Rooj, A. K., Krasemann, S., Carter, B. S., Chen, C. C., Steed, T., Treiber, J., Rodig, S., Yang, K., Nakano, I., … Chiocca, E. A. (2018). Immune evasion mediated by PD-L1 on glioblastoma-derived extracellular vesicles. *Science Advances 4*(3):eaar2766.

Rodriguez-Cerdeira, C., Molares-Vila, A., Carnero-Gregorio, M., & Corbalan-Rivas, A. (2018). Recent advances in melanoma research via "omics" platforms. *Journal of Proteomics 188*, 152-166.

Ruivo, C. F., Adem, B., Silva, M., & Melo, S. A. (2017). The biology of cancer exosomes: insights and new perspectives. *Cancer Research 77*(23), 6480-6488.

Shannan, B., Perego, M., Somasundaram, R., & Herlyn, M. (2016). Heterogeneity in melanoma. *Cancer Treatment and Research 167*, 1-15.

Sharma, P., Diergaarde, B., Ferrone, S., Kirkwood, J. M., & Whiteside, T. L. (2020). Melanoma cell-derived exosomes in plasma of melanoma patients suppress functions of immune effector cells. *Scientific Reports 10*(1), 92.

Sharma, P., Ludwig, S., Muller, L., Hong, C. S., Kirkwood, J. M., Ferrone, S., & Whiteside, T. L. (2018). Immunoaffinity-based isolation of melanoma cell-derived exosomes from plasma of patients with melanoma. *Journal of Extracellular Vesicles 7*(1):1435138.

Subramanian, L., Crabb, J. W., Cox, J., Durussel, I., Walker, T. M., van Ginkel, P. R., Bhattacharya, S., Dellaria, J. M., Palczewski, K., & Polans, A. S. (2004). Ca2+ binding to EF hands 1 and 3 is essential for the interaction of apoptosis-linked gene-2 with Alix/AIP1 in ocular melanoma. *Biochemistry 43*(35), 11175-11186.

The Human Protein Atlas https://www.proteinatlas.org/.

The TCGA Research Network https://www.cancer.gov/tcga.

Theodoraki, M. N., Yerneni, S. S., Hoffmann, T. K., Gooding, W. E., & Whiteside, T. L. (2018). Clinical significance of PD-L1(+) exosomes in plasma of head and neck cancer patients. *Clinical Cancer Research 24*(4), 896-905.

Tripp, M. K., Watson, M., Balk, S. J., Swetter, S. M., & Gershenwald, J. E. (2016). State of the science on prevention and screening to reduce melanoma incidence and mortality: the time is now. *CA: A Cancer Journal for Clinicians 66*(6), 460-480.

Valenti, R., Huber, V., Iero, M., Filipazzi, P., Parmiani, G., & Rivoltini, L. (2007). Tumor-released microvesicles as vehicles of immunosuppression. *Cancer Research 67*(7), 2912-2915.

Weiss, S. A., Wolchok, J. D., & Sznol, M. (2019). Immunotherapy of melanoma: facts and hopes. *Clinical Cancer Research 25*(17), 5191-5201.

Wendt, H. W. (1972). Dealing with a common problem in Social science: a simplified rank-biserial coefficient of correlation based on the U statistic. *European Journal of Social Psychology 2*(4), 463-465.

Whiteside, T. L. (2014). Induced regulatory T cells in inhibitory microenvironments created by cancer. *Expert Opinion on Biological Therapy 2014*, 1-15.

Whiteside, T. L. (2017). Exosomes carrying immunoinhibitory proteins and their role in cancer. *Clinical and Experimental Immunology 189*(3), 259-267.

Whiteside, T. L., Demaria, S., Rodriguez-Ruiz, M. E., Zarour, H. M., & Melero, I. (2016). Emerging opportunities and challenges in cancer immunotherapy. *Clinical Cancer Research 22*(8), 1845-1855.

Wieckowski, E. U., Visus, C., Szajnik, M., Szczepanski, M. J., Storkus, W. J., & Whiteside, T. L. (2009). Tumor-derived microvesicles promote regulatory T cell expansion and induce apoptosis in tumor-reactive activated CD8+ T lymphocytes. *Journal of Immunology 183*(6), 3720-3730.

Willms, E., Cabanas, C., Mager, I., Wood, M. J. A., & Vader, P. (2018). Extracellular vesicle heterogeneity: subpopulations, isolation techniques, & diverse functions in cancer progression. *Frontiers in Immunology 9*, 738.

Wisniewski, J. R., & Gaugaz, F. Z. (2015). Fast and sensitive total protein and Peptide assays for proteomic analysis. *Analytical Chemistry 87*(8), 4110-4116.

Wisniewski, J. R., Zougman, A., Nagaraj, N., & Mann, M. (2009). Universal sample preparation method for proteome analysis. *Nature Methods 6*(5), 359-362.

Yaguchi, T., & Kawakami, Y. (2016). Cancer-induced heterogeneous immunosuppressive tumor microenvironments and their personalized modulation. *International Immunology 28*(8), 393-399.

Yu, G., & He, Q. Y. (2016). ReactomePA: an R/Bioconductor package for reactome pathway analysis and visualization. *Molecular Biosystems 12*(2), 477-479.

Yu, G., Wang, L. G., Han, Y., & He, Q. Y. (2012). clusterProfiler: an R package for comparing biological themes among gene clusters. *Omics 16*(5), 284-287.

SUPPORTING INFORMATION

Additional supporting information may be found online in the Supporting Information section at the end of the article.

How to cite this article: Pietrowska M, Zebrowska A, Gawin M, et al. Proteomic profile of melanoma cell-derived small extracellular vesicles in patients' plasma: a potential correlate of melanoma progression. *J Extracell Vesicles*. 2021;10:e12063. https://doi.org/10.1002/jev2.12063

cells

MDPI

Article

Proteomic and Metabolomic Profiles of T Cell-Derived Exosomes Isolated from Human Plasma

Aneta Zebrowska [1,†], Karol Jelonek [1,†], Sujan Mondal [2,†], Marta Gawin [1], Katarzyna Mrowiec [1], Piotr Widłak [3,*], Theresa Whiteside [2,4,5,*] and Monika Pietrowska [1,*]

1 Maria Sklodowska-Curie National Research Institute of Oncology, 44-102 Gliwice, Poland; aneta7zebrowska@gmail.com (A.Z.); karol.jelonek@io.gliwice.pl (K.J.); marta.gawin@io.gliwice.pl (M.G.); katarzyna.mrowiec@io.gliwice.pl (K.M.)
2 UPMC Hillman Cancer Center, University of Pittsburgh Cancer Institute, Pittsburgh, PA 15232, USA; mondals@upmc.edu
3 Clinical Research Support Centre, Medical University of Gdańsk, 80-210 Gdańsk, Poland
4 Department of Pathology, University of Pittsburgh School of Medicine, Pittsburgh, PA 15261, USA
5 Department of Medicine, University of Pittsburgh School of Medicine, Pittsburgh, PA 15261, USA
* Correspondence: piotr.widlak@gumed.edu.pl (P.W.); whitesidetl@upmc.edu (T.W.); monika.pietrowska@io.gliwice.pl (M.P.); Tel.: +48-58-349-2767 (P.W.); +1-412-624-0096 (T.W.); +48-32-2789672 (M.P.)
† These authors contributed equally to this work.

Abstract: Exosomes that are released by T cells are key messengers involved in immune regulation. However, the molecular profiling of these vesicles, which is necessary for understanding their functions, requires their isolation from a very heterogeneous mixture of extracellular vesicles that are present in the human plasma. It has been shown that exosomes that are produced by T cells could be isolated from plasma by immune capture using antibodies that target the CD3 antigen, which is a key component of the TCR complex that is present in all T lymphocytes. Here, we demonstrate that CD3(+) exosomes that are isolated from plasma can be used for high-throughput molecular profiling using proteomics and metabolomics tools. This profiling allowed for the identification of proteins and metabolites that differentiated the CD3(+) from the CD3(−) exosome fractions that were present in the plasma of healthy donors. Importantly, the proteins and metabolites that accumulated in the CD3(+) vesicles reflected the known molecular features of T lymphocytes. Hence, CD3(+) exosomes that are isolated from human plasma by immune capture could serve as a "T cell biopsy".

Keywords: CD3 antigen; exosomes; immune capture; T lymphocytes; metabolomics; proteomics; small extracellular vesicles

check for updates

Citation: Zebrowska, A.; Jelonek, K.; Mondal, S.; Gawin, M.; Mrowiec, K.; Widłak, P.; Whiteside, T.; Pietrowska, M. Proteomic and Metabolomic Profiles of T Cell-Derived Exosomes Isolated from Human Plasma. *Cells* **2022**, *11*, 1965. https://doi.org/10.3390/cells11121965

Academic Editor: Francesc E. Borràs

Received: 24 May 2022
Accepted: 17 June 2022
Published: 18 June 2022

1. Introduction

Exosomes are small extracellular vesicles (sEVs) that are sized between 30–150 nm. They are produced by all types of cells via the endosome pathway and are present in all body fluids, including plasma, urine, cerebrospinal fluid, synovial fluid and breast milk [1–3]. The molecular and genetic cargo of sEVs reflects the content of their parent cells and thus, exosomes are considered to be promising components of "liquid biopsy". Exosomes are key mediators in different aspects of cell-to-cell communication, including those involved in disease-related mechanisms. Tumor cells produce and release large numbers of sEVs, which are also referred to as tumor-derived exosomes or TEXs [4–7]. However, vesicles in human plasma are a heterogeneous mix of circulating sEVs that originated from multiple tissues, including immune cells [6–8]. Consequently, the EV component of plasma consists of many individual subsets of exosomes that share a common biogenesis but have unique phenotypic/functional characteristics. This heterogeneity causes difficulties in understanding exosome-mediated intercellular crosstalk in vivo without attributing their molecular/functional features to specific subsets of sEVs that are produced by various

tissues or circulating parental cells. To be able to determine the molecular signatures of the different subsets of exosomes, novel strategies are required for their isolation and separation from human plasma for downstream molecular/genetic profiling. An emerging approach is the separation of particular tissue-derived sEVs based on their specific antigens using an immune capture strategy, as we recently reported for the case of sEVs in the plasma of melanoma patients [9–11].

Exosomes that are released by T cells, which comprise a large fraction of the sEVs in human plasma [12], are key messengers between tissue cells, malignant tumors and the immune system [13–16]. Therefore, the isolation of T cell-derived exosomes may result in substantial knowledge being gained about the crosstalk between immune cells and tissue-resident normal or pathologically altered cells. We previously reported on the success of an immune capture strategy that relies on the use of a specific mAb for the CD3 antigen (a component of the TCR signaling complex), which separates CD3(+) T cell-derived exosomes from CD3(−) exosomes that are released by other immune or non-immune cells [12,15,17]. These exosome fractions have been characterized functionally, which has revealed their important immunomodulatory role in patients with head and neck cancers [12]. Here, the same immune capture strategy for CD3(+) exosomes was utilized for the in-depth characterization of the differences between the proteome and metabolome compositions of exosomes that are released by T cells versus other types of CD3(−) exosomes that are present in the plasma of healthy individuals. We found that under physiologically normal conditions, the immune-captured CD3(+) exosomes reflected the proteomic and metabolomic features of their parental T cells and thus, could serve as a "liquid T cell biopsy".

2. Materials and Methods

2.1. Isolation of Total sEVs from Human Plasma

Blood samples were obtained from 10 consenting healthy donors (HDs) (IRB approval #04-001). The blood samples were processed to separate the plasma, which was divided into aliquots and stored at −80 °C until thawed and was then used for the exosome isolation. The thawed and pre-cleared plasma was processed by ultrafiltration, followed by size exclusion chromatography (SEC) as previously described in [9]. Briefly, the thawed plasma samples were centrifuged at 2000 × *g* for 10 min, followed by centrifugation at 10,000 × *g* for 30 min at 4 °C and they were then ultrafiltered through 0.22-µm filters (EMD Millipore, Billerica, MA, USA). An aliquot (1 mL) of plasma was loaded onto a 10-cm SEC column and 1 mL fractions were eluted with PBS. The void volume fraction #4, which contained the majority of the non-aggregated and morphologically intact sEVs, was collected and used for further analyses. The transmission electron microscopy (TEM), vesicle size range, particle numbers and protein content of fraction #4 were determined as previously described in [9,18,19]. The sEV protein concentration was determined using the BCA method (Pierce Biotechnology, Rockford, CA, USA), as per the manufacturer's instructions. The sEVs were concentrated using Vivaspin 500 (100,000 MWCO, Sartorius, Göttingen, Germany).

2.2. Isolation of CD3(+) Exosomes Using Immune Capture

The T cell-derived exosomes (CD3(+) exo) were separated from the non-T cell-derived exosomes (CD3(−) exo) using immune capture with anti-CD3 mAbs, which recognize an epitope that is selectively expressed on T cell receptor-positive (TCR+) T cells [12,15]. An aliquot of the sEVs that were present in fraction #4 (10 µg of protein) was used for the immune capture by biotin-labeled anti-CD3 mAbs (Biolegend #300304, San Diego, CA, USA) and streptavidin-labeled magnetic beads (ExoCap™, MBL International, Woburn, MA, USA). The vesicles were incubated with the biotin-labeled anti-CD3 mAbs overnight and then 100 µL of streptavidin-coated magnetic beads (washed twice with PBS) were added, which was followed by overnight incubation. The recovered CD3(+) vesicles that were captured by the anti-CD3 mAbs on the beads were washed twice with PBS and re-suspended in 100 µL of PBS as the CD3(+)exo fraction. Exosomes that were not captured on the beads,

i.e., the soluble CD3(−)exo fraction, were also harvested. The detection of proteins that were present on the surface of the CD3(+)exo and CD3(−)exo fractions was performed using on-bead flow cytometry, as previously described in [12]. The separated exosome fractions were used for the downstream analyses.

2.3. Sample Preparation for Metabolomics and Proteomics Analyses

Sterile PBS (350 µL) was added to the thawed samples of CD3(+)exo on the beads, vortexed for 30 sec and then mixed (50 rpm) using a HulaMixer (HulaMixer™ Sample Mixer, Thermo Fisher Scientific, Waltham, MA, USA) for 15 min at 4 °C. The samples of the non-captured CD3(−)exo fraction were vortexed and centrifuged; then, each sample was adjusted to the final volume of 350 µL using sterile PBS. All samples containing 350 µL of suspension were transferred to new 2-mL Eppendorf tubes (in the samples containing beads with CD3(+)exo, a brown precipitate was visible). Extraction with ice-cold 100% MeOH was performed using vigorous vortexing for 1 min (the final MeOH concentration was 80%); then, the samples were mixed using a HulaMixer (50 rpm) for 10 min at 4 °C and centrifuged for 10 min at 14,000× g and 4 °C. The supernatants were collected into new tubes for metabolomics analysis, while all pellets were frozen at −20 °C for proteomics analysis. The supernatants were vacuum-concentrated using a SpeedVac concentrator (SpeedVac DNA 120, SAVANT Instruments, Inc., Ramsey, MN, USA) in 500 µL aliquots to reach the final remaining sample volume of 50 to 70 µL and were then stored at −80 °C until further processing.

2.4. Targeted Metabolomics Analysis

The methanol-extracted samples (see paragraph above) were analyzed using a targeted quantitative approach with an Absolute IDQ p400 HR kit (test plates in the 96-well format; Biocrates Life Sciences AG, Innsbruck, Austria), according to the manufacturer's protocol. The samples were applied to the wells in a few 10–20 µL aliquots (dried under nitrogen) and were then analyzed using combined direct flow injection (for lipids) and liquid chromatography (for small metabolites) high-resolution mass spectrometry (HR-MS). The method combined the derivatization and extraction of the analytes with selective mass-spectrometric detection using integrated isotope-labeled internal standards for absolute quantification. This approach hypothetically allowed for the simultaneous quantification of 407 metabolites (or their isomer groups) into 42 amino acids and biogenic amines, 55 acylcarnitines, 60 di- and triglycerides, 196 (lyso)phosphatidylcholines, 40 sphingolipids, 14 cholesteryl esters and hexose. The mass spectrometry analyses were carried out on an Orbitrap Q Exactive Plus (Thermo Fisher Scientific, Waltham, MA, USA), which was equipped with a 1290 Infinity UHPLC (Agilent, Santa Clara, CA, USA) system that was controlled by Xcalibur 4.1 software (Thermo Fisher Scientific, Waltham, MA, USA). The acquired data were processed using Xcalibur 4.1 and MetIDQ DB110-2976 (Biocrates Life Sciences AG, Innsbruck, Austria) software.

2.5. Peptide Preparation for Proteomics Analysis

The pellets that were collected during the sample preparation (see paragraph above) were dissolved in 100 µL of lysis buffer (0.1 M Tris–HCl pH 8.0, 0.1 M DTT, 4% SDS), heated for 1 h at 99 °C with shaking (800 rpm) and then cooled down. The samples were subsequently centrifuged at 20,000× g for 10 min at RT; then, the supernatants were collected and subjected to filter-aided sample preparation (FASP) [20] using a Microcon-30 kDa Centrifugal Filter Unit with an Ultracel-30 membrane (Millipore, Billerica, MA, USA). The proteins that were retained on the membrane were alkylated using 50 mM of iodoacetamide and digested with sequencing grade modified trypsin (Promega, Madison, WI, USA) at an enzyme to protein ratio of 1:50 (m/m). The digestion was performed in a humid chamber at 37 °C for 18 h. The obtained tryptic peptides were released from the filter membrane using 160 µL of water, acidified with trifluoroacetic acid (final concentration of TFA: 0.2% v/v) and desalted using StageTips [21], which contained an Empore C18 SPE extraction disk

(Supelco, Bellefonte, PA, USA). The peptides that were retained on the sorbent were eluted with 60% ACN and 0.1% TFA, dried using a vacuum concentrator and resolved in 20 µL of water; then, the peptide concentration was assessed using the tryptophan fluorescence method [22]. Before the LC-MS/MS analysis, the purified peptide samples were acidified with TFA (final concentration: 0.1% v/v).

2.6. Protein Identification by LC-MS/MS Analysis

The LC-MS/MS analysis of the tryptic peptides (see paragraph above) was performed using the Dionex UltiMate 3000 RSLC nanoLC system coupled with a Q Exactive Plus Orbitrap mass spectrometer (Thermo Fisher Scientific, Waltham, MA, USA). The peptides were separated on a reverse-phase Acclaim PepMap RSLC nanoViper C18 column (75 µm × 25 cm, 2 µm granulation) using 0.1% FA in LC-MS grade water (as mobile phase A) and 80% acetonitrile with 0.1% FA in LC-MS grade water (as mobile phase B) at 30 °C and a flow rate of 300 nL/min (for 200 min). For additional desalting purposes, the samples were loaded onto a C18 trap column for 3 min using 0.1% FA in LC-MS grade water as a loading buffer. After desalting, the trap column was switched with the analytical column and the peptides were eluted using the binary gradients of 3–8% of mobile phase B for 7 min, 8–35% of mobile phase B for 130 min and 35–60% of mobile phase B for a further 20 min. Finally, the rinsing off of the column in 80% of mobile phase B for 20 min and equilibration in 3% of mobile phase B for another 20 min were performed. The spectrometer was operated in data-dependent MS/MS mode with survey scans that were acquired at a resolution of 70,000 at m/z 50 in MS mode and 17,500 at m/z 200 in MS2 mode. The spectra were recorded using the positive ion scanning mode in the range of 350–1500 m/z and higher energy collisional dissociation (HCD) was used to fragment the ions.

The protein identification was performed using a reviewed Swiss-Prot human database (release 2018_11_30, which contains 11,378,269 sequence entries) with a precision tolerance of 10 ppm for the peptide masses and 0.02 Da for the fragment ion masses. All raw data that were obtained for each dataset were imported into Proteome Discoverer v.1.4 (Thermo Fisher Scientific, Waltham, MA, USA) <Thermo raw files> for protein identification and quantification (Sequest engine was used for the database searches). Protein was considered as positively identified when at least two peptides per protein were found by the search engine and the peptide score reached the significance threshold of FDR = 0.01 (assessed by the Percolator algorithm). A protein was further considered as "present" when it was detected in at least one sample of a given type. The abundance of the identified proteins was estimated in Proteome Discoverer using the Precursor Ions Area detector node, which calculates the abundance of a given protein based on the average intensity of the three most intensively distinct peptides for that protein with further normalization to the total ion current (TIC).

2.7. Statistical Analyses

The significance of difference of the levels of proteins/metabolites that was used in the quantitative analyses (compounds with less than 50% of the initial "zero" values in each group were used in a given comparison) was measured using the Wilcoxon signed-rank test. Additionally, the chi-squared independence test was applied to test whether the absence/presence status of a given compound was a group-related feature. The FDR correction was applied using the Benjamini–Hochberg procedure, when necessary. All statistical hypotheses were tested at the 5% significance level. The STRINGdb database [23] was used to predict the relationships between the chosen proteins.

3. Results

3.1. Separation of CD3(+) and CD3(−) Vesicles

The total populations of sEVs were isolated from the plasma of healthy donors using size-exclusion chromatography (SEC) and then separated into T cell-derived sEVs (CD3(+)exo) and other cell-derived sEVs (CD3(−)exo) using the immune capture method

with anti-CD3 monoclonal antibodies. The total sEVs that were isolated from plasma by SEC (fraction #4) were characterized according to the MISEV2018 guidelines [24]. Morphology, size and the presence of endocytic protein markers (as well as the absence of cytoplasmic proteins) indicated that the majority of isolated sEVs represented exosomes. Figure 1A documents typical characteristics of isolated sEVs. The separation of the exosomes into the CD3(+) and CD3(−) fractions was monitored by on-bead flow cytometry, which revealed the enrichment of CD3 antigens in the CD3(+)exo fraction and the lack of CD3 antigens in the CD3(−)exo fraction (Figure 1B). We concluded that the combination of SEC for the isolation of the total plasma sEVs with the morphological and molecular characteristics of exosomes followed by the immune capture method with anti-CD3 mAbs allowed for the isolation of exosomes that were released by T lymphocytes and their separation from exosomes that were produced by other cells. The protein and lipid profiles of the resulting exosome fractions were assessed by mass spectrometry for 10 donors and the abundance of each identified component was compared in paired CD3(+)exo and CD3(−)exo vesicles from the same donor.

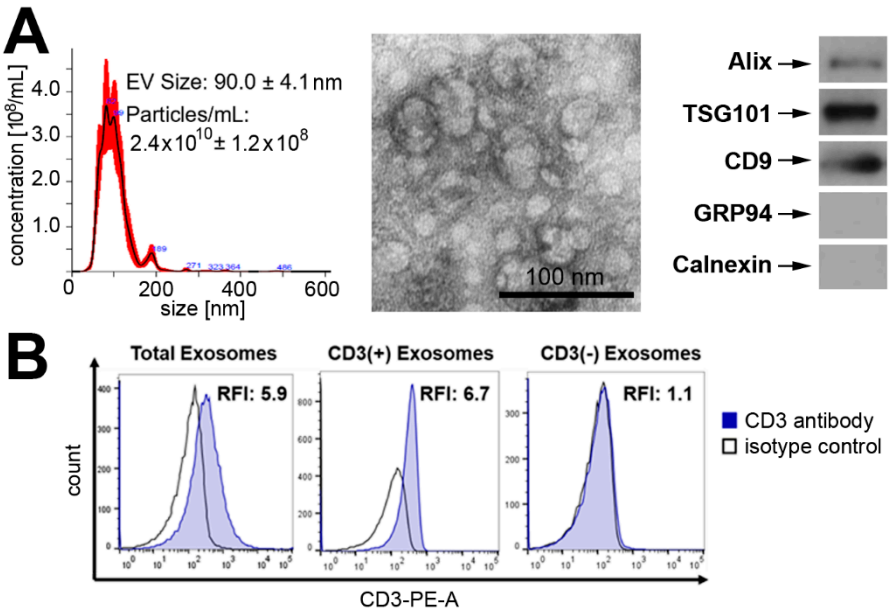

Figure 1. The characteristics of the analyzed vesicles: (**A**) the size, morphology and presence of exosome markers (from left to right), as analyzed by NanoSight, TEM and Western blots, respectively, in the total sEVs that were purified from the plasma; (**B**) the presence of CD3 in the CD3(+)exo and CD3(−)exo fractions, as analyzed by on-bead flow cytometry. RFI, MFI sample/MFI isotype control; TCR, T cell receptor CD3.

3.2. Comparison of the Protein Contents of CD3(+) and CD3(−) Vesicles

Using a shotgun proteomics approach, 418 proteins were identified (listed in the Supplementary Materials, Table S1), including 99 high-abundance plasma proteins that usually co-purify with plasma sEVs [25]. These putative plasma "contaminants" were excluded from all further analyses of the sEV components and were addressed separately. The quantitative analysis of the sEVs revealed several proteins that had an abundance that was significantly different (FDR < 0.05) in the CD3(+)exo and CD3(−)exo fractions (Figure 2A, left). We found 36 sEV proteins that were upregulated in the CD3(+)exo fraction and 56 sEV proteins that were upregulated in the CD3(−)exo fraction. On the other hand, almost half of the putative plasma proteins were upregulated in the CD3(−)exo fraction. This observation suggested that some of the plasma proteins that were putatively co-purifying with total sEVs (fraction #4) were removed from the CD3(+)exo fraction during the washing of the bead-captured vesicles.

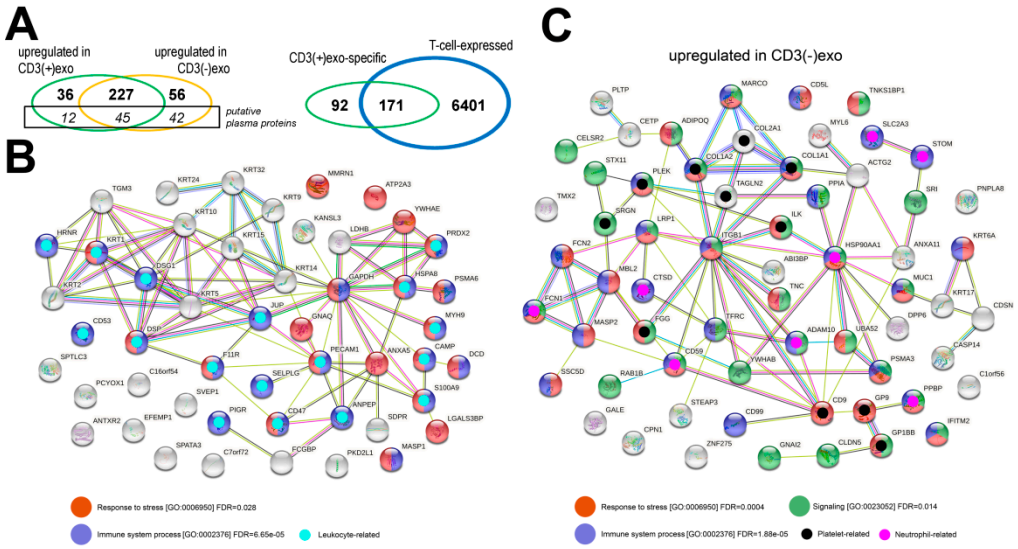

Figure 2. The proteins that were identified in the CD3(+) and CD3(−) fractions of the sEVs from human plasma: (**A**, **left**) a Venn diagram showing the numbers of proteins that were significantly upregulated in either fraction (FDR < 5%) with putative plasma proteins shown separately; (**A**, **right**) a Venn diagram showing the overlap between the CD(3+)exo-specific proteins and the T cell-expressed proteins (the latter dataset was taken from [26]); (**B**) the functional networks of proteins that were upregulated in the CD3(+)exo fraction; (**C**) the functional networks of proteins that were upregulated in the CD3(−)exo fraction. Proteins that were associated with the selected biological processes are color-coded, along with the significance of the process overrepresentation. The putative interactions between the proteins and associated processes were found using the STRINGdb database.

Moreover, we compared the set of proteins that were identified in the CD3(+) exosomes to a set of proteins that were detected in T lymphocytes. We used the proteomics dataset that was provided by Joshi et al. [26], who performed an in-depth analysis of $CD3^+/CD4^+/CD8^-$ T cells and identified 6572 proteins. We found that the majority of the protein characteristics for the CD3(+)exo fraction, i.e., neither upregulated in the CD3(−)exo nor the putative plasma components, were also detected in the T lymphocytes (Supplementary Materials, Figure 2A, right). On the other hand, the protein characteristics for the CD3(+)exo fraction that were not detected in the $CD3^+/CD4^+/CD8^-$ T cells (92 proteins) were mostly associated with exosome-based transport and putatively represented components that are specific to extracellular vesicles (Supplementary Materials, Figure S1). It is noteworthy that a few reports have addressed functions of sEVs that are produced by different classes of T lymphocytes, including $CD4^+$ cells (sEVs mediate co-stimulatory functions), $CD8^+$ cells (sEVs from activated cells mediate suppressive functions), Treg cells (sEVs are strongly immunosuppressive) [14,27,28]. There are no data available on sEVs that are produced by naïve or memory T cells. However, none of the abovementioned studies comprehensively addressed the proteome composition of sEVs that are released by T lymphocytes. Therefore, our proteomics data that were obtained with sEVs that were produced in vivo by the overall population of T lymphocytes could not be compared to other proteomics datasets in this study.

In the next step, we identified the biological functions/processes that were associated with the differentially expressed proteins (DEPs) that were upregulated in either the CD3(+)exo or CD3(−)exo fractions. The complete lists of the overrepresented functions and processes are provided in the Supplementary Materials, Tables S2 and S3. The potential interactions among the DEPs that were specific to both fractions of vesicles are also illustrated in the Supplementary Materials, Figure 2B,C. We found that among the most abundant subsets of proteins that were upregulated in either the CD3(+)exo or CD3(−)exo fractions, there were proteins that were associated with immune-related processes (GO:0002376; 20 and 26 DEPs were upregulated in the CD3(+) and CD3(−) fractions, respectively) and

the stress response (GO:0006950; 20 and 28 DEPs in the CD3(+) and CD3(−) fractions, respectively). Moreover, among the significantly overrepresented processes that were associated with the proteins that were upregulated in the CD3(−)exo fraction, there was "signaling" (GO:0023052; 31 DEPs). It is noteworthy, however, that the immune-related proteins that were upregulated in the CD3(+)exo and CD3(−)exo fractions of the plasma sEVs were associated with different types of immune cells. The immune-related proteins that were upregulated in the CD3(+)exo vesicles were primarily associated with leukocytes (GO:0045321 and GO:0050900; 17 DEPs were associated with "leukocyte activation" or "leukocyte migration"). On the other hand, the immune-related proteins that were upregulated in the CD3(−)exo fraction were primarily associated with neutrophiles (GO:0043312; nine DEPs were associated with "neutrophil degranulation"). Furthermore, a large subset of the proteins that were upregulated in the CD3(−)exo fraction was associated with platelets (GO:0030168 and GO:0002576; 11 DEPs were associated with "platelet activation" and "platelet degranulation"). Hence, the functions that were associated with the proteins that were upregulated in the two analyzed fractions of plasma exosomes confirmed their origin from T lymphocytes, which carried CD3 antigens (CD3(+)exo fraction) and other types of cells (CD3(−)exo fraction), including platelets and neutrophils.

3.3. Comparison of the Lipid and Small Metabolites Content of CD3(+) and CD3(−) Vesicles

In the second type of analysis, 338 metabolites (lipids and small metabolites) were identified and quantified using high-resolution mass spectrometry, including 287 putative membrane components (di/triglycerides, phosphatidylcholines, sphingolipids and cholesteryl esters), as well as a few acylcarnitines, amino acids, biogenic amines and hexoses (all compounds are listed in the Supplementary Materials, Table S4). The analysis revealed that several metabolites had an abundance that was significantly different (FDR < 0.05) between the CD3(+)exo and CD3(−)exo fractions. There were 96 metabolites that were upregulated in the CD3(+)exo fraction and 74 metabolites that were upregulated in the CD3(−)exo fraction of the plasma sEVs (Figure 3A). The majority of metabolites that were detected in the analyzed sEVs were lipids and lipid-related compounds. When small metabolites were considered, only hexoses (including glucose and fructose), which were highly accumulated in the CD3(+)exo fraction, discriminated between the fractions of the plasma exosomes.

The lipidomic profile characteristics for the CD3(+) and CD3(−) fractions of the plasma exosomes were identified. When the putative components of the vesicle membranes were analyzed, higher total amounts of cholesterols and sphingomyelins (SM) were observed in the CD3(+)exo fraction, while higher total amounts of phosphatidylcholines (PC) were observed in the CD3(−)exo fraction. In the case of acylglycerols, we noted higher amounts of triglycerides (TG) in the CD3(+)exo fraction, while we noted higher amounts of diglycerides (DG) in the CD3(−)exo fraction. Moreover, higher total levels of ceramides and acylcarnitines were characteristic for the CD3(+)exo fraction (Figure 3B). It was shown that the plasma membranes of lymphocytes were relatively enriched with cholesterol and sphingomyelins but depleted in phosphatidylcholines [29] and that cholesterols and sphingolipids were essential components of the plasma membranes that were involved in the proper functioning of the T cells [30]. Hence, the lipid composition of the CD3(+) sEVs that was revealed in the present study reflected the features of the plasma membranes of the T cells. Furthermore, ceramides (another class of metabolites that accumulated in the CD3(+) sEVs) were critical mediators that were associated with different functions of the T cells [31]. Similarly, the high concentration of glucose in the CD3(+) sEVs seemed to reflect a very high demand for this compound in the activated T cells [32]. Therefore, it should be noted that the features of the metabolic profiles that discriminated the CD3(+)exo fraction from the CD3(−)exo fraction of the plasma vesicles reflected the composition of the plasma membrane and other metabolic features of the T cells.

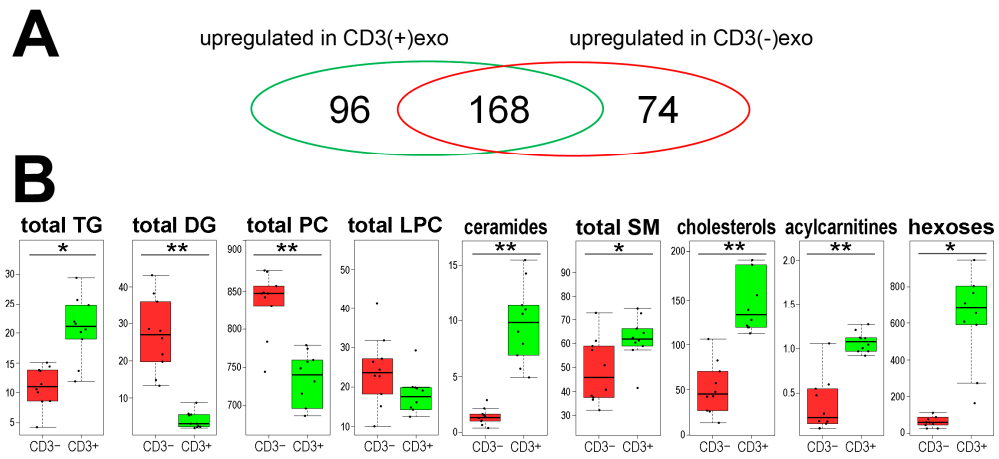

Figure 3. The metabolites that were identified in the CD3(+) and CD3(−) fractions of the sEVs from human plasma: (**A**) a Venn diagram showing the numbers of metabolites that were significantly upregulated in either fraction (FDR < 5%); (**B**) the abundance of the major classes of metabolites that were detected in the CD3(+) and CD3(−) fractions of the sEVs. The aggregated amounts of the major classes of lipids are also shown (TG, triglycerides; DG, diglycerides; PC, phosphatidylcholines; LPC, lysophosphatidylcholines; SM, sphingomyelins). The box plots represent the minimum, lower quartile, median, upper quartile and maximum. The dots represent the individual samples. The significance of difference between both fractions of sEVs is marked with asterisks (* FDR < 0.05; ** FDR < 0.001).

4. Conclusions

The exosomes that were released by T cells could be effectively separated from other types of sEVs that were present in human plasma using the immune capture method with antibodies that were specific for the CD3 antigen, which is a key component of the TCR signaling complex and is exclusively present in all subpopulations of T lymphocytes. The isolated and immunoselected vesicles represented a feasible material for high-throughput molecular profiling using proteomics and metabolomics, which allowed for the identification of the proteins and metabolites that differentiated the CD3(+) and CD3(−) fractions of the exosomes in the plasma of healthy donors. Importantly, the proteins and metabolites that accumulated in the CD3(+) vesicles reflected the known molecular features of T cells. Moreover, the protein characteristics for the CD3(+) vesicles were detected in the $CD3^+$ lymphocytes. Hence, the exosomes that were purified from human plasma using the immune capture method with anti-CD3 mAbs appeared to serve as a "T cell biopsy". Importantly, the discrimination of the exosome subsets in the plasma of HDs could provide a basis for future investigations on the CD3(+) exosomes in the plasma of patients with pathological conditions, including autoimmune diseases or cancers. A "T cell biopsy" using the exosomes from pathological plasma could replace the currently used analyses of T lymphocytes from blood or other body fluids. In addition, the CD3(−)exo fraction, which putatively reflected the attributes of other circulating or tissue-infiltrating immune and non-immune cells, could inform us as to their general activation or functional status.

Supplementary Materials: The following supporting information is available at https://www.mdpi.com/article/10.3390/cells11121965/s1, Table S1: The proteins that were identified in the CD3(+) and CD3(−) exosomes from the plasma of healthy donors, Table S2: The functions that were associated with proteins that were upregulated in the CD3(+) exosomes, Table S3: The functions that were associated with proteins that were upregulated in the CD3(−) exosomes, Table S4: The metabolites that were identified in the CD3(+) and CD3(−) exosomes from the plasma of healthy donors, Figure S1: The functional network of proteins characteristic for the CD3(+)exo fraction that were not detected in $CD3^+/CD4^+/CD8^-$ T cells. Proteins that were associated with the selected biological processes are color-coded, along with the significance of the process overrepresentation. The putative interactions between the proteins and associated processes were found using the STRINGdb database.

Author Contributions: Conceptualization, M.P., T.W. and P.W.; methodology, A.Z., K.J., S.M. and M.G.; software, M.P. and K.J.; formal analysis, K.J. and A.Z.; investigation, A.Z., K.J., S.M. and K.M.; resources, M.P. and T.W.; writing—original draft preparation, A.Z., M.P., T.W. and P.W.; writing—review and editing, M.P., T.W., P.W. and M.G.; visualization, S.M., M.P. and P.W.; supervision, M.P. and T.W.; project administration, M.P. and T.W.; funding acquisition, M.P. and T.W. All authors have read and agreed to the published version of the manuscript.

Funding: This research was funded by the National Science Centre, Poland (grant number 2016/22/M/NZ5/00667 to M.P., A.Z. and P.W.) and in part by the NIH (grant numbers R01-CA168628 and U01-DE029759 to T.W.).

Institutional Review Board Statement: The study was conducted in accordance with the Declaration of Helsinki and was approved by the Institutional Review Board of the University of Pittsburgh School of Medicine (IRB approval #04-001).

Informed Consent Statement: Informed consent was obtained from all subjects involved in this study.

Data Availability Statement: Not applicable.

Conflicts of Interest: The authors declare no conflict of interest.

References

1. Brinton, L.T.; Sloane, H.S.; Kester, M.; Kelly, K.A. Formation and role of exosomes in cancer. *Cell Mol. Life Sci.* **2015**, *72*, 659–671. [CrossRef] [PubMed]
2. Zebrowska, A.; Widlak, P.; Whiteside, T.; Pietrowska, M. Signaling of Tumor-Derived sEV Impacts Melanoma Progression. *Int. J. Mol. Sci.* **2020**, *21*, 5066. [CrossRef] [PubMed]
3. Zebrowska, A.; Skowronek, A.; Wojakowska, A.; Widlak, P.; Pietrowska, M. Metabolome of Exosomes: Focus on Vesicles Released by Cancer Cells and Present in Human Body Fluids. *Int. J. Mol. Sci.* **2019**, *20*, 3461. [CrossRef] [PubMed]
4. Kalluri, R.; LeBleu, V.S. The biology, function, and biomedical applications of exosomes. *Science* **2020**, *367*, eaau6977. [CrossRef] [PubMed]
5. Whiteside, T.L. Tumor-Derived Exosomes and Their Role in Cancer Progression. *Adv. Clin. Chem.* **2016**, *74*, 103–141. [CrossRef] [PubMed]
6. Kok, V.C.; Yu, C.C. Cancer-Derived Exosomes: Their Role in Cancer Biology and Biomarker Development. *Int. J. Nanomed.* **2020**, *15*, 8019–8036. [CrossRef] [PubMed]
7. Whiteside, T.L. The effect of tumor-derived exosomes on immune regulation and cancer immunotherapy. *Future Oncol.* **2017**, *13*, 2583–2592. [CrossRef]
8. Azambuja, J.A.; Ludwig, N.; Yerneni, S.; Braganhol, E.; Whiteside, T.L. Arginase-1+ Exosomes from Reprogrammed Macrophages Promote Glioblastoma Progression. *Int. J. Mol. Sci* **2020**, *21*, 3990. [CrossRef]
9. Pietrowska, M.; Zebrowska, A.; Gawin, M.; Marczak, L.; Sharma, P.; Mondal, S.; Mika, J.; Polańska, J.; Ferrone, S.; Kirkwood, J.M.; et al. Proteomic profile of melanoma cell-derived small extracellular vesicles in patients' plasma: A potential correlate of melanoma progression. *J. Extracell. Vesicles* **2021**, *10*, e12063. [CrossRef]
10. Ferrone, S.; Whiteside, T.L. Targeting CSPG4 for isolation of melanoma cell-derived exosomes from body fluids. *HNO* **2020**, *68*, 100–105. [CrossRef]
11. Sharma, P.; Ludwig, S.; Muller, L.; Hong, C.S.; Kirkwood, J.M.; Ferrone, S.; Whiteside, T.L. Immunoaffinity-based isolation of melanoma cell-derived exosomes from plasma of patients with melanoma. *J. Extracell. Vesicles.* **2018**, *7*, 1435138. [CrossRef] [PubMed]
12. Theodoraki, M.N.; Hoffmann, T.K.; Whiteside, T.L. Separation of plasma-derived exosomes into CD3(+) and CD3(−) fractions allows for association of immune cell and tumour cell markers with disease activity in HNSCC patients. *Clin. Exp. Immunol.* **2018**, *192*, 271–283. [CrossRef] [PubMed]
13. Whiteside, T.L.; Diergaarde, B.; Hong, C.S. Tumor-Derived Exosomes (TEX) and Their Role in Immuno-Oncology. *Int. J. Mol. Sci.* **2021**, *22*, 6234. [CrossRef] [PubMed]
14. Shao, Y.; Pan, X.; Fu, R. Role and Function of T Cell-Derived Exosomes and Their Therapeutic Value. *Mediators Inflamm.* **2021**, *2021*, 8481013. [CrossRef]
15. Theodoraki, M.N.; Hoffmann, T.K.; Jackson, E.K.; Whiteside, T.L. Exosomes in HNSCC plasma as surrogate markers of tumour progression and immune competence. *Clin. Exp. Immunol.* **2018**, *194*, 67–78. [CrossRef]
16. Seo, N.; Akiyoshi, K.; Shiku, H. Exosome-mediated regulation of tumor immunology. *Cancer Sci.* **2018**, *109*, 2998–3004. [CrossRef]
17. Theodoraki, M.N.; Yerneni, S.; Gooding, W.E.; Ohr, J.; Clump, D.A.; Bauman, J.E.; Ferris, R.L.; Whiteside, T.L. Circulating exosomes measure responses to therapy in head and neck cancer patients treated with cetuximab, ipilimumab, and IMRT. *Oncoimmunology* **2019**, *8*, 1593805. [CrossRef]

18. Ludwig, N.; Hong, C.S.; Ludwig, S.; Azambuja, J.H.; Sharma, P.; Theodoraki, M.N.; Whiteside, T.L. Isolation and Analysis of Tumor-Derived Exosomes. *Curr. Protoc. Immunol.* **2019**, *127*, e91. [CrossRef]
19. Ludwig, N.; Razzo, B.M.; Yerneni, S.S.; Whiteside, T.L. Optimization of cell culture conditions for exosome isolation using mini-size exclusion chromatography (mini-SEC). *Exp. Cell Res.* **2019**, *378*, 149–157. [CrossRef]
20. Wiśniewski, J.R.; Zougman, A.; Nagaraj, N.; Mann, M. Universal sample preparation method for proteome analysis. *Nat. Methods* **2009**, *6*, 359–362. [CrossRef]
21. Rappsilber, J.; Ishihama, Y.; Mann, M. Stop and go extraction tips for matrix-assisted laser desorption/ionization, nanoelectrospray, and LC/MS sample pretreatment in proteomics. *Anal. Chem.* **2003**, *75*, 663–670. [CrossRef] [PubMed]
22. Wiśniewski, J.R.; Gaugaz, F.Z. Fast and sensitive total protein and Peptide assays for proteomic analysis. *Anal. Chem.* **2015**, *87*, 4110–4116. [CrossRef] [PubMed]
23. Szklarczyk, D.; Gable, A.L.; Lyon, D.; Junge, A.; Wyder, S.; Huerta-Cepas, J.; Simonovic, M.; Doncheva, N.T.; Morris, J.H.; Bork, P.; et al. STRING v11: Protein-protein association networks with increased coverage, supporting functional discovery in genome-wide experimental datasets. *Nucleic Acids Res.* **2019**, *47*, D607–D613. [CrossRef] [PubMed]
24. Théry, C.; Witwer, K.W.; Aikawa, E.; Alcaraz, M.J.; Anderson, J.D.; Andriantsitohaina, R.; Antoniou, A.; Arab, T.; Archer, F.; Atkin-Smith, G.K.; et al. Minimal information for studies of extracellular vesicles 2018 (MISEV2018): A position statement of the International Society for Extracellular Vesicles and update of the MISEV2014 guidelines. *J. Extracell. Vesicles* **2018**, *7*, 1535750. [CrossRef]
25. Smolarz, M.; Pietrowska, M.; Matysiak, N.; Mielańczyk, Ł.; Widłak, P. Proteome Profiling of Exosomes Purified from a Small Amount of Human Serum: The Problem of Co-Purified Serum Components. *Proteomes* **2019**, *7*, 18. [CrossRef]
26. Joshi, R.N.; Stadler, C.; Lehmann, R.; Lehtiö, J.; Tegnér, J.; Schmidt, A.; Vesterlund, M. TcellSubC: An Atlas of the Subcellular Proteome of Human T Cells. *Front Immunol.* **2019**, *10*, 2708. [CrossRef]
27. Azoulay-Alfaguter, I.; Mor, A. Proteomic analysis of human T cell-derived exosomes reveals differential RAS/MAPK signaling. *Eur. J. Immunol.* **2018**, *48*, 1915–1917. [CrossRef]
28. Tung, S.L.; Boardman, D.A.; Sen, M.; Letizia, M.; Peng, Q.; Cianci, N.; Dioni, L.; Carlin, L.M.; Lechler, R.; Bollati, V.; et al. Regulatory T cell-derived extracellular vesicles modify dendritic cell functions. *Sci. Rep.* **2018**, *8*, 6065. [CrossRef]
29. Hildebrand, J.; Marique, D.; Vanhouche, J. Lipid composition of plasma membranes from human leukemic lymphocytes. *J. Lipid Res.* **1975**, *16*, 195–199. [CrossRef]
30. Gombos, I.; Kiss, E.; Detre, C.; László, G.; Matkó, J. Cholesterol and sphingolipids as lipid organizers of the immune cells' plasma membrane: Their impact on the functions of MHC molecules, effector T-lymphocytes and T-cell death. *Immunol. Lett.* **2006**, *104*, 59–69. [CrossRef]
31. Adam, D.; Heinrich, M.; Kabelitz, D.; Schütze, S. Ceramide: Does it matter for T cells? *Trends Immunol.* **2002**, *23*, 1–4. [CrossRef]
32. Maciver, N.J.; Jacobs, S.R.; Wieman, H.L.; Wofford, J.A.; Coloff, J.L.; Rathmell, J.C. Glucose metabolism in lymphocytes is a regulated process with significant effects on immune cell function and survival. *J. Leukoc. Biol.* **2008**, *84*, 949–957. [CrossRef] [PubMed]